ALTERNATIVE STRATEGIES FOR SECURITY LABELLING/ENCODING OF PAPER AND PLASTIC PRODUCTS

SIMON J. OFFICER

PhD 2005

ALTERNATIVE STRATEGIES FOR SECURITY LABELLING/ENCODING OF PAPER AND PLASTIC PRODUCTS

SIMON J. OFFICER

A thesis submitted in partial fulfilment of

The Robert Gordon University

for the degree of Doctor of Philosophy.

April 2005

This research work was carried out in collaboration with

NCR Financial Solution Group Ltd Dundee.

Alternative Strategies for Security Labelling/Encoding of Paper and Plastic Products

By Simon Officer for the degree of Doctor of Philosophy

Abstract

A literature and patent review of current optical security techniques has been carried out and identified a need in the market for an improved optical security label to rival molecular fluorescent dyes. The label proposed was a rare earth (RE) doped borosilicate glass host that was excited and fluoresced in the visible region. Suitable RE dopants were found to be europium, terbium and dysprosium. The ability to triple dope a single glass and to be able to detect all three dopants based on their discrete fluorescence signals and unique fluorescence lifetimes has been achieved with an in-situ detector. This has advantages over current fluorescent dye labels which have broadband spectra that quickly overlap each other reducing their number of permutations.

Energy transfer between the dopants was noted. This can be used to increase the security level as the fluorescence signals were altered by these interactions. Europium was found to be enhanced with the addition of dysprosium or terbium whilst dysprosium enhanced terbium. Environmental studies of the doped glasses were carried out under various extreme conditions. These results concluded that no affect was found on their fluorescence signals or weight.

Fluorescence lifetime studies on the single RE doped glasses was successfully carried out. These results were used for the detection system design to increase the selectivity of the RE dopants over background fluorescence. Subsequently an initial single channel detector system was designed and built that could selectively detect 5 mm diameter pieces of 3 mol% europium doped glass.

The application of doped glass dispersed in ink and printed onto various media was also successfully demonstrated. With the production of micron sized particles, the glass could be incorporated into a wide variety of media increasing their possible applications in brand protection. Additionally, initial tests for compatibility with the detector system were achieved proving the capabilities of the detector system to detect the doped samples whilst mixed in various media.

Acknowledgements

I wish to offer my thanks to the following people who contributed towards this research project.

Firstly to the supervisory team, Dr Pat Pollard, Dr Catherine Hunter, Prof Peter Robertson and Dr Gary Ross from NCR for all their help, advice and support throughout this project enabling me to complete this thesis. Special thanks also go to Dr R Prabhu for all his help and advice with the detector system, barcode printing techniques and various other experiments carried out to complete this work.

I would also like to thank all the technician staff who helped throughout my PhD including Iain Tough for carrying out the SEM analysis, Bruce Thomson for his help with particle size analysis, Stephen Allardyce for fabricating the PCB boards, Steven Pirie for all his help in the workshop making the detector housing and John Wood for his help with FT-IR.

Further thanks also go to Morgan Adams for his advice and friendship for the past three years and to my girlfriend Lindsay and my family for putting up with me during my writing up period.

Contents

Table of Figures

Abbreviations

AC	-	Alternating current
ACG	-	Anti-counterfeiting group
ANOVA	-	Analysis of variance
ATM	-	Automated teller machine
BP	-	Band-pass
Calgon	-	Sodium hexametaphosphate
CW	-	Continuous wave
DC	-	Direct current
EDXA	-	Energy dispersive x-ray analysis
EU	-	European Union
FT-IR	-	Fourier transform-infrared
FWHM	-	Full width half maximum
GND	-	Ground
IR	-	Infrared
LED	-	Light emitting diode
LISFM	-	Laser induced scanning fluorescence microscope
LP	-	Long-pass
MS	-	Mean square
NBO	-	Non-bridging oxygen
NMR	-	Nuclear magnetic resonance
PCR	-	Polymerase chain reaction
PMT	-	Photomultiplier tube
RE	-	Rare earth
RI	-	Refractive index
SD	-	Standard deviation
SEM	-	Scanning electron microscope
Tg	-	Glass transition temperature
Tm	-	Melting temperature
UV	-	Ultraviolet

CHAPTER 1 - INTRODUCTION

1.1 OVERVIEW

The need for security features for valuable documents is well known. Human senses, particularly those of sight and touch, are the simplest detectors yet are some of the most dependable forms of validation in existence. These senses can detect a range of features including watermarks, security threads, raised print, holograms, and other variable optical devices. The features incorporated for human recognition are obvious, by definition, but are not usually conducive to automated processes either for document recognition or authentication. Features for simple automatic processes, such as bar codes, do exist but are readily reproduced. This is because such features are passive and always visible and due to the advances in scanner, copier and printer technologies can be effectively reproduced at low cost [1].

According to the ACG (Anti-Counterfeiting Group) the effect of all fake products (including videos, music and software) could be as high as £250 billion in the EU (European Union) through piracy and counterfeiting [2]. The Organisation for Economic Co-operation & Development has estimated that trade in fakes steals 7-9 % of world trade each year. In the credit card industry, every €100 spent on European VISA cards accounts for a loss of eight cents to fraud representing a fraud-to-sales ratio of 0.08 % [3]. This equates to absolute losses of €0.5 billion or €3 for each VISA card issued in Europe. In the automobile industry, one in ten car parts sold in Europe are fake according to France's anti-counterfeit agency [2]. In the UK alone, £289 million is lost to counterfeits of perfume and toiletries [4]. There is also a large problem concerning fuel tax fraud across Europe where a new chemical marker has now been launched that could save the UK government £500 million in lost tax revenue [5]. These statistics clearly indicate the size of the problem world-wide due to counterfeit products in numerous industries and indicates the need for new and improved security labels to combat this problem.

Increasingly features not visible in sunlight or artificial white light, or with properties other than optical are being incorporated into products and documents to increase security. The most common of these are magnetic inks and fluorescing inks. Magnetic inks can be formed into bar codes that are only read by a machine, and contain recognition data. However, readily available magnetic toner could be used to reproduce these codes reducing their level of security. Fluorescing inks can also be used to produce machine-readable bar codes, pictures or patterns (Figure 1-1) which tend to be for human verification but only while the product or document is exposed to UV (ultra violet) radiation. The inks in use have wide spectral bandwidths, precluding the use of several inks to form complex labels. This is because the individual bandwidths quickly overlap and become indistinguishable from each other, background fluorescence and ambient light.

Figure 1-1. Example fluorescent image (right) of original document (left)

Chemical and biochemical taggants (also known as labels, markers or tags) have been added to products as entities that can be subsequently detected as proof of authenticity. However, these tend to be detected in a two-stage process where the taggant has to be extracted and analysed. This is both time consuming and expensive and renders such techniques inappropriate for on-line, high-speed examination as would be needed in a self-service environment.

1.2 LITERATURE AND PATENT REVIEW

Labelling strategies are varied as they cover a wide range of applications and levels of security. In addition there are various techniques and approaches used to detect and validate the labels depending on their size, cost, speed and safety factors, which makes them unsuitable for on-line, high speed applications. Descriptions of labelling strategies are split into four categories; chemical and biochemical markers (1.2.1), optical markers (excluding fluorescence) (1.2.2), embedded fluorescent markers (1.2.3) and printed fluorescent markers (1.2.4).

1.2.1 Chemical and Biochemical Markers

One approach to achieve non-visible tagging is to use chemical markers embedded into the subject. Verification is then achieved by the extraction of the marker followed by its detection using well-known chemical analysis techniques such as PCR (polymerase chain reaction), electron microscopy, flow cytometry, NMR (nuclear magnetic resonance), IR (infrared), spectroscopic techniques or UV (ultra violet) microscopy.

Biochemical techniques for in-product marking are also finding use in covert product marking. The markers in such systems (e.g. The Biocode marking system [6]) comprise of simple organic chemicals, which are invisible and inert. Related systems utilise nucleotide markers (DNA is a subset of these) and require a second complementary nucleotide sequence with a suitable marker for easy detection. Basically one known sequence "finds" its partner sequence. Examples of such markers include substances capable of forming micelles, a strain or an antigen [7]. Another format involves microbeads that contain a nucleic acid marker [8]. The chemical marker to combat fuel tax fraud mentioned earlier, is called *Solvent Yellow 124* and is being described as the new "Euromarker*"* as it will be used throughout Europe as its standard marker [5]. Whilst designed for tagging liquids, such markers can be included in the paper manufacture process or included in inks used to print security documents.

In all such chemical and biochemical systems the marker must be extracted from the product (usually chemically) prior to detection. This two step process is often time-consuming, labour intensive and may require user expertise and very specialised equipment, but more importantly involves a form of destructive analysis. It is therefore not suited to self-service automation or other real time, on-line applications.

1.2.2 Optical Markers

Optical based techniques have been used for non-visual encoding of a range of products such as credit cards, passports, coupons and key cards. One of the simplest automated and invisible optical encoding techniques involves creating a pattern of holes in paper products that are read using an optical encoding transmission device. An example of such a system is that developed by Webcraft Technologies [9], which utilises a laser to produce the code on to the paper that is subsequently read using an optical scanning system.

For credit cards, a code has been embossed or electromagnetically recorded on to the card that contains information about the card [10]. This involves a layer of relatively high coercivity magnetisable material being laminated into the credit card, which is then encoded with a magnetically readable code. Furthermore, this same code is made as a human-readable mark on the card; therefore there is both a covert and overt security feature on the card that can be verified against each other. A variety of other systems based on optical or infrared reflective or transmission encoding techniques have also been developed. Holographic encoding has found favour in recent years in a number of applications, particularly for banks and credit cards. An example of such a system is the discrete wavelength implantation for security holograms developed by Tobin [11]. However, holograms can be replicated relatively easily and therefore do not offer a high level of security.

A new type of security thread has been developed for semi-covert security [12]. This technique is based on the properties of reversible thermochromic inks that change colour above a certain activation temperature. By inserting these inks into threads, the label can be inserted into any banknote or paper product. The operator then heats up the exposed thread with a finger to reveal the underlying text to verify its authenticity. This feature called Thermotext [13] can be seen on Microsoft manual covers and Marks and Spencer's gift vouchers, for example.

Such features require to be incorporated into substrates at the source. For example a laser written code is unlikely to be produced within an ATM (automated teller machine). With the thread, if it is the security feature then the stock of documents has to be kept secure. None of these give the option of coding the document within the ATM or making it valid at the point of issue. This does not give opportunities for increasing security through the use of encryption, based on the security feature, as codes cannot be produced.

1.2.3 Embedded Fluorescent Markers

One of the most widely employed optical labelling strategies is the incorporation of fluorescent labels. The first example utilises microbeads containing nucleic acid markers [8]. These markers then require a specific recognition molecule, which contains the fluorescent tag. Applications include the ability to use an aerosol to spray any individual attempting to remove the article. Furthermore, the nucleic acid markers can be incorporated into different types of beads, which may contain the fluorescent label.

A different approach is to use two different labels [7]. Here the first label is a type of DNA, which is invisible to everyone, whereas the second label is easily detectable and indicates the presence of the first label. However, as with the chemical and biochemical markers, described in 1.2.1, these approaches suffer from being multiple step techniques.

A two step marking method that utilises chelates has been developed [14]. Chelates are a class of co-ordination or complex compounds consisting of a central atom of a metal attached to a large molecule (ligand). For this type of application, rare earth (RE) chelates were found to be particularly advantageous. The first step involves pre-marking during the document production so as not to form the chelate. The second step adds the necessary elements to form the chelate during authentication. This can be achieved by applying an aqueous solution by printing, brushing, stamping or with a pen. After which, illumination of UV light causes the visible fluorescent emission. Deactivation requires an acidic or alkaline solution to be added by the methods described in the authentication step.

For securing credit cards and security documents, another label that involved RE metals has been produced [15]. This idea consists of a crystalline powder containing rare earth metals that can be inserted into the card, during its manufacture, as slurry. Excitation in the IR region produced fluorescence that can be detected mainly in the green visible region. Authentication of a positive response is based on the well defined rise and decay times of the label to differentiate it from any other background signal.

This second method could have applications in self-service document security as it could be applied, via ink, to a document at the time of dispense. It does appear limited in the number of variants and therefore codes that could be produced.

1.2.4 Printed Fluorescent Markers

The article by Williams [16] gives a good overview of the different types of security inks available for media security. As there is a total market size of $380 million for security inks alone, its little wonder there is such an interest in developing a new label that can be added to ink.

One such fluorescent ink includes a porphyrin dye that can be applied to paper via an ink jet system [17]. This approach produces an image that is only visible under UV light. Rare earth metals and a chelating ligand have also been used for security marking [18]. This label was based on fluorescent jet ink that is invisible to the naked eye but visible after UV excitation. A refinement of the basic dye labelling strategy is the encapsulation of the dye molecules in microbeads, as in the system developed by Dainippon Ink and Chem Inc [19]. This type of system is readily automated, however the dye molecules used have broadband absorption and fluorescence spectra. This limits the number of dyes which can be incorporated into a given marker (as the spectra will become indistinguishable from each other as shown in Figure 1-2) and thus severely restrict the number of permutations available for coding. Additionally a complex optical detection system is required to resolve the spectra. Furthermore, the instability of the dyes to a range of environmental parameters, such as oxygen, is well established and further restricts their use [20].

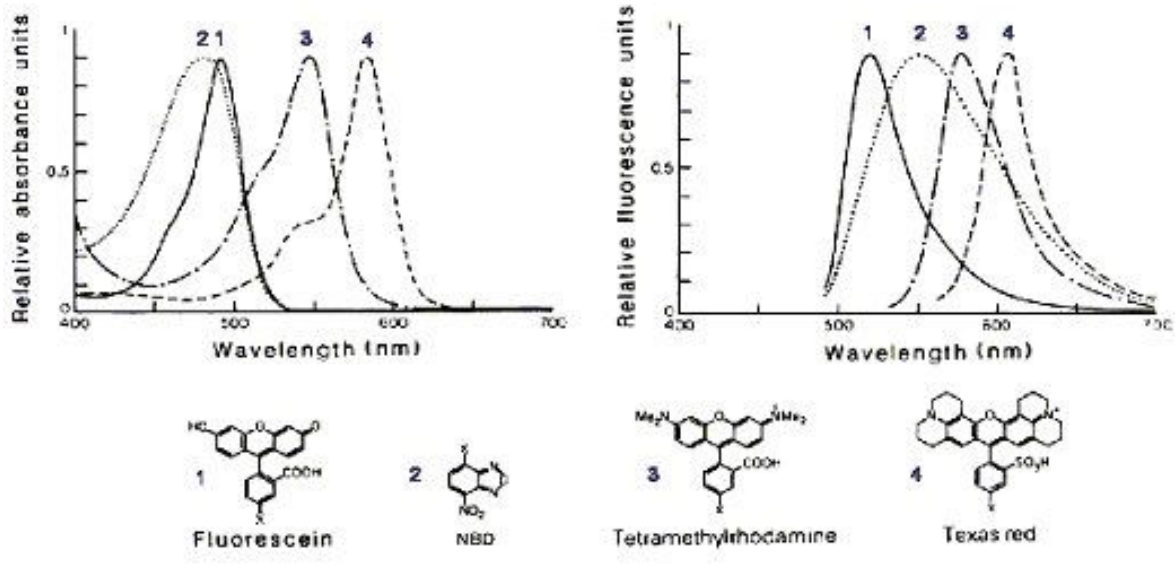

Figure 1-2. The absorption and emission spectra of four fluorescent dyes [21]

Ink that incorporates fluorophores and absorbs in the infrared and fluoresces outside of the visible region (wavelengths greater than 650 nm) has also been described [22]. Applications for this invention included security documents, metal surfaces and credit cards. Another form of security ink is described where any encrypted data can be printed on to a transparent tape using invisible ink [23]. This ink then becomes visible when exposed to either UV or IR light depending upon the dyes in the ink.

An application for use on bank checks and bags of cement or potatoes has utilised a form of ink [24]. This idea employs rare earth ions as ligands in either organic or inorganic chromophoric groups and produces ink that absorbs in the UV region and emits in the visible. A different fluorescent ink that uses a rare earth oxysulphide has been produced [25, 26]. This time both visible and invisible dyes are used on the secure document to give both covert and overt features. This is suitable for security documents because the inks are invisible under normal viewing conditions but visible once illuminated with light in the infrared region.

An overt security device involving luminophores, that are excited and fluoresce very close to each other, can be added to paper material, the printing ink, mottling fibres or security threads [27]. This way the fluorescence signal cannot be seen as it is overlapped by the much stronger test signal whilst detection is by the decay behaviour of the luminescence emission. A similar technique to this entails a luminescent substance based on a host lattice that is doped with at least one rare earth metal [28]. This technique is said to absorb

in the visible spectra and emit in the near infrared making its application in document security. Again the luminescence substance is exposed to a light source with an emission spectrum largely overlapped by the excitation spectrum of the rare earth metal.

Another ink utilises rare earth metal luminophores, which emit outside the visible spectrum after excitation by either infrared or ultraviolet light [29]. With the incorporation into various matrices, the luminophores can then be included in the printing ink. Testing is done with a device that is opaque to visible light but allows both invisible excitation light and luminescence light to pass through thus blocking visible light interference.

1.2.5 Discussion

From this review of security labelling techniques, it becomes evident that there is still room for new and improved security labels to fulfil the requirements of the self-service and brand protection industries. By employing new methods, the levels of fraud could be reduced by making the forger's task much harder. The limitations of conventional fluorescent labels and detection methods in discriminating between specific fluorescence signals from non-specific background signals, particularly in complex biological mixtures are well known. This factor is the major limit to the sensitivity of most assays of biological material.

There is therefore a need for a taggant system which has specific characteristics such as the biochemical taggants yet can utilise fast, cost effective detection techniques such as those of the conventional fluorescent inks. A combination of the two characteristics would allow fast on line detection and allow combined taggants for encoding information for recognition. Such a marker would be very difficult to identify and reproduce. Even if it could be reproduced, a family of such markers could be used to produce near infinite combinations of coded markers that would add further security to a system.

The requirements for a novel security label are therefore; narrow spectral emission bands thereby producing a large number of possible permutations, a simple detection system that is suitable for automation and for the security label to be resistant to environmental degradation to increase the shelf life of the label.

Rare earth ions would therefore appear suitable based on their discrete sharp spectra that would enable multi-RE doping, of a suitable host material, to produce different codes. The selection of excitation and emission wavelengths in the visible region of the spectrum would also be possible with suitable REs. This would increase the selectivity of the security label as it would require matched excitation sources and emission filters to produce the signal and would reduce any background signals as the majority of dyes are only excited in the UV region. Furthermore, their inherent long fluorescence lifetimes could be utilised to further distinguish them from background molecular fluorescence. A decay time in ms would provide a suitable length of time to be distinguished from any background molecular fluorescence and to be longer than the response time of the detector system.

Suitable host materials could include glass or polymers to protect the RE ions from environmental degradation. The chosen host would be required to have low manufacturing costs and would enable the fluorescence transitions to occur in the REs in comparison to their solution spectra. A simple detection system based on readily available components and optics would also reduce its cost for mass production.

1.3 PROJECT AIM

To overcome all the limitations of the above techniques, the development of a novel covert security label is proposed. This label will consist of a host matrix doped with RE ions. This will then be embedded into/onto the document and excited and subsequently detected in an online environment and takes advantage of the narrow bandwidth and relatively long fluorescent lifetimes of the REs, to maximise the security information content.

This aim will be achieved through the following milestones:

1. Analysis of different glass compositions to determine their suitability as a possible host matrix
2. Development of methodologies for single rare earth ion doping of glass with selected rare earth ions
3. Optimisation of rare earth doping methodologies
4. Spectral analysis of the rare earth ion doped glasses
5. Rare earth doped glass lifetime studies by a modified laser induced scanning fluorescence microscope (LISFM) system
6. Investigation of multi-ion doped glasses and their spectral characterisation
7. Determination of any deterioration to the doped glass fluorescence and glass structure under various environmental conditions
8. Development of an initial in-situ detection system
9. Testing of the doped glasses for their compatibility with the in-situ detection system
10. Particle size analysis to determine the possibility of bead size production and verification of dopant ions presence in separate beads
11. Incorporation of doped glass beads into or onto a paper document
12. LISFM scans of paper samples with added doped glass beads to verify the detection capabilities and printing methods

This work was part of a larger project with Dr R Prabhu working in collaboration; therefore milestones 5 and 11 were carried out mainly by Dr Prabhu with only some of this work reported here. Milestone 8 replaced this work and was carried out before the arrival of Dr Prabhu who then carried this work further.

1.4 DEVELOPMENT OF GLASS PRODUCTION TECHNIQUES

A large literature search indicated that glass was suitable for doping with RE ions due to the interest in lasers using RE fluorescence. Although polymers could still be used, less literature was found in this area and was therefore not selected for this project. Therefore the suitable host composition that had to be doped with the fluorescent species found glass as being most suitable and was used in this project for two reasons:

- Less susceptible to environmental effects and
- Glass can be produced in a variety of formats to be used in various applications

Glass is defined as an amorphous solid without long range order or periodicity of atomic structures and which exhibits a glass transition temperature (*Tg*) [30]. Oxides have various roles in the formation of glasses depending on their chemistry (see Table 1-1).

Network Formers	**Conditional (intermediate)**	**Network Modifiers**
SiO_2	Al_2O_3	Na_2O
B_2O_3	TiO_2	K_2O
GeO_2	ZrO_2	CaO
P_2O_5	Ga_2O_3	MgO
		PbO
		BaO
		ZnO

Table 1-1. Role of oxides in glass formation

Network formers will form glasses on their own, conditional oxides do not form glasses on their own, but will do when mixed with some network modifiers. Network modifiers never form glasses but do alter the structure and properties of the glasses e.g. decrease melting temperature (*Tm)* or lower the viscosity (η) [30-32].

Pure silica (SiO_2) glass is often the ideal medium. This is because of its very low thermal expansion, high thermal stability and extremely high UV transmission [31]. However, because the Si-O bonds are so strong their *Tm* is 1715 °C [30] and require a furnace temperature of greater than 2000 °C to pour the glass making production expensive and

difficult. In order to make the glass more workable and cheaper to produce; additives are used to lower the *Tm* value. For example, boric oxide (B_2O_3) forms triangular units compared to the tetrahedral units formed by silicate glass and therefore form a much more open structure. With the addition of a suitable quantity of boric oxide to silica, the subsequent *Tm* value can be lowered to 800°C therefore making the glass more workable.

The addition of alkali metal oxides (Na_2O, K_2O or Li_2O) lowers the *Tm* and produces a much more open structure. The alkali metal oxides introduce non-bridging oxygens (NBO) into the glass matrix that are used to maintain the charge balance throughout the glass structure [30]. However, too much can cause glass microspheres to become excessively hydrophilic, whilst too little results in poor melting behaviour.

Alumina (Al_2O_3) contributes strength as well as improving chemical resistance as it enters the network of SiO_4 tetrahedra filling any gaps [31]. Furthermore, it increases the viscosity in lower temperature ranges and suppresses crystallisation [33]. However, if too much is added, the melting property is lowered and the glass becomes unstable.

It is easy to see that different oxides in different amounts will alter the properties of the glass depending upon the user requirements, which adds a further security feature to the proposed label. This is because the exact glass matrix would have to be known in order to replicate the label.

1.4.1 Production Methods

One of the main challenges in this project would be the preparation of glass containing a uniform distribution of RE ions. Various methods can be employed to achieve this and each one has its own advantages and disadvantages. The various techniques for preparing doped glass that may be used here are:

For glass production from raw materials or constituent oxides:

- Melting and quenching
- Sol-gel

For doping glass already produced:

- Diffusion
- Ion exchange

Due to RE ions having a high co-ordination number, it is difficult to incorporate a uniform distribution of ions without clustering [34]. This occurs when the RE's have to share the limited number of NBO atoms in the glass matrix. These clusters are formed through RE-O-RE bonding and facilitate energy migration among the RE and fluorescence quenching from cross relaxation. However, it has been found that by co-doping with aluminium (from Al_2O_3), the RE clustering becomes dispersed and thus reduces the energy migration. This is because Al^{3+} has a lower coordination number, in comparison to RE, and this increases the probability of Al-O-RE bonds forming.

1.4.1.a Melting and quenching

This method was the traditional laboratory method to produce glass until the middle of the 1980s. The glass is prepared by melting the powdered starting materials (based on glass composition) in a suitable crucible between 950 and 1500 °C depending upon the glass composition [33, 35-50]. The melt is then kept at this temperature for approximately 2 hours to homogenise before it is poured into a stainless steel cast and annealed before cooling to room temperature. Rare earth ions are normally added into this type of glass as an aqueous nitrate solution, or as a powdered salt, before the mixture is fired [46].

1.4.1.b Sol-gel

Due to the high melting temperature of SiO_2, it is quite difficult to make silica glasses doped with RE ions using the traditional technique as described above [51]. The literature survey indicates that the sol-gel method has passed the melting and quenching technique as the main way of producing RE doped glasses [34, 51-62].

The sol-gel method is a low temperature solution (therefore high purity) method based on the inorganic polymerisation of hydrolysed metal alkoxides. The dopant RE ions can be incorporated into the initial solution in various forms including:

- Inorganic salts
- Metal alkoxides
- Encapsulated metal complexes

A porous gel is formed because the hydrolysis and condensation reactions, which drive the polymerisation, continue. This gel is then dried and densified to form a glass. It has been noted [34] that conventional silica glasses cooled from a melt have a maximum RE dopant concentration of about 0.5 wt% (equivalent to approximately 0.1 mol%). Any higher concentration was noted to result in phase separation during cooling. However, by utilising the sol-gel technique, silica glass can be produced containing a RE concentration of up to 10 wt% (equivalent to approximately 2 mol%) and has a more uniform distribution [54, 63]. Unfortunately, the sol-gel process does have the disadvantage of the time required to make the glass equalling over two weeks in comparison to only a few hours with the melting and quenching technique. Furthermore, it was found that the fluorescence value increased with increased gadolinium dopant concentration up to 3 mol% in oxyfluoroborate glass whereas any higher dopant concentration resulted in concentration quenching [47]. These findings indicated the optimum dopant concentrations were dependent on the particular dopant, the host matrix and the method of production.

1.4.1.c Diffusion

In the diffusion method ions are allowed to move into the glass structure or onto its surface by movement alone. This process is normally used to try and improve at least one property of the glass such as its surface strength [64]. To achieve this, the glass is immersed in a solution of the required ions for a fixed period of time. A solution that contains an acidifying substance [65], such as $K_2Cr_2O_7$, weakens the diffusion barrier at the interface between the material and the medium and improves the diffusion process. This process has very specific applications with the ions that can diffuse into or onto the glass and may only be appropriate where surface exchange is sufficient. Since this project requires a bulk glass with a homogeneous distribution of dopant ions, this procedure would not be suitable.

1.4.1.d Ion-exchange

The ion-exchange method involves alkali/alkaline ion exchange, especially M^+ or M^{2+}. Similar to the diffusion process, this method is used to improve certain properties of the glass such as its strength [66, 67]. The majority of literature on this subject involves the exchange between Na^+ and Ag^+ [68, 69]. The experimental procedure involves the exposure of commercial soda-lime glass to nitrate melts ($AgNO_3/NaNO_3$) for about 310

hours at 330 °C. This temperature is well below the glass transition temperature of the glass (*Tg* = 535 °C), however, by increasing the temperature of the reaction the rate of exchange can be increased as long as the temperature remains below the *Tg* to prevent devitrification.

1.5 FLUORESCENCE

Fluorescence spectroscopy was the most widely used analytical technique employed throughout this project. The high level of sensitivity and large linear concentration range of fluorescence methods made this type of analysis ideal for this project. In comparison to absorption spectroscopy, fluorescence spectroscopy can be two to three orders of magnitude better [70].

The process of luminescence occurs when the radiation of light from a body is produced by means other than heat. This process is subdivided into fluorescence and phosphorescence. If a short time elapses between the excitation process (absorption of radiation) and the emission (luminescence), of the order 10^{-7}-10^{-9} seconds, so that the process occurs almost simultaneously, the phenomenon is called fluorescence. If the process takes longer, then it is called phosphorescence.

To produce fluorescence, the species must absorb a certain amount of energy [71]. Quantum theory has shown that the radiation causing luminescence has a higher frequency than the luminescence it produces, called Stokes shift. This is why it is possible to excite a species with UV light and produce a fluorescence spectrum in the visible region.

There are three factors that reduce or quench the lifetime of an active ion in its excited state in a glass:

- Self quenching between two neighbouring ions, often referred to as concentration quenching.
- Transfer of excited state energy to vibrational modes in the glass network called nonradiative multiphonon relaxation.
- Transfer of excited state energy to impurities including transition metal ions and residual (OH^-) groups, present in glass.

A Perkin Elmer LS 50B Luminescence Spectrometer and a purpose built LISFM was used to determine the fluorescence spectroscopy of the samples and to scan an area to produce a fluorescence map of the samples respectively. The LISFM could be adapted to allow the fluorescence lifetimes to be determined, which was a critical part of the project.

1.6 LANTHANIDES

The lanthanide series consists of the elements from lanthanum to lutetium inclusively. As their properties are extremely similar to each other, they were originally thought to be a single element until 1907 [72]. Furthermore, they used to be called the rare earths (REs), but this name is no longer appropriate because most of the elements are not particularly rare. With the exception of promethium, which has only radioactive isotopes, the rarest lanthanides (lutetium and thulium) are still more abundant than the elements bismuth, mercury and silver [73]. However, the term rare earth is still used in the literature today and will be referred to here interchangeably with lanthanide.

In 1930, optical glasses contained lanthanide ions, especially lanthanum [31]. These expanded the range of optical glasses into the area of high refractive index and high Abbé values and were decisive in further eliminating image defects in lens systems. In the 1960s, much work was involved in demonstrating which ions lased in glass and how their spectroscopic properties could be altered by changing the host composition [74]. According to Weber in 1990 [75] all glass lasers to this date had used trivalent REs as the active ion including the ions Pr^{3+}, Nd^{3+}, Pm^{3+}, Er^{3+} and Tb^{3+}.

However, possibly the greatest and well known impact on daily life by REs was due to the red emission band of europium used to produce the red colour in televisions [73]. Other applications of REs are their use in; alloys for cigarette lighter flints, steel making, permanent magnets, fluorescence concentrators to collect solar energy to feed photovoltaic cells [73], sensors [76], radiation resistant glasses and catalytic converters [77] to name a few.

In this project, RE ions are used to produce fluorescence in the visible spectrum by a range of excitations. The fluorescence properties of the REs are due to their unfilled 4f electron shell, which are screened from the crystal field by the outer 5s and 5p electrons [78]. From this electronic state, RE containing solids have isolated "free" ions that are only weakly influenced by the environment. It is from the f-f electron transitions between the Stark levels of the $4f^n$ configurations that extremely sharp and clear peaks are produced in the optical spectra. This process involves purely electronic transitions and weaker transitions due to lattice vibrations. These properties result in very narrow, well-defined emission bands that can be easily detected and identified. This is unlike most of the fluorophores present in the environment, as they usually exhibit molecular fluorescence with resultant broad band spectrum that makes them unsuitable for producing an encoding pattern/combination (see Figure 1-2).

CHAPTER 2 - THEORY

2.1 ULTRA-VIOLET/VISIBLE ABSORPTION THEORY

When an atom or molecule encounters UV or visible radiation, an interaction may occur between the radiation and the electrons of the atom or molecule [79]. This process is very specific and results in one of the outer or bonding electrons being promoted from a 'ground state' energy level into one of higher energy. These levels are separated by a discrete energy increment determined by the nature of the atom or molecule with only a quantum of radiation being absorbed. A quantum is related to frequency and wavelength of radiation by:

$$E = h\nu = hc/\lambda$$

h = Planck's constant (6.63×10^{-34} Js)
c = velocity of light (2.998×10^{8} ms^{-1})
λ = m

Since even the simplest molecules have a large number of energy levels, their absorption spectra can be quite complex. Furthermore, each electronic energy level has a group of closely spaced vibrational levels associated with it due to small increments in the energy of the molecule caused by the relative motion of its constituent atoms. However, these vibrational bands tend to overlap such that most spectrometers are unable to resolve them and subsequently produce a broad bell-shaped peak.

The most important formula for absorption is the Beer-Lambert Law which tells us quantitatively how the amount of attenuation (decrease in intensity) of the incident light depends on the concentration of the absorbing molecules and the pathlength over which the absorption occurs [70]:

$$A = \varepsilon lc = \log {I_0}/{I}$$

A = absorbance

ε = molar absorptivity at a specific wavelength

l = pathlength of the sample cell in cm

c = molar concentration.

I_o = incident radiant power

I = transmitted beam power

Absorption is also related to transmittance (T) in a logarithmic manner, where transmittance is the fraction of incident radiation transmitted by the solution expressed as:

$$T = {I}/{I_0}$$

Furthermore, as absorption is comparing the difference between the incident radiation to the transmitted radiation, the source power does not have to be very intense. This is in comparison to fluorescence instruments where the intensity of the light source can enhance the fluorescence signal and improve the sensitivity of the instrument as fluorescence is measured from a zero background as the excitation and emission wavelengths are different.

2.1.1 Absorption Instrumentation

For absorption in the UV/visible region, the instrumentation is generally made up of five components shown in Figure 2-1 [70]. This consists of a stable source of radiant energy in the UV/visible region (1); a wavelength selector that can isolate a region of the spectrum suitable for the measurement of the sample (2); a sample container for one or more samples (3); a radiation detector that can convert the radiation signal to a measurable electrical signal (4); and a signal processor and a computer that can process the data into a useable format, in this case an absorption spectrum that can then be determined (5).

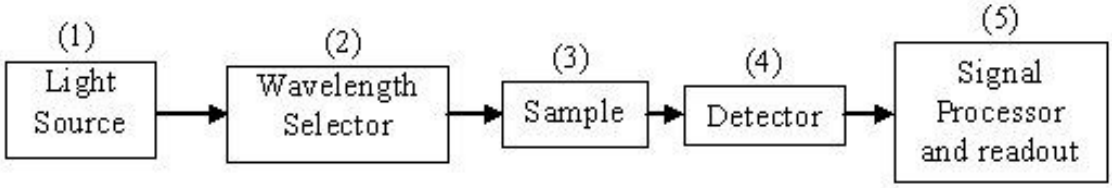

Figure 2-1. Components of a UV/Vis spectrometer

2.2 FLUORESCENCE THEORY

Fluorescence is the photoluminescence process of atoms or molecules being excited by the absorption of electromagnetic radiation before the excited species relax back to the ground state giving off their excess energy as photons [70]. This emission of radiation is of longer wavelength (lower energy) than the excitation radiation due to loss of energy by non-radiative transitions covered below.

The main advantages of molecular fluorescence are its inherent sensitivity of three orders of magnitude higher than absorption spectroscopy and the large linear concentration range of fluorescence methods is significantly greater than that of absorption spectroscopy. This is because it is inherently easier to measure a small signal (fluorescence intensity) in comparison to measuring the difference between two large signals (I and I_o) in absorption spectrometry. Furthermore, the fluorescence intensity can be increased by increasing the incident radiation I_o (under certain conditions) therefore increasing sensitivity, whereas this has no effect on absorption as I is simultaneously increased proportionally therefore there is no increase in sensitivity. However, fluorescence methods are much less widely applicable than absorption because of the relatively limited number of chemical systems that show appreciable fluorescence.

2.2.1 Principles of Molecular Fluorescence

A sample is first excited at the absorption wavelength, also called the excitation wavelength, and subsequently the emission at a longer wavelength, called the fluorescence wavelength, is measured. Usually the fluorescence is measured at right angles to the incident beam to avoid interference from the incident radiation. Short lived emissions are called fluorescence whereas much longer lasting luminescence is called phosphorescence. Florescence generally occurs in 10^{-5} seconds or less whereas phosphorescence can last for several minutes or even hours.

2.2.2 Relaxation Processes

After the molecule has been excited to a higher energy level, several processes can occur that cause the molecule to lose the excess energy. The most important of these mechanisms are non-radiative relaxation and fluorescence emission.

The non-radiative relaxation methods are;

- Vibrational relaxation which occurs during collisions between excited molecules and molecules of the solvent.
- Internal conversion which is the process of non-radiative relaxation between the lower vibrational levels of an excited electronic state and the higher vibrational levels of another electronic state.

The net result of these processes is a tiny increase in the temperature of the medium.

Almost all fluorescence transitions are from the lowest-lying excited electronic state to the ground state. Fluorescence usually occurs only from the lowest vibrational level of E_1 (see Figure 2-2) to various vibrational levels of E_0 because internal conversion and vibrational relaxation processes are very rapid in comparison to fluorescence. Hence a fluorescence spectrum usually consists of only one band with many closely spaced lines representing transitions from the lowest vibrational level of the excited state to the many different vibrational levels of the ground state. Fluorescence is usually of lower energy than that of excitation due to loss of energy from non-radiative relaxation processes, and is called Stokes shift.

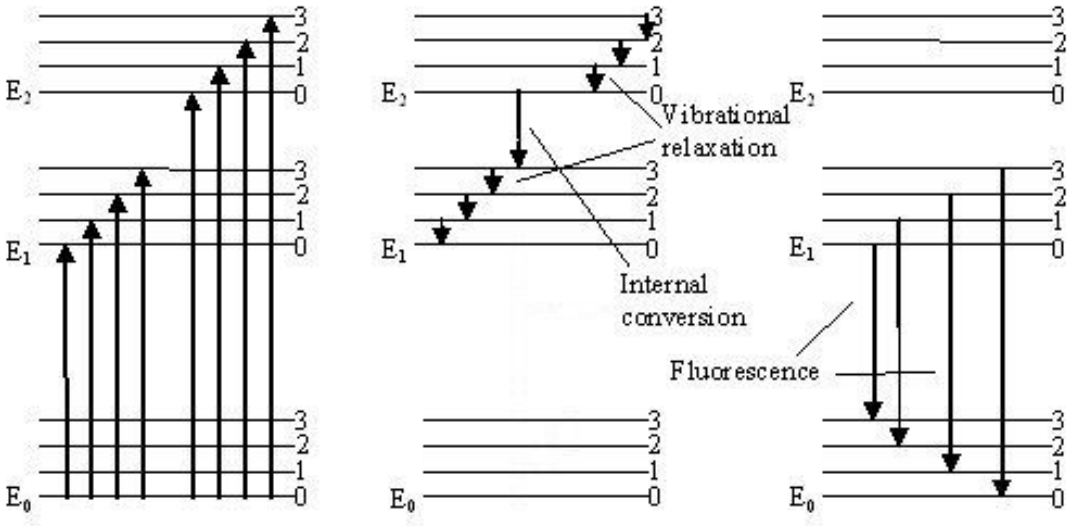

Figure 2-2. Energy level diagram showing the process of radiative and non-radiative emissions

Figure 2-1 shows the process of fluorescence in three different stages. The first is the excitation of electrons from the ground state (E_o) to various vibrational energy levels of E_1 and E_2. The second stage shows the mechanism of non-radiative processes including vibrational relaxation and internal conversion. The final stage depicts fluorescence from the higher energy levels back down to the ground state.

2.2.3 Principles of Atomic Fluorescence

The basis of the fluorescence involved in this thesis was atomic since the lanthanides were doped into the glass in the form X^{3+} (where X is the lanthanide), and the resulting fluorescence was based on the lanthanide energy level transitions. The main observed difference between molecular and atomic spectroscopy is the width of the peaks. In molecular spectroscopy, broad peaks are produced due to the large number of vibrational and rotational states of the excited molecule [70]. However, in atomic spectroscopy, well defined narrow lines are caused only by the electronic transitions of the outermost electrons [80].

For any electronic transition to occur, there are certain selection rules that need to be obeyed as follows [81]:

Spin selection rule: $\Delta S=0$ (changes in multiplicity are forbidden)

Laporte selection rule: There must be a change in parity

allowed transitions: g↔u (g=even and u=odd)

forbidden transitions: g↔g u↔u

This leads to the selection rule: $\Delta l=\pm 1$ (where l is the orbital quantum number and determines the shape of the atomic orbital)

allowed transitions are: s→p, p→d, d→f

forbidden transitions are: s→s, p→p, d→d, f→f, s→d, p→f etc

Therefore the transitions of the lanthanides that occur between the f→f energy levels are strictly forbidden. This leads to the problem of why these transitions are then still exhibited.

These transitions are allowed due to spin-orbit coupling, which is more significant than crystal-field splitting [81, 82]. Crystal-field splitting is due to the arrangement and type of ligands surrounding the ion having differing strengths of effect on the different atomic orbitals of the ion. If the effect was spherical, then all the energies of the electrons would be affected by the same amount and are raised uniformly, although this is not generally the case. If the effect was octahedral, then this causes the energy of electrons in the 4f level that point directly at the ligand to be raised whilst lowering those electrons that point between the ligands with respect to the spherical field. Spin orbit coupling is also called Russell-Saunders or LS coupling and involves the interaction, when several electrons are

present in a subshell, between the total orbital angular quantum number L (due to the overall effect of individual orbital angular momenta, l) and the spin quantum number S (due to the overall effect of individual spins, m_s) [72]. This effect splits the terms into a number of levels (J) with J=L+S, L+S-1, ...|L-S|. The multiplicity of J levels is equal to 2S+1 and follows the rules:

- For less than half-filled shells, smallest J lies lowest
- For more than half-filled shells, largest J lies lowest.

Therefore the full level term symbol is written as $^{2S+1}L_J$.

Since the f orbital of the lanthanides are well shielded by the surrounding 5s and 5p electrons, the various states from the f^n configurations are only split by approximately 100 cm^{-1} by external fields (caused by ligand vibrations) [72, 83]. Therefore, the f→f electronic transitions from one J state to another J state of the same configuration results in very sharp absorption bands similar to the free atom and have weak intensities due to the low probability of the f→f transitions.

As l=3 for an f electron, m_l can be 3, 2, 1, 0, -1, -2 or -3 and can give rise to high values of L for certain lanthanide ions. For example, praseodymium (Pr^{3+}) has two f electrons and the highest values for M_L of 6, 5, 4, 3, 2, 1 and 0. For two electrons the highest S value is +1 (as each electron can be +1/2 or -1/2) making 2S+1=3, and the highest L value with S=1 would be 5. According to Hund's rule, where the term with the highest S value lies lowest in energy and if there are several terms with the same S, the one with the highest L lies lowest, the ground state of Pr^{3+} is $^3H_4$. Furthermore, the terms S, P, D, F, G and I are also possible (relating to M_L values of 0, 1, 2, 3, 4 and 6 respectively) and each having many different values of J. Even taking into account the selection rules mentioned above, the number of possible transitions is large, and therefore, the number of rare earth absorptions can be large. Furthermore, some lanthanide M^{3+} ions with greater or equal to three f electrons have one or more transitions that show an increase in intensity when H_2O is replaced by other ligands [83]. This is because the hydroxyl groups have a strong absorption band, which when nearby the RE ion, allows a non-radiative decay mechanism that causes fluorescence quenching [34]. This feature will be investigated by comparing the spectra of the lanthanide doped glass samples with those from their solution.

2.2.4 Concentration and Fluorescence Intensity

Radiant power of fluorescence (F) is proportional to the radiant power of the excitation beam absorbed (I_0-I) and the fluorescence efficiency (ø) of the fluorescent species (quantum yield) [70]:

$$F = \text{ø}(I_0 - I)$$

I_0 = radiant power of bean incident on the sample

I = power after it traverses a path length l of the medium

ø = fluorescence quantum efficiency = ratio of number of photons fluorescing to the number absorbed

To relate the fluorescence intensity to the concentration requires Beer's law:

$$Log\left(I_0 / I\right) = \varepsilon lc$$

ε = molar absorptivity of the fluorescence species

εlc = Absorbance

By multiplying both sides by -1 and taking the antilog, this can be written as:

$$I / I_0 = 10^{-\varepsilon lc}$$

$$1 - \left(I / I_0\right) = 1 - 10^{-\varepsilon lc}$$

$$\left(I_0 / I_0\right) - \left(I / I_0\right) = 1 - 10^{-\varepsilon lc}$$

$$I_0 - I = I_0(1 - 10^{-\varepsilon lc})$$

Substituting this into $F = \text{ø}(I_0 - I)$:

$$F = \text{ø}\mathrm{I}_0\left(1 - 10^{-\varepsilon lc}\right)$$

And converting the exponential term into a series expansion:

$$F = \text{ø}\mathrm{I}_0\left[2.3\varepsilon lc - \frac{(-2.3\varepsilon lc)^2}{2!} - \frac{(-2.3\varepsilon lc)^3}{3!} - .....\right]$$

The factor 2.3 is the factor when converting base 10 to base e.

If εlc = A < 0.05 then all the terms in the subsequent terms in the square brackets are small in comparison to the first therefore:

$$F = \phi I_0 2.3\varepsilon lc$$

Or $$F = K\varepsilon lc$$

At a constant incident radiant power under the above circumstances, F is directly proportional to the analyte concentration. Thus a plot of fluorescent radiant power versus the concentration of emitting species should be linear at low concentrations. When concentration (c) is such that the absorbance is greater than 0.05, linearity is lost and F begins to reach a plateau. This type of quenching is called 'primary absorption inner filter effect'. At high concentrations fluorescence radiant power can even decrease with increasing concentration.

2.2.5 Fluorescence Instrumentation

Two wavelength selectors are used for the excitation and emission wavelengths. If these are both filters then the instrument is called a fluorometer whereas if they are both monochromators then it is a spectrofluorometer. Additionally it is possible to design a hybrid of an excitation filter and an emission monochromator. Fluorescence instruments can also incorporate a double beam design to compensate for changes in radiant power with time and wavelength.

In fluorescence instruments, the excitation sources are generally more powerful than typical absorption sources. This is because the radiant power is directly proportional to the source intensity, under the above conditions, whereas absorbance is independent of source intensity as it is related to the ratio of radiant powers (covered earlier).

Figure 2-3 depicts a block diagram of a typical fluorometer instrument. This includes an external source of radiation usually a xenon lamp (1); a wavelength selector to select the excitation wavelength and a separate wavelength selector for the emission wavelengths (2); a sample holder (3); a radiation detector usually a photomultiplier tube which can convert radiation to an electrical signal (4); and a computer to display the fluorescence spectrum (5).

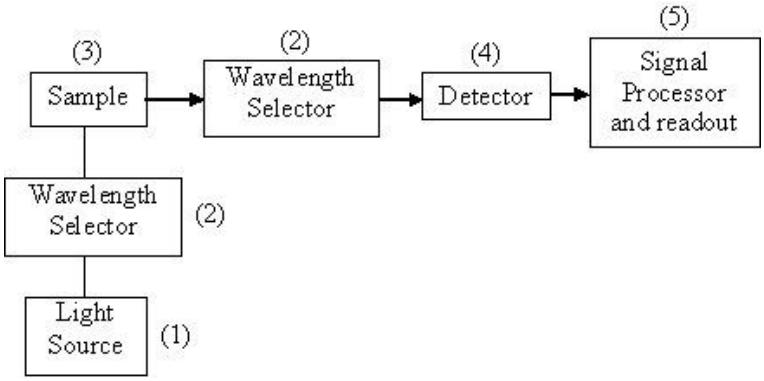

Figure 2-3. Components of a fluorometer

2.3 PARTICLE SIZE ANALYSIS

The ability to determine the size of a particle requires the knowledge of the shape and dispersion processes [84]. This is because only one shape can be described by a single number and that is a sphere. Even a cube can not be described by a single number as the number may refer to an edge or to a diagonal. Unfortunately, the majority of samples investigated for their particle size are not perfectly spherical and so some assumptions are made in order to simplify the procedure. One method is the equivalent sphere theory which measures the weight of the particle and converts this weight into the weight of a sphere:

$$Weight = \left(4/3\right)\pi r^3 . \rho$$

ρ = density

This method produces a unique one number (2r) for the diameter of the equivalent sphere which is the same weight as the sample. However, this can cause some problems when the shape and weight of the sample changes; fortunately we are still able to determine whether the sample was larger or smaller than previous samples.

There can be numerous ways to determine the particle size of a sample. The true way to remain consistent throughout a series of experiments is to compare measurements on a powder using the same technique. However, there are different methods of calculation, based on measuring a different property of the particle, that all produce a correct but different answer with the most important described below.

- D [v,0.5] - Volume median diameter. This figure has 50 % of the distribution above and 50 % below this value. It divides the distribution exactly in half.

- D [4,3] - Volume mean diameter. This is the diameter of the sphere that has the same volume as an ideal sphere. $D\,[4,3] = \sum d^4 \Big/ \sum d^3$

- D [v,0.9], D [v,0.1] - These are 90 % and 10 % cut-offs respectively for the distribution. Where D [v,0.9] has 90 % of the distribution below this value and D [v,0.1] has 10 % of the distribution below this value.

2.3.1 Particle Size Instrumentation

The instrument used for all measurements in this work was the Malvern Mastersizer /E which is based on the principles of laser ensemble light scattering [85]. This instrument falls into the category of a non imaging optical system as it determines the particle size without forming an image of the particle onto the detector (see Figure 2-4). There are two forms of optical configuration possible with this machine:

1) Conventional Fourier optics
2) Reverse Fourier optics

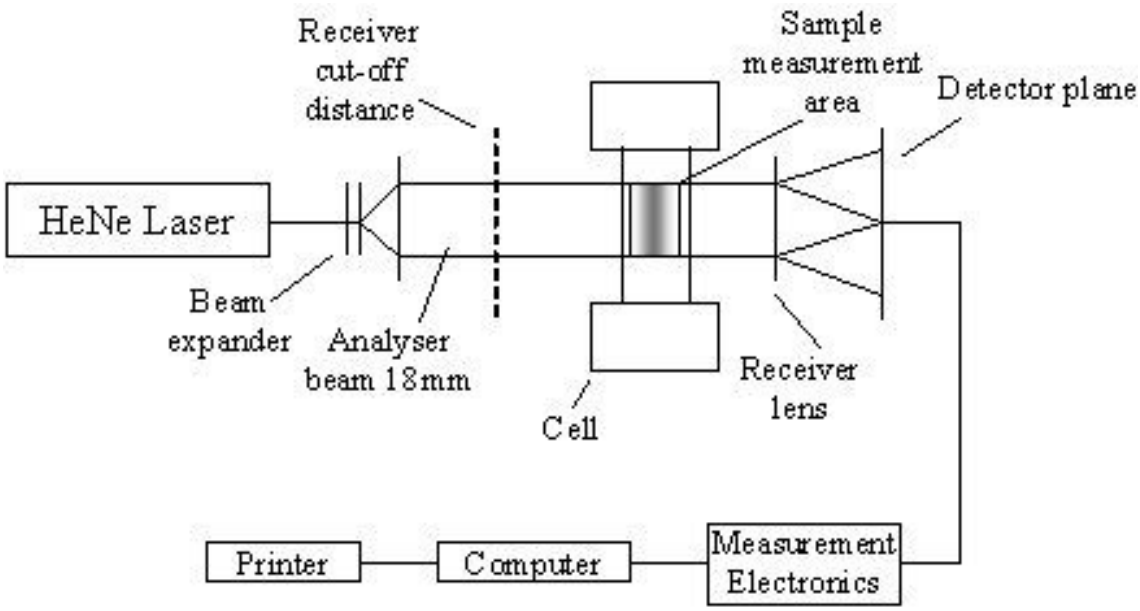

Figure 2-4. Block diagram of laser diffraction experiment

For the conventional Fourier optics method, light (analyser beam) is first collected to typically 18 mm in diameter and any particle present will scatter the laser light. The light scattered by the particles and the unscattered remainder are incident onto a receiver lens (range lens). This operates as a Fourier transform lens forming the far field diffraction pattern of the scattered light at its focal plane. The detector used is a series of 31 concentric annular sections and gathers the scattered light over a range of solid angles of scatter. The unscattered light is focused on the detector and passes through a small aperture in the detector and passes out of the optical system. This process is monitored to allow the determination of the sample volume concentration. The range lens configuration has the useful property that keeps the diffraction pattern stationary and centred on the range lens optical axis wherever the particle is in the analyser beam. Therefore it does not matter if the particle is moving through the analyser beam.

Reverse Fourier optics is used to measure accurately the scattering at higher angles (smaller particles) than feasibly possible by the conventional method. This method was not used here and therefore is not covered.

In practice many particles can be simultaneously present in the analyser beam and the scattered light measures the sum of all the individual patterns overlaid on the central axis. Typically the number of particles needed in the beam simultaneously to obtain an adequate measurement of the scattering would be 100-10,000 dependent on their size. Therefore measurements are not done by one instantaneous measurement but are time averaged as the material is continuously passed through the analyser beam.

When the particles scatter the light, they produce unique light intensity characteristics with an angle of observation. Basically the particles scatter the light resulting in the measured energy on the detector to have a peak at a favoured scattering angle related to its diameter (see Figure 2-5). Large particles have peak energies in small angles of scatter whilst small particles have peak energies in high angles of scatter.

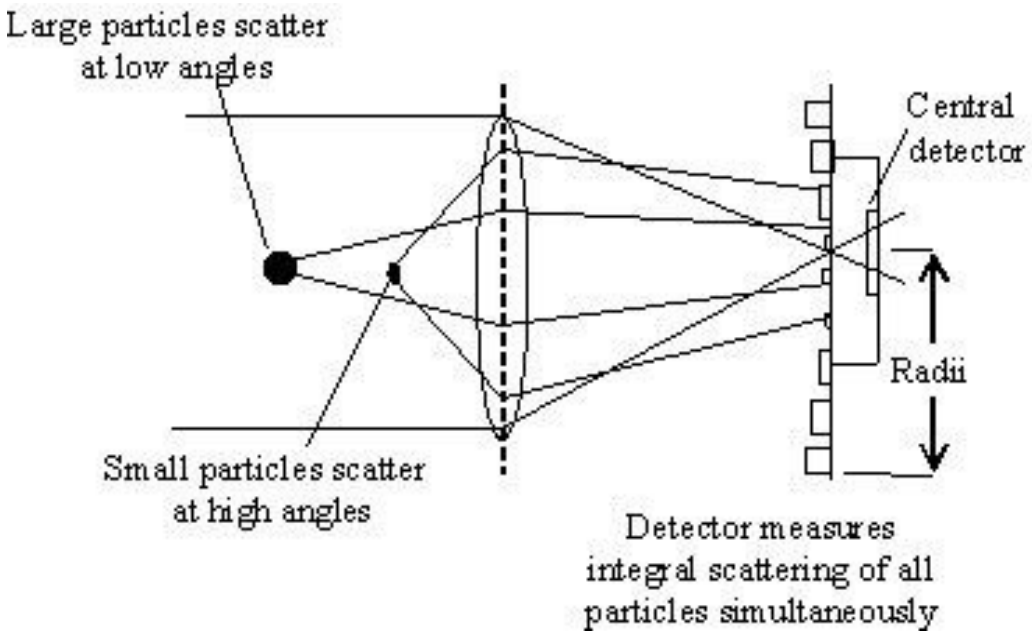

Figure 2-5. Properties of the scattered light

When the sample is over 2 μm in diameter the scattering versus angle is largely independent of the optical properties of the material or the suspension medium and is caused by the diffraction of light around the particle thus any light absorbed by the particles can be ignored. The Mastersizer / E has three standard size ranges and the expected size of the sample particles determines which focal lens is utilised as shown in Table 2-1.

Configuration	Scaling Constant (focus)	Size Range (μm)
Reverse Fourier	45 mm	0.1-80
Fourier	100 mm	0.5-180
Fourier	300 mm	1.2-600

Table 2-1. Standard size ranges for the Malvern Mastersizer/E

2.4 SUMMARY

Based on the capabilities of the above techniques, each technique shall be utilised to characterise the samples. Since the absorption analysis is very quick, this will initially be used to determine the suitability of the dopant REs by the appearance of absorption peaks in the visible region. Furthermore, the determination of a suitable host matrix will require a low absorption signal in the visible region so as not to interfere with the dopant signal. Fluorescence analysis would then be carried out to characterise the emission wavelengths for the dopants and the host in order to determine the optimum wavelengths to use for the detection system and to investigate any affects of multi-RE doping. Particle size analysis will be used to investigate the possibility of producing single micron sized particles of the doped host for use in printing applications.

CHAPTER 3 - MATERIALS AND METHODS

3.1 DEVELOPMENT OF METHODOLOGIES FOR THE PRODUCTION SINGLE RE DOPED GLASSES

The initial experiment was the diffusion of molecular fluorescent dyes onto commercial glass beads. This was used to determine whether or not the dyes would attach to the glass and to act as a standard to use with the Laser Induced Scanning Fluorescent Microscope (LISFM) and the fluorescent microscope. Since the fluorescent dyes (rhodamine B and fluorescein) have known fluorescent properties (Table 3-1), the selection of filters and excitation wavelengths were known. The glass beads used were soda lime beads of 100 μm in diameter and were a free sample from British Optical Limited. On account of their known diameter, the sensitivity of the systems could be monitored for future tests. These beads are normally used in chromatography columns and for sieve calibrations.

Dye	Excitation Wavelength Maximum / nm	Emission Wavelength Maximum / nm
Rhodamine B	550	580
Fluorescein	490	510

Table 3-1. Typical fluorescence values for fluorescent dyes

3.1.1 Method 1 - Diffusion of Molecular Fluorescent Dyes into Commercial Glass Beads

Two 2 g samples of glass were weighed out and placed into volumetric flasks containing an excess solution of each dye. The solution concentrations were 1 mol l^{-1} for rhodamine B and $1x10^{-6}$ mol l^{-1} for fluorescein. The flasks were shaken well and left for 72 hours, after which some of the glass beads were extracted and filtered using 45 μm filter paper and washed with distilled water to remove excess solution. These beads were subsequently placed in an oven for 30 minutes at 100 °C to dry.

The dried beads were first analysed under a fluorescent microscope (Leica DMRB Fluorescence Microscope) that used a mercury lamp as the excitation source and different broad band filters to select different wavelengths. When a selection of the rhodamine B and fluorescein beads were examined at 100x magnification, different fluorescent colours could be seen under the different filters as shown in Figure 3-1.

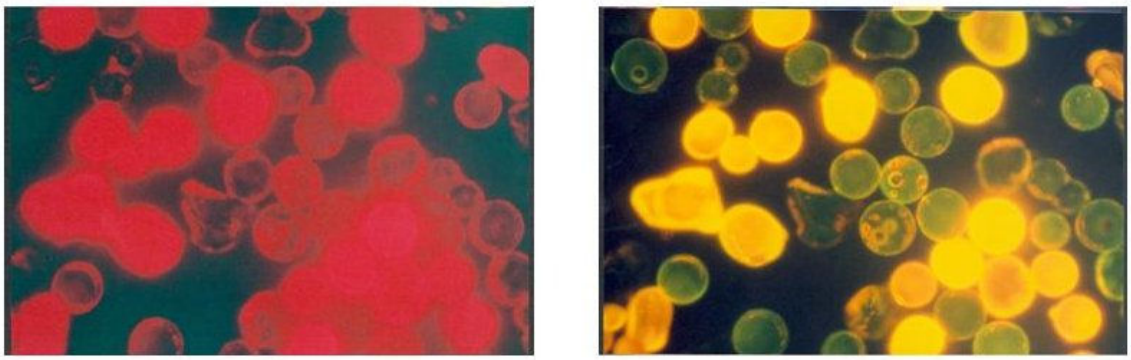

Figure 3-1. Rhodamine and fluorescein coated glass beads fluorescence pictures under various excitation wavelengths: (a) green, (b) blue

The strong red fluorescence shown in Figure 3-1(a) came from the rhodamine coated beads. The characteristic yellow/green fluorescence of fluorescein could only be seen in Figure 3-1(b) as it was cut off by the emission filters in Figure 3-1(a). The faint red glow of the fluorescein coated beads observed in Figure 3-1(a) was reflected red light coming from the rhodamine coated beads. The weaker fluorescence coming from the fluorescein coated beads was due to the use of a less concentrated solution in comparison to the rhodamine solution. Rhodamine beads were selected because of their strong fluorescence and because they can be detected using the same excitation filter as the europium doped glass described later.

Figure 3-2 shows a selection of rhodamine coated beads placed on a glass slide and their fluorescence pictures taken under various excitation filters. All four pictures were taken with 100x magnification.

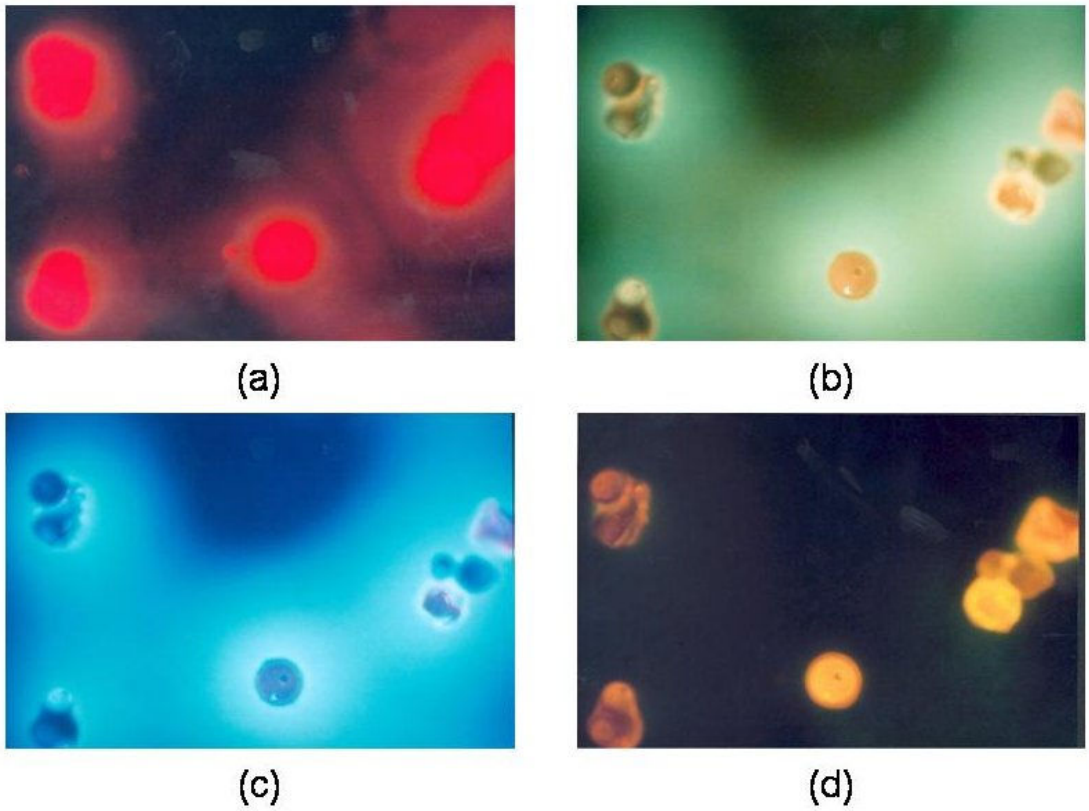

Figure 3-2. Rhodamine coated glass beads fluorescence pictures under various excitation wavelengths: (a) green, (b) violet, (c) UV, (d) blue

Table 3-2 shows the specification for all four filters used with the fluorescence microscope. A band-pass (BP) filter allows light to pass through between the two values and blocks wavelengths above and below that range, whilst a long-pass (LP) filter allows light of greater wavelength than the value stated to pass.

Excitation range	Excitation filter wavelength / nm	Emission filter wavelength / nm
UV	BP 340-380	LP 425
Violet	BP 355-425	LP 470
Blue	BP 450-490	LP 515
Green	BP 530-595	LP 615

Table 3-2. Specification of microscope filters. BP: band-pass, LP: long-pass

This diffusion experiment was used as a quick and simple test to determine whether the dyes would attach to the glass. Although the dye coated beads will not be used in the final product, they could be used as a standard to calibrate any future systems due to the standard size of the beads and the fluorescence signal from the dye.

3.1.2 Method 2 - Preparation of a Blank Borate Glass

The second experiment was to produce a blank glass without any dopant ions. This was achieved by melting sodium tetraborate decahydrate as the base glass composition as it can produce a glass on its own without adding any other oxides and has a relatively low melting point.

3.1.2.a Method

10 g of sodium tetraborate decahydrate was transferred to a porcelain crucible and heated with a bunsen burner to remove the water molecules. Once this had been achieved, the crucible was placed into a muffle furnace at 950 °C and allowed to completely melt. This temperature was greater than the melting point of sodium tetraborate decahydrate (743 °C) to ensure the formation of a homogeneous liquid. After 20 minutes, the crucible was removed and quenched at room temperature.

The melting and quenching technique was used here mainly because of the low melting temperature of sodium tetraborate decahydrate, and to gain experience making and handling glass. This process worked well in that it produced a transparent glass for background fluorescent measurements that did crack after quenching.

3.1.3 Method 3 - Preparation of Rare Earth - Doped Borate Glasses

From the claim [48] that greater than 3 mol% of the RE dopant, would produce a decrease in the fluorescent value from concentration quenching, it was therefore decided to add 3 mol% of europium to sodium tetraborate decahydrate and measure the fluorescence produced. Table 3-3 shows the weights of the base glass and the RE dopant used.

	Weight of $Na_2B_4O_7.10H_2O$	**Weight of $EuCl_3.6H_20$**
Blank	10g	0g
3 mol% Eu	10g	0.2881g

Table 3-3. Weights used to produce doped glass containing 3 mol% of RE dopant

3.1.3.a Method

The weighed powder was mixed together in a glass mortar and pestle using acetone to create a slurry and produce a homogeneous mixture. The acetone was subsequently removed by placing the sample in a drying oven. This now dry, mixed powder was transferred to a porcelain crucible and heated to remove water before repeating the melting and quenching process as described for the blank glass.

3.1.4 Method 4 - Preparation of Rare Earth - Doped Soda Lime Glasses

Sodium borate glasses are susceptible to moisture attack from the atmosphere. Therefore to improve the chemical properties of the host matrix a soda lime glass was doped with a RE ion. The soda lime glass beads were from British Optical Ltd which had the composition shown in Table 3-4.

Oxide	Weight percent (wt%)
SiO_2	72.5
Na_2O	13.7
CaO	9.8
MgO	3.3
Al_2O_3	0.4
FeO, Fe_2O_3	0.2
K_2O	0.1
B_2O_3	0

Table 3-4. Chemical composition of soda lime glass beads

This glass matrix had a softening point of 740 °C and therefore required a higher temperature in order to form a melt.

3.1.4.a Method

The same procedure as the borate glass was used except 2 g of the soda lime beads were first crushed in a stainless steel ball mill for 10 minutes before adding the resultant crushed powder to the mortar and pestle with the required RE salt. Subsequently the mixed sample was melted in a muffle furnace at 1100 °C and quenched at room temperature.

3.2 OPTIMISATION OF RARE EARTH GLASS DOPING METHODOLOGY

3.2.1 Method 5 - Preparation of Rare Earth – Doped Borosilicate Glass

The resultant soda lime glasses had some problems as the glass produced was blue and not free of bubbles. The blue colour was due to the stainless steel ball mill which caused the contamination of the glass matrix. The air bubbles were due to the temperature of the furnace being too low to completely melt the soda lime glass. However, the blue colour contamination was removed by using an agate ball mill but the new furnace with a higher temperature range could still not produce a bubble free liquid melt. Therefore, to lower the *Tm*, boric oxide (B_2O_3) was added to the soda lime glass.

3.2.1.a Method

The soda lime glass beads were initially crushed in the agate ball mill for 5 minutes to produce powdered glass. 5 g of this crushed powder was added to 2 g of boric oxide and mixed together in the agate ball mill for 3 minutes. This produced a mixed dry powder that was subsequently transferred to a platinum crucible. The crucible was heated up to 550 °C for 30 minutes to allow the boric oxide to melt slowly to reduce the possibility of rising over the crucible walls. The temperature was then increased to 900 °C, 1000 °C and 1100 °C for 1 hour at each stage before pouring the molten mixture out at 1250 °C onto a brass mould and thus reduces the likelihood of cracking. The brass mould was heated on a hot plate to anneal the glass and reduce shock.

This process produced a clear blank glass that was bubble free and allowed various shapes of samples to be made. Doping the glass with the rare earths involved adding the dopants to the mixture of crushed soda lime glass and boric oxide before mixing in the ball mill.

3.3 ANALYTICAL TECHNIQUES

3.3.1 Method A - UV-Vis Absorption

The UV-Visible instrument used was a Perkin Elmer Lambda 2 UV/Vis Spectrophotometer. Each sample was inserted into a quartz cuvette, to minimise the background signal, and scanned from 900 – 190 nm. The data were then saved in a format that could be used in Microsoft Excel where the axis could be altered to achieve the optimum spectrum.

3.3.2 Method B - Fluorescence

A Perkin Elmer LS50B Luminescence Spectrometer was used to determine the fluorescence spectra for each sample. In the initial experiments, the samples were irregular pieces with sharp edges therefore the light from the Spectrometer would be scattered minimising the intensity of the excitation light and subsequently the emission intensity. The samples were therefore placed in a liquid of approximately equal refractive index (RI) to reduce the amount of scatter. Toluene was therefore chosen as its RI is 1.4967 whilst the glass samples were assumed to be approximately 1.5 [86]. This is advantageous due to the hydrophilicity of the borate glass. To maximise the glass sample alignment with the excitation light, glass from a broken pipette was used to pack the lower part of the cuvette and the sample placed on top. Typical settings used to produce a 3D spectrum of the samples are shown in Table 3-5.

Emission Scan Range Parameters					
Start (nm):	320	**End (nm):**	800	**Excitation (nm):**	300
Ex Slit (nm):	7.5	**Em Slit (nm):**	9	**Scan Speed (nm/min):**	1500
3D Scan Range Parameters					
Number of Scans:	400			**Excitation Increment (nm):**	1

Table 3-5. Typical settings for 3D fluorescence spectrum

These settings allowed the full spectrum of the RE doped glass to be acquired with sufficient fluorescence intensity to characterise each sample based on literature results. To reduce the time required for a 3D scan, the settings were optimised for a specific range where the fluorescence was known to occur. For the borosilicate glass samples, the toluene and broken pipette glass were not required as larger samples could be produced.

3.3.3 Method C - Particle Size Analysis

To determine the particle size of the crushed samples, a Malvern Mastersizer/E was used. Water, acetone or a 0.1 % solution of sodium hexametaphosphate (calgon) was used as a dispersion liquid to disperse the sample in the sample cell to allow an averaged value of particle size to be calculated. Once samples were smaller than 45 μm, a drop of surfactant (decon) was required to "wet" the sample i.e. to break up any agglomerates and to stop the sample from sitting on top of the liquid (only added when the dispersant was water or acetone). The 100 mm focusing lens was used to measure the size range of 0.5-180 μm. The quantity of sample added was determined by the software program on the computer attached to the instrument, which gave an indication of the optimum amount as the sample was added to the cell.

3.4 SUMMARY

These methods enabled the absorption and fluorescence spectral characterisation for all the samples produced in this work. By analysing the RE solutions first, suitable dopants can be selected that would then be doped in a glass matrix. An ideal matrix would have to be analysed for its spectral and resistant properties to determine the most suitable host. On completion of this, particle size analysis would produce an indication of the sample size in order to determine what crushing conditions are required to produce single micron samples.

CHAPTER 4 - DEVELOPMENT OF A NOVEL GLASS TRACER

4.1 RARE EARTH AQUEOUS SOLUTIONS

The selection of suitable dopants with at least one sharp fluorescence peak in the visible region involved an extensive literature search. A table of the maximum excitation and emission wavelengths [87] is given (Table 4-1) for eight rare earth ions doped in borate glass that have visible emissions.

RE Ions	Strongest Excitation Peak Wavelength / nm	Strongest Emission Peak Wavelength / nm
Ce^{3+}	250	355
Pr^{3+}	445	595
Sm^{3+}	360	598
Eu^{3+}	395	614
Tb^{3+}	360	545
Dy^{3+}	360	575
Er^{3+}	450	570
Tm^{3+}	360	454

Table 4-1. Luminescence properties of RE borate glasses [87]

The RE dopants chosen for initial testing were Eu^{3+}, Tb^{3+}, Pr^{3+}, Er^{3+} and Dy^{3+} because of their visible emission wavelengths. The absorption and fluorescence spectra for each of the RE dopant solutions was determined by analysing each sample following Methods A (3.3.1) and B (3.3.2) respectively.

Each RE was purchased in the form $XCl_3.6H_2O$ (where X is Eu, Tb, Pr, Er or Dy) from Sigma Aldrich with a purity of 99.9%. The concentration of the solutions was 0.3 mol l^{-1} for each dopant to allow comparisons between their absorption and fluorescence spectra.

4.1.1 UV-Vis Absorption

All the absorption analyse were carried out in 0.5 cm cuvettes and background corrected with distilled water as a blank, therefore allowing the absorbance values to be compared with each other. All of the resulting spectra can be found in Appendix A (Figures A-1 to A-4). An example absorption spectrum for the europium solution is shown in Figure 4-1A. These results indicated the sharp characteristic peaks of the RE ions with the strongest peaks confined to the UV region. Furthermore, some weaker peaks were found in the visible range (Figure 4-1B) which suggested europium could be a suitable dopant with regards to the project aims (section 1.3).

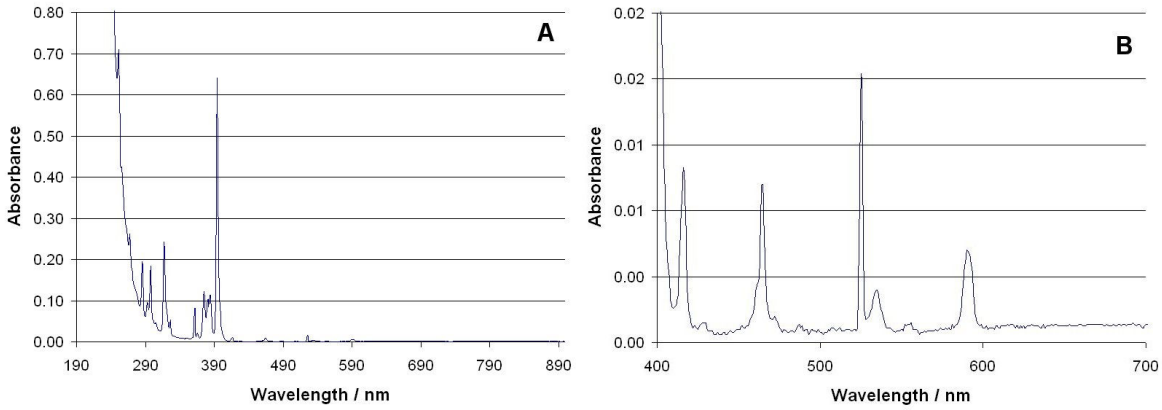

Figure 4-1. UV-Visible absorption spectrum of 0.3 mol l^{-1} $EuCl_3$

A table of the wavelengths of the six most intense peaks and their respective absorbance for each RE are given in Table 4-2 for all the solutions tested, except for praseodymium where only four peaks were found.

0.3 mol l^{-1} $EuCl_3$		0.3 mol l^{-1} $TbCl_3$		0.3 mol l^{-1} $PrCl_3$	
Absorption Wavlength / nm	Absorbance (Arb. Units)	Absorption Wavlength / nm	Absorbance (Arb. Units)	Absorption Wavlength / nm	Absorbance (Arb. Units)
251	0.7062	265	0.3587	444	1.8405
394	0.6403	284	0.1363	468	1.3296
267	0.2621	369	0.1192	482	0.9927
317	0.2399	351	0.1132	590	0.6273
285	0.1950	377	0.0832		
298	0.1836	318	0.0676		

0.3 mol l^{-1} $ErCl_3$		0.3 mol l^{-1} $DyCl_3$	
Absorption Wavlength / nm	Absorbance (Arb. Units)	Absorption Wavlength / nm	Absorbance (Arb. Units)
255	1.0358	350	0.8022
379	0.8392	365	0.6240
523	0.5203	325	0.5442
364	0.4282	387	0.2945
487	0.3843	295	0.1686
653	0.3639	256	0.1612

Table 4-2. Selection of the strongest intensity absorption peaks and their relative wavelengths for the RE solutions

Results show that all the strongest absorptions are in the UV range for Eu, Tb and Dy although Pr and Er had peaks in the visible range. Any peaks in the visible range were generally weak in comparison with the UV as the visible transitions are more forbidden in a solution. However, some of these transitions will become allowed once doped in a glass host due to the greater effect of the surroundings on the dopant ions and will be looked at later. The strongest absorption intensities were observed for Pr and Er, with Tb the weakest.

4.1.2 Fluorescence

Leading on from the absorption results, the same approach for the fluorescence analysis was carried out. The europium solution fluorescence spectra are shown in Figure 4-2 and Figure 4-3 as an example, and a table of the highest intensity wavelengths for all the samples given in Table 4-3. The remaining spectra can be found in Appendix A (Figures A-5 to A-12).

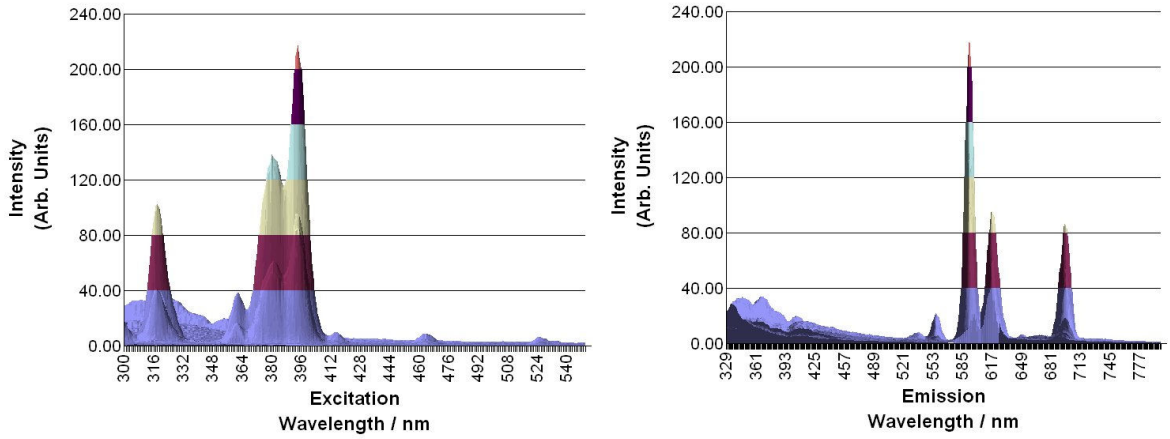

Figure 4-2. Fluorescence spectrum of the 0.3 mol l^{-1} $EuCl_3$ solution

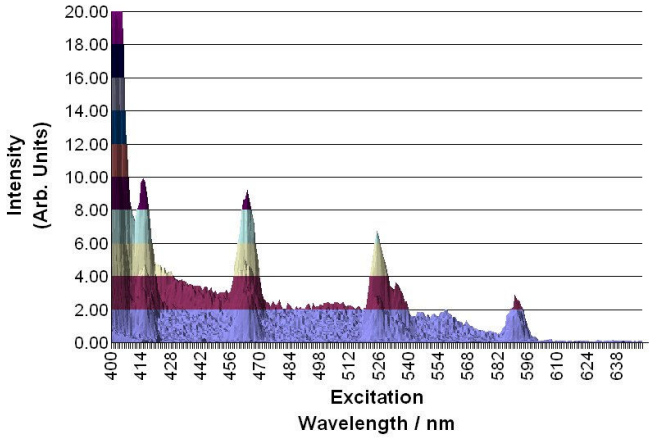

Figure 4-3. Emission spectrum for the visible range excitation of the 0.3 mol l^{-1} $EuCl_3$

0.3 mol l^{-1} $EuCl_3$			0.3 mol l^{-1} $TbCl_3$		
Excitation Wavlength / nm	Emission Wavlength / nm	Intensity (Arb. Units)	Excitation Wavlength / nm	Emission Wavlength / nm	Intensity (Arb. Units)
394	592.5	218.89	352	545.0	324.97
380	592.5	138.77	371	545.0	313.52
318	592.5	103.07	352	488.5	183.95
394	616.5	95.71	371	488.5	177.58
394	696.5	85.97	352	587.0	91.33
381	618.0	62.39	370	587.0	90.51
0.3 mol l^{-1} $PrCl_3$			0.3 mol l^{-1} $ErCl_3$		
Excitation Wavlength / nm	Emission Wavlength / nm	Intensity (Arb. Units)	Excitation Wavlength / nm	Emission Wavlength / nm	Intensity (Arb. Units)
300	355.0	81.75	322	348.0	348.05
			322	368.0	245.58
			322	389.0	204.86

0.3 mol l^{-1} $DyCl_3$		
Excitation Wavlength / nm	Emission Wavlength / nm	Intensity (Arb. Units)
387	479.0	121.81
350	479.0	119.81
363	479.0	101.57
387	574.5	93.86
350	574.5	90.29
364	574.5	77.68

Table 4-3. Selection of the strongest intensity fluorescence peaks and their relative wavelengths for the RE solutions

The europium results indicated the strength of the peaks in the UV range in comparison with the visible as was evident in the absorption spectra. However, the appearance of discrete, sharp peaks in the visible range was encouraging and made europium appear to be a suitable dopant.

For the other dopants, only Tb and Dy appeared promising whilst Er and Pr did not produce any discrete peaks near the visible region. Although a low intensity, Tb had a discrete peak in the visible region (487 nm excitation and 545 nm emission) indicating Tb as a possible dopant for the security label. In addition, dysprosium was promising as it produced numerous peaks in the UV and visible regions.

4.1.3 Rare Earth Solution Conclusion

Analysis of the solution absorption and fluorescence results identified europium, terbium and dysprosium as suitable dopants for the security label whereas praseodymium and erbium only appear to have very weak fluorescence or no visible fluorescence when in solution. It is known that changing the environment of the ion can change its fluorescence spectrum of the rare earths and this would have to be investigated to determine the degree of change possible [74, 88]. The suitable dopants would then be doped into the glass matrix and their absorption and fluorescence spectra repeated to compare results with their solution.

4.2 DETERMINATION OF A SUITABLE GLASS MATRIX

To incorporate the dopants into a glass various techniques could be used including the melting and quenching technique and the sol-gel technique. However, the sol-gel technique is specialised and can take one month to produce a single glass sample. Since the melting and quenching technique can be achieved in one day, this method was selected to produce the glass samples.

Various matrices of glass have been produced and tested for their suitability as the host for the lanthanide ions. Specific properties required of a potential host included:

- None or little amount of overlapping spectral properties (must not fluoresce in region of interest)
- Must be optically transparent
- Low melting temperature for cheaper manufacture
- Resistant to environmental effects

These criteria were very important in order to reduce any background fluorescence signal being generated from the glass and to make it possible to make the glass using the equipment available. For initial experiments, europium was used for determining whether the glass host would be suitable. This was because europium has been researched most intensively of all the REs, allowing literature data to be used for comparison.

Literature results indicated that the maximum concentration certain rare earths could be incorporated into a glass was 3 mol% [47]. In order to maximise the fluorescence intensity, 3 mol% was chosen as the dopant concentration. It was known that the absorption and emission spectra of the rare earth dopants in glasses would be inhomogeneously broadened because of the contribution of ions in different sites throughout the glass matrix [89]. Therefore, as a guide to the expected wavelengths due to the europium dopant, a table of emissions from Erostyak et al [90] is given in Table 4-4.

Transition	Emission Wavelength / nm
$^5D_1$-$^7F_1$	538
$^5D_0$-$^7F_0$	580
$^5D_0$-$^7F_1$	592
$^5D_0$-$^7F_2$	615
^5D_O-$^7F_3$	652
$^5D_0$-$^7F_4$	703

Table 4-4. Emission wavelengths and their transitions for europium in Eu/TTA/Phen/TX-100 system [90]

4.2.1 Borate Glass

Sodium tetraborate decahydrate ($Na_2B_4O_7.10H_2O$) was used as the base glass as this could be melted and form a glass upon quenching. The melting and quenching technique was used here because of the low temperatures of $Na_2B_4O_7$ (Tm 743 ^oC), and to gain experience in making and handling glass.

Unfortunately, borate glasses are not commercially important because they are water-soluble [30]. This was shown when, after some time, the transparent glass became opaque. Subsequently the glass had to be stored in a desiccator or drying oven to reduce any moisture from the air affecting the glass.

The borate glass was made following Method 2 (section 3.1.2). This process worked well in that it produced a transparent glass for background fluorescent measurements that did crack after quenching. Since this glass was not cast in a mould, only small pieces of glass were removed from the crucible. Subsequently the fluorescence analysis involved adding

toluene and broken pipette glass into the cuvette to raise the small sample to be inline with the excitation light as described in Method B (section 3.3.2).

4.2.1.a Fluorescence

Initial experiments did not have the same settings as those described in section 3.3.2; instead these were produced with the settings in Table 4-5. The optimum settings, for the slit widths described in Method B, were determined as more experiments were carried out and were used for future samples.

Emission Scan Range Parameters					
Start (nm):	320	**End (nm):**	700	**Excitation (nm):**	300
Ex Slit (nm):	2.5	**Em Slit (nm):**	5	**Scan Speed (nm/min):**	1500
3D Scan Range Parameters					
Number of Scans:	50			**Excitation Increment (nm):**	5

Table 4-5. Fluorescence settings for 3D fluorescence spectrums

The fluorescence spectrum of a cuvette with blank borate glass, toluene and the broken pipette glass is shown in Figure 4-4. This spectrum has a very strong (saturated) fluorescence from the toluene in the UV range but no fluorescence peaks due to the blank borate glass. Fortunately only peaks in the visible range are of interest therefore the toluene should not interfere with any of the peaks of interest. The 3 mol% europium doped borate glass fluorescence is shown in Figure 4-5.

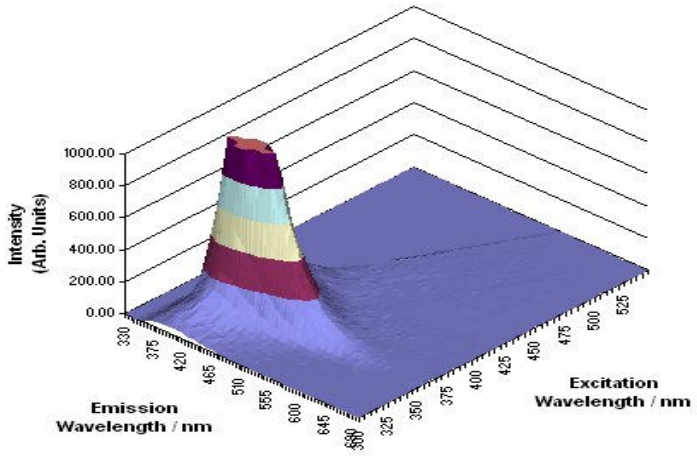

Figure 4-4. Fluorescence spectrum of blank borate glass raised by broken pipette glass and immersed in toluene

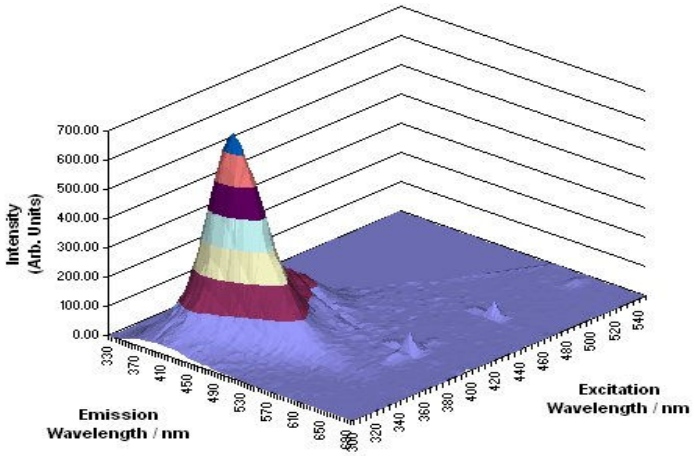

Figure 4-5. Fluorescence spectrum of 3 mol% europium doped borate glass raised by broken pipette glass and immersed in toluene

The spectrum again shows the very strong UV fluorescence of the toluene as well as some small peaks with an emission in the visible range. A closer look at these small peaks is shown in Figure 4-6.

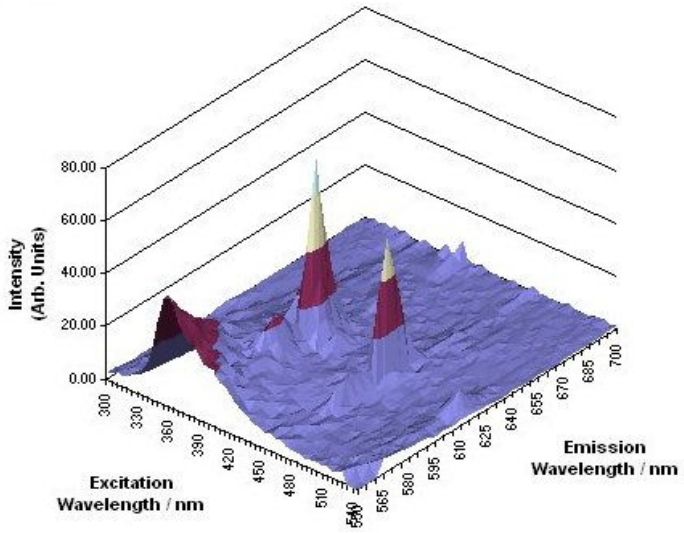

Figure 4-6. Selected fluorescence spectrum of 3 mol% europium doped borate glass

The peaks shown above are tabulated in Table 4-6. These results show the europium fluorescence in the doped borate glass, although due to the small sample size, the fluorescence intensity was small.

Excitation Wavelength / nm	Emission Wavelength / nm	Intensity (Arb. Units)
380	614.0	21.909
395	614.0	76.607
415	614.0	11.360
465	614.0	57.191
535	614.0	9.999
395	593.0	25.213
465	593.0	13.258
395	650.5	5.266
465	650.5	3.310

Table 4-6. Strongest fluorescence peaks in the visible and near UV range

4.2.1.b Borate glass conclusion

Although the europium fluorescence could still be detected in the borate glass, the fluorescence intensity was very weak due to the sample size. However, due to the hydrophilic nature of borate glass, this was not a suitable host matrix.

4.2.2 Soda Lime Glass

After initial experiments with borate glass, another glass matrix was tested to reduce the water solubility effect seen from the borate glass [30]. This time soda lime glass was used. A sample of commercial soda lime glass beads was acquired from British Optical Limited, with the composition shown in Table 4-7.

Oxide	**Weight percent (wt%)**
SiO_2	72.5
Na_2O	13.7
CaO	9.8
MgO	3.3
Al_2O_3	0.4
FeO, Fe_2O_3	0.2
K_2O	0.1
B_2O_3	0

Table 4-7. Chemical composition of soda lime glass beads

These beads had a softening point of 740 ^{o}C and therefore required a much higher temperature to form a melt. Therefore a doped soda lime glass was prepared by following Method 4 (section 3.1.4). Unfortunately the resultant glass contained problems. Firstly the glass could not be poured out of the crucible due to the limitations of the furnace temperature and the glass contained air bubbles because it was not completely melted. Secondly the glass was blue due to contamination with the stainless steel ball mill used to mix the powders together. However, the resultant glass was analysed to determine if the europium dopant could still be detected.

4.2.2.a Fluorescence

To reduce any effects from the blue colour on the fluorescence spectrum, the sample was crushed into a powder and dispersed over the broken pipette glass in the cuvette to try and have some of the sample in the correct region for analysis. Again toluene was added to the cuvette and therefore only the selected region as used in Figure 4-6 is shown in Figure 4-7 to remove the toluene fluorescence.

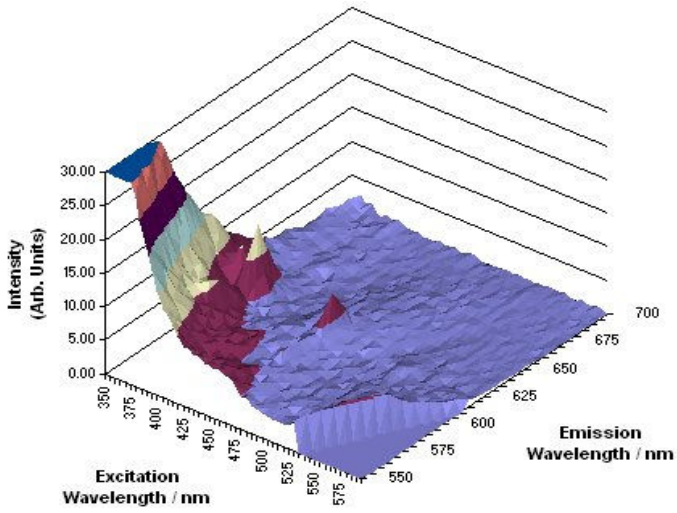

Figure 4-7. Selected fluorescence spectrum of 3 mol% Eu doped soda lime glass

The spectrum still shows the europium fluorescence at the strongest wavelengths of 395 nm and 465 nm excitation and the emission at 613 nm. The remaining peaks as mentioned for the borate glass could still be present but were too weak to be seen on the above spectrum.

4.2.2.b Soda lime glass conclusion

Although the soda lime matrix did not show signs of hydrophilicity as with the borate host, the matrix was not suitable due to its high melting temperature. This caused difficulties in production of samples with the limitations of the available furnace. Therefore a compromise was required to combine the low melting temperature of the borate glass with the greater chemical resistance of the soda lime glass.

4.2.3 Phosphate glass

Another type of glass tested was phosphate glass because of its low melting point temperature and ease of manufacture.

4.2.3.a Method

A base glass of composition Na_2O:P_2O_5 (ratio of 2:3) was produced by mixing molten sodium dihydrogen phosphate with ammonium dihydrogen phosphate. This mixture was then transferred to a crucible and heated over a bunsen burner to drive off the water of crystallisation before transferring the crucible to a furnace at 1000 °C for 20 minutes. The melt was then poured onto a brass mould.

4.2.3.b UV-Vis absorption

The absorption spectrum of the blank phosphate glass is shown in Figure 4-8. This spectrum appeared to be spectrally suitable as there was not much background absorption signal above 300 nm.

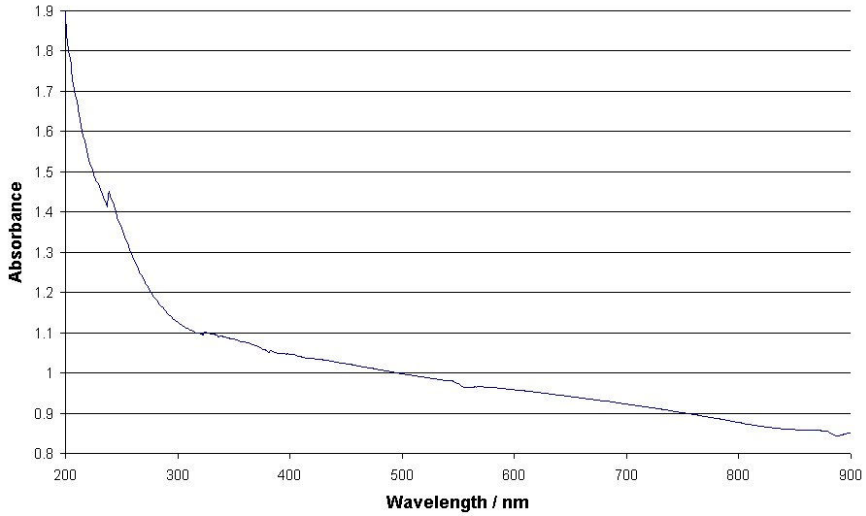

Figure 4-8. UV-Vis absorption spectrum of the blank phosphate glass

4.2.3.c Fluorescence

However, upon scanning the fluorescence spectrum of the blank glass, shown in Figure 4-9, it was found that the phosphate glass had a large fluorescence signal over a broad section of the spectrum. Therefore no further phosphate samples were tested.

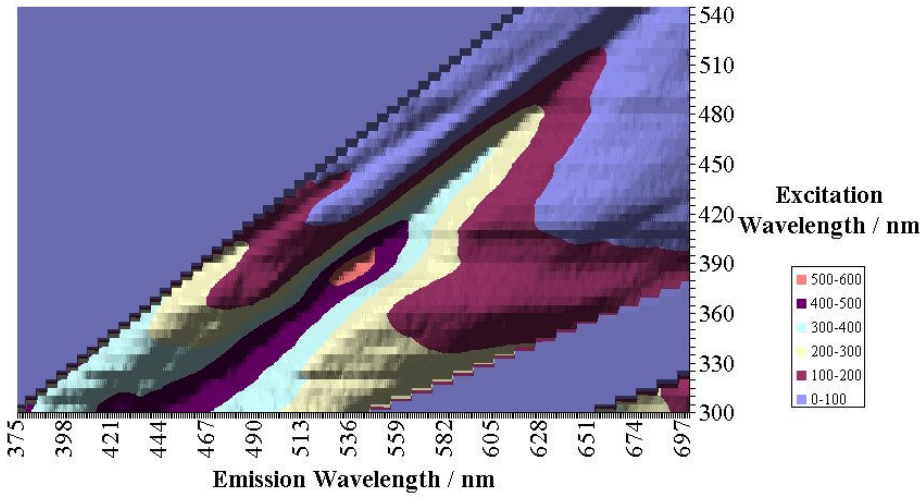

Figure 4-9. 3D spectrum of blank phosphate glass

4.2.3.d Phosphate glass conclusion

Phosphate glass was therefore not ideal as a suitable host because the background signal would be too large. Furthermore, the phosphate glass absorbed water from the atmosphere causing the glass to turn opaque after time. This was a similar problem as the borate glass and therefore there was still a requirement to produce a suitable glass matrix as a host.

4.2.4 Borosilicate glass

To try and produce a glass with a low melting temperature, low background fluorescence spectrum and resistant to environmental conditions, a mixture of the borate and soda lime glass would be required. A study of the relevant phase diagram for the composition Na_2O-B_2O_3-SiO_2 (see Figure 4-10) enabled a tailor made matrix with the required properties to be produced.

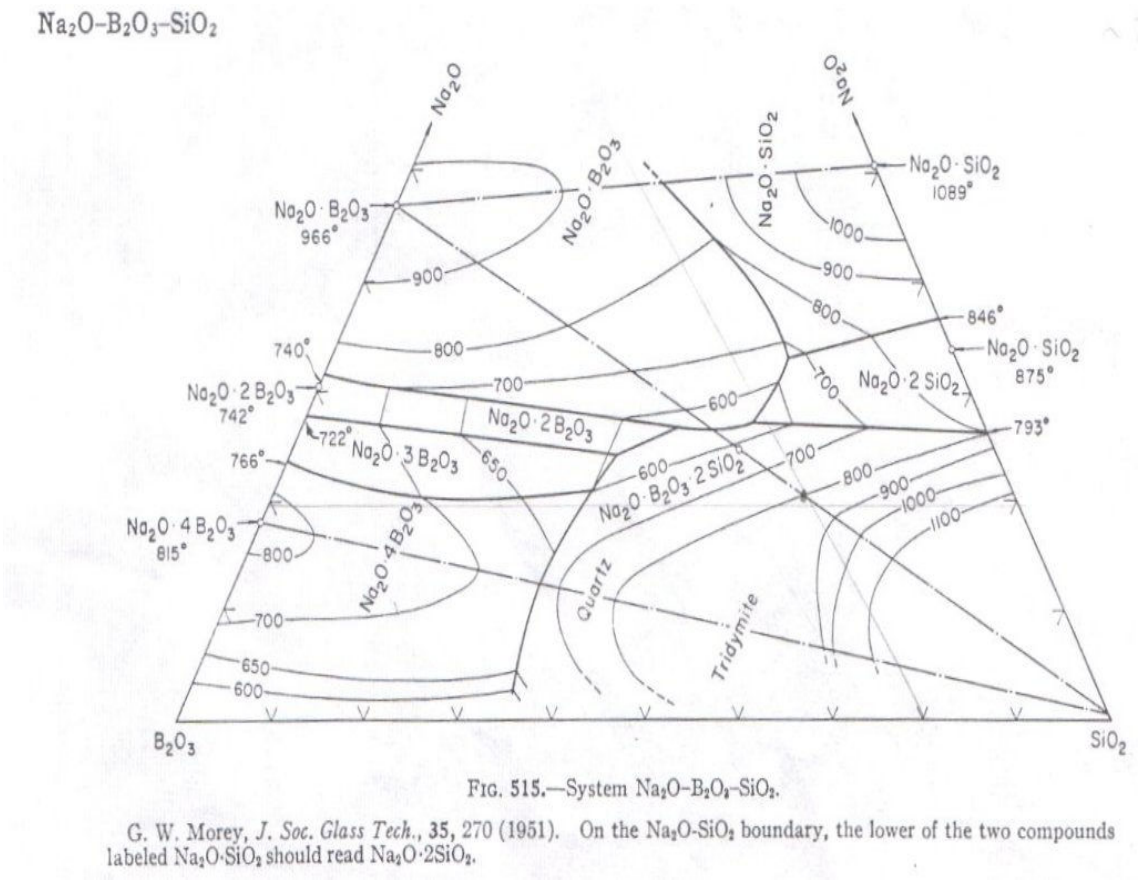

FIG. 515.—System Na_2O–B_2O_3–SiO_2.

G. W. Morey, *J. Soc. Glass Tech.*, **35**, 270 (1951). On the Na_2O-SiO_2 boundary, the lower of the two compounds labeled $Na_2O·SiO_2$ should read $Na_2O·2SiO_2$.

Figure 4-10. Tertiary phase diagram for a borosilicate glass matrix [91]

Adding enough boric oxide to give the composition in Table 4-8 produced the new matrix.

	Percentage weight	
Oxide	**Soda Lime**	**Borosilicate**
SiO_2	72.5	51.79
Na_2O	13.7	9.79
CaO	9.8	7
MgO	3.3	2.36
Al_2O_3	0.4	0.29
FeO, Fe_2O_3	0.2	0.14
K_2O	0.1	0.07
B_2O_3	0	28.56

Table 4-8. Chemical composition of soda lime and the new borosilicate glass

Subsequently by lowering the percentage of SiO_2, the melting temperature of the glass was reduced. Furthermore, by only adding approximately 30 weight percent boric oxide, the glass will still have the chemical properties of the soda lime glass without the water-soluble property of the borate glass.

Once a new furnace was purchased (the Carbolite 1600) much higher temperatures could be achieved in comparison to the previous furnace that had a maximum temperature of 1100 °C. This increased the possibility of pouring the molten glass into a mould and creating larger pieces of glass that would not require the broken pipette glass or toluene for analysis. An agate vial and zirconia balls were purchased from Spex CertiPrep to remove any possibility of contamination from the ball mill.

To produce this new glass matrix, Method 5 (section 3.2.1) was followed. This removed all the problems with the stainless steel ball mill contamination and the air bubbles previously found with the soda lime glass.

4.2.4.a UV-Vis absorption

The absorption spectra for the blank borosilicate glass are shown in Figure 4-11 for the whole range and just the visible region. These results indicated a strong absorption in the UV range but not in the visible, therefore for this application, there would not be any spectral interferences with the RE dopants fluorescence in the visible range.

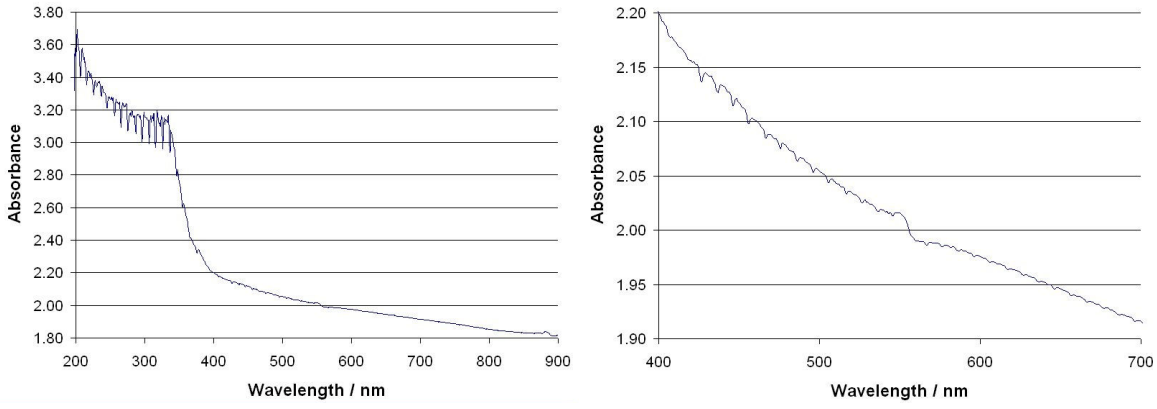

Figure 4-11. Absorption spectra of the blank borosilicate glass

The fluorescence was then analysed with the spectra shown in Figure 4-12. A strong broad fluorescence peak ranging from approximately 300-350 nm excitation and emission between 350-440 nm, correlated with the absorption results. Furthermore, no fluorescence peaks were found in the visible range (see Figure 4-13), therefore making borosilicate glass suitable for doping.

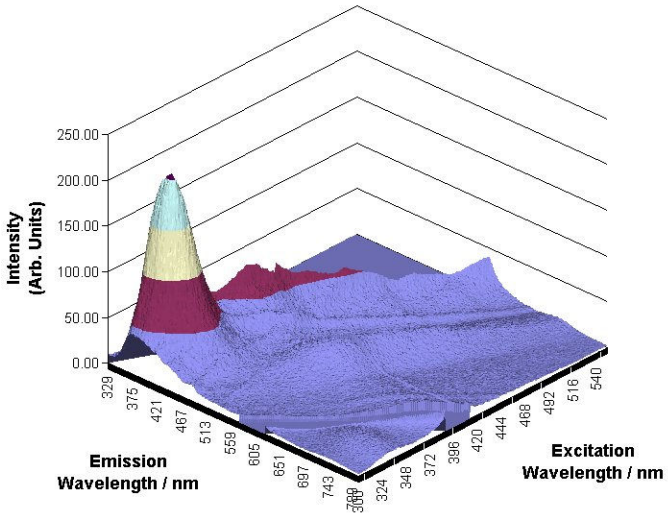

Figure 4-12. Fluorescence spectrum of the blank borosilicate glass

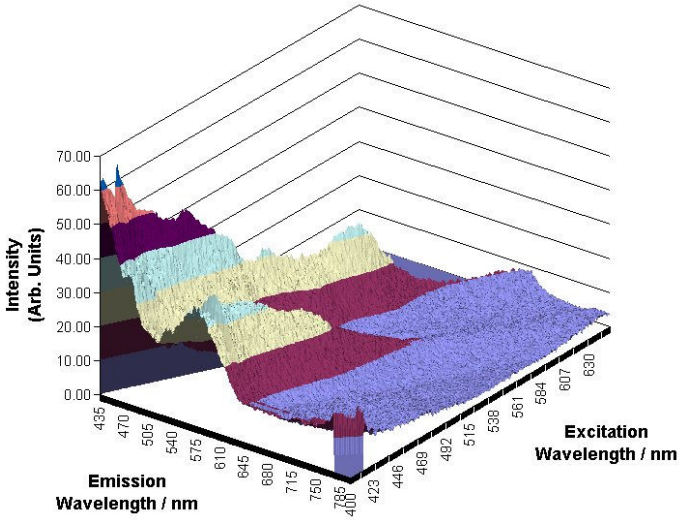

Figure 4-13. Fluorescence spectrum of blank borosilicate glass in the visible region

4.2.5 Base glass conclusion

The above spectra did not show any fluorescence signal in the visible region in comparison to the UV. Therefore the blank glass did not show any significant fluorescence that would interfere with the rare earth dopants enabling the europium doped glass to be analysed. Borosilicate glass was therefore chosen as the host matrix for the dopant ions and was used for all future doped samples. Therefore the fluorescence spectrum and further analysis of the europium doped glass could be carried out.

4.3 SINGLE RARE EARTH DOPED BOROSILICATE GLASS

Initial single doped glass experiments were carried out with europium, terbium and dysprosium in order to determine their suitability for their use in the security label by analysing their spectral characterisation and by comparison with their solution spectra. This was necessary in order to determine the matrix effects on the RE spectra and to select discrete fluorescence peaks in the visible range because the visible region would allow a more selective and therefore secure tag. The greater the number of discrete wavelengths from different RE ions that could be selected for use with the detector system, the greater the number of security code permutations. It was known from literature [92] that the fluorescence peaks would become wider in an amorphous glass host in comparison with solution due to the site broadening effect. Sarkies et al [92] reported that the rare earth ions are coordinated by a well defined solvation shell and therefore all the ions experience a similar field whilst in solution. However, once doped in a glass, an inhomogeneous broadening effect due to the dopant ions inhomogeneously distributed throughout the glass matrix, causes the peak widths to increase. This is because of the slightly different surrounding environments of the dopant ions causing slight deviations on the electronic energy level splitting.

Each of the three REs was doped in the borosilicate glass with a concentration of 3 mol% and their absorption and fluorescence spectra analysed. The europium absorption results are shown in (Figure 4-14), as an example, with those for terbium and dysprosium found in Appendix B (Figures B-1 and B-2).

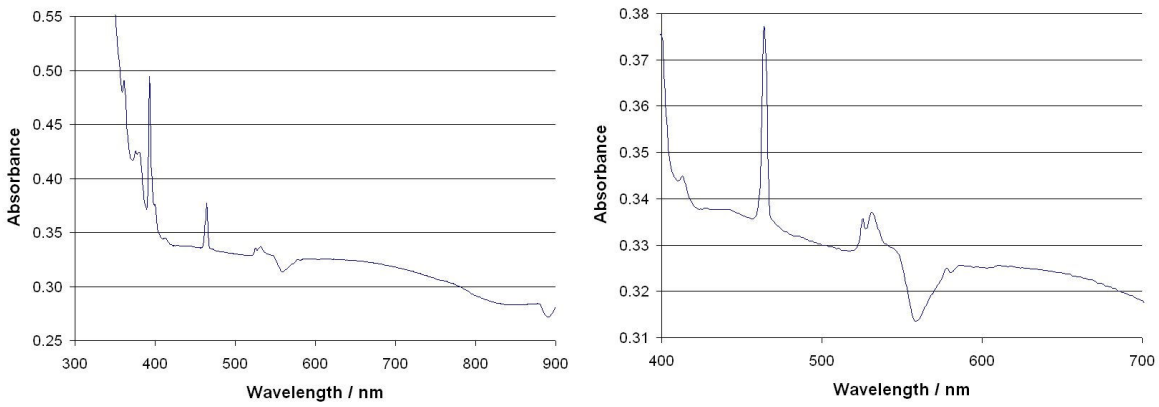

Figure 4-14. Absorption spectra of 3 mol% europium doped borosilicate glass

All the energy level assignments are given in Table 4-9 with reference to Carnall [93] who had analysed europium in an aqueous solution of $HClO_4$ and made a comparison to europium in the form $EuCl_3$. These results were in agreement with those reported with the majority of excitation peaks in the UV and visible range present in the europium doped borosilicate glass. The peak at 532 nm relates to the transition from $^7F_1$-$^5D_1$ whereas all the transitions in the table are from the ground state $^7F_0$.

Terms from $^7F_0$	Excitation Wavelength / nm
$^5D_4$	362
$^5G_6$	377
$^5G_2$	381
$^5L_6$	393
$^5D_3$	413
$^5D_2$	464
$^5D_1$	526
$^5D_0$	579

Table 4-9. Energy level assignments for Eu^{3+} doped in borosilicate glass

Terbium and dysprosium both produced absorption spectra with discrete wavelengths in the UV and visible regions. Tb produced one peak in the visible at 484 nm excitation whereas Dy produced four with the strongest absorbance of these at 452 nm. Tables of their energy level assignments based on the work by Tonooka and Nishimura [56], Aruna and Buddhuda [94] and Kam and Budduda [95] for terbium and Jayasankar and Rukmini [96] for dysprosium are found in Appendix B (Table B-1 and Table B-2).

4.3.1 Comparison with solution

The fluorescence spectra were then compared with their solution spectra in order to determine the matrix effects of the glass on the RE fluorescence. This was achieved by analysing the peak wavelengths and their relative intensities within each sample. Complete tables of all the fluorescence wavelengths, relative intensities and energy level transitions for each doped glass are in Appendix B (Table B-3 to Table B-5). All of the doped glass samples showed strong intensity peaks and a very low background due to the glass host, as no toluene or broken pipette glass was required in the analysis.

The first comparison was with the europium fluorescence of the doped glass and solution shown in Figure 4-15 and Figure 4-16 respectively. In comparison to the europium solution fluorescence, a number of the relative peak intensities were visually altered due to the change in host environment, although the peak wavelengths were not. This was also evident for terbium (Figure 4-17 and Figure 4-18) and dysprosium (Figure 4-19 and Figure 4-20). In the europium solution the strongest emission wavelength was 591 nm which changed to 615 nm when in the glass. The peak at 483 nm for terbium became stronger relative to the UV wavelengths once in the glass whilst in dysprosium, the largest variation was the strongest emission wavelength changing from 483 nm in the solution to 577 nm in the glass. The reason for these changes in peak intensities could be due to the forced electric dipole transitions becoming allowed when in the glass environment as opposed to the free ion state (in solution) where these transitions are forbidden by the parity rule [97].

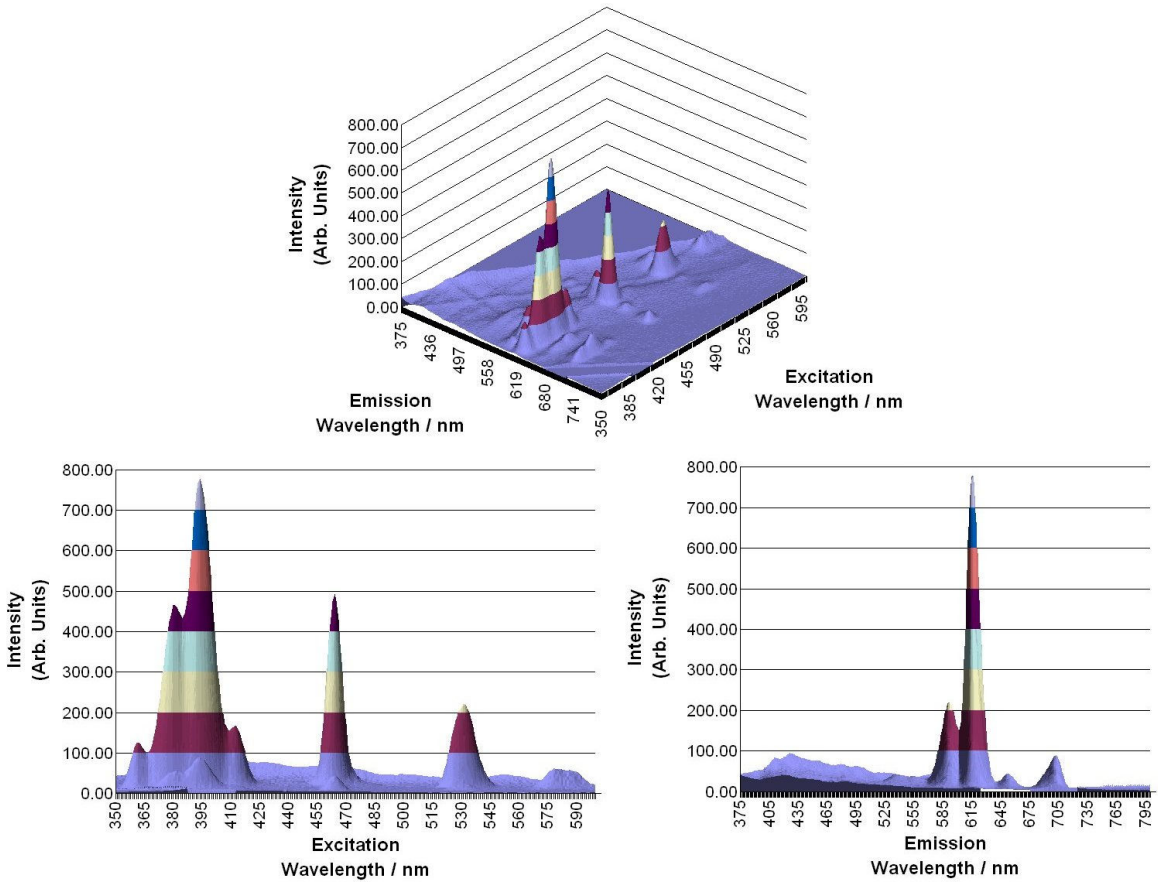

Figure 4-15. Fluorescence spectra of 3 mol% europium doped borosilicate glass

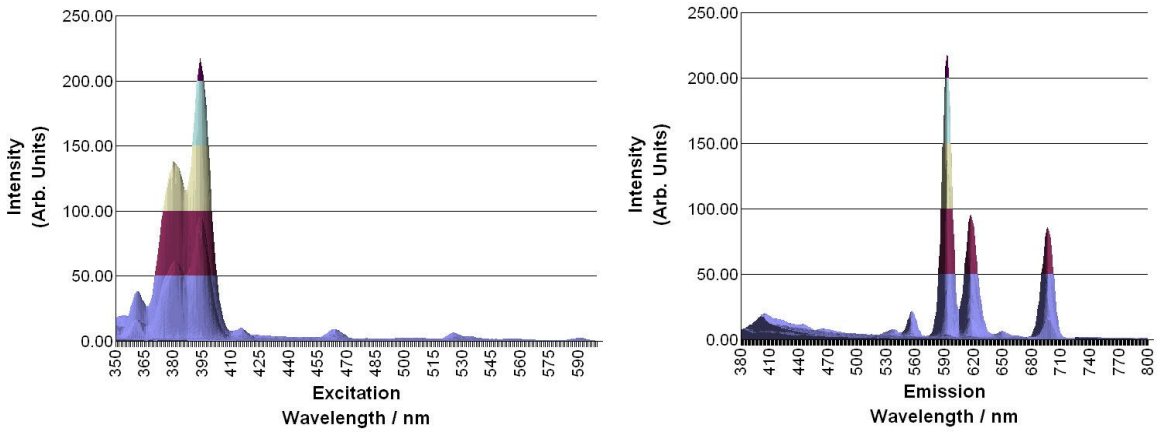

Figure 4-16. Fluorescence spectrum of 0.3 mol l^{-1} $EuCl_3$ solution

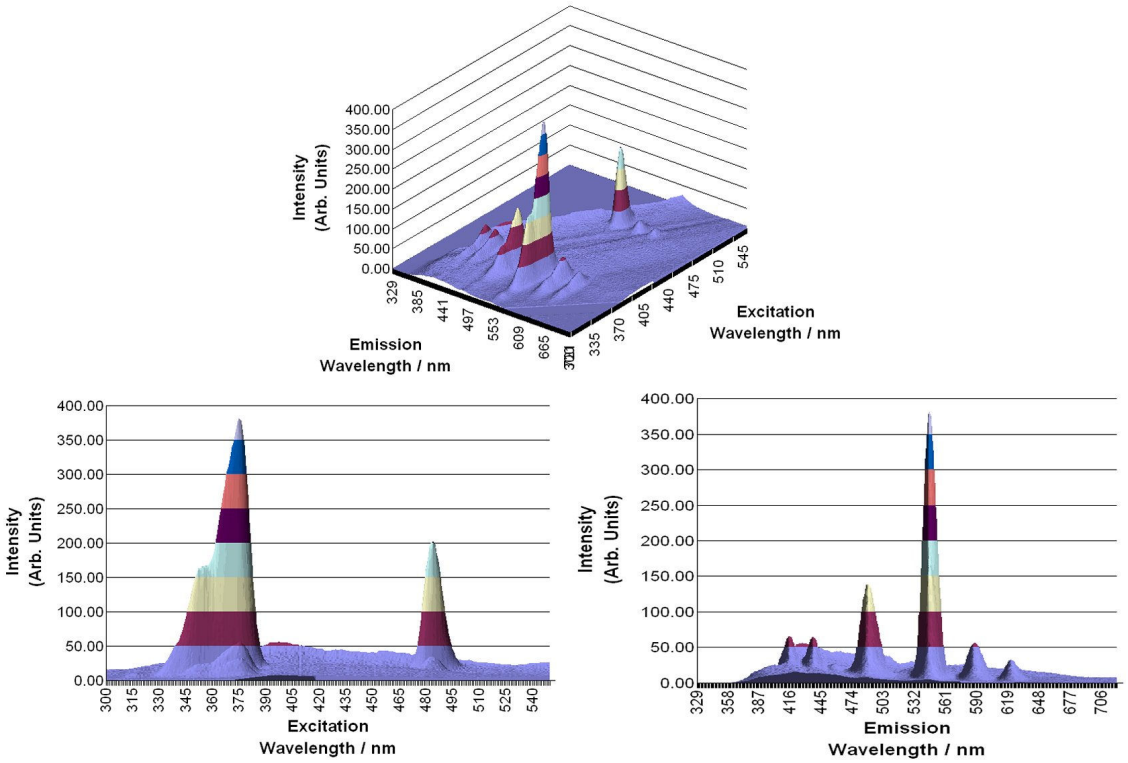

Figure 4-17. Fluorescence spectrum of 3 mol % terbium doped borosilicate glass

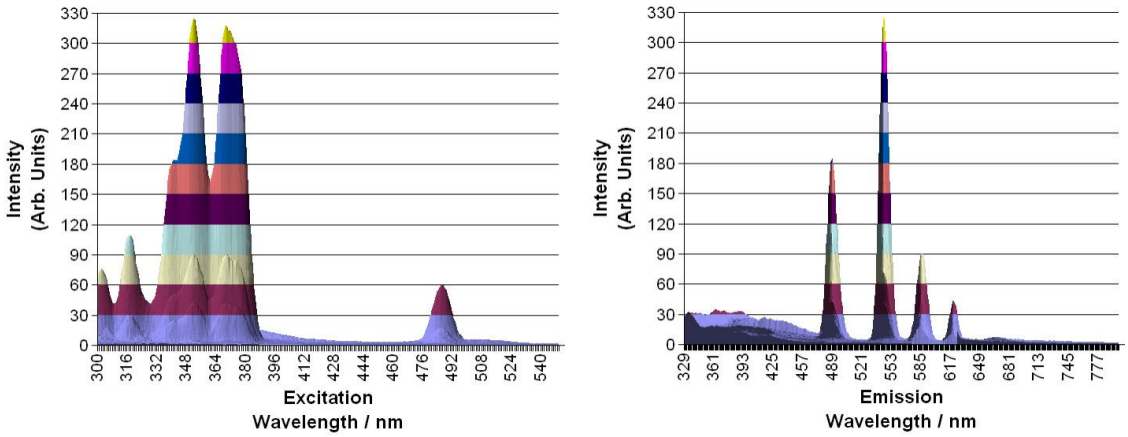

Figure 4-18. Fluorescence spectrum of the 0.3 mol l^{-1} $TbCl_3$ solution

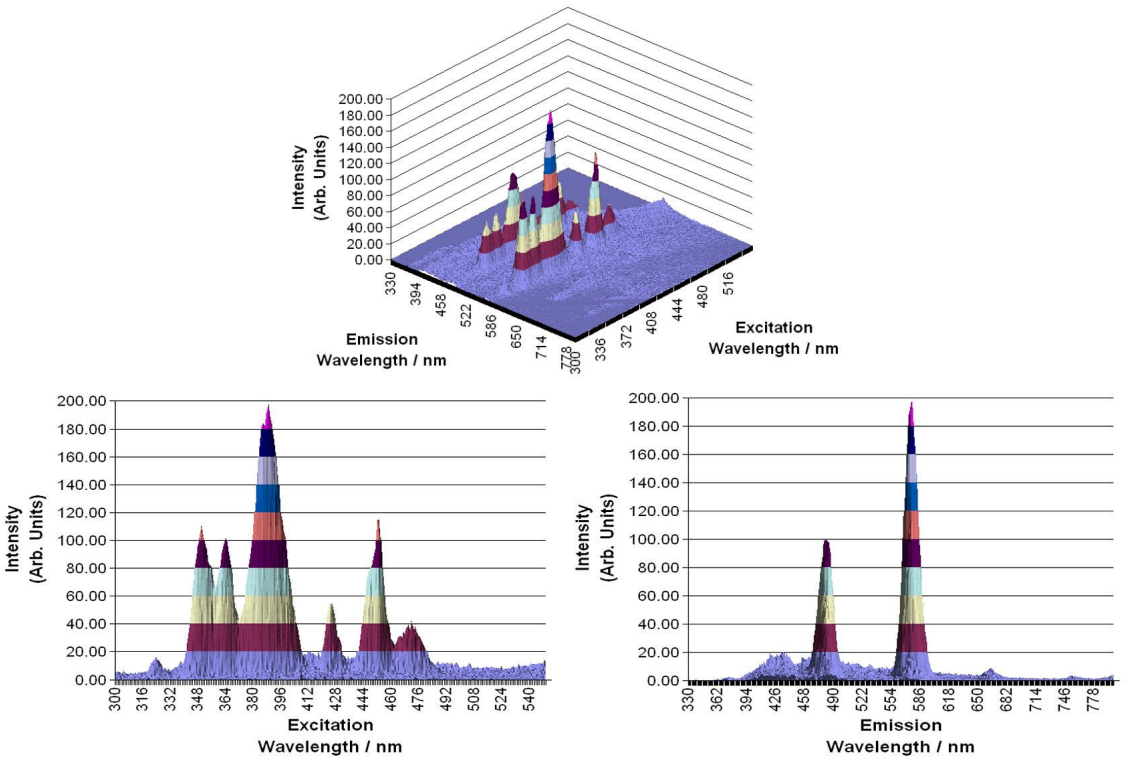

Figure 4-19. Fluorescence spectra of 3 mol% dysprosium doped borosilicate glass

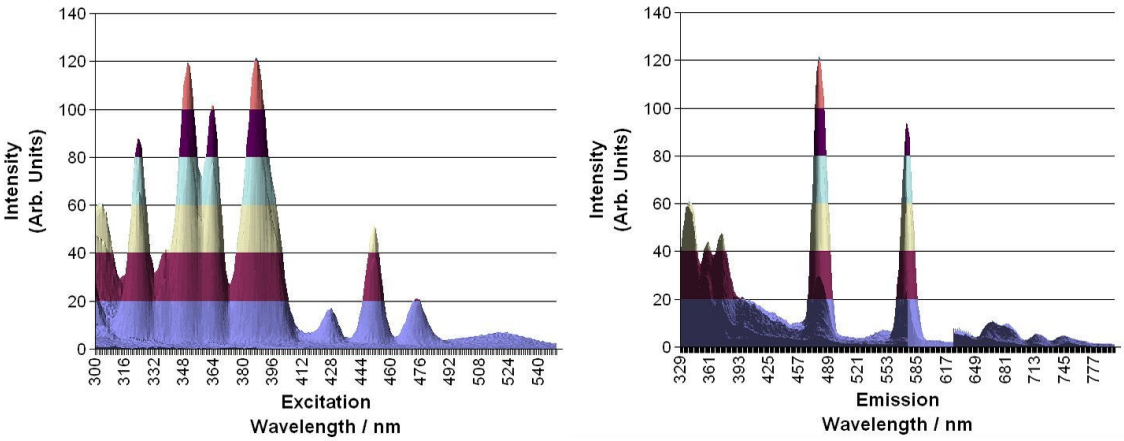

Figure 4-20. Fluorescence spectrum of 0.3 mol l^{-1} $DyCl_3$ solution

To further compare this difference from solution to glass, a table comparing the six most intense peaks in the solution and glass is shown in Table 4-10. Although a direct comparison between the relative intensities can not be made due to different concentrations, it is the peak wavelengths that are of interest. For each of the doped glasses, an excitation peak in the visible region appears as the second most intense wavelength. This is in direct contrast with the solution wavelengths that were all in the UV range. Furthermore, the changes in emission wavelengths noted above for europium and dysprosium are evident here.

0.3 mol l^{-1} $EuCl_3$			3 mol% Eu doped borosilicate glass		
Excitation Wavlength / nm	Emission Wavlength / nm	Relative Intensity (Arb. Units)	Excitation Wavlength / nm	Emission Wavlength / nm	Relative Intensity (Arb. Units)
394	592.5	218.89	393	615.5	768.13
380	592.5	138.77	465	615.5	479.06
318	592.5	103.07	381	615.5	465.88
394	616.5	95.71	531	615.5	220.97
394	696.5	85.97	393	591.5	218.76
381	618.0	62.39	412	615.5	166.91
0.3 mol l^{-1} $TbCl_3$			3 mol% Tb doped borosilicate glass		
Excitation Wavlength / nm	Emission Wavlength / nm	Relative Intensity (Arb. Units)	Excitation Wavlength / nm	Emission Wavlength / nm	Relative Intensity (Arb. Units)
352	545.0	324.97	375	546.0	382.28
371	545.0	313.52	483	545.0	200.31
352	488.5	183.95	354	546.5	164.13
371	488.5	177.58	376	488.5	139.36
352	587.0	91.33	354	488.5	65.29
370	587.0	90.51	376	438.0	65.12
0.3 mol l^{-1} $DyCl_3$			3 mol% Dy doped borosilicate glass		
Excitation Wavlength / nm	Emission Wavlength / nm	Relative Intensity (Arb. Units)	Excitation Wavlength / nm	Emission Wavlength / nm	Relative Intensity (Arb. Units)
387	479.0	121.81	389	577.0	197.69
350	479.0	119.81	452	577.0	111.25
363	479.0	101.57	352	577.0	101.13
387	574.5	93.86	364	577.0	100.68
350	574.5	90.29	389	483.0	96.76
364	574.5	77.68	364	483.0	56.20

Table 4-10. Comparison of the most intense fluorescence peaks of the REs in a solution and glass environment

4.3.2 Derivative Ultraviolet-Visible Absorption

Derivative spectroscopy can be utilised for the separation of overlapping bands, a higher precision of flat maxima and the isolation of shoulders and weak signals from unwanted background [98]. Solid materials are known to show complicated spectrophotometric measurements due to light scattering particularly in the UV region. Subsequently the actual spectrum of the interested species becomes superimposed on top of the background and loses some of its intensity. In order to remove any problems with uncontrollable base line shifts between samples, light scattering, turbidity of test solutions and dust or fingerprints on the cuvette, derivative spectra can be used.

An example of profiles produced by the derivative spectra is given in (Figure 4-21), which was adapted from Dixit [98]. The second derivative was chosen because it has a greater resolution than the normal and first derivative spectra and the characteristic minimum at the signal peak is easy to identify, whereas the first order has the peak at the cross point of the axis which is difficult to measure. Additionally, higher orders can be used, however, signal to noise ratio decreases with higher orders.

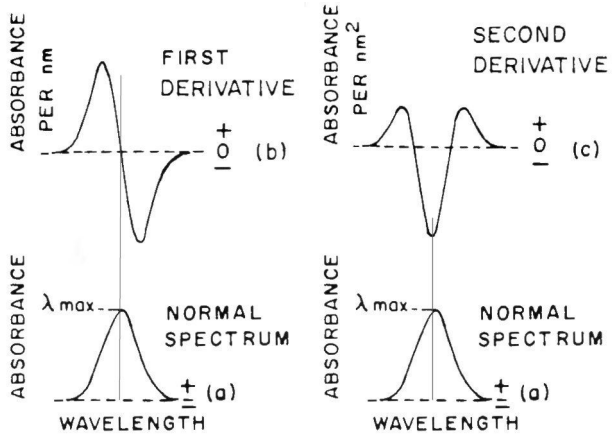

Figure 4-21. Characteristic profile of the 1st and 2nd order derivatives of a Gaussian band

Since the absorption spectra for the single RE doped samples did not contain all of the excitation wavelengths found in the fluorescence spectra, the second derivative was used to improve the resolution. This would remove the constant background caused by the glass scattering the light leaving the RE ions spectra. Although all three dopants were analysed, the spectra and tables for terbium and dysprosium can be found in Appendix B (Figures B-3 to B-6 and Tables B-6 to B-7).

Each of the second derivative results was correlated to the excitation wavelengths labelled on their fluorescence spectrum, as demonstrated with the europium spectra in Figure 4-22 and Figure 4-23. A table was then made to compare the absorption and second derivative results with the fluorescence excitation wavelengths, shown in Table 4-11 for europium.

Figure 4-22 shows a flat background and more discrete peaks in comparison to the normal UV visible spectrum. Although there were 11 discrete peaks in the derivative spectrum, there were only 7 excitation peaks visible in the fluorescence spectrum. This was because some of the absorption peaks had become merged into a single excitation peak causing the broader peaks in the fluorescence spectrum. Due to the randomly situated europium ions within the glass matrix, slight variations on the excitation wavelength caused the peaks to become grouped together.

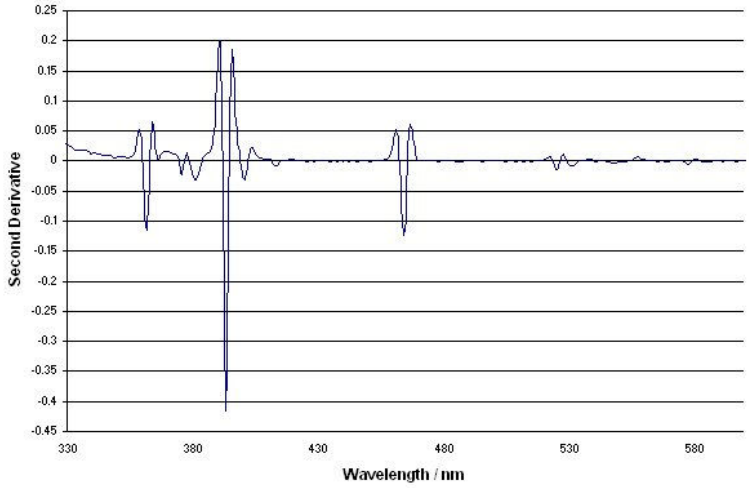

Figure 4-22. Second derivative absorption spectrum of 3 mol% Eu doped borosilicate glass

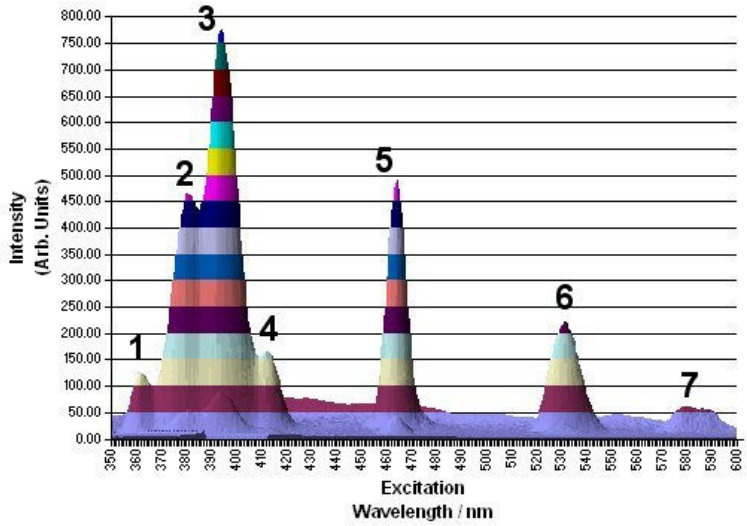

Figure 4-23. Fluorescence spectrum of 3 mol% Eu doped borosilicate glass with main peaks numbered

Label	Normal UV / nm	Second Derivative / nm	Excitatin maximum on fluorescence spectrum / nm
1	362	362	362
2		367	
	376	376	
	380	382	381
3	393	393	393
		401	
4	413	414	412
5	464	464	465
6	526	526	
	532	532	531
7		578	579

Table 4-11. Comparing UV results with second derivative and fluorescence results for europium doped glass

For the terbium results, the second derivative spectrum contained more detail below 378 nm with the resulting peaks corresponding with the fluorescence excitations. This was also evident with dysprosium. All of the second derivative results correlated well with the excitation peak widths found in the fluorescence spectra. Although the majority of peaks could be seen in the normal UV visible absorption spectra, the second derivative spectra made it easier to pick out the peak wavelengths and removed the background signal caused by the glass. For future samples, both the normal UV visible absorption spectrum and the second derivative spectrum will be analysed and used together to characterise the results.

4.4 FOURIER TRANSFORM-INFRARED CHARACTERISATION OF THE HOST GLASS

Although the strong red fluorescence of europium was observed in the borosilicate glass (due to the $^5D_0$-$^7F_2$ transition) peaks from higher energy levels ^5D_J (J>1) were not observed. This was because of the energy transfer from these electronic energy levels to the surrounding glass vibrations [97]. These interactions tend to reduce the quantum yields of fluorescence and generally the greater the energy difference between the two electronic states, the smaller the probability for a non-radiative transition. Therefore, these non-radiative decays from the europium level ^5D_J (J>1) to the $^5D_0$ level are assisted by the phonon of the glass host through multiphonon relaxation. According to Reisfeld [97], the responsible vibrational phonons for the quenching of various glasses are those reproduced in Table 4-12.

Bond	Stretching Frequencies / cm^{-1}
Silicate Si-O	1010-1115
Metaphosphate P-O	1140-1300
Borate B-O	1310-1380
Germanate Ge-O	840-930

Table 4-12. Table of the host phonon vibrational frequencies for various glasses

Furthermore, considerable quenching occurs when the difference between energy levels is less than about the energy equivalence of four phonons. For example, in borate glasses, quenching would occur between levels separated by approximately 5000 cm^{-1} and therefore the non-radiative relaxation in europium is very high whilst lowest in germanate glasses because there are fewer borate phonons required to bridge the energy gap. If fluorescence from the higher energy levels was required, then germanate glass hosts should be used. Fluoride glasses have a low phonon energy and have been reported as emitting fluorescence from the higher energy levels of europium [99]. For the borosilicate glass host, the FT-IR (Fourier Transform-Infrared) spectrum was recorded in order to determine the host vibrational energies.

4.4.1 Method

A KBr disc was produced by mixing 0.8 mg of the crushed blank borosilicate glass sample, of under 45 μm diameter, with 245.7 mg Analar KBr. This mixture was pressed together under 8 tons of pressure for six minutes to form a transparent disc. The disc was subsequently inserted into the Perkin Elmer GX FT-IR spectrometer and scanned five times to reduce the signal to noise ratio of the spectrum by averaging the signals.

4.4.2 FT-IR Results

The resulting spectrum for the blank borosilicate glass sample is shown in Figure 4-24 with the table of the main peaks and their related bonds adapted from the results in [41, 100, 101] shown in Table 4-13.

Frequency / cm^{-1}	Bond
442	Si-O-Si bonding vibrations
686	Boroxyl ring vibrations
1015	B-O stretching of tetrahedral BO_4 units
1396	B-O stretching of trigonal BO_3 units

Table 4-13. Table of the main FT-IR peaks and their relative bond assignments

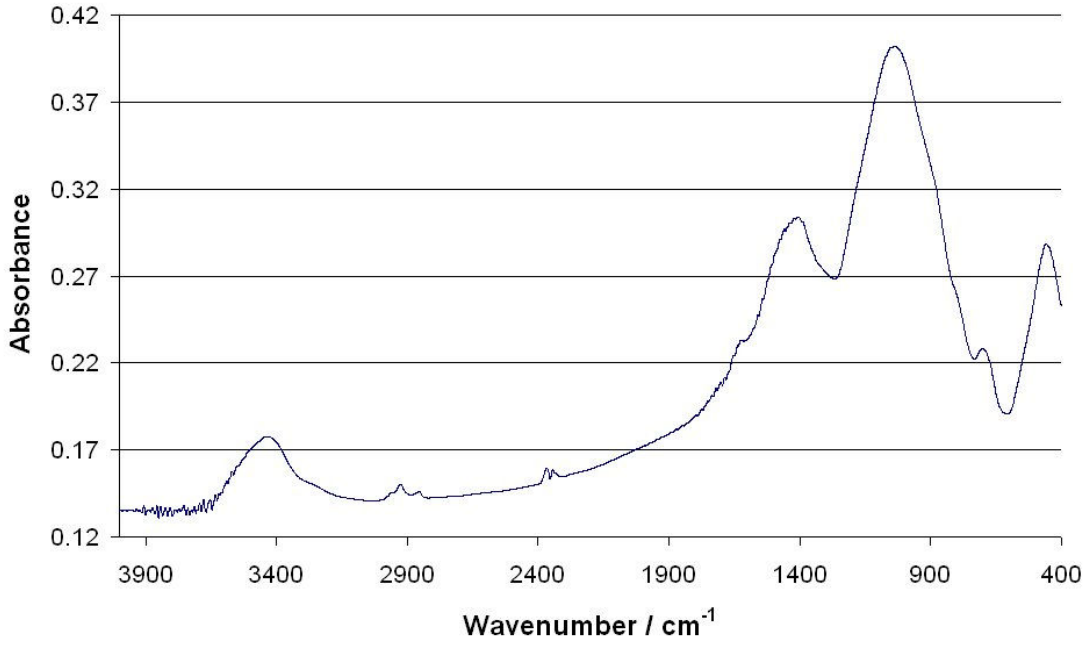

Figure 4-24. FT-IR absorbance spectrum of the blank borosilicate glass

The strongest peak at 1015 cm^{-1} was probably a mixture of both B-O and Si-O bonds (1106 cm^{-1} Si-O-Si stretching vibrations [101]) as both are present in the borosilicate glass. Therefore quenching will occur in this matrix when the energy level difference is approximately below 4060 cm^{-1} and/or 5584 cm^{-1} which relates to four phonons of the strongest bonds. Since 615 nm is equivalent to a wavenumber of 16,260 cm^{-1} this emission is radiative from the metastable $^5D_0$ level of Eu^{3+} whereas the energy difference between ^5D_J (J=2 or 3) and $^5D_0$ are very small (less than three phonons), and therefore non-radiatively relax to the $^5D_0$ level with the excess energy being absorbed by the host bonds [102].

This information is very important as the host matrix can completely quench the fluorescence emission depending on the dopant. Altering the host matrix would not only change the intensities and lifetimes of the fluorescence signals but would also change the allowed transitions of the dopant making the knowledge of the host matrix very important.

With reference to the energy levels of the REs (Figure 4-25) reproduced from Dieke and Crosswhite [103], it is possible to predict which REs should produce fluorescence in the borosilicate glass host. This is based on the energy difference between radiant energy levels and from the FT-IR results from the borosilicate glass. To achieve fluorescence, these gaps would have to be greater than approximately 5500 cm^{-1} which accounts for the equivalence of four host phonons mentioned earlier. Although the energy levels from Dieke and Crosswhite were calculated from RE doped crystal lattices, where the REs retained their sharp energy levels, the energy values would not change significantly when doped in the borosilicate host as they are dependent on the trivalent state of the RE and not the glass host. The difference occurs due to the slight variations in the surroundings of each RE ion in the glass, as glass is amorphous, resulting in inhomogeneous line broadening. This is not the case in a crystal where each dopant ion would have exactly the same surroundings and therefore smaller line widths. Furthermore, the probability of any radiative transition is dependent on the specific host matrix and would have to be taken into account.

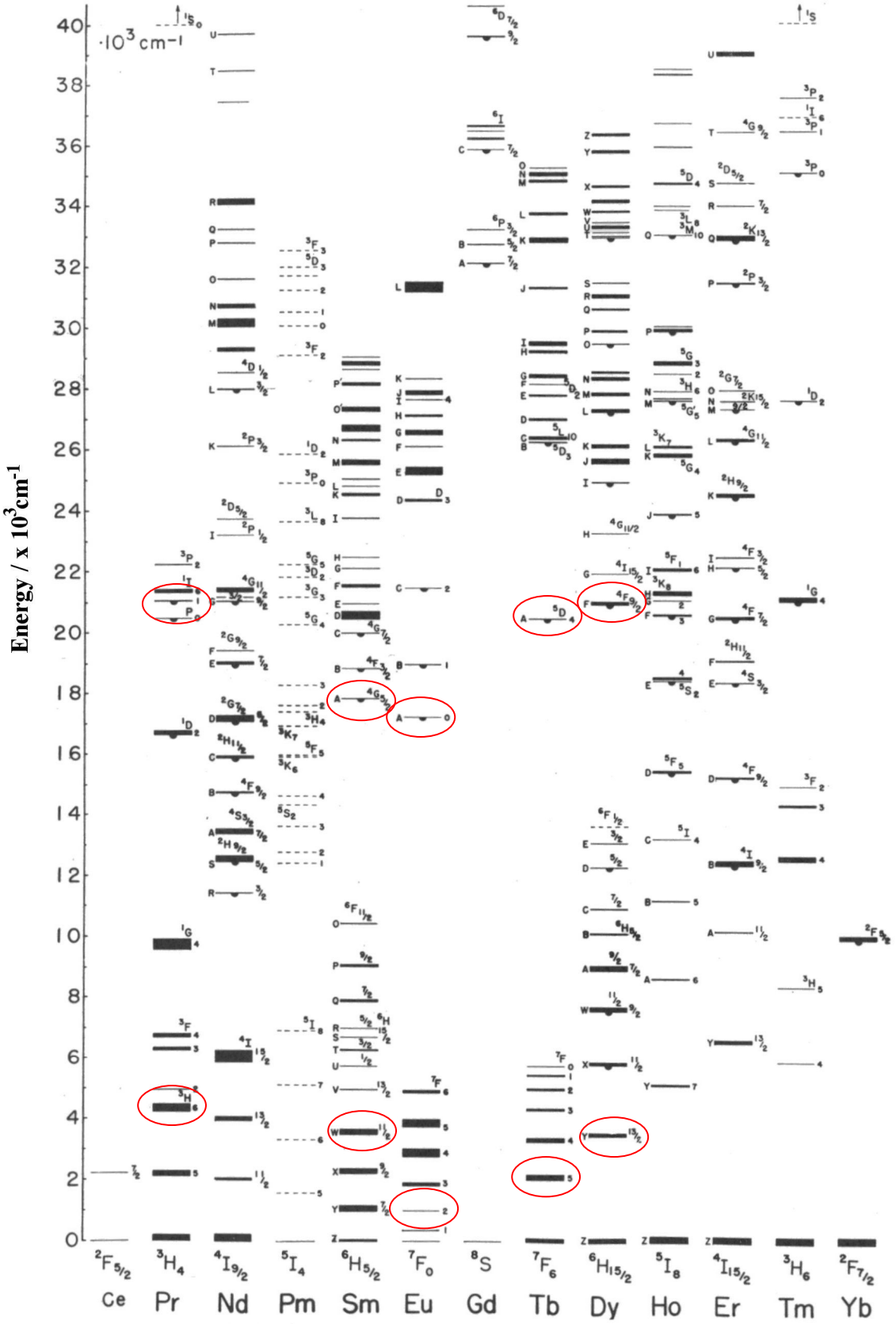

Figure 4-25. Observed energy levels of the trivalent rare earth ions [103]

This therefore allows an initial estimation, of possible RE ions that should fluorescence in the borosilicate matrix, to be made based on crystal lattice data that would then be confirmed experimentally for the particular host. Additionally, experiments would be required to determine the line width of each transition (dependent on the host matrix), their fluorescence lifetime and the suitability of the peak to be used in this taggant system because of the detector system requirements covered later. A strong discrete peak in the visible range would be required that did not interfere with other dopants spectrally.

4.4.3 FT-IR Conclusion

From Figure 4-25, possible dopants that have energy level differences greater than approximately 5500 cm^{-1} (circled in red on the figure) suitable for visible range emissions are Pr^{3+}, Sm^{3+}, Eu^{3+}, Tb^{3+} and Dy^{3+} whereas Gd^{3+} and Yb^{3+} would emit outside of the visible range. Although praseodymium did not appear to be a suitable dopant from its solution spectra, a doped glass sample was prepared based on the energy difference between fluorescent levels. Dopant REs that have energy level differences of similar values as the host phonons may still be useable as sensitisers for other REs or as possible extra dopants and would need to be investigated further.

4.5 PRASEODYMIUM DOPED BOROSILICATE GLASS

Based on the FT-IR results of the borosilicate glass, Pr^{3+} appeared to have energy levels that would produce a visible emission when in the borosilicate glass. In order to test this, a doped glass of 0.3 mol% Pr^{3+} was produced. 3 mol% was not chosen here due to the green colour of the praseodymium salt that would have caused a strong green colour to the glass. A 0.3 mol% concentration produced a pale green glass that would minimise any interference.

The absorption spectra of the full range and visible range are shown in Figure 4-26. These spectra show three strong absorption peaks in the visible range, although they were not very discrete. A table of their relative transitions are given in Table 4-14 and were adapted from the results by Nachimuthu and Ishizaka [104, 105]. These results agreed well with those reported with all the transitions in the table from the ground state $^3H_4$.

Terms from $^3H_4$	Excitation Wavelength / nm
$^3P_2$	440
$^1I_6$	465
$^3P_1$	470
$^3P_0$	481
$^1D_2$	591

Table 4-14. Energy level assignments for Pr^{3+} doped in borosilicate glass

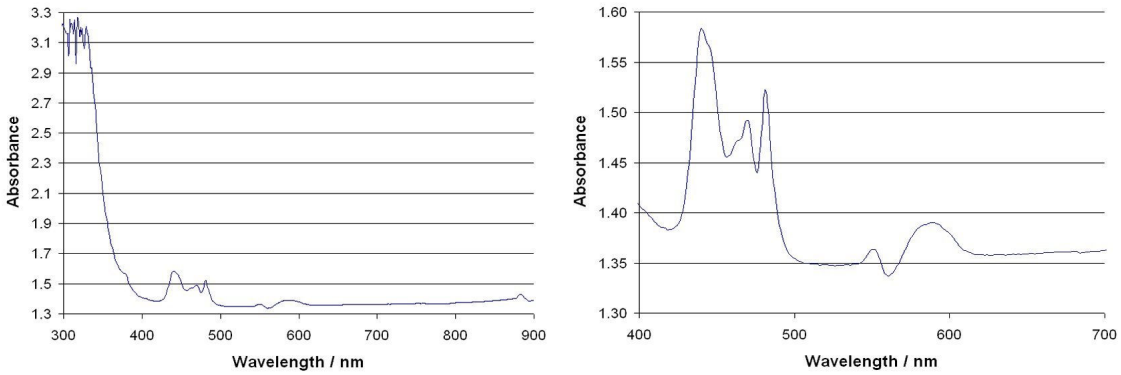

Figure 4-26. UV-absorption spectra of 0.3 mol% Pr^{3+} doped borosilicate glass

The small peak and dip about 550nm was due to the blank glass and not from praseodymium as this was evident in the blank glass absorption spectrum (Figure 4-27). These results appeared promising because of the strong absorption in the visible region, therefore the fluorescence spectrum was analysed and is shown in Figure 4-28. A table of all the relative transitions from the fluorescence spectra were adapted from Hormadaly and Nachimuthu [104, 106] and can be found in Appendix B (Table B-8).

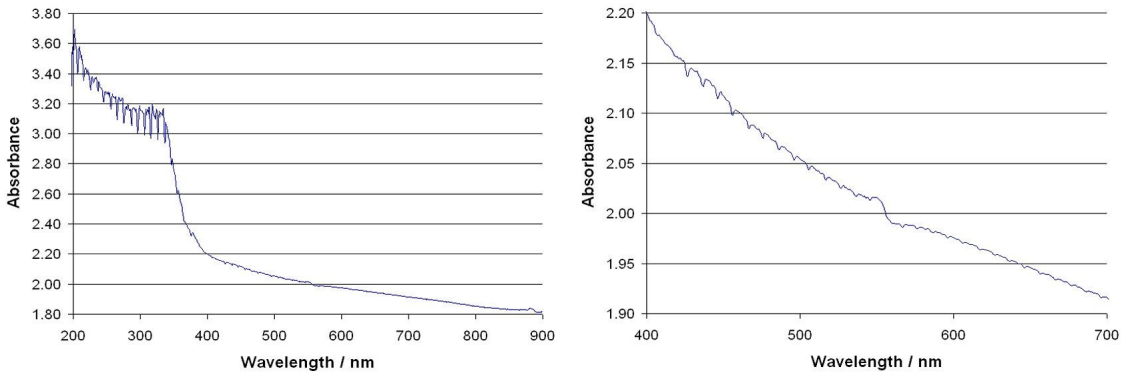

Figure 4-27. Absorption spectra of the blank borosilicate glass

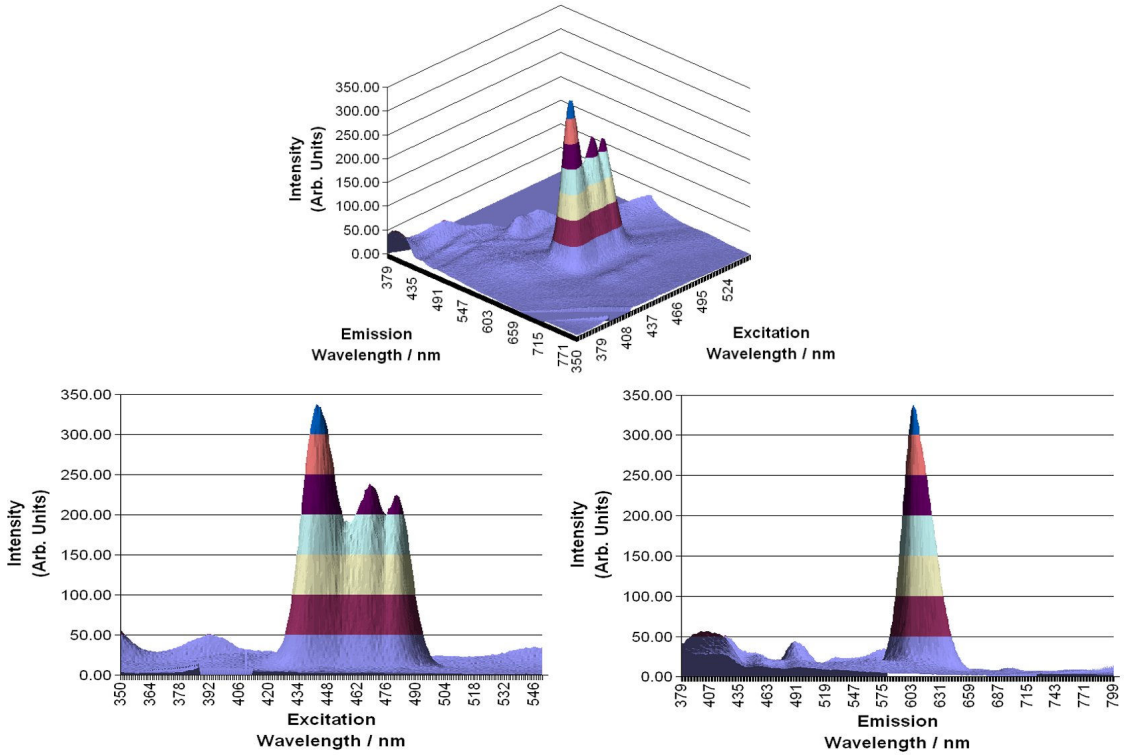

Figure 4-28. Fluorescence spectrum of the 0.3 mol% Pr^{3+} doped borosilicate glass

4.5.1 Praseodymium Doped Borosilicate Glass

These results correlated well with the absorption results; however, as in the absorption spectrum, the peaks overlapped each other and therefore were not discrete. This could cause problems with the detection system as the selectivity would be reduced. Unlike the analysis of the other single doped glasses, the solution spectrum of praseodymium was not compared here as there were no peaks found in the visible region of the spectrum for the solution. However, these results do not rule out praseodymium as a possible sensitiser as it does have a very strong absorption in the visible range which could be used to enhance the signal of other dopants at low concentrations.

4.6 DEVELOPMENT OF A NOVEL GLASS TRACER CONCLUSION

The solution spectral characterisation for the REs concluded that europium, terbium and dysprosium would be suitable for use in the security label based on the discrete fluorescence peaks found in the visible region. A suitable host matrix was found to be a borosilicate glass because of its low spectral background and chemical resistant properties.

Single RE doped borosilicate glasses based on the REs selected from the solution results, were analysed and found discrete fluorescence peaks for europium (465 nm excitation and 616 nm emission), terbium (483 nm excitation and 545 nm emission) and dysprosium (452 nm excitation and 577 nm emission). In comparison to the solution spectrum, the fluorescence spectrum of the doped glass was noted to have changed because of the different environment surrounding the dopant ions. This change caused an increase in the relative intensity of the peaks in the visible region, which is beneficial for the security label.

The derivative absorption spectrum was also analysed and was found to enhance the absorption results by removing the background absorbance caused by the glass host and made it easier to determine the absorption maximum wavelengths in comparison to the normal absorption spectrum. Future analysis will therefore include the derivative spectrum.

FT-IR analysis of the host glass concluded that Pr, Sm, Eu, Tb and Dy should all produce visible range fluorescence when doped in the glass based on the host phonon energy. Gd and Yb would also fluoresce; however these would be outside of the visible region and therefore are not suitable for this application. Based on the FT-IR results, a Pr doped glass was analysed for its spectral characteristics and found a strong fluorescence in the visible region. However, this fluorescence was not discrete and therefore Pr was not selected as a suitable dopant based on the specifications set out for this work. Based on these conclusions, an initial detector system can now be designed and tested based on the spectral characteristics of the chosen dopants.

CHAPTER 5 - DESIGN AND CONSTRUCTION OF AN ON-LINE SINGLE CHANNEL DETECTOR SYSTEM TO MEASURE THE NOVEL TRACERS

The aim of the work in this chapter was to build a circuit capable of detecting the fluorescence of the doped glass samples with little interference from other fluorescent species. The requirement from NCR was for a small and as cheap as possible detector with sensitivity and size as the key issues. Therefore instead of trying to build a highly sensitive and expensive detector utilising a photomultiplier tube (PMT) detector and a laser as the excitation source, the cheaper option (required for application to a mass market) of a light emitting diode (LED) for excitation and a photodiode as a detector was used. This option, reduced the cost and size of the detector considerably.

Rather than building a multi-channel detector with an array of LED light sources and a single detector, the system used a number of single channel detectors each for a specific wavelength and frequency. Consequently the design comprised of three single channel detectors (for the three selected dopants) placed side by side, as in an array, to detect each dopant separately reducing the complexity and cost of the system.

5.1 DEVELOPMENT OF OPTICAL TESTING & CHARACTERISATION METHODS

Before an on-line single channel detector system could be developed, the fluorescence properties of the glasses were tested using small bandwidth, high bright light sources such as lasers and LEDs. For the study of smaller samples a fluorescence microscope and an in-house built LISFM system were used. The LISFM system had to be adapted to measure the fluorescence lifetime of each dopant in order to also measure the laser pulse profile. These experiments were necessary in order to optimise the detector system.

5.2 LASER INDUCED FLUORESCENCE

A 532 nm green laser was used to excite two pieces of glass, the first one being non-doped, the second one doped with europium. The two pieces of glass are shown in Figure 5-1. The pictures were taken in white light without any filter in front of the camera (Figure 5-1A) and in total darkness through a red bandpass filter when the green laser light passed through the glass (Figure 5-1B).

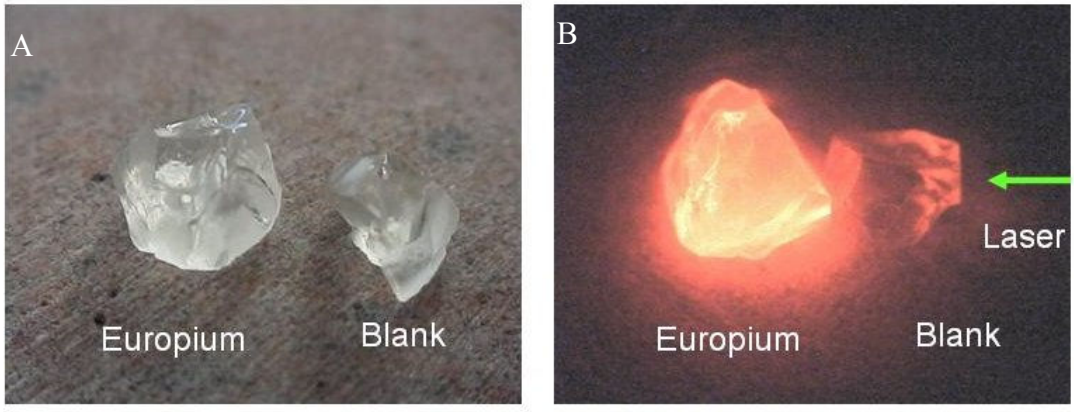

Figure 5-1. Blank and Europium doped glass, (A) white light picture and (B) fluorescence picture

The laser light in Figure 5-1b was directed through the blank glass sample (shown by the green arrow) then through the europium sample. The bright red glow was due to the 615 nm fluorescence of the europium whilst the faint red glow in the blank sample came from the reflection of the red light coming from the doped sample. This wide shift in wavelength (green to red) demonstrated the large Stokes shift of the RE fluorescence.

5.3 FLUORESCENCE MICROSCOPE

Some of the initial europium doped borate glass was crushed with a mortar and pestle and observed under a fluorescence microscope using the mercury lamp as the excitation source and different broad band filters to select different excitation/emission wavelengths combination. Figure 5-2 shows the fluorescence images of the europium sample on a glass slide using 100x magnification and different filter combinations.

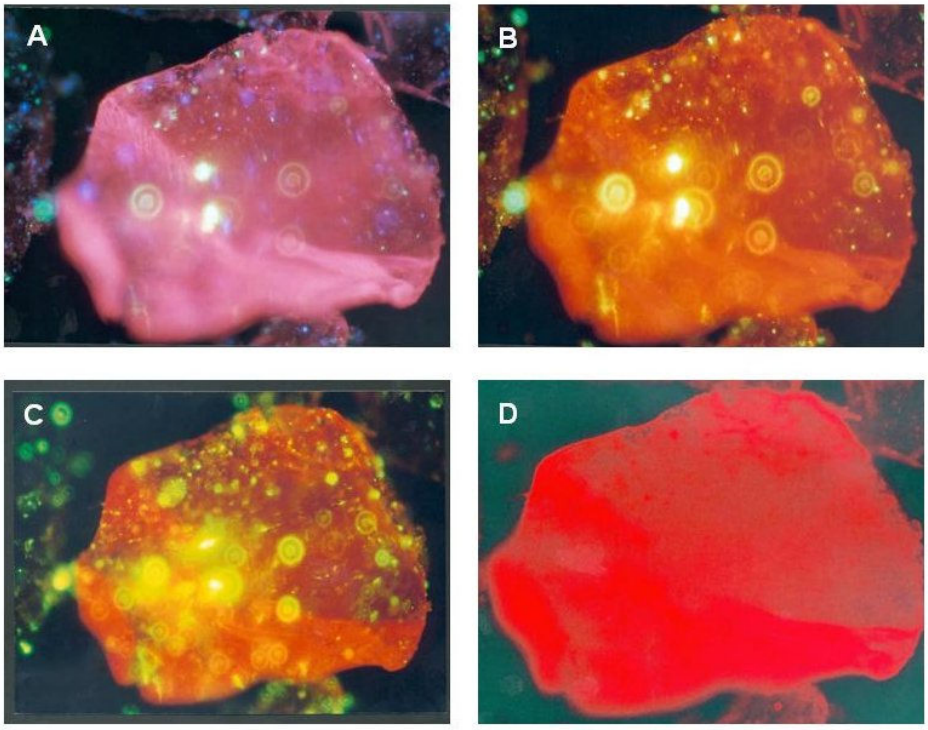

Figure 5-2. Europium doped glass fluorescence pictures under various excitation wavelengths: (A) UV, (B) violet, (C) blue, (D) green

Figure 5-2 shows europium doped glass particle fluorescence under UV (A), violet (B), blue (C) and green (D) excitation. The emission filters were longpass filters that allowed light of slightly longer wavelength than the excitation to be collected. The excitation filters present in the microscope covered each part of the spectrum where europium doped glass could be excited as indicated from the spectroscopic analysis covered in Chapter 4. These pictures demonstrated that europium doped glass could be successfully excited by a range of excitation wavelengths and still fluoresce in the red region, around 615 nm. Figure 5-2 also shows some green spots on the glass. Further investigation under the fluorescence microscope revealed that these green spots were due to the presence of particulate contamination, probably quartz, coming from the porcelain crucibles used in the initial experiments. This problem was eliminated once platinum crucibles were used for the borosilicate glass manufacture.

5.3.1 Europium Doped Glass

Figure 5-3A shows europium doped glass on a glass slide, whilst Figure 5-3B shows an additional white piece of paper underneath the slide. Both pictures were taken using a blue excitation filter. This demonstrated the strong red fluorescence of the glass and that by using the appropriate filter the glass could be detected on white paper. When a green excitation filter was used, Figure 5-3C, the picture was completely red as the filter could not distinguish the different emissions from the background and the sample.

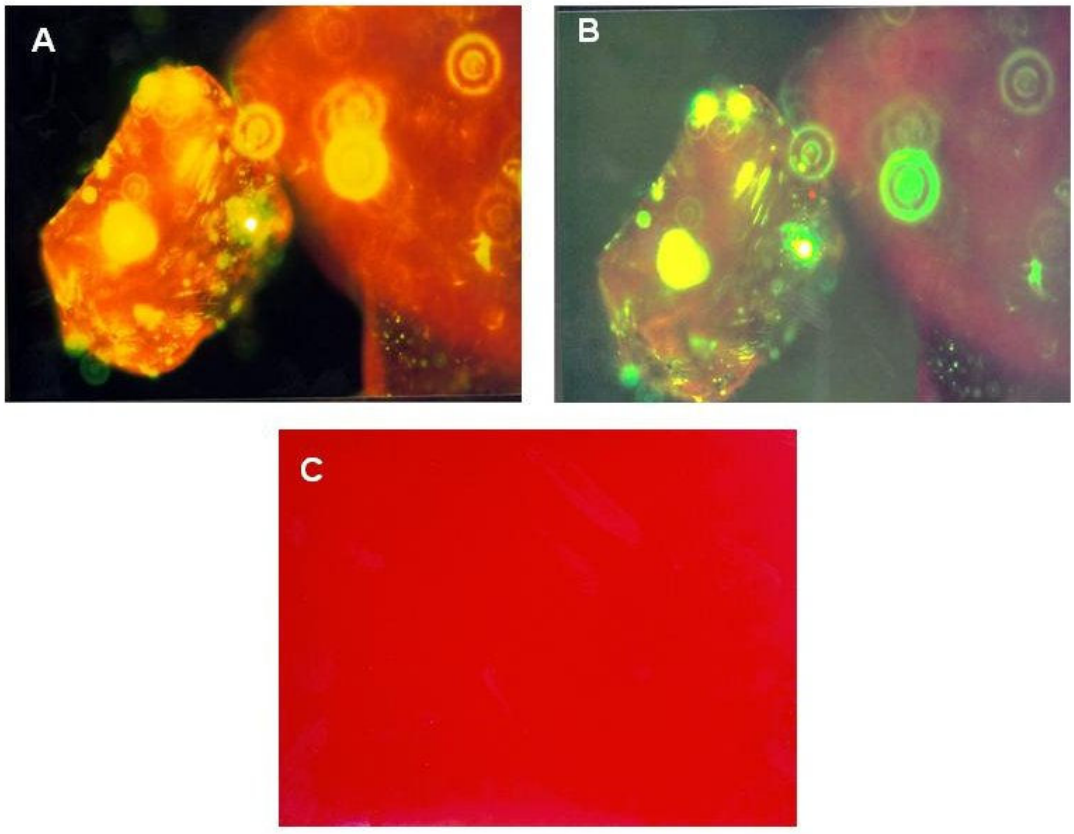

Figure 5-3. Fluorescence pictures of europium doped glass with and without white paper under various excitation wavelengths: (A) blue, (B) blue with paper and (C) green with paper

5.3.2 Conclusion

These two experiments highlighted the necessity for knowing and selecting the appropriate optimum excitation and emission wavelength filters. Furthermore, it proved that the glass beads could be separated spectrally from the background fluorescence of white paper.

5.4 LASER SPECTROSCOPY OF DOPED GLASSES

Lasers are, spectroscopically, narrow bandwidth light sources with high brightness. Due to their high intensity, they can be used for testing fluorescence from even small micron-sized fluorescent glass samples. Here, the laser induced fluorescence of the dye based beads (produced by Method 1 in section 3.1.1) and RE-doped glass powders on paper samples were investigated using the LISFM system.

5.4.1 Laser Induced Scanning Fluorescence Microscope

A Nd:YAG laser emitting at 532 nm was used in the LISFM system shown in Figure 5-4. In this system the sample was placed on an XY scanning table that moved automatically under a fluorescence microscope. Recording (using a computer) the signal as the sample was scanned obtained a full fluorescence map of the sample. The fluorescence wavelength measured was selected by a series of interference filters placed in front of the detector.

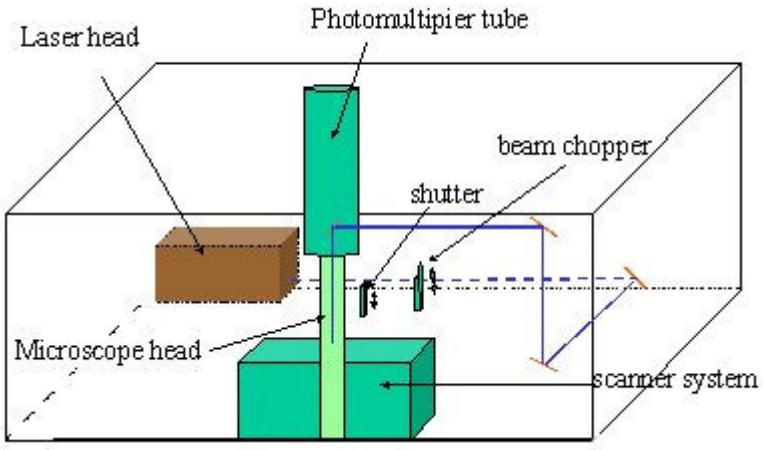

Figure 5-4. Laser Induced Scanning Fluorescence Microscope

5.4.1.a Dye based beads

In order to test the LISFM system sensitivity, some of the 100 μm diameter rhodamine B doped beads were arranged on a glass slide to make an NCR logo (shown in Figure 5-5a) and were kept in place using optical glue. Due to the small field of view available with the standard fluorescence microscope, only pictures of details of the logo could be taken.

Figure 5-5b was the picture taken of the area marked on Figure 5-5a with a white box. The picture was at 100x magnification and used a blue filter.

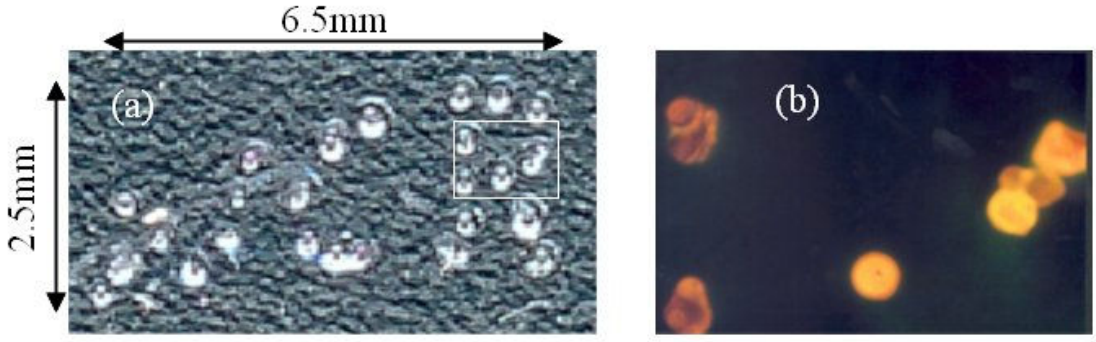

Figure 5-5. (a) NCR logo made out of beads and (b) detail fluorescent picture of the highlighted R section

Figure 5-6 shows the LISFM scan of the slide in Figure 5-5a. This initial test demonstrated the system in terms of fluorescence sensitivity and scanning capabilities. With a comparison of Figure 5-6 to Figure 5-5a, it can be seen that these capabilities were met. The LISFM system was capable of detecting single 100 μm diameter beads and recording the fluorescence map of a sample surface.

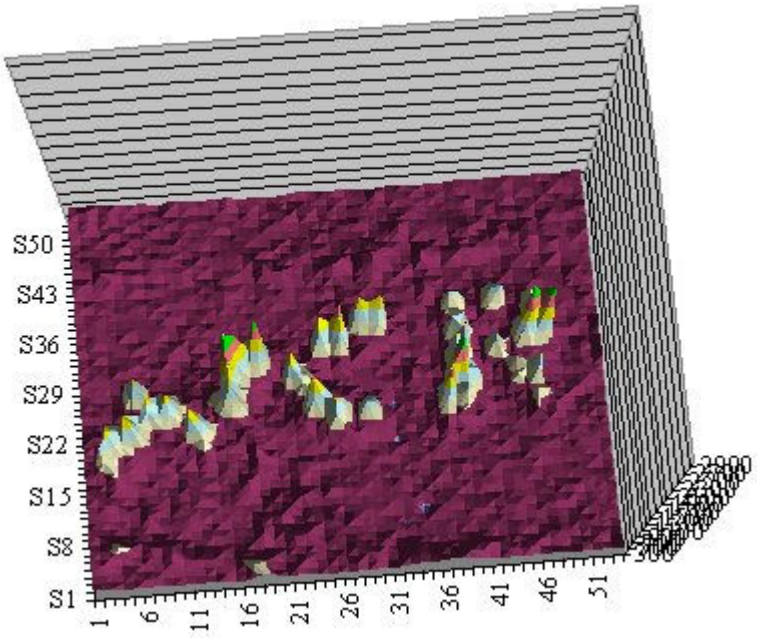

Figure 5-6. LISFM scan of rhodamine beads

5.4.1.b Europium doped glass powder

Some of the crushed europium doped borate glass was shaped into an N and a picture was again taken using the standard fluorescence microscope shown in Figure 5-7(a). The modulator speed of the LISFM had to be slowed down in comparison to that used for the rhodamine coated beads. It was found that this was due to the longer fluorescence lifetime of the europium fluorescence. Any detector system design would therefore have to accommodate for this longer lifetime.

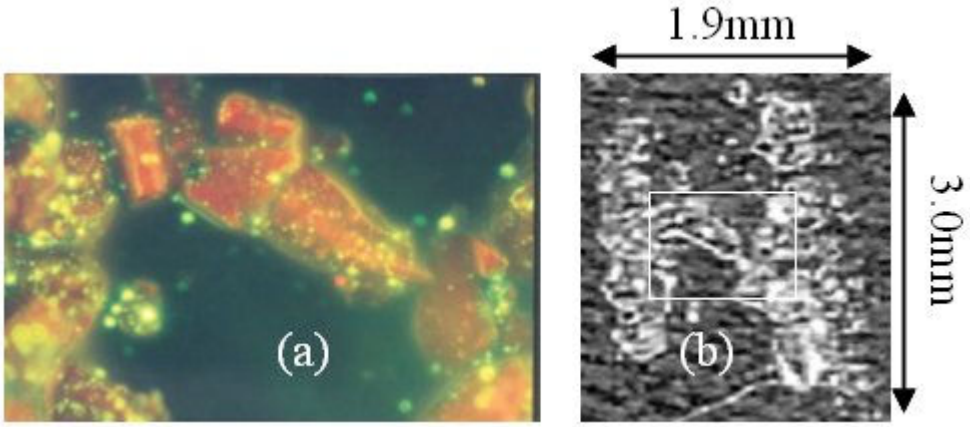

Figure 5-7. (a) Fluorescent picture of N and (b) the scanned image of the whole N

Figure 5-7(a) was taken at 100x magnification, using the blue excitation filter and shows the section of the N highlighted by the white box in the scanned image shown in Figure 5-7(b). To acquire the whole image with the fluorescence microscope, a smaller objective, i.e. x5, would have been required. The slide shown in Figure 5-7(b) was also analysed with the LISFM system and is shown in Figure 5-8(a).

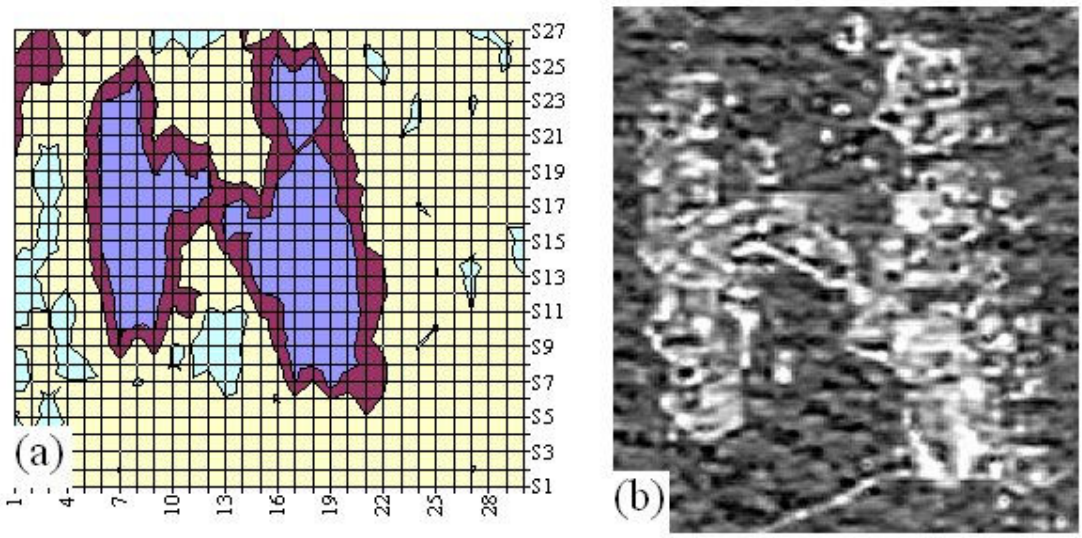

Figure 5-8. (a) LISFM scanned image of europium doped glass and (b) a scanned image of the whole pattern

5.4.1.c Conclusion

In summary, these studies have shown that the fluorescence from dye based beads and RE-doped glass beads differ in wavelength and their fluorescence lifetimes. High frequency excitation pulses can be used in the case of dye based beads but due to the longer fluorescent lifetimes of RE-ions, low frequency laser pulses can be selected to excite the RE-doped glass samples, to increase the temporal resolution.

5.5 LIFETIME STUDIES OF THE RE DOPED GLASSES

Before the fluorescent decay time of the RE ions can be used as a method to selectively discriminate against short lived background molecular fluorescence, it was important to check the fluorescent lifetimes of the doped RE ions inside the glass. The fluorescent decay time of each RE ion inside single doped borosilicate glass was measured.

In order to measure the lifetimes, time resolved fluorescence studies were carried out using the modified LISFM system. In this setup the microscope focused the laser light on to the RE doped glass sample and collected the fluorescence. Short laser pulses of appropriate wavelength, generated from a continuous wave (CW) ILT Model 5500A Ar-ion laser (with tuneable wavelengths of 457.9, 465.8, 476, 488, 496.5, 501 and 514 nm) by a mechanical chopper, were used to excite the fluorescence and the corresponding temporal fluorescence intensity variations were detected using a highly sensitive PMT. A set of filters were placed in front of the detector to filter-out unwanted wavelengths. The laser pulses were monitored using a photodiode with the help of a partially reflecting glass plate (microscopic glass slide) as a reference. A Tektronix TDS 380 digital real-time oscilloscope was used to display and record the signals.

5.5.1 Europium

The spectral characterisation of the europium doped samples has shown a strong absorption peak around 465 nm with a corresponding emission peak around 615 nm. Hence an argon-ion laser wavelength of 465 nm was selected for the excitation and an interference filter with a transmission peak at 620 nm (Full Width at Half Maximum, FWHM = 10 nm) was chosen as the fluorescence filter. The transmitted intensity was detected using a PMT and was displayed/recorded using the oscilloscope. A typical laser pulse is shown in Figure 5-9 with a pulse width of almost 500 μs (FWHM). The corresponding fluorescent pulse from a sample of the 3 mol% $EuCl_3$ doped borosilicate glass is shown in Figure 5-10. These results showed the fluorescence pulse was much longer than the pump pulse (nearly 7 ms base width) and had a FWHM of approximately 2 ms.

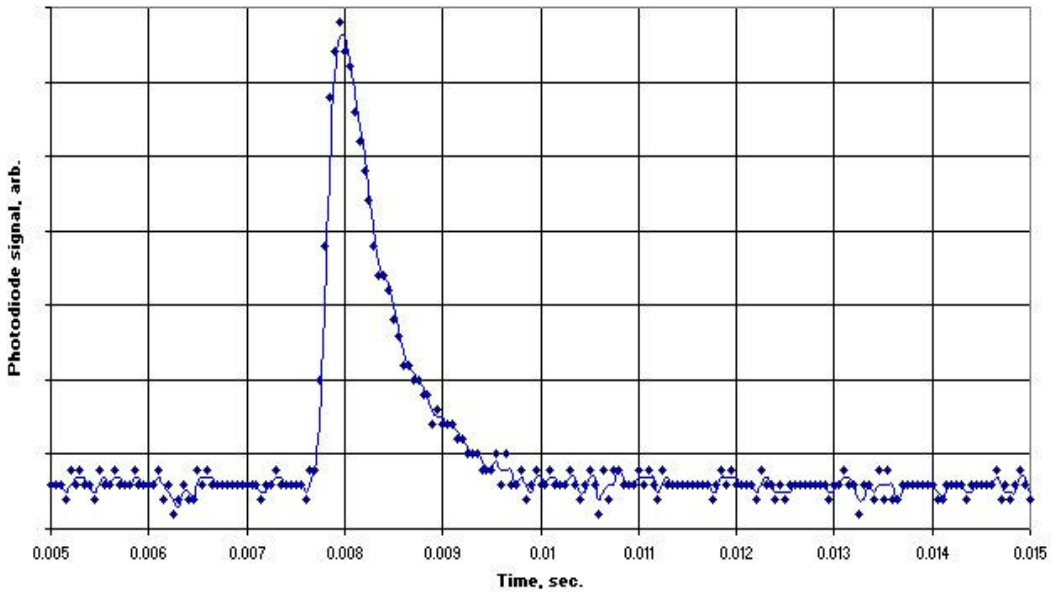

Figure 5-9. A typical 465 nm laser pulse

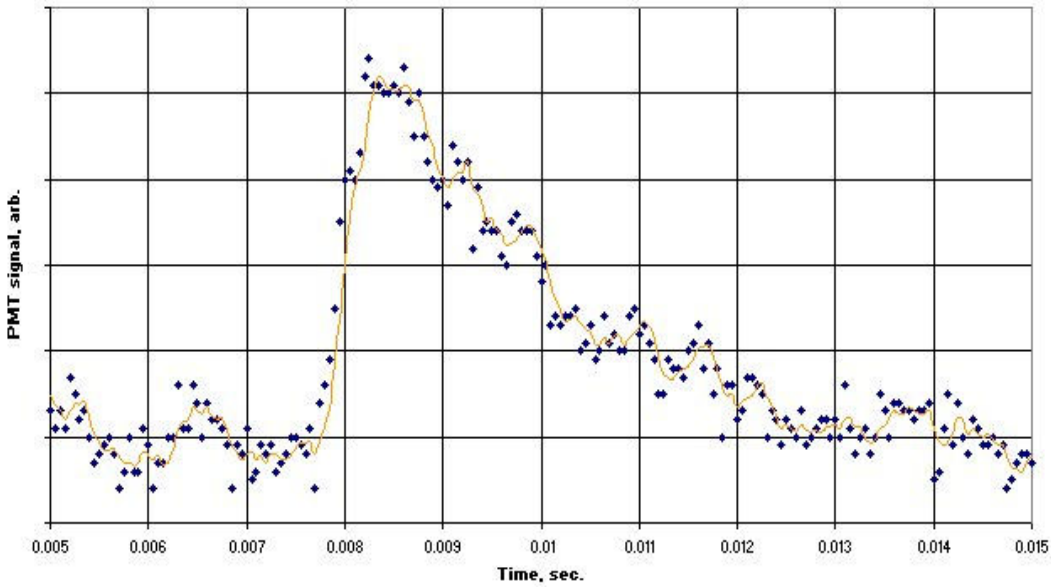

Figure 5-10. Europium doped borosilicate glass 620 nm fluorescent pulse profile under a 465 nm laser pulse excitation

5.5.2 Terbium

The second suitable dopant selected from the spectral studies was terbium and the spectral characteristics had shown a strong excitation and emission peak centred on 485 nm and 543 nm respectively. Hence the strong laser line at 488 nm from the argon-ion laser was selected as the excitation wavelength. The same experimental setup was retained except for the laser wavelength and the filters. A PMT was used to detect the fluorescence intensity filtered through an interference filter with transmission peak at 543 nm. In addition, a holographic notch filter (488 nm) was used to block the strong laser pulses leaking into the detector. Laser pulses were generated at a frequency of around 10 Hz by controlling the speed of the chopper with a typical laser pulse detected by the photodiode shown in Figure 5-11 with a FWHM of approximately 500 μs. The resulting fluorescence pulse recorded from the borosilicate glass doped with 3 mol% $TbCl_3$ is shown in Figure 5-12 and had a larger width in comparison to the excitation pulse. As can be seen in Figure 5-12, it has a fast rise time of 1 ms and a long decay time of nearly 7 ms with a FWHM of 2.2 ms. This indicated the long fluorescent lifetime for Tb ions in the borosilicate glass.

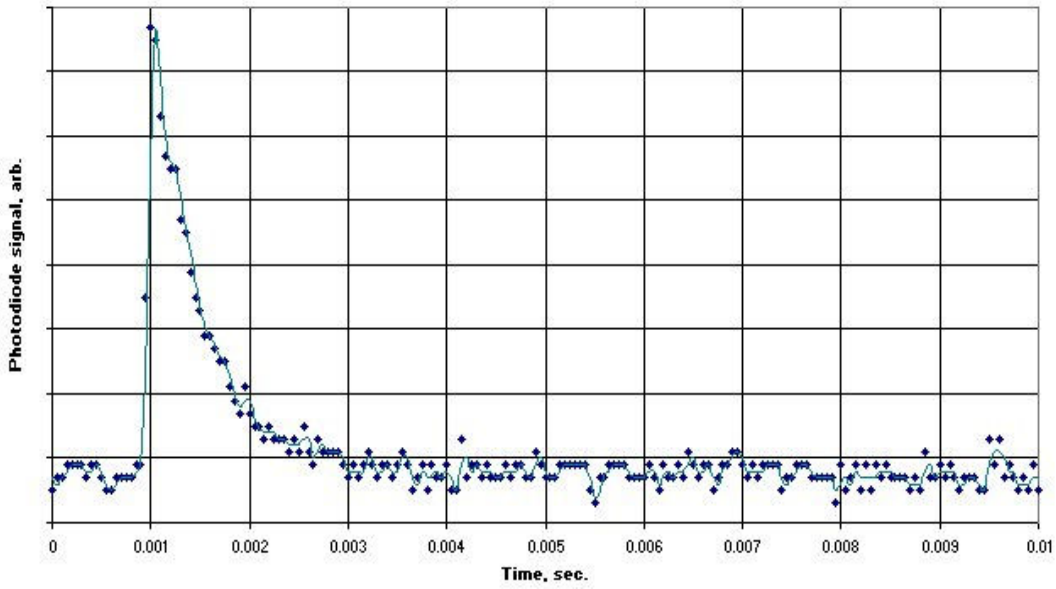

Figure 5-11. A typical 488 nm laser pulse

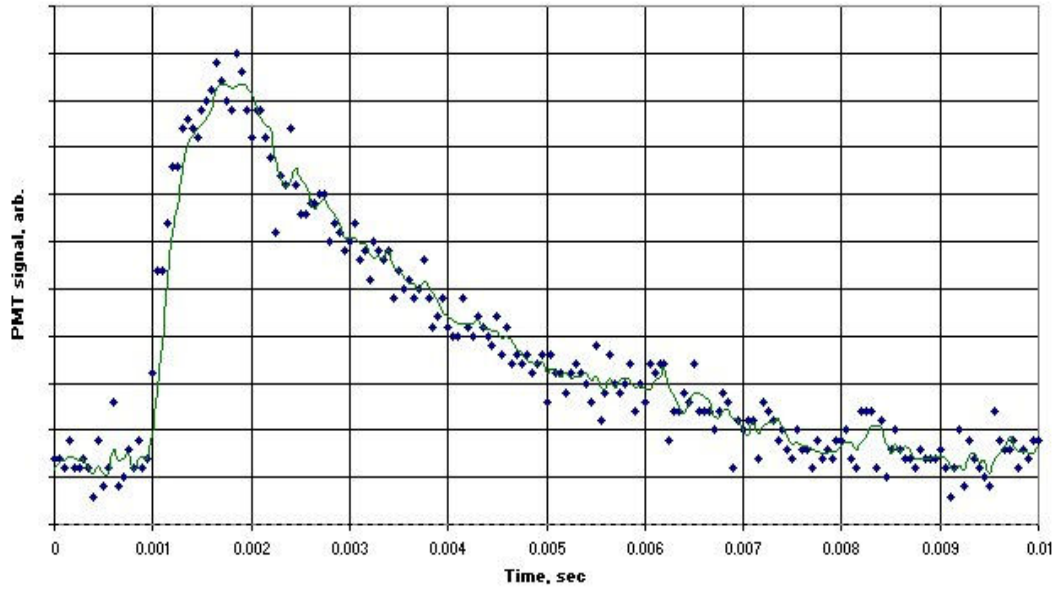

Figure 5-12. Terbium doped borosilicate glass 543 nm fluorescent pulse profile under a 488 nm laser pulse excitation

5.5.3 Dysprosium

The proposed third dopant was dysprosium and had shown a useful sharp excitation peak centred on 453 nm with the corresponding fluorescence around 577 nm. Therefore the 457 nm argon-ion laser line was chosen as the excitation wavelength and an interference filter with transmission peak at 578 nm (10 FWHM) was chosen as the fluorescence filter. 1 ms (FWHM) laser pulses were generated (Figure 5-13) by chopping the laser beam with the mechanical chopper operating at 4 Hz. These pulses were directly pumped into the glass sample to resonantly excite the dysprosium ions and the corresponding fluorescent signals recorded (Figure 5-14). These results indicated dysprosium had a short rise time and a relatively long decay time extending for nearly 15 ms with a FWHM of approximately 7 ms. A summary of all the lifetime results is shown in Table 5-1.

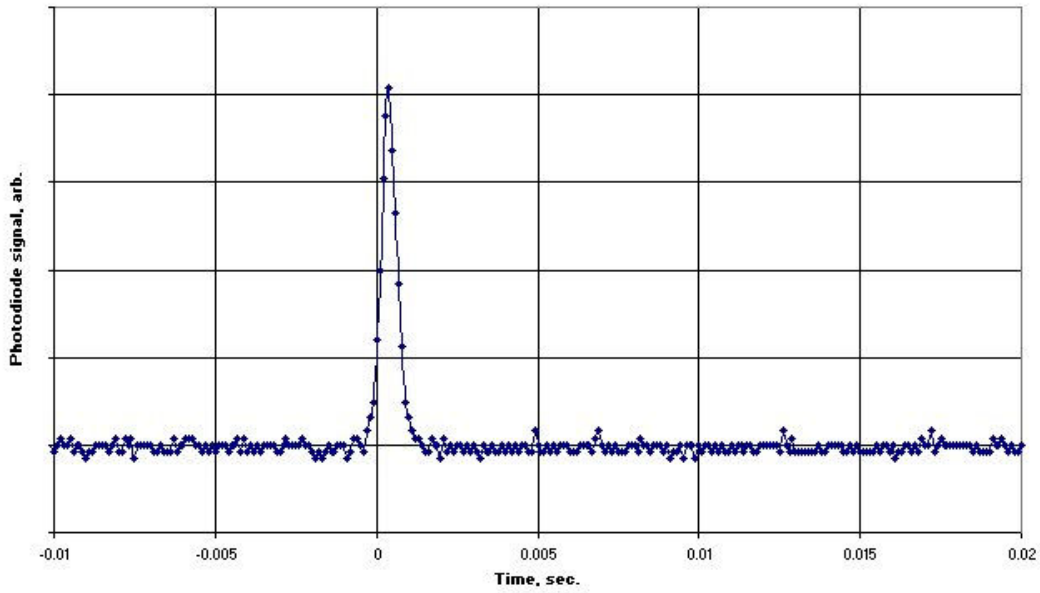

Figure 5-13. A typical 457 nm laser pulse

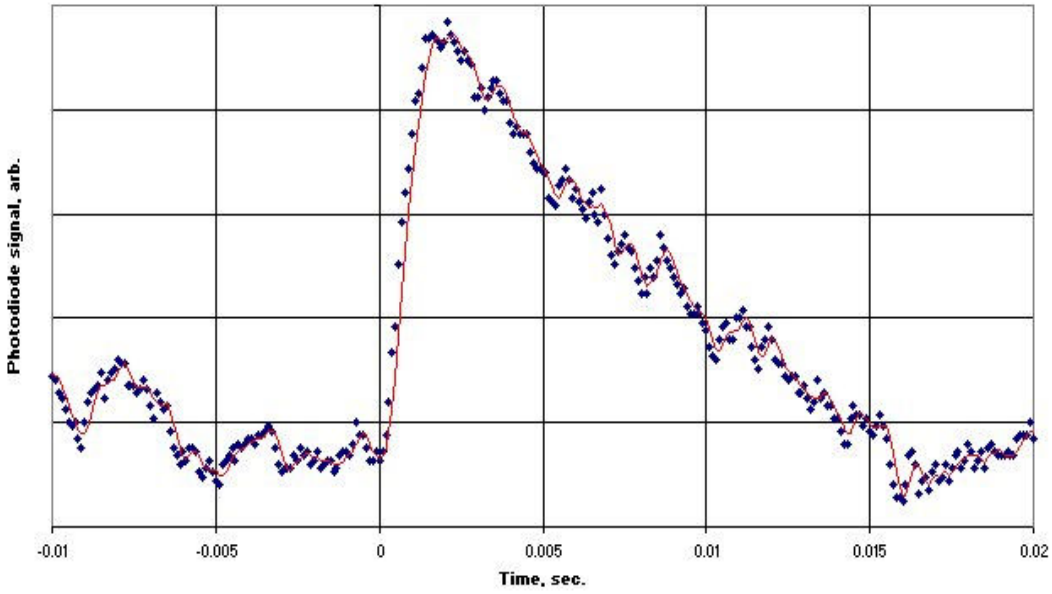

Figure 5-14. Dysprosium doped borosilicate glass 578 nm fluorescent pulse profile under a 457 nm laser pulse excitation

Ion	Excitation Wavelength / nm	Fluorescence Wavelength / nm	Laser Excitation Wavelength / nm	Laser Pulse Lifetime FWHM / ms	Fluorescence Lifetime FWHM / ms
Eu	465	615	465	0.5	2
Tb	485	543	488	0.5	2.2
Dy	453	577	457	1	7

Table 5-1. Summary of the fluorescent lifetime results

5.5.4 Conclusion

In summary, all three dopants in the single doped borosilicate glasses have shown relatively long (greater or equal to 2 ms FWHM) fluorescent lifetimes. Europium and terbium had shown fluorescent pulse widths of nearly 2 ms whilst that of dysprosium was almost 7 ms. This can therefore be used as a clear distinguishing feature of the RE doped borosilicate glass, thus providing higher selectivity and hence higher security to the detector system in comparison with the traditional detection of molecular based dyes.

5.6 DETECTION PRINCIPLE

To distinguish the fluorescence of the doped glasses from other background fluorescing species that could be on the valuable article e.g. white paper and ink, the long lifetimes of the lanthanides were utilised. Since most interfering fluorescence lifetimes are short in comparison to the lanthanide fluorescence, a pulsed excitation signal would produce a pulsed fluorescence of the same frequency, producing an Alternating Current (AC). However, if the pulsed frequency were of a speed where the fluorescence of the lanthanide-doped sample did not have enough time to decay before the next pulse, then a Direct Current (DC) signal was produced. This DC signal could therefore be detected without any AC signal interference by incorporating a low pass active filter. Each part of the detector circuit and holder is discussed below for the initial single channel detector system.

5.7 THE CIRCUIT

The specifications from NCR were for a small, cheap and simple detection system in order to minimise the cost for use in a mass market. Therefore, LEDs and photodiodes were chosen as the excitation sources and detectors respectively. Initially, the detector system was designed to be operated by a battery supply in order to produce a hand-held system. All of the components were supplied by RS components whilst the lenses and filters were from Comar Instruments.

5.7.1 Voltage

The amount of voltage required for the majority of the circuit was 5 V. However, to operate a 5 V regulator (see Figure 5-15) required an input between +2 to +30 V DC. This was supplied from either a 9 V battery or a 9 V-power supply from a wall socket. The 5 V regulator stopped any fluctuation of voltage to protect the circuit. The two capacitors between both the V_{in} and V_{out} to ground (GND) were used to prevent any oscillations due to instability.

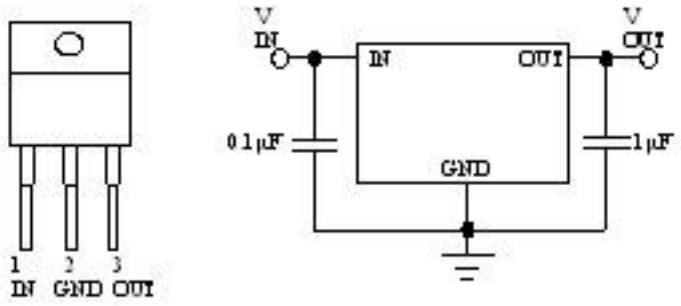

Figure 5-15. 5 V regulator schematic and circuit diagram

However, ±15 V was also required to power the photodiode and amplifier, therefore a DC/DC converter (see Figure 5-16) was used to convert the +5 V from the regulator to produce ±15 V. From these chips the whole circuit was powered.

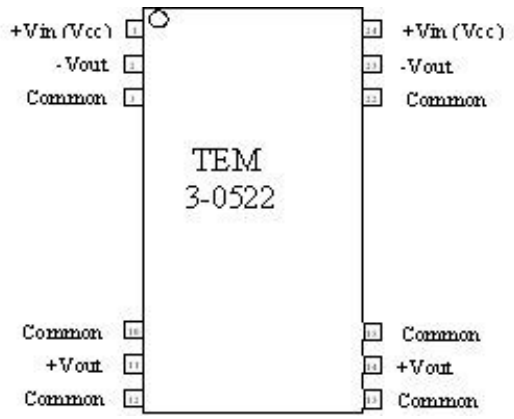

Figure 5-16. Schematic of the 15 V DC/DC Converter

The DC converter did not require any additional components other than wires to connect the +5 V to $+V_{in}$, GND to Common and to take out the ±15 V from $+V_{out}$ and $-V_{out}$.

5.7.2 Timer

Based on the lifetime measurements, a short pulsed excitation with a large duty cycle would remove any background short lived molecular fluorescence whilst still detecting the RE fluorescence. Therefore, to generate a pulse for the LED, a timer was used to set a frequency for the excitation (see Figure 5-17).

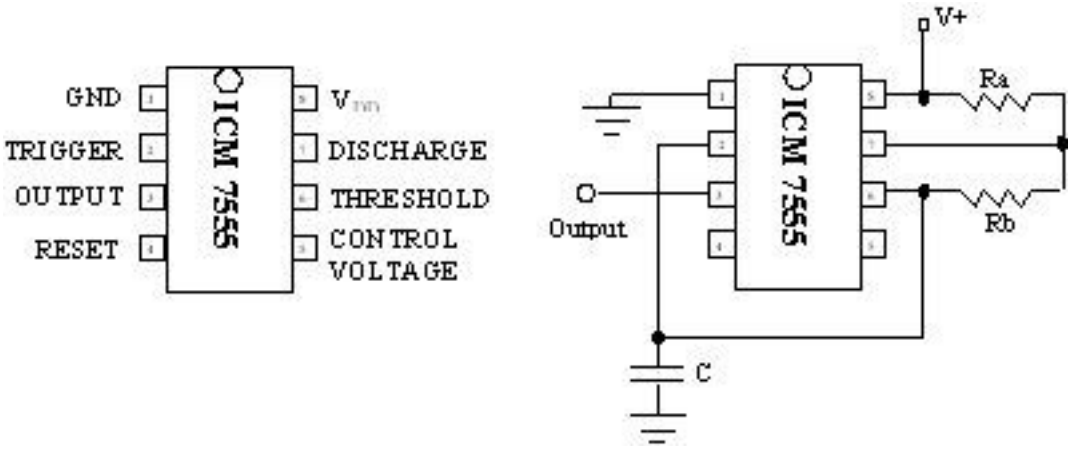

Figure 5-17. Schematic and circuit diagram for the timer

The timer used the +5 V and a GND signal input and by following the equations stated in the accompanying datasheet:

$$f = \frac{1.46}{(Ra + 2Rb)C} \qquad D = \frac{Rb}{Ra + 2Rb}$$

Where:

f	=	frequency of the pulse	=	1.4 kHz
Ra	=	resistance value of resistor a	=	2 kΩ
Rb	=	resistance value of resistor b	=	10 kΩ
C	=	capacitor value	=	47 nF
D	=	duty cycle	=	50 %

A duty cycle of 50 % was required and achieved by having a much larger Rb compared to Ra. This meant that changing the capacitor value could change the timer frequency. For the europium-doped glass, having a capacitor value of 47 nF produced a frequency of approximately 1.4 kHz and produced a DC output signal.

5.7.3 Light Source

Europium-doped glass was selected for initial tests to optimise a single channel detector system due to its strong fluorescence. The LED used was an Ultra blue, wide angle and round LED that emitted a wavelength of approximately 467 nm. This was chosen because it was close to 465 nm, which was a suitable excitation wavelength for the europium-doped glass.

To prevent the LED from being supplied with too much current, an adjustable resistor was placed before the LED from the +5 V supply to reduce the current to approximately 25 mA (see Figure 5-18). Connecting the timer output to the LED via a transistor, that acted as a switch (see Figure 5-19), and the other end to the +5 V, the LED was able to pulse at the frequency set by the timer.

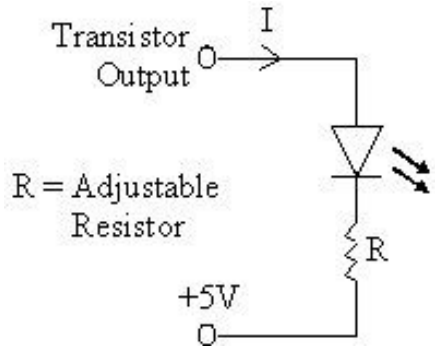

Figure 5-18. Circuit diagram for the LED

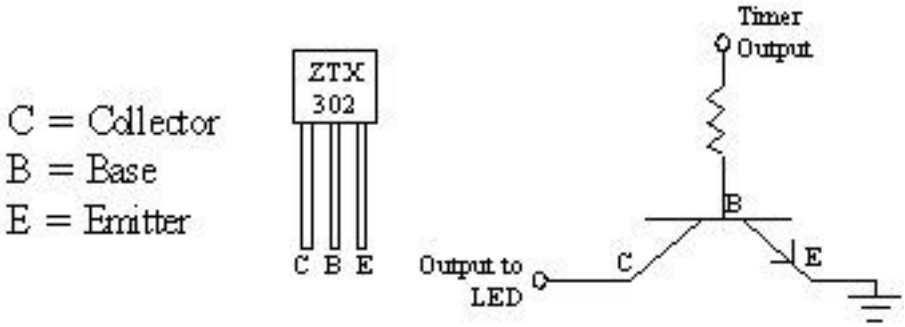

Figure 5-19. Schematic and circuit diagram for the transistor

5.7.4 Detector

The europium-doped sample fluoresced in the red part of the spectrum (615 nm) therefore a photodiode with a good spectral response in this region, was selected (shown in Figure 5-20). The detector required ±15 V and a GND signal to power the diode. With the addition of a 10 MΩ resistor, a 10 times amplification of the output signal was achieved due to the built in amplifier. For initial testing purposes, the detector was designed to be easily repositioned by hand, therefore the diode was attached to a separate circuit board with long wires connecting it to the main circuit.

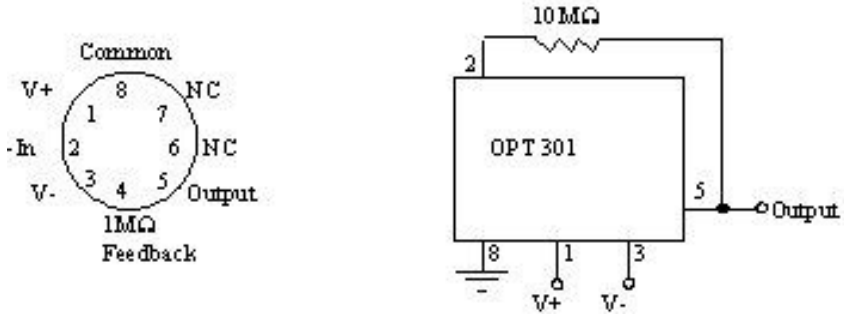

Figure 5-20. Schematic and circuit diagram of the photodiode

5.7.5 Amplifier

The output from the photodiode was too weak to be detected when crushed glass was used; therefore the signal needed to be amplified (Figure 5-21). The amplifier used produced a gain of up to 1000 times (Table 5-2) without adding any or very little, noise.

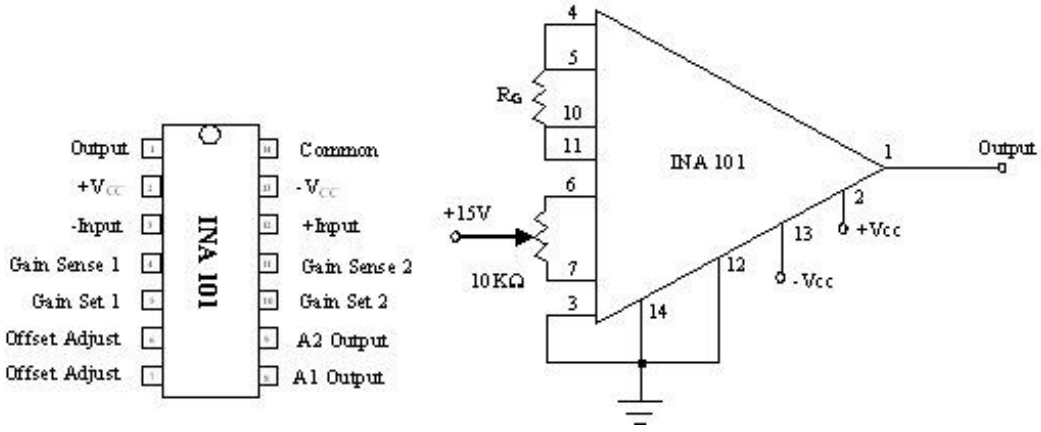

Figure 5-21. Schematic and circuit diagram of the amplifier

Gain	R_G / Ohms
1	> 40 K
10	> 4 K
100	> 400
1000	> 40

Table 5-2. Resistor values to set the gain for the amplifier

The addition of a low pass active filter (Figure 5-22) before the signal reached the amplifier reduced the AC signal so only the europium fluorescence was amplified.

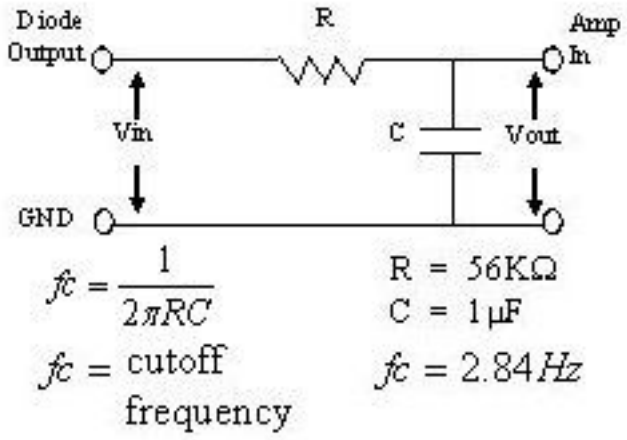

Figure 5-22. Circuit diagram of the low pass active filter

The low pass filter reduced any signals above a frequency of 2.84 Hz therefore removing the majority of the AC signal [107]. This effect become greater as the frequency increased whereas the signal remained the same below the cutoff frequency leaving the DC signals unaffected. Since the excitation frequency was 1.4 KHz, this was easily removed from the background. Furthermore, this addition did not slow down the response time of the detector in comparison to without the filter.

5.7.5.a Signal output

The output signal from the amplifier, without any doped glass present, gave a negative reading. Although this was not a problem, it did mean for future work the output could not be connected to a PC via a data logger such as a PicoLog ADC 11, because the PicoLog could not handle negative numbers. To overcome this problem, a potentiometer was added to produce an offset adjust to raise the blank reading to an approximately positive value (Figure 5-23).

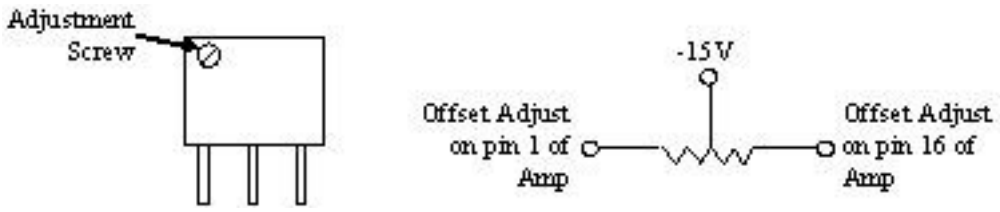

Figure 5-23. Schematic and circuit diagram of the potentiometer

The potentiometer varied the voltage by changing the resistance in the circuit when the screw, shown on the schematic in Figure 5-23, was turned. This allowed a simple method for zeroing the system quickly.

5.7.6 Single Channel Circuit

All of the above components were then combined together to form a PCB design using Number One Systems Easy-PC for Windows version 4.0.4 software. The resulting PCB design is shown in Figure 5-24. Each of the components was soldered to the board according to their individual descriptions mentioned above. This detector was capable of detecting a sample of europium doped glass that was approximately 5 mm in diameter with the output displayed on a digital oscilloscope. All the required components and their required values are shown in Table 5-3.

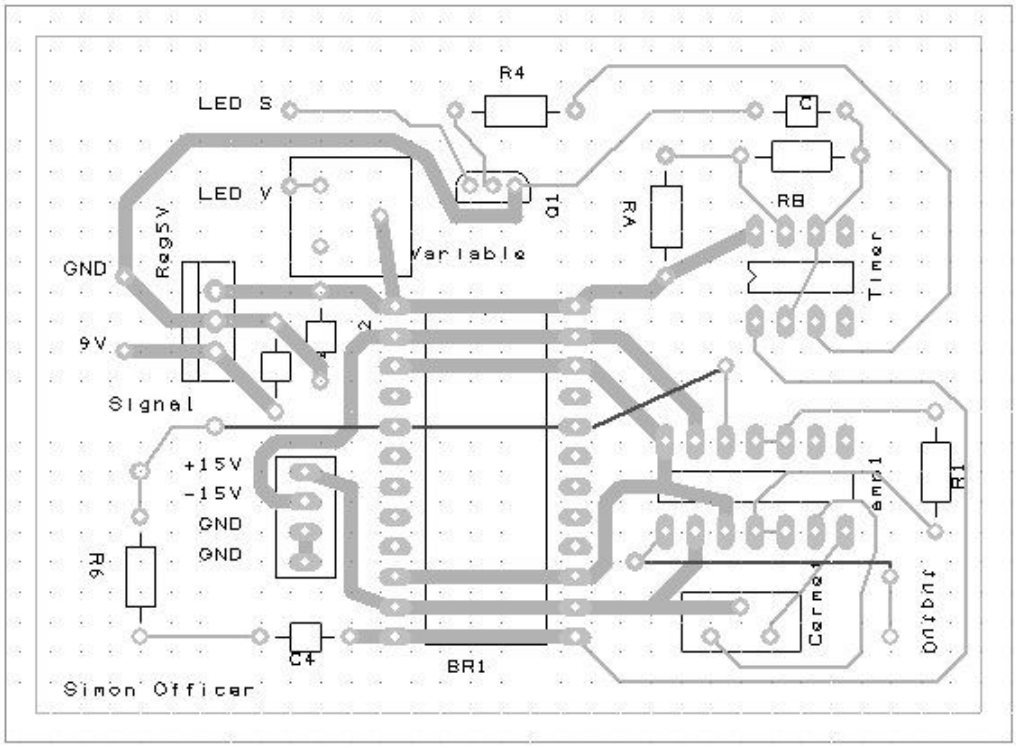

Figure 5-24. Schematic of the PCB design for a single channel detection system

Component	Name	Value/Model
amp1	Instrumentation amplifier	INA 101
BR1	DC/DC converter	TEM 3-0522
C	Capacitor	47 nF
C1	Capacitor	100 nF
C2	Capacitor	1000 nF
C4	Capacitor	1000 nF
Cermet	Cermet trimmer	200 Ohms - 1K Ohm
Q1	Transistor	ZTX 302
R1	Resistor	40 Ohm
R4	Resistor	12K Ohm
R6	Resistor	56K Ohm
RA	Resistor	2K Ohm
RB	Resistor	10K Ohm
Reg5V	5V regulator	MIC 294OA
Timer	Timer	ICM 7555
Variable	Variable resistor	0-220 Ohm

Table 5-3. Table of single channel detector components and respected values

5.8 OPTICS AND DETECTOR HOLDER

Once the circuit was finished, the detector holder had to be designed and produced to test the system. The design of the holder involved having the light source entering from one side and the detector at the other. Having the holder cut at 45° meant the detector could be flush on the article surface and reduce any background light from entering. The LED could then excite the sample and the fluorescence be detected by the photodiode. For improved sensitivity of the detector, lenses were added to focus the LED excitation onto one spot on the surface and to focus the fluorescence light onto the photodiode surface. Initial designs were made out of wood in the workshop before an optimised design was built in aluminium with the draft design shown in Figure 5-25. All design work was drawn out using EDS Solid Edge version 11 software.

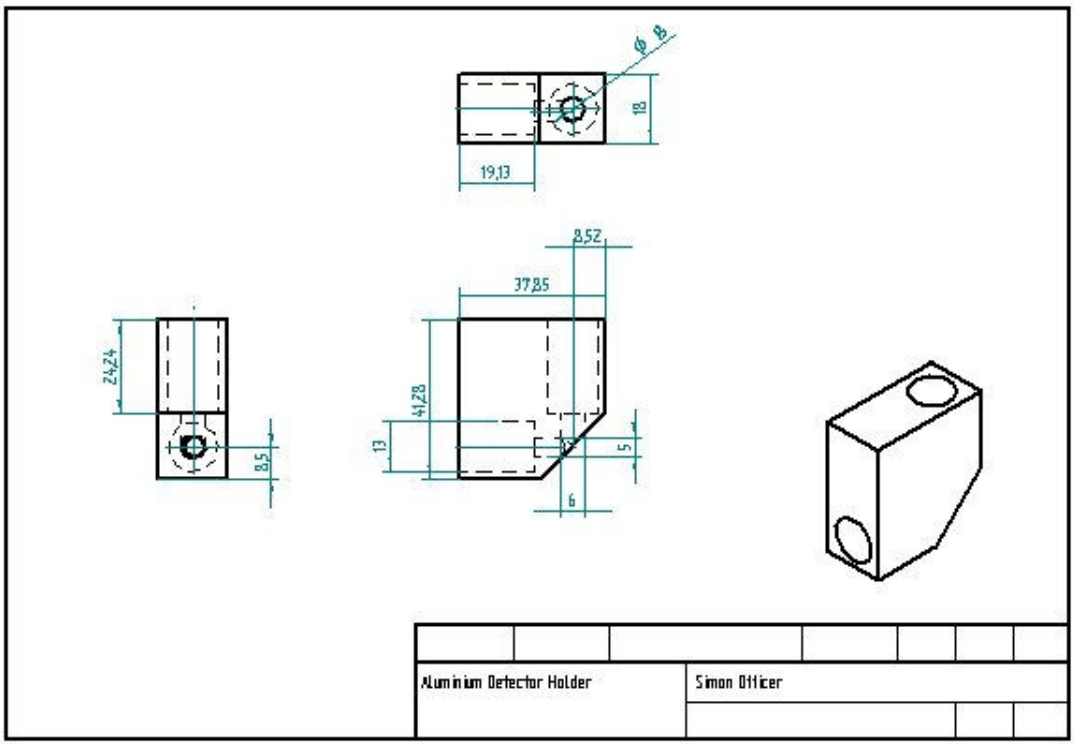

Figure 5-25. Draft view of the aluminium single channel detector holder

A 467 nm (blue) filter was placed in front of the LED to select the correct excitation wavelength of europium (465 nm) previously found from the spectrofluorometer measurements, whilst a 620 nm (red) filter was placed before the photodiode so only the red europium fluorescence (615 nm) was detected to reduce any interfering wavelengths.

An exploded view showing all the components in their correct orientation is shown in Figure 5-26. The LED and diode holders were made of aluminium so that the LED and photodiode could be held in place in the tubes of the detector holder. A small circuit to connect the photodiode pins for its power and the output signal was made and inserted into a metal box. This circuit was then attached to the main circuit, described above, for the amplification of the signal and for supplying the power for the photodiode. A completed view of the detector is shown in Figure 5-27 with all the components inserted. This detection system was able to detect Eu doped glass pieces but further modification was required to detect micron sized particles; however this work is not covered here as it was carried out by Dr Prabhu.

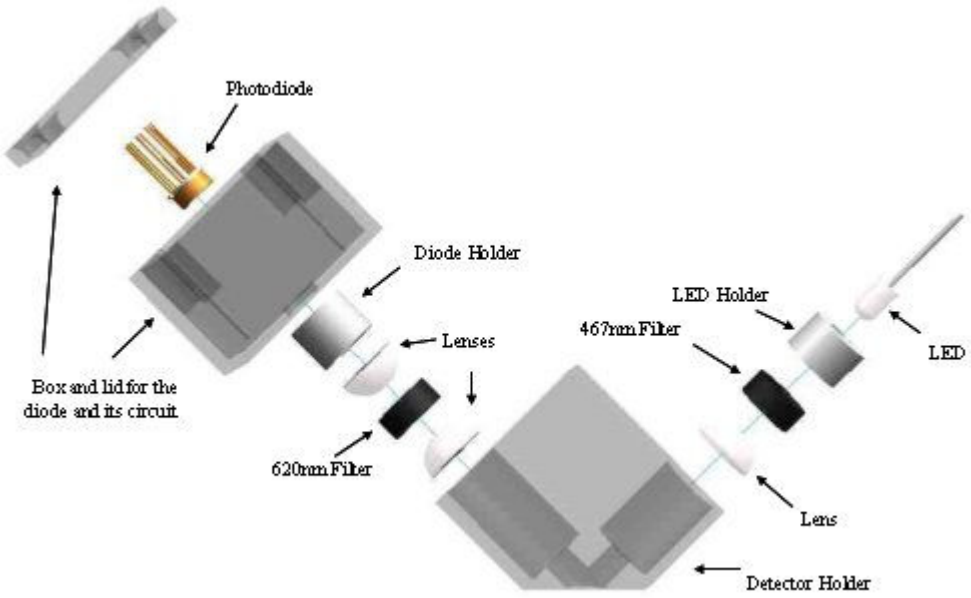

Figure 5-26. Labelled exploded view of the single channel detector holder

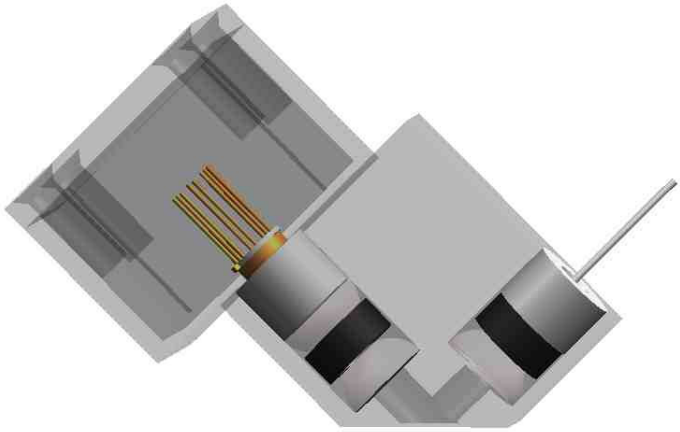

Figure 5-27. See through picture of the assembled single channel detector

5.8.1 Multi-Channel Detector System

Individual channels would be required for each different RE dopant selected and the relevant filters and excitation wavelengths selected based on their spectral characteristics. One design possibility for this multi-channel detector system would be to have a linear arrangement of single channel detector heads as shown in Figure 5-28. This arrangement has four channels with different LEDs and filters (the box for the detector is not shown for clarity). The circuit would have to be altered to deal with four channels as an increase in current was required in order to control four LEDs. Greater selectivity to distinguish between the REs may be achieved by altering the timer signal based on individual fluorescent lifetimes of each dopant, therefore requiring more components on the circuit to tailor the timer signal.

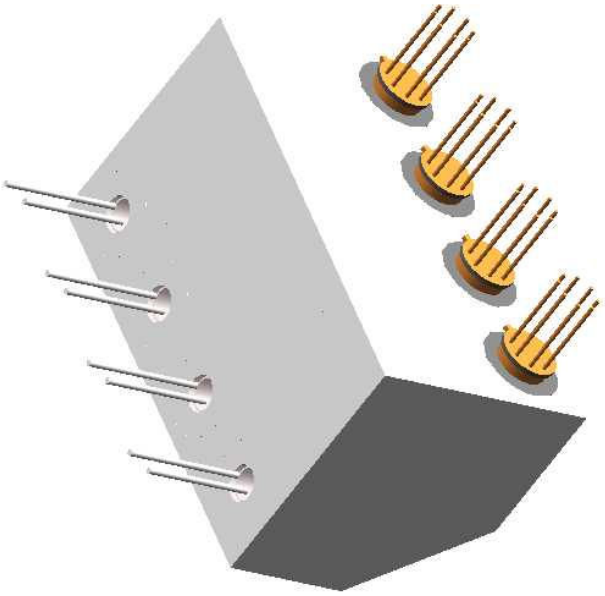

Figure 5-28. Illustration of a possible multi-channel detector system

5.9 DETECTOR SYSTEM CONCLUSION

As this work was only to produce an initial detection system, further work and optimisation was carried out by Dr R Prabhu in collaboration with this work and is not reported here. However, this work had successfully produced an initial detector system that could selectively detect 5 mm diameter europium doped glass, from background molecular fluorescence, that could then be taken further. It can be noted that a multi-channel detector system has now been constructed that can detect samples down to a diameter of 45 μm and that this was based on the initial work and detection principles reported here.

5.10 INCORPORATION OF DOPED GLASS BEADS INTO/ONTO PAPER

NCR had proposed that one of the aims of this work was to be able to read a fluorescent barcode made up of RE doped glass beads. Therefore, the compatibility of the fluorescence detector head with the RE doped glass beads buried inside and attached onto the surface of paper was investigated. The first step to make these barcode lines involved crushing europium doped glass pieces with a mortar and pestle. These doped beads were then incorporated inside and onto the surface of freshly prepared wet paper. The paper was made using a craft paper making kit purchased from The House of Crafts Ltd., Leicester.

Paper pulp in water was prepared by soaking small craft paper pieces in boiling water and stirring for an hour in a glass beaker. A paper bath was then prepared by mixing the pulp in a bucket containing water to get an even distribution. To deposit paper from the mixture, a circular mesh (around 55 mm diameter) was made by fixing a nylon mesh to a circular ring. Then the mixture was filtered through the mesh to achieve a sufficiently thick layer of paper on the mesh. Since the intention was to detect barcodes with the detector head, a mask to create a rectangular pattern (thick or thin lines) was made. This mask was made from thin aluminium foil by cutting out rectangular patterns with a sharp knife. The mask pattern contained three rectangular openings (two thin and one thick) and is shown in Figure 5-29 with the dimensions in mm.

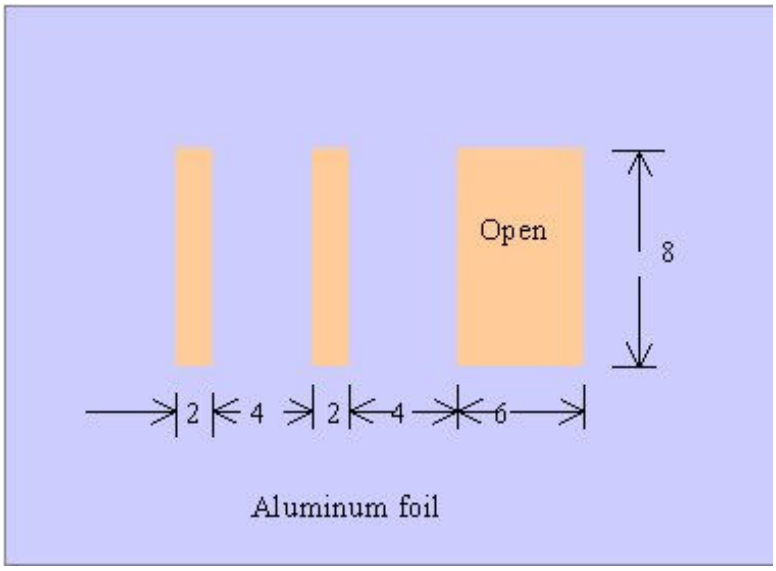

Figure 5-29. Mask made from aluminium foil with the orange section showing the opening

A further application possibility was to print the beads through an ink jet printer directly onto an article. However, no suitable ink jet printer could be found within the project time scale therefore screen printing was chosen as another option. Furthermore, this method would allow larger particles to be used, as the mesh size of the screen was much larger than the nozzles of a printer (ink jet print heads are usually less than 5 μm in diameter). Using screen printing however, particle sizes between 45 μm and 75 μm could pass through the screen mesh without any problems and would also increase the signal intensity for the detector system in comparison with using 5 μm paricles.

5.10.1 Incorporation of Doped Beads Onto Paper

To make the paper with glass bead barcodes on the paper surface, europium doped glass beads were sprinkled over the wet paper through the mask. The paper was subsequently pressed between two metal blocks for better adherence of the beads onto the paper and to obtain a flatter surface. After flattening, the paper was left to air dry for approximately 12 hours.

5.10.2 Incorporation of Doped Beads Into Paper

Paper with the glass beads incorporated under the paper surface was prepared in two stages. First, rectangular patterns of beads were made on the wet paper as explained above. Over this wet paper, another layer of paper was deposited by filtering the pulp mixture, therefore a thin layer of glass beads could be incorporated inside the paper. After pressing and drying the paper, the paper sheets were removed from the mesh and tested for their compatibility with the detector head.

5.10.3 Screen Printing

A beginner's screen printing kit (see Figure 5-30) was purchased from Specialist Crafts in order to test its applicability. However, the inks supplied with the kit were all bright water based colours with a very high viscosity. Therefore, different inks had to be sourced.

Figure 5-30. Picture of the purchased screen printing kit

White water-based and white acrylic inks had been sourced which would reduce any spectral interference making detection simpler. Additionally, the acrylic ink would adhere to metals and plastics allowing the security label to be used as a barcode on NCR equipment (for example), whereas the water based ink would only be suitable for paper and card.

Ideally a transparent ink would be used to reduce any interference and make the label more covert. 3M Scotchprint did have a selection of screen printing inks, including a transparent series [108], however when queried, only approved Scotchprint graphics manufacturers were authorised to use it. There also appeared to be a transparent overcoat varnish that is used to extend the lifetime of the screen print by covering the design with this protective coating. This could be suitable for future work.

5.10.3.a Distribution of particles

A homogeneous layer of particles would be required on the screen print, therefore the distribution and dispersion of the particles throughout the ink was very important. For the dispersion of glass spheres a solution of 0.1 % Calgon was used [109]. If a sample of glass powder was first mixed in a solution of calgon, then this solution can be mixed with the ink as two liquids. This would increase the mixing process instead of trying to add the powder to the ink directly. Furthermore, the dispersion of the powder by the Calgon reduced the agglomeration of the powder when added to the ink producing a more homogeneous distribution.

5.11 TESTING BEAD DOPED PAPER COMPATIBILITY WITH THE IN-SITU DETECTOR

The compatibility of the detector system with the doped glass was checked with a fixed detector head and moving paper. The glass bead doped papers were attached to an X-Y scanning stage (attached to the LISFM set-up) with the detector head positioned one millimetre above the paper. X-Y translation was controlled using the LISFM software and detector signals were transferred to the computer via the Picolog ADC 11 attached to the printer port. The scanned image, of the beads doped onto the paper surface, is shown in Figure 5-31 as a 3D plot of the fluorescent intensity variations over the paper (displacement [x,y] vs. fluorescent intensity [z]). The red line shows the cross sectional intensity variations. A similar response from the beads doped into the paper is shown in Figure 5-32.

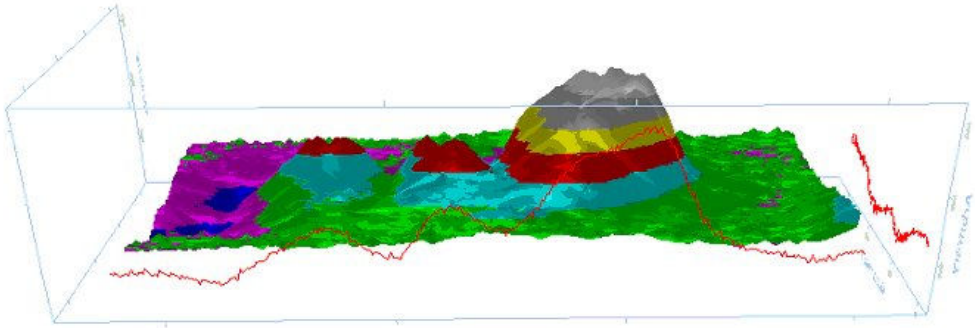

Figure 5-31. Scanned image of glass beads doped onto paper

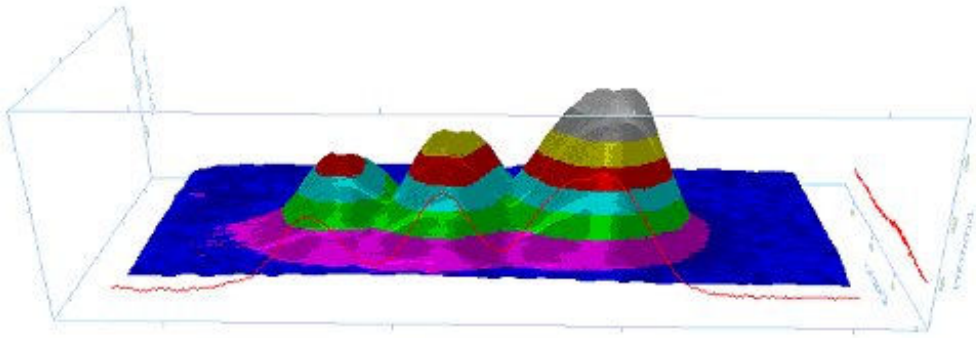

Figure 5-32. Scanned image of glass beads in paper

As demonstrated in Figure 5-31 and Figure 5-32, the barcodes could be detected using the detector head (from the separate peaks) but the spatial resolution and background noise levels were not ideal as the peaks merged together.

It was observed that the beads doped onto the paper surface were easily detached if the paper was bent as seen in Figure 5-31 where some peaks appeared attenuated from the other peaks because glass beads have fallen off. In order to overcome this problem barcode lines using beads mixed in printing ink and glue were printed. A test was carried out to check the attenuation of fluorescent signals due to the printing ink. Two identical lines (1.5 x 11 mm separated by 2.5 mm), one with bare europium doped glass beads and another with europium doped glass beads in black ink were made. These lines were scanned using the LISFM (with a green laser diode as the source and a photodiode as the detector) and the signal levels recorded as shown in Figure 5-33. The fluorescent signal from glass beads on the paper was strong but the same signal from the beads in ink was attenuated due to the absorption of the light by the ink.

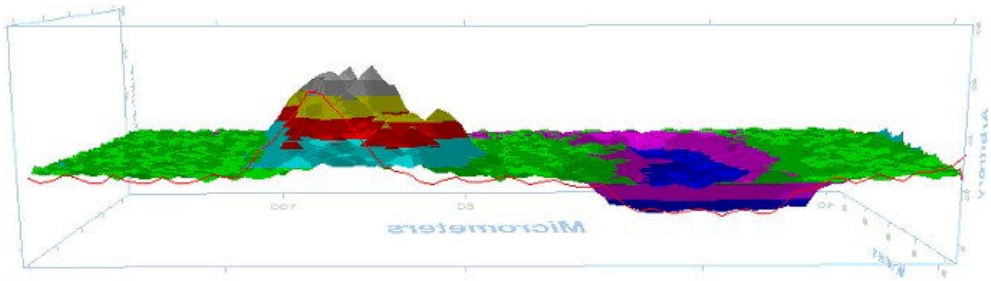

Figure 5-33. LISFM scanned image of barcode to demonstrate the effect of printing ink

An optically transparent glue layer was tested to bond the beads to the paper. Optically transparent Loctite superglue was stamped onto the paper (1.5 x 11 mm separated by 2.5 mm) before the beads were sprinkled over it. This produced good binding of the first layer of beads but not for subsequent layers. In addition to this, the superglue was drying fast (in a few seconds) and the stamping of barcodes was difficult. The signal response from this is shown in Figure 5-34.

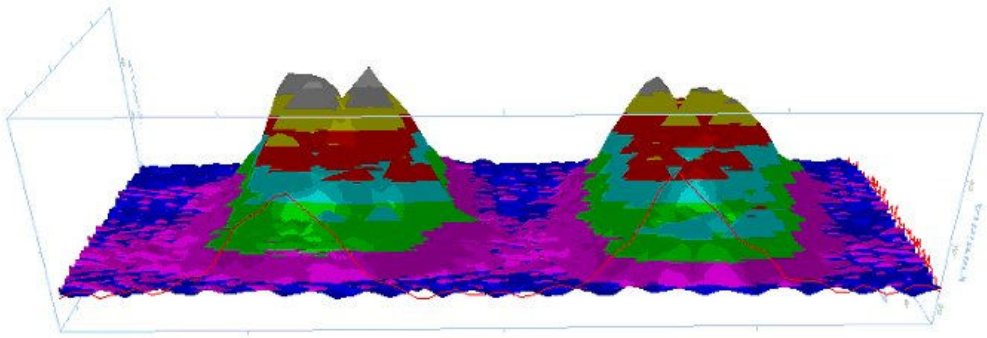

Figure 5-34. LISFM scanned image of barcodes made by stamping Loctite glue over paper and sprinkling europium doped glass beads on it

To increase the bonding, it was decided to use an optically transparent, UV curable glue (Loctite 350) to mix the beads and use a photolithographic or painting technique to make thin barcode lines. The barcodes were made with a thin layer of bead mixed glue (1:1 ratio by weight of 3 mol % europium doped glass beads to UV glue) painted onto a piece of paper before the glue was selectively cured with UV light passing though the aluminium mask for one minute. The uncured glue was then removed from the paper by washing it with acetone to leave only the UV cured barcode. The bonding of these beads was good and provided sharp edges for the barcodes which can be seen from the LISFM scanned image shown in Figure 5-35.

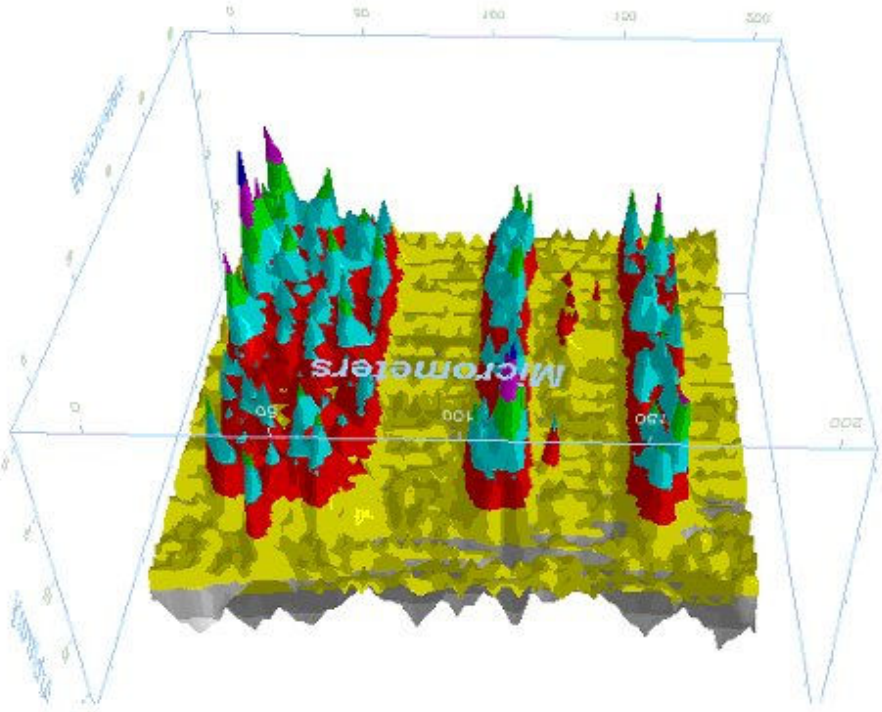

Figure 5-35. LISFM scanned image of photolithographyically made barcode

5.12 APPLICATION AND TESTING OF DOPED GLASS BEADS WITH THE DETECTOR SYSTEM CONCLUSION

The printing application of the RE doped beads to paper was demonstrated by various techniques. Results from the initial detector system were promising and allowed work to be carried out to optimise the intensity and selectivity response of the detector. If a suitable transparent ink could be sourced, it would have been tested to apply the beads to different surface materials such as metals. Ink jet printing would also be advantageous if a suitable printer could be sourced as this would increase the possible applications of the beads as a point of issue security label e.g. printing the label directly onto concert tickets at kiosks. However, more work would have to be carried out in order to distribute the beads throughout the printing ink and to maintain a reproducible output of beads.

CHAPTER 6 - INVESTIGATION AND SPECTRAL CHARACTERISATION OF MULTI-ION DOPED GLASSES

6.1 DOUBLE DOPED GLASSES

Following the successful results for the single rare earth doped borosilicate glasses europium, terbium and dysprosium were chosen to investigate their suitability in double rare earth doped glasses. Ideally the rare earth fluorescence signals should not overlap each other to allow a more secure fluorescence signal to be produced. Combinations of Eu-Tb, Eu-Dy and Dy-Tb were produced in order to account for all of the possible combinations of the three single dopants. Spectral characterisation of the glasses was carried out in order to determine whether the peaks could be resolved spectrally and whether there were any interactions between the dopants. If these were successful, the ability to produce spectrally encoded samples with their own unique fluorescence fingerprint would produce a very secure tag that would be very difficult to replicate.

6.2 EUROPIUM AND TERBIUM

A 1:1 ratio of europium to terbium doped borosilicate glass was produced. The concentration selected was 3 mol% for each dopant to compare their relative intensities together. The glass was produced following Method 5 (section 3.2.1).

6.2.1 UV-Vis Absorption

The absorption spectrum of the europium-terbium doped glass is shown in Figure 6-1. Only the range between 350-700 nm is shown as this range covers all the relevant peaks found from the single doped glass results. The spectrum shows the strong absorption peaks from europium at both 395 nm and 465 nm and two relatively weak absorbance peaks from terbium at 378 nm and 485 nm. Furthermore, as the terbium absorbance was weak, the second derivative spectrum is shown in Figure 6-2.

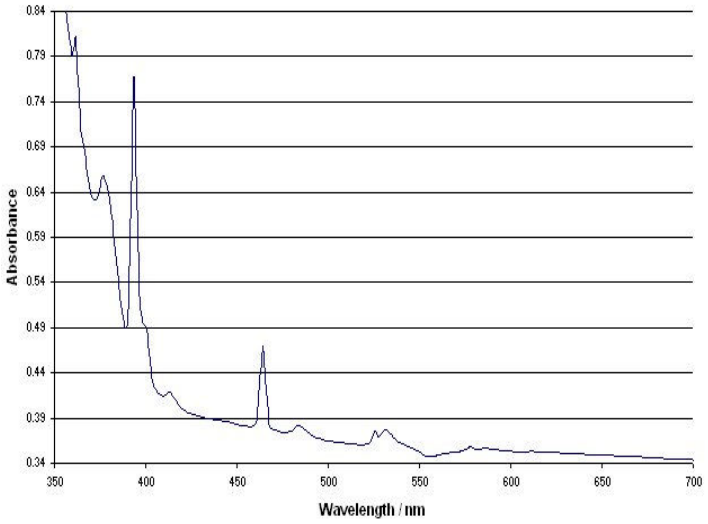

Figure 6-1. Absorption spectrum of the 3Eu-3Tb doped borosilicate glass

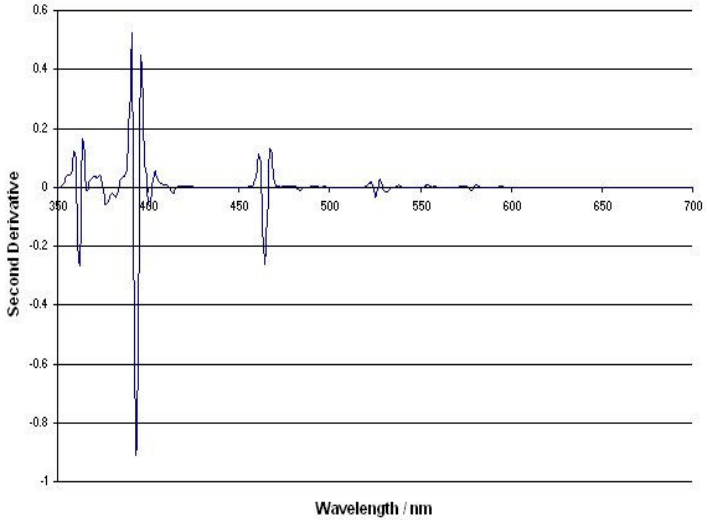

Figure 6-2. Second derivative absorption spectrum for the 3Eu-3Tb doped borosilicate glass

From the above results, it was easy to see that the absorption from the terbium was much lower than the europium absorbance, with an expanded view shown in Figure 6-3. Consequently, this would imply that the terbium fluorescence signal would be much weaker than the europium and could cause problems later on.

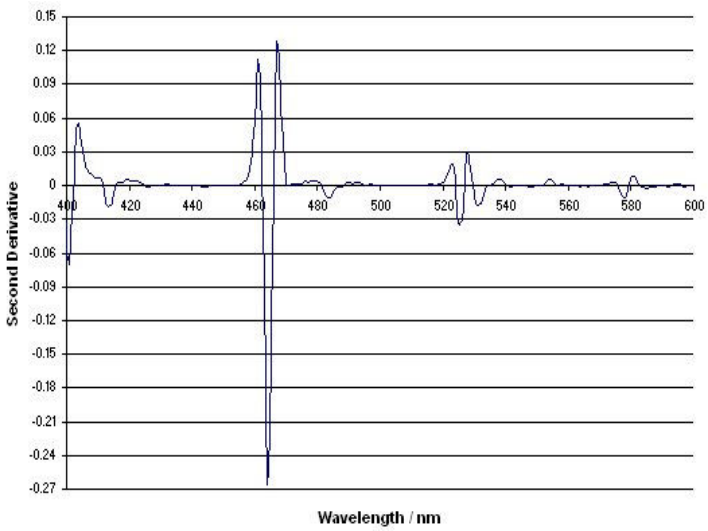

Figure 6-3. 400-600 nm range second derivative spectrum for 3Eu-3Tb doped borosilicate glass

6.2.2 Fluorescence

The fluorescence spectrum for the Eu-Tb doped glass is shown in Figure 6-4 with a table of all the transitions in Table 6-1. The majority of the peaks found in the single Eu and Tb doped glasses were present. However, a number of the peaks were now merged together especially in the UV range resulting in some wider peak widths. Furthermore, because the terbium absorption was much weaker than europium, it was expected that some of the terbium peaks might not be strong enough to be detected.

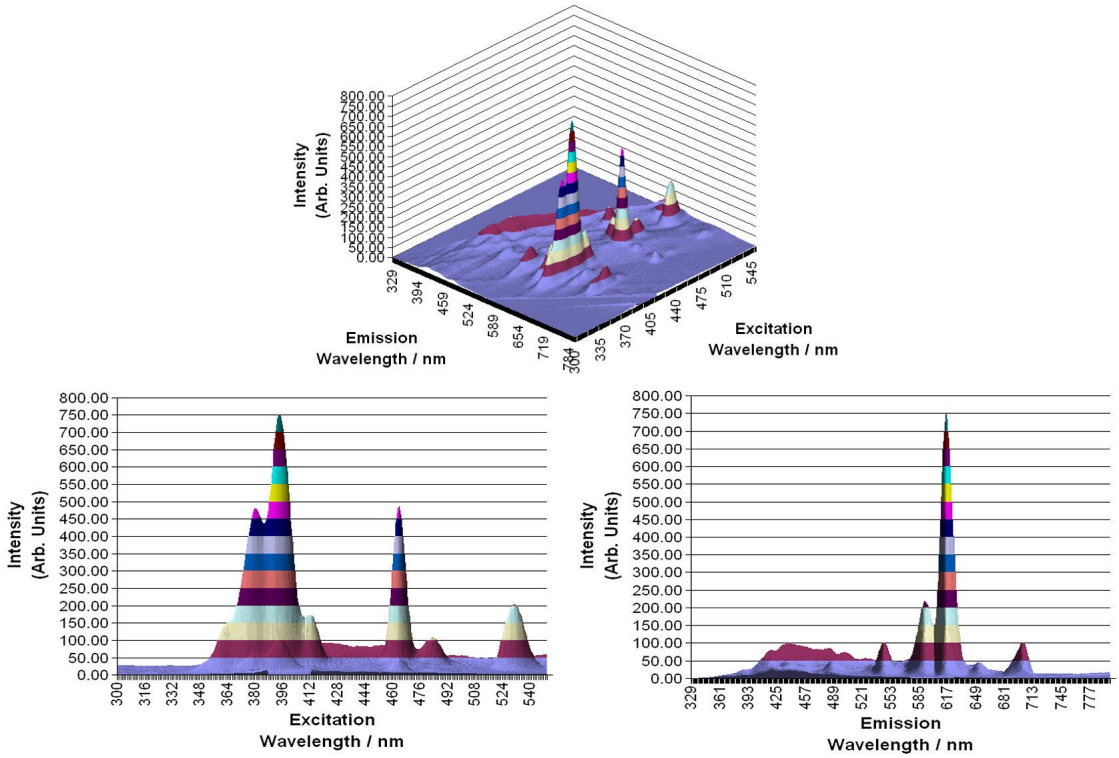

Figure 6-4. Fluorescence spectrum of 3 mol% Eu^{3+} and 3 mol% Tb^{3+} doped borosilicate glass

				Peak width			
Peak label	Excitation Wavelength / nm	Emission Wavelength / nm	Intensity	Ex Wavelength		Em Wavelength	
Eu	364	615.5	152.19	354-366	12	602-638.5	36.5
Tb	375	414	51.27			401.5-425.5	24.0
Tb	375	436.5	43.39			428-445	17.0
Tb	375	488.5	50.36	359-392	33	474.5-509.5	35.0
Tb	375	546	99.30	340-393	53	530.5-563	32.5
Eu	380	615.5	482.79	368-385	17	602-638.5	36.5
Eu	381	592.5	145.10	367-384	17	568.5-601	32.5
Eu	381	652.5	31.29	357-385	28	642-671	29.0
Eu	381	702	66.25	367-384	17	675.5-719	43.5
Tb	386	457.5	38.63	367-392	25	455.5-470.5	15.0
Eu	393	702	101.44	385-407	22	674.5-720.5	46.0
Eu	394	591.5	218.94	386-407	21	566-602	36
Eu	394	616	752.67	386-407	21	602-640.5	38.5
Eu	396	653	44.36	385-407	22	642-671	29.0
Tb	408	487.5	43.80	395-416	21	478.5-505	26.5
Eu	410	653	20.46	409-419	10	644-667	23
Tb	411	546	45.95	395-422	27	531.5-556.5	25
Eu	412	701.5	27.81	409-423	14	678.5-716.5	38
Eu	413	591	76.37	408-422	18	573.5-602	28.5
Eu	413	615	173.37	408-420	12	602-638.5	36.5
Tb	455	547.5	28.55	446-465	19	535.5-558.5	23.0
Eu	463	593.5	128.05	454-473	19	570-600.5	30.5
Eu	463	652	44.32	455-474	19	644-674.5	30.5
Eu	463	701.5	52.05	453-473	20	678.5-718.5	40.0
Eu	464	615.5	487.69	454-473	19	602-640.5	38.5
Tb	483	589.5	46.27	474-498	24	571.5-602	30.5
Tb	483	616.5	108.68	475-495	20	604-634.5	30.5
Tb	484	545.5	101.88	469-498	29	531.5-566	34.5
Tb	484	700	20.23	477-494	17	693.5-714.5	21
Eu	529	656	19.82	519-540	21	644-667	23
Eu	531	615.5	204.31	519-544	25	602-638.5	36.5
Eu	531	702	33.29	518-543	25	680.5-718.5	38.0
Eu	532	589	64.98	518-542	24	573.5-600.5	37
Eu	577	701	13.64	572-595	23	682.5-713	30.5
Eu	582	613.5	64.46	568-585	17	606-634.5	28.5
Eu	582	650	12.04	569-587	18	644-671	27

Table 6-1. Table of all the fluorescence peaks found for the 3Eu-3Tb doped borosilicate glass

6.2.3 Discussion

A comparison has also been made for the strongest peak in the UV and the visible region in the single doped glasses with the corresponding peaks found in the double doped glass in Table 6-2.

				Peak Width		
Glass	**Ex / nm**	**Em / nm**	**Intensity**	**Ex / nm**	**Em / nm**	**Ratio**
3 mol% Eu	393	615.5	768	22	34.5	1.60
	465	615.5	479	22	32.5	
3 mol% Tb	375	546	382	31	36.5	1.91
	483	545	200	27	36.5	
3Eu-3Tb	394	616	753	21	38.5	1.54
	464	615.5	488	19	38.5	
	375	546	99	53	32.5	0.97
	484	545.5	102	29	34.5	

Table 6-2. Comparison of the strongest peak in the UV and visible range in the single doped and double doped glasses

Analyses of the ratios in the above table indicated a change in the terbium peaks had occurred. This change resulted in the ratio of 1.91 dropping to 0.97 from the single to the double doped glass respectively. If there were no interactions between the dopants and or between the dopant and glass matrix, then these ratios should remain constant as shown with the europium ratio; however, now the visible peak for terbium at 484 nm was larger than the 375 nm peak. This could be explained by the appearance of a peak at 483 nm excitation and 616.5 nm emission as this peak was not present in either of the single doped glasses. There was a peak in the terbium single doped glass at 483 nm excitation and 622.5 nm emission but this was less than $1/10^{th}$ the intensity (30) of the 375 nm/546 nm peak in the terbium glass. This new peak had an intensity of 109 in the double doped glass which was stronger than any of the terbium assigned peaks. Therefore, as 483 nm is a terbium absorption wavelength and 616.5 nm is a europium emission wavelength, this would appear to be the consequence of an energy transfer between terbium and europium. This shift with multi-doped beads can be used to advantage to increase the number of changeable variables for encoding.

Figure 6-5 shows three single excitation scans to produce an emission of 615 nm in the single Eu, Tb and double doped Eu-Tb glasses. The spectra showed the 464 nm and 531 nm excitation peaks from the europium in both the double doped and the single europium doped glasses, which were missing in the single terbium doped glass. However, the peak at 483 nm only appeared in the double doped glass and not in either of the single doped samples. Therefore, this peak seems likely to be due to the energy transfer between terbium and europium. According to Joshi [110], terbium and europium have an electrostatic interaction with each other causing the terbium emission to decrease and the europium to increase. The energy from the terbium level $^5D_4$ (484 nm excitation) relaxes to the europium level of $^5D_0$ non-radiatively through $^5D_1$ as this energy level lies lower than that of the $^5D_4$ and the difference in energy being absorbed by the host. This resulted in an emission peak at approximately 615 nm ($^5D_0$-$^7F_2$) and a reduced emission from terbium at 545 nm ($^5D_4$-$^7F_5$). This was confirmed by the results shown here.

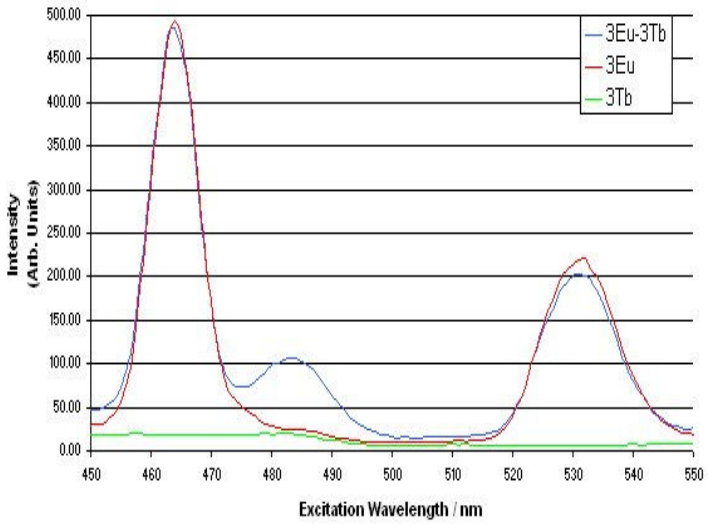

Figure 6-5. Excitation wavelengths for 615 nm emission in single Eu, Tb and double Eu-Tb glasses

To further analyse this transfer, the emission spectra for 484 nm excitation is shown in Figure 6-6 with a closer look in Figure 6-7. These showed the 3Eu doped glass had no emission peaks at 545, 591, 650 or 700 nm but very weak emission peaks at 582 and 619 nm when the close up spectra was analysed. This meant the peaks at 545, 589 and 623 nm were solely due to the terbium ions. However, in the double doped glass, peaks at 545, 590, 615.5, 652.5 and 700 nm were all present and related to the transitions $^5D_4$-$^7F_5$ (Tb), $^5D_0$-$^7F_1$ (Eu), $^5D_0$-$^7F_2$ (Eu), $^5D_0$-$^7F_3$ (Eu) and $^5D_0$-$^7F_4$ (Eu) respectively. These results proved that terbium was transferring energy to the $^5D_0$ level of europium causing emission at 652.5 and 700 nm to appear in the Eu-Tb glass. Furthermore, the 589 nm and 623 nm

peaks in 3Tb shifted to 590 nm and 615.5 nm respectively, which signified an energy transfer from Tb to Eu. A similar investigation could have looked at the 375 nm excitation (another terbium excitation wavelength); however, this peak overlapped the 381 nm excitation of Eu that would emit all the europium wavelengths mentioned above and mask any effect due to terbium.

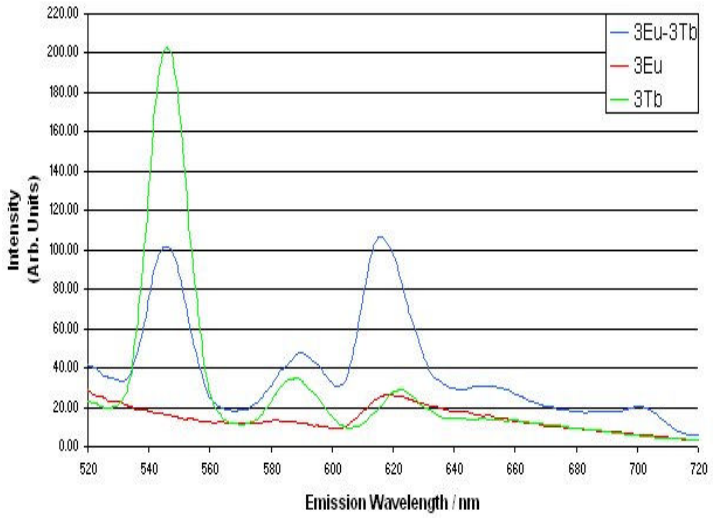

Figure 6-6. Emission spectra comparing the single europium, terbium and double doped glasses under 484 nm excitation

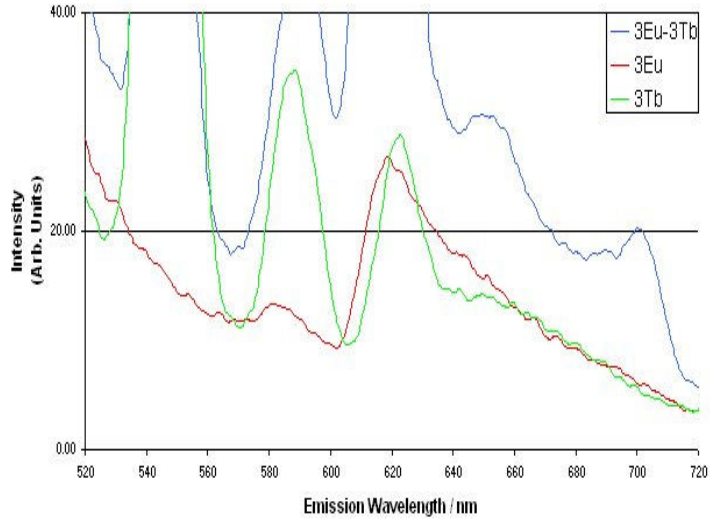

Figure 6-7. Close up of the emission spectra comparison for single europium, terbium and double doped glasses

6.2.4 Europium and Terbium Double Doped Borosilicate Glass Conclusion

All these results further enhance the security levels of the label. This is because to replicate the signals, the counterfeiter would have to know the concentrations required producing the required energy transfer between the dopant ions. Therefore enhancing the complexity of the fluorescence signal further.

6.3 EUROPIUM AND DYSPROSIUM

A 1-1 ratio with 3 mol% of each ion added to the glass matrix was produced. However, this glass showed the appearance of phase separation [30]. The glass sample appeared to have a colloidal precipitate inside and therefore an investigation into the maximum dopant concentration would have to be carried out. This can occur when a heterogeneous mixture is produced e.g. oil and water. However, in this case the problem could be due to the saturation of RE dopant ions in the glass matrix because there is only a certain amount of dopant that can be distributed homogeneously.

6.3.1 UV-Vis Absorption

The UV-visible spectrum is shown in Figure 6-8. This spectrum contained all the Eu and Dy peaks previously found in the single doped glasses and therefore the fluorescence spectrum was analysed.

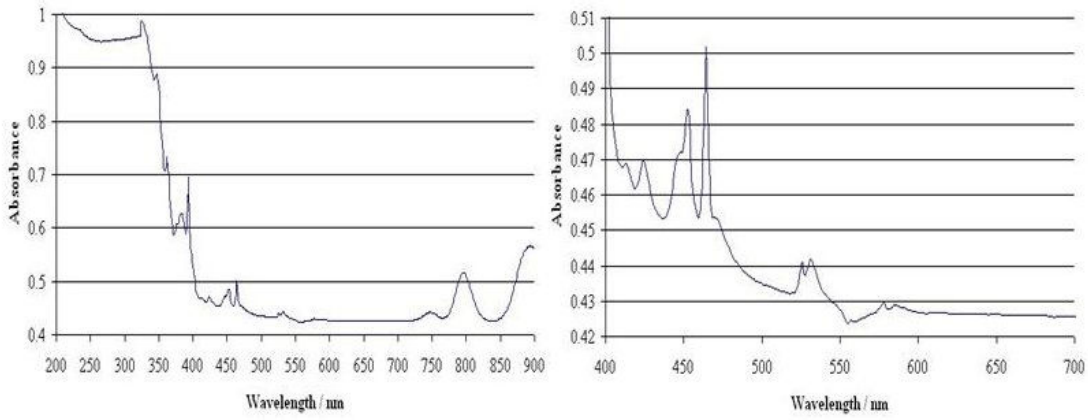

Figure 6-8. Absorption spectrum of 3 mol% Eu^{3+} and 3 mol% Dy^{3+} doped borosilicate glass

6.3.2 Fluorescence

The fluorescence spectrum for the Eu-Dy glass is shown in Figure 6-9 and a table of all the transitions is shown in Table 6-3.

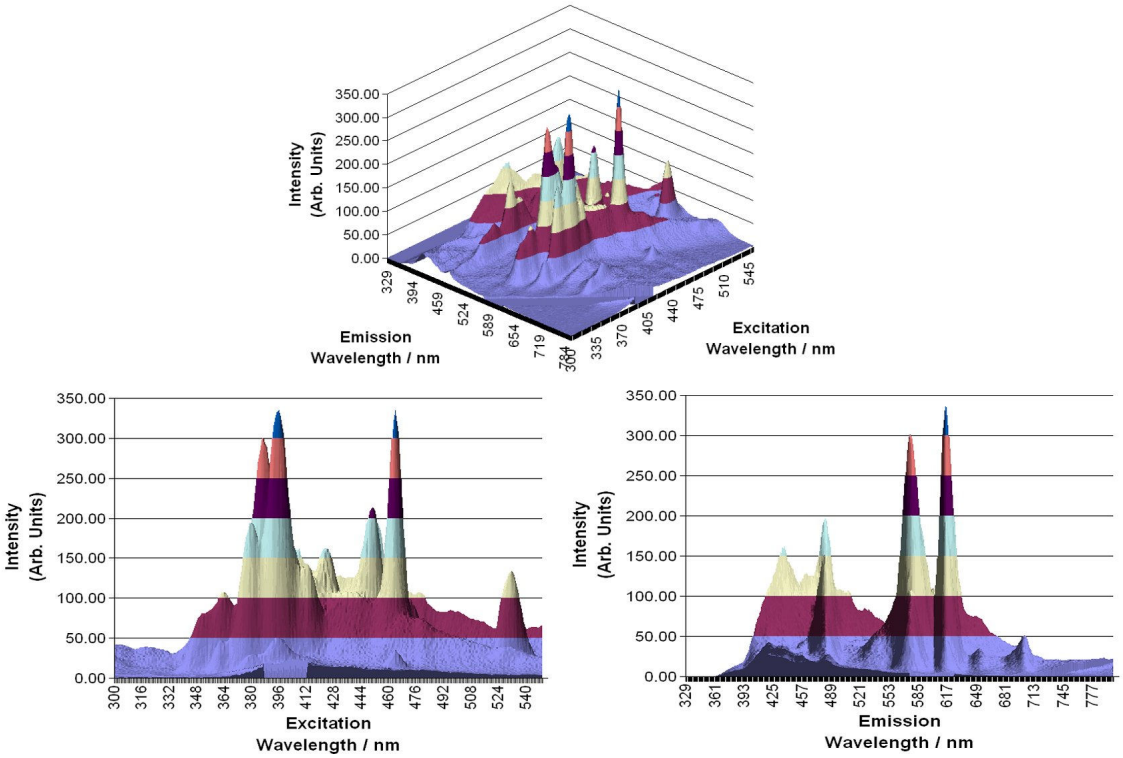

Figure 6-9. Fluorescence spectrum of 3 mol% Eu^{3+} and 3 mol% Dy^{3+} doped borosilicate glass

				Peak width					
				Excitation			Emission		
Peak label	Excitation Wavelength / nm	Emission Wavelength / nm	Intensity	From	To	PW	From	To	PW
Eu	362.0	702.5	6.39	358.0	365.0	7.0	685.5	709.0	23.5
Eu	363.0	615.5	47.29	353.0	367.0	14.0	602.5	636.0	33.5
Dy	364.0	483.5	79.27	357.0	370.0	13.0	462.0	501.0	39.0
Dy	364.0	577.5	108.01	357.0	368.0	11.0	554.5	602.5	48.0
Eu	379.0	615.5	193.96	368.0	386.0	18.0	602.5	639.0	36.5
Eu	382.0	702.5	29.78	365.0	384.0	19.0	679.5	716.0	36.5
Dy	386.0	576.0	297.58	372.0	396.0	24.0	553.0	602.5	49.5
Dy	387.0	483.0	153.12	373.0	394.0	21.0	462.0	501.0	39.0
Eu	396.0	615.5	336.10	386.0	409.0	23.0	601.0	637.5	36.5
Eu	396.0	702.0	50.92	386.0	410.0	24.0	679.5	717.5	38.0
Dy	397.0	579.5	214.19	396.0	411.0	15.0	560.5	601.0	40.5
Eu	397.0	653.5	35.63	367.0	418.0	51.0	641.5	665.5	24.0
Eu	412.0	702.5	27.58	410.0	423.0	13.0	689.5	715.0	25.5
Eu	413.0	614.5	142.01	407.0	423.0	16.0	604.0	636.0	32.0
Dy	424.0	578.0	162.37	414.0	435.0	21.0	550.5	605.0	54.5
Dy	426.0	482.0	98.52	414.0	432.0	18.0	467.5	500.0	32.5
Eu	441.0	613.0	108.12	425.0	451.0	26.0	599.5	653.0	53.5
Dy	451.0	576.5	214.18	437.0	462.0	25.0	554.5	598.0	43.5
Dy	455.0	483.0	198.97	437.0	459.0	22.0	480.0	501.0	21.0
Eu	463.0	702.0	34.01	454.0	474.0	20.0	682.5	716.0	33.5
Eu	465.0	615.5	322.01	454.0	474.0	20.0	599.5	639.0	39.5
Dy	470.0	577.5	100.95	465.0	481.0	16.0	554.5	597.0	42.5
Eu	480.0	653.5	72.71	449.0	537.0	88.0	602.5	695.0	92.5
Eu	532.0	615.0	133.79	518.0	546.0	28.0	602.5	636.0	33.5
Eu	532.0	701.5	38.55	518.0	549.0	31.0	646.0	723.0	77.0
Eu	579.0	613.5	61.56	568.0	584.0	16.0	606.5	633.5	27.0

Table 6-3. Table of all the fluorescence data found in the 3Eu-3Dy doped borosilicate glass

6.3.3 Discussion

These results indicated that all the fluorescence peaks were still detectable in the phase separated sample. However, because of the colloidal precipitate in the glass scattered the light, the background level of the spectrum had increased between the fluorescence peaks and caused the peaks to merge into each other reducing their selectivity. Furthermore, there did appear to be some interaction between the two RE ions as illustrated by the strongest Eu peak changing from an excitation wavelength at 395 nm to 465 nm. However, the results did show that the wavelengths previously selected in the single doped glasses, could still be resolved in the double doped sample and that the variation caused by the interaction between the ions can be used to enhance the security of the label.

6.3.4 Europium and Dysprosium Double Doped Borosilicate Glass Conclusion

Although the Eu and Dy peaks were detected, it was too difficult to determine any energy transfer effects due to the sample being phase separated. This analysis would require more samples (with varying concentrations) in order to determine the mechanism and is looked at further in the triple doped glass section later. From these results it could be concluded that there may have been some interference between Eu and Dy due to their close excitation wavelengths (465 nm and 450 nm respectively) that may cause problems in their detection.

6.4 INVESTIGATION INTO THE OPTIMUM RARE EARTH DOPANT CONCENTRATION

Leading on from the Eu-Dy doped glass, an investigation to determine the optimum mol% possible for a single RE dopant was carried out. A 5 mol% Dy doped glass was produced to check the solubility limit and its absorption spectrum is shown in Figure 6-10.

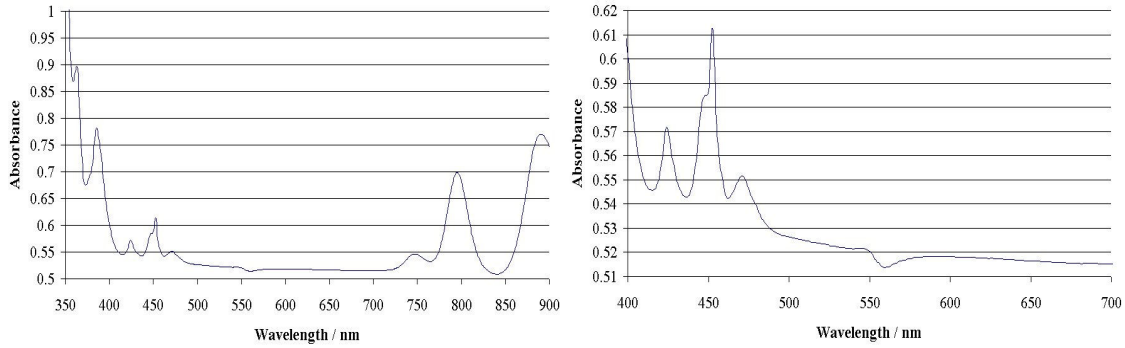

Figure 6-10. Absorption spectra of 5 mol% Dy^{3+} doped borosilicate glass

It was shown that the 5 mol% Dy absorption spectrum contained all of the data found in the 3 mol% spectrum and two additional peaks at 348 and 364 nm. However, as the samples could not be directly compared due to their variations in sample shape and size, a peak ratio analysis was used to determine any variations within each sample and the results are tabulated in Table 6-4.

	Relative Absorbance		Ratio	
Absorption Wavelength / nm	3 mol%	5 mol%	3 mol%	5 mol%
385	0.80	0.78	1.46	1.37
424	0.55	0.57		
448	0.56	0.58	0.96	0.96
452	0.59	0.61		
471	0.53	0.55	0.94	1.01
746	0.56	0.55		
797	0.69	0.70	0.89	0.91
888	0.77	0.77		

Table 6-4. Comparison between 3 and 5 mol% Dy absorbance peaks ratio

These results indicate the relative peaks absorbance remained consistent with the largest difference found between the peaks at 471 and 746 nm. With the additional peaks in the UV range now detectable, the 5 mol% does not appear to have suffered self-quenching or phase separation problems. According to Sobha and Rao [111] concentration quenching of Dy in NTP glass ($Na_5TiP_3O_{12}$) occurred around 4 wt% (equivalent to 5.3 mol%). Although concentration quenching was not evident here, the glass matrix was very different with the additional aluminium oxide in the borosilicate matrix. This has been known to reduce clustering of the RE ions which would lead to self quenching. Further work would be required to investigate higher dopant concentrations in this matrix but for this work 5 mol% Dy doped glasses can be produced successfully.

6.5 TERBIUM AND DYSPROSIUM

From the Eu-Dy and 5 mol% Dy^{3+} glasses described earlier, future multi-ion doped glasses will have a maximum dopant concentration of 5 mol%. This should stop any future phase separation problems whilst keeping the fluorescence signals as high as possible.

The concentration of each dopant was decided using past results that showed the Tb fluorescence to be much weaker than the Eu or Dy fluorescence. To try and keep a strong signal, 2.5 mol% terbium and 1 mol% dysprosium was selected.

6.5.1 UV-Vis Absorption

The absorption spectra for the Tb-Dy glass are shown in Figure 6-11. These results still contained the Dy and Tb absorption peaks as discussed in the single doped glasses, although they did appear quite weak.

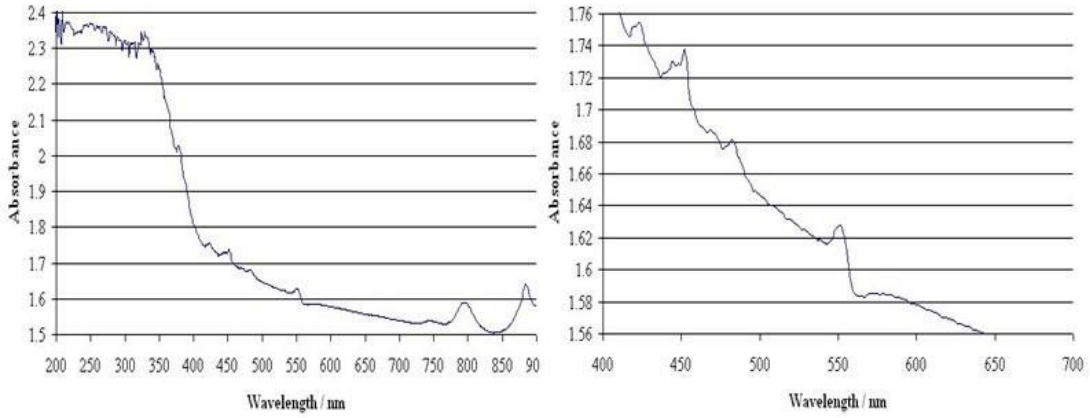

Figure 6-11. Absorption spectrum of 1 mol% dysprosium and 2.5 mol% terbium doped borosilicate glass

6.5.2 Fluorescence

The fluorescence spectrum is shown in Figure 6-12 and a table of the transitions given in Table 6-5.

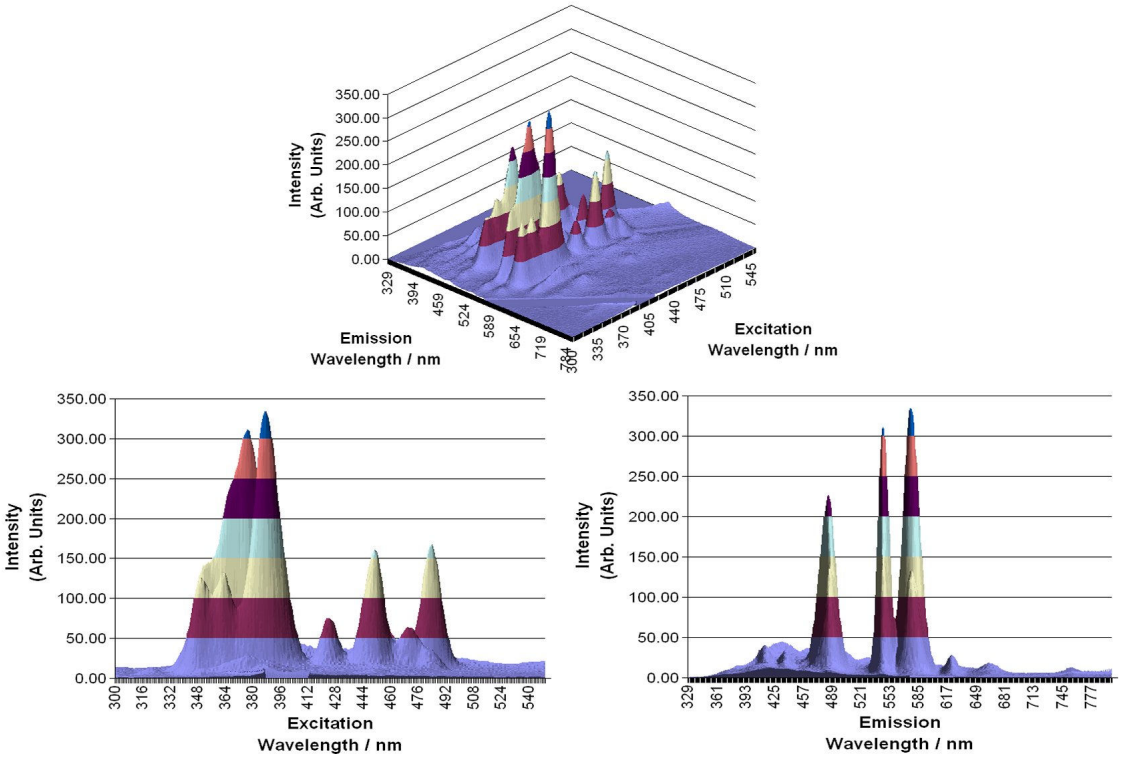

Figure 6-12. Fluorescence spectrum of 1 mol% Dy^{3+} and 2.5 mol% Tb^{3+} doped borosilicate glass

				Peak width					
				Excitation			Emission		
Peak label	**Excitation Wavelength / nm**	**Emission Wavelength / nm**	**Intensity**	**From**	**To**	**PW**	**From**	**To**	**PW**
Tb	321.0	545.0	11.42	308.0	327.0	19.0	533.5	560.5	27.0
Tb	322.0	438.0	13.07	310.0	329.0	19.0	428.5	446.0	17.5
Tb	322.0	459.0	10.28			0.0	453.5	467.0	13.5
Dy+Tb	322.0	486.0	13.45	311.0	329.0	18.0	468.5	507.0	38.5
Dy	324.0	577.5	9.69	311.0	330.0	19.0	560.5	600.5	40.0
Dy+Tb	350.0	485.0	103.93	338.0	355.0	17.0	461.0	510.5	49.5
Tb	350.0	545.5	134.13	341.0	358.0	17.0	529.5	560.5	31.0
Dy	351.0	577.0	123.86	333.0	355.0	22.0	562.0	606.0	44.0
Tb	352.0	622.5	12.45	335.0	355.0	20.0	610.0	640.5	30.5
Dy	363.0	577.0	133.06	357.0	371.0	14.0	562.0	606.0	44.0
Dy	364.0	486.5	135.55	358.0	370.0	12.0	461.0	510.5	49.5
Tb	376.0	416.0	40.36	359.0	384.0	25.0	404.0	427.0	23.0
Tb	376.0	437.5	33.85	344.0	386.0	42.0	428.5	449.5	21.0
Tb	376.0	622.5	28.39	355.0	409.0	54.0	608.0	638.5	30.5
Tb	378.0	545.5	310.39	358.0	409.0	51.0	528.0	562.0	34.0
Dy	387.0	485.5	227.79	371.0	411.0	40.0	457.5	510.5	53.0
Dy	387.0	576.0	333.94	371.0	409.0	38.0	558.5	606.0	47.5
Dy	387.0	663.0	18.31	373.0	409.0	36.0	640.5	693.5	53.0
Dy	422.0	665.0	6.54	416.0	433.0	17.0	655.5	678.5	23.0
Dy	425.0	483.5	54.79	414.0	433.0	19.0	467.0	501.0	34.0
***	425.0	546.5	45.44	416.0	433.0	17.0	531.5	558.5	27.0
Dy	425.0	576.5	74.72	412.0	435.0	23.0	558.5	602.0	43.5
***	427.0	623.0	13.26	416.0	430.0	14.0	611.5	638.5	27.0
***	449.0	622.5	19.29	438.0	458.0	20.0	610.0	642.0	32.0
***	450.0	545.5	98.86	436.0	462.0	26.0	531.5	558.5	27.0
Dy	450.0	576.5	159.15	436.0	462.0	26.0	560.5	604.0	43.5
Dy	450.0	665.0	12.01	436.0	460.0	24.0	646.0	690.0	44.0
Dy	452.0	483.5	123.95	436.0	460.0	24.0	472.5	509.0	36.5
Dy	471.0	576.0	62.96	462.0	492.0	30.0	560.5	596.5	36.0
Tb	484.0	546.0	167.82	473.0	498.0	25.0	539.5	564.0	24.5
Tb	484.0	621.5	20.89	473.0	500.0	27.0	608.0	640.5	32.5
Tb	519.0	622.0	5.25	511.0	525.0	14.0	611.5	632.5	21.0

Table 6-5. Table of fluorescence peaks, their intensities and relative transitions

6.5.3 Discussion

The majority of peaks from the single doped glasses reported earlier were found in the double doped glass. However, new peaks labelled *** in the table were found. These four peaks appeared at 425, 427, 449 and 450 nm excitations, which were known Dy excitation wavelengths. The emission wavelengths were 546.5, 623, 622.5 and 545.5 nm and were Tb emission wavelengths. This indicated there was an energy transfer between the Dy and Tb ions in the glass. To investigate this, the ratios of the dysprosium peaks at 425 and 450 nm excitation were compared in different concentration doped glasses and the double doped Dy-Tb glass shown in Table 6-6.

Sample	Excitation Wavelength / nm	Emission Wavelength / nm	Intensity	Ratio
1 mol% Dy	425	482	79.90	0.57
	424	575.5	139.73	
	451	482	189.85	0.59
	451	577.5	324.07	
3 mol% Dy	426	483	30.20	0.60
	426	577	50.74	
	452	483	55.22	0.50
	452	577	111.25	
1Dy + 2.5Tb	425	483.5	54.79	0.73
	425	576.5	74.72	
	452	483.5	123.95	0.78
	450	576.5	159.15	

Table 6-6. Comparison of ratios involved in energy transfer between Dy and Tb

These results suggested that the ratio between the Dy peaks in the 1 mol% and 3 mol% glasses remained similar. However, in the double doped glass, the ratios increased becoming closer to 1. This would indicate that some energy had left the dysprosium ions and caused a change in intensity for dysprosium.

In order to visualise the energy transfer, the emission spectra of the single and double doped Dy^{3+} and Tb^{3+} glasses under 450 nm excitation are shown in Figure 6-13. These spectra clearly show an extra peak at approximately 545 nm in the double doped glass that was not present in either single doped spectra. Since 450 nm was not a terbium excitation wavelength, this emission must have been caused by an energy transfer from dysprosium to terbium. The intensity of this peak was 98.86 whilst the terbium peak 485/545 nm was 167.82 (in the double doped glass) therefore this extra peak increases the 545 nm emission by approximately 58.9 %. A closer look at the emission spectra Figure 6-14 now shows a weak peak at 623 nm that was also due to terbium emission.

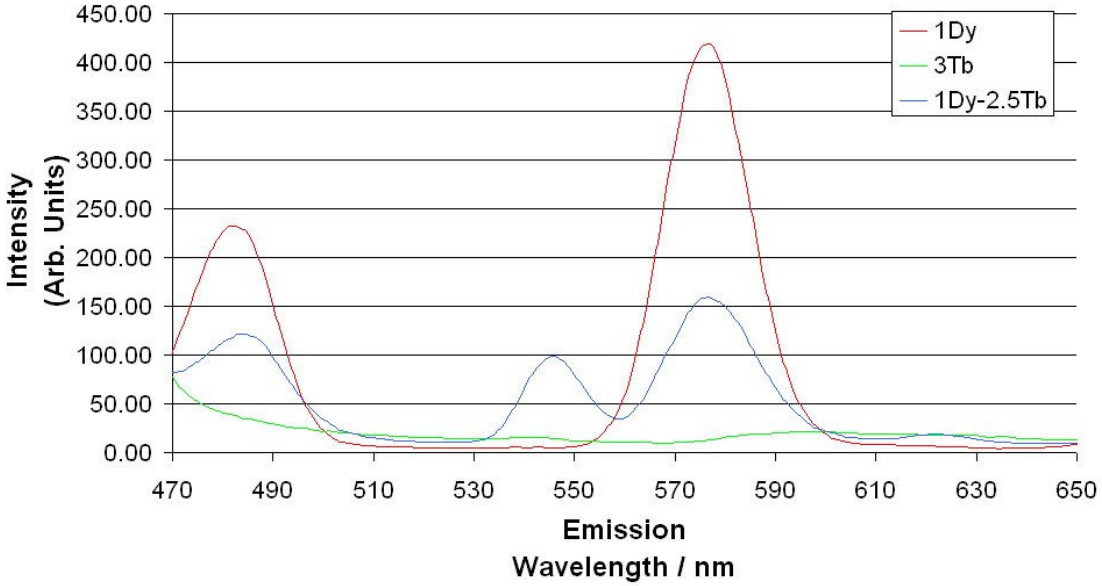

Figure 6-13. Comparison of emission spectra for single Dy, Tb and double doped Dy-Tb glasses under 450nm excitation

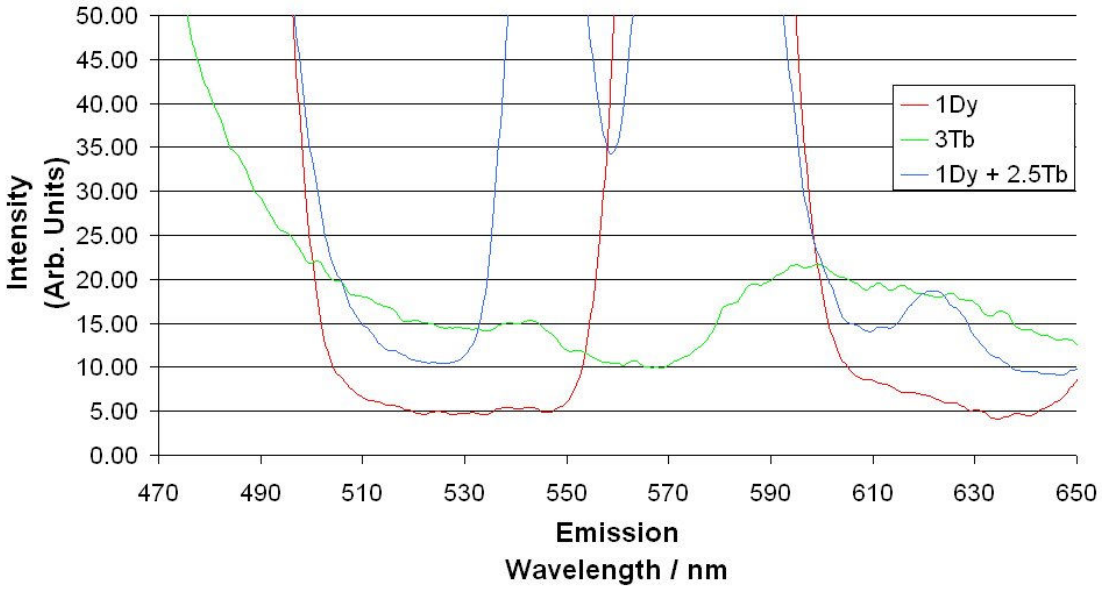

Figure 6-14. Closer look at the emission spectra of the Dy and Tb glasses under 450nm excitation

According to Sobha etal [111] the peak at 482 nm can be due to both dysprosium (482 nm) and terbium (487 nm), therefore this peak should increase with the presence of terbium whilst the peak at 577 nm, due to dysprosium only, decreases due to the energy transfer to terbium. However, the peak at 487 nm emission was not found for the single doped terbium at 487 nm excitation, because this peak was under the excitation light from the instrument. Furthermore, there were peaks at 488.5 nm for the higher energy excitations, implying that a similar peak would have been seen for an excitation at 487 nm.

In conjunction with the peaks appearing at the terbium emission wavelengths, this would imply that the terbium was gaining energy from dysprosium [111, 112]. This transfer occurs because of the similar energies of the $^4F_{9/2}$ level of Dy and the $^5D_4$ level of Tb (refer to energy level diagram in section 4.5.2), therefore allowing emissions from $^5D_4$-$^7F_5$ (546.5 and 545.5 nm) and $^5D_4$-$^7F_3$ (623 and 622.5 nm) to occur from the 425 and 450 nm excitation of dysprosium.

6.5.4 Dysprosium and Terbium Double Doped Borosilicate Glass Conclusion

A further investigation into the energy transfer will be looked at in the triple doped section where more samples with varying concentrations were analysed. It would appear from these results that only the 577 nm of dysprosium was reduced by the presence of terbium as the 482 nm peak was simultaneously enhanced by the enhanced terbium emission.

This interaction would further enhance the security level of the label by increasing the complexity of the signals due to energy transfer. Knowledge of the wavelengths involved in producing this effect would have to be known in order to try and replicate the relevant signal strengths.

6.6 TRIPLE RE DOPED GLASSES

For the triple RE doped glasses, the excitation and emission peaks in Table 6-7 would be used in the detection system. These peaks were shown in the single and double doped samples to be discrete and non-overlapping with each other. Furthermore, a single excitation for each dopant simplifies the initial detector system with the ability to select further wavelengths a possibility to enhance the complexity.

RE Ion	Excitation Wavelength / nm	Emission Wavelength / nm
Eu	465	615
Tb	485	545
Dy	453	577

Table 6-7. Chosen wavelengths for the detection system

As was illustrated, each dopant has different levels of intensity to one another and this property would be utilised in the security label to try and produce various codes. Altering the concentrations of each dopant ion causes the relative intensities of each peak to be changed and consequently would change the fluorescence fingerprint signal. Additionally, it is worth noting that the fluorescence levels were not always directly related to concentration as the ions interacted with each other and enhanced or reduced each other's signals, as demonstrated with the double doped samples. This adds another level to the security of the label so that the counterfeiter has to know the dopant ions used (and to ensure the correct fluorescence lifetime), the wavelengths selected for detection and the relative intensities to each of the dopants in order to reproduce the same signal.

To try and control this security code, it was very important to understand the relationship between the three RE dopants and their fluorescence signal to manufacture sufficiently different codes that could be distinguished by the detector system. In order to achieve this, various combinations of the three RE doped glasses had to be produced and their signals analysed. The glasses that were analysed are shown in Table 6-8. From previous work (section 6.4), 5 mol% was chosen as the optimum concentration for a single RE dopant. Therefore the total concentration of the three RE ions was set at 4.5 mol% with 2.5 mol% as the highest concentration of any individual dopant in an attempt to stop any concentration quenching or phase separation. The exception to this was the 2Eu-3Tb-3Dy

combination that was produced to maximise the fluorescence intensity although it did contain a total of 8 mol% RE dopant concentration. This sample was used in the particle size analysis covered later. All six glasses were produced following Method 5 (section 3.2.1).

	Eu (mol%)	Tb (mol%)	Dy (mol%)
(a)	1	1	1
(b)	1	2	1
(c)	1	2.5	1
(d)	1.5	2	1
(e)	1	2	1.5
(f)	2	3	3

Table 6-8. Composition of three RE doped glasses produced

6.6.1 UV-Vis Absorption

UV-visible absorption spectra were recorded to confirm the presence of all three dopants within the matrix. All the triple doped samples showed all the absorption peaks expected for a triple RE doped glass, therefore only one example (1Eu-1Tb-1Dy sample) of the absorption and second derivative spectra are shown in Figure 6-15 and Figure 6-16 respectively, which have the three selected peaks labelled for clarity.

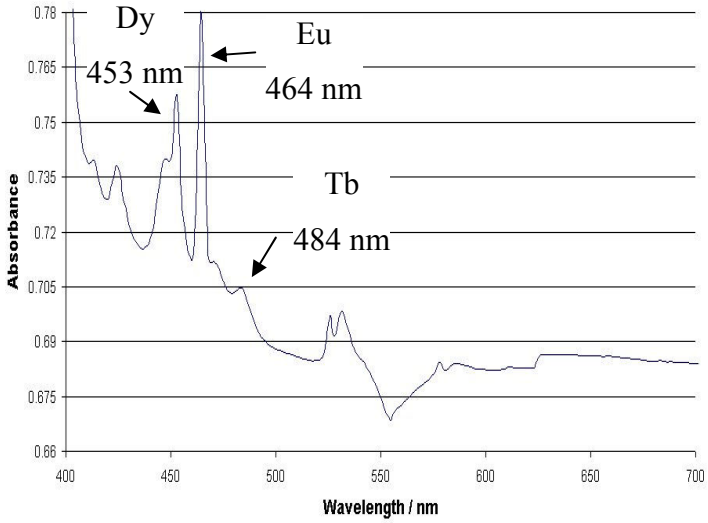

Figure 6-15. Absorbance spectrum of 1Eu-1Tb-1Dy doped borosilicate glass

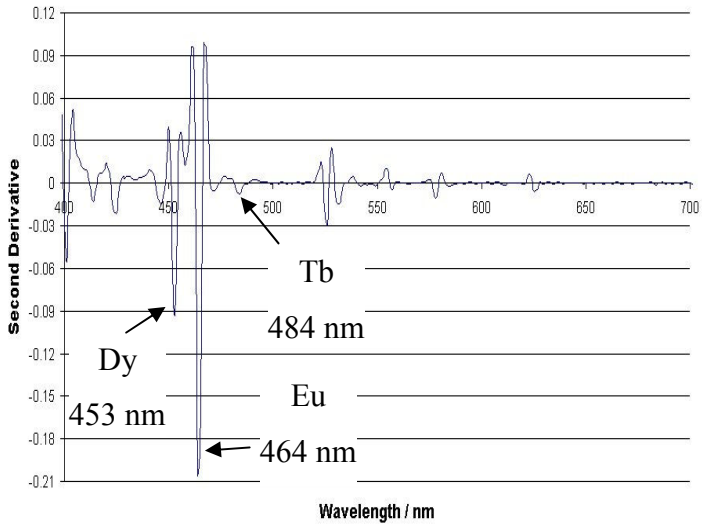

Figure 6-16. Second derivative absorption spectrum of 1Eu-1Tb-1Dy doped borosilicate glass

Since this glass contained the same concentration of each dopant, it gave a good indication of the absorption intensity for each dopant relative to one another. Here the europium dominates being twice as large as dysprosium which in turn was ten times larger than terbium. By measuring the maximum vertical distance between successive maxima and minima peaks in the second derivative spectra enabled a comparison between different dopant concentrations. For each sample only those with a change in concentration of one dopant (with the other two dopants remaining constant) could be compared in order to analyse changes with concentration. Therefore, a graph of the vertical distances for each of the selected excitation wavelengths divided by the vertical distance of the strongest peak (395 nm) to normalise each set of results, is shown in Figure 6-17. The 395 nm peak was not shown on Figure 6-16 due to its greater size from the peaks of interest and would have made it impossible to see the terbium peak.

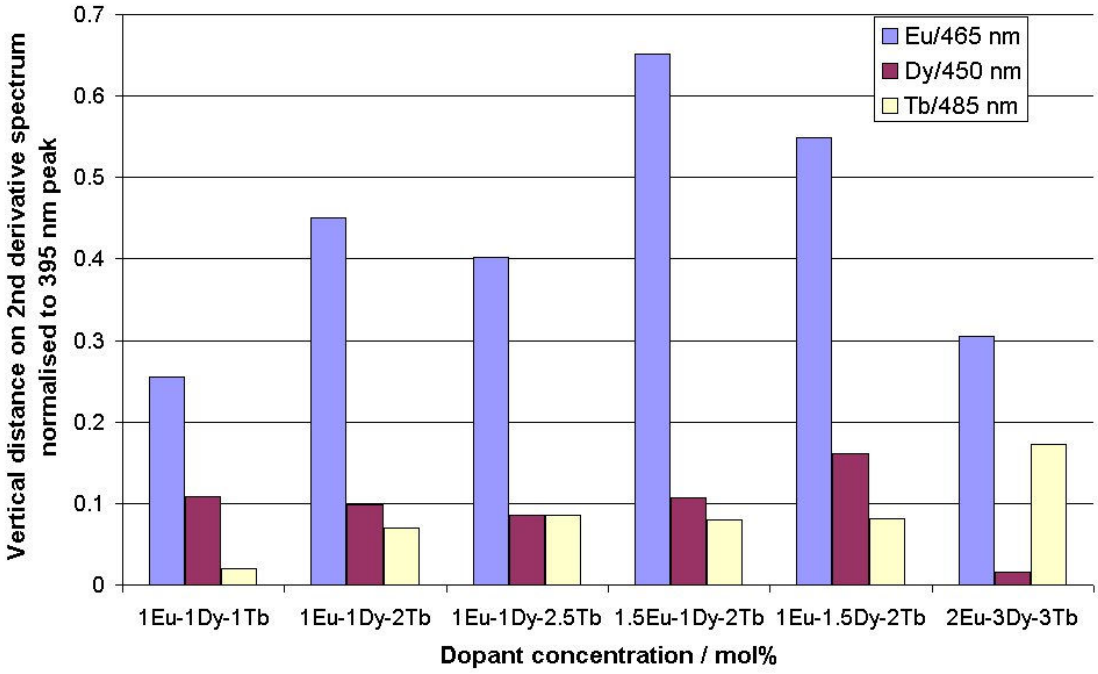

Figure 6-17. Comparison of the absorption intensity with varying concentrations in the triple doped glasses

This graph shows how large the europium absorption peak was in comparison to the terbium and dysprosium peaks and that they did appear to follow an increase with concentration. The terbium absorption at 2 mol% became equal to that of dysprosium at 1 mol% and was larger when both concentrations were 3 mol%. Furthermore, this showed that the dopant enhancement effects observed with fluorescence do not affect the absorption results.

6.6.2 Fluorescence

The fluorescence spectrum for the 1Eu-1Tb-1Dy glass is shown in Figure 6-18 and includes labelled red circles over the three wavelengths selected for the detection system. This shows the complexity of the spectrum if the sample was scanned from 300-550 nm excitation in order to determine the wavelengths used in the security label. From these data, knowledge of the exact peaks of interest would have to be known in order to determine the corresponding lifetimes and wavelengths of each peak. Other wavelengths could be selected as reference points to act as an internal standard for verification, which would also increase the security level of the label.

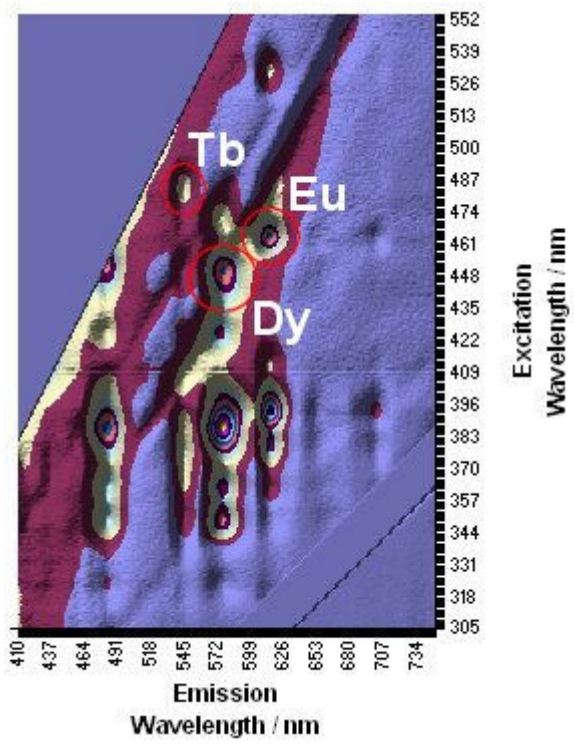

Figure 6-18. Top surface view of the fluorescence spectrum for 1Eu-1Tb-1Dy with the peaks used for the detector system circled in red

The fluorescence spectra for the six triple doped glasses are shown in Figure 6-19. These spectra demonstrated the effect of altering the concentrations of each dopant. Only the emission wavelength range 440-650 nm was shown to simplify the spectra and to focus on the wavelengths highlighted in Table 6-7. All four emission peaks are labelled for simplicity with two Dy emission peaks visible in this range.

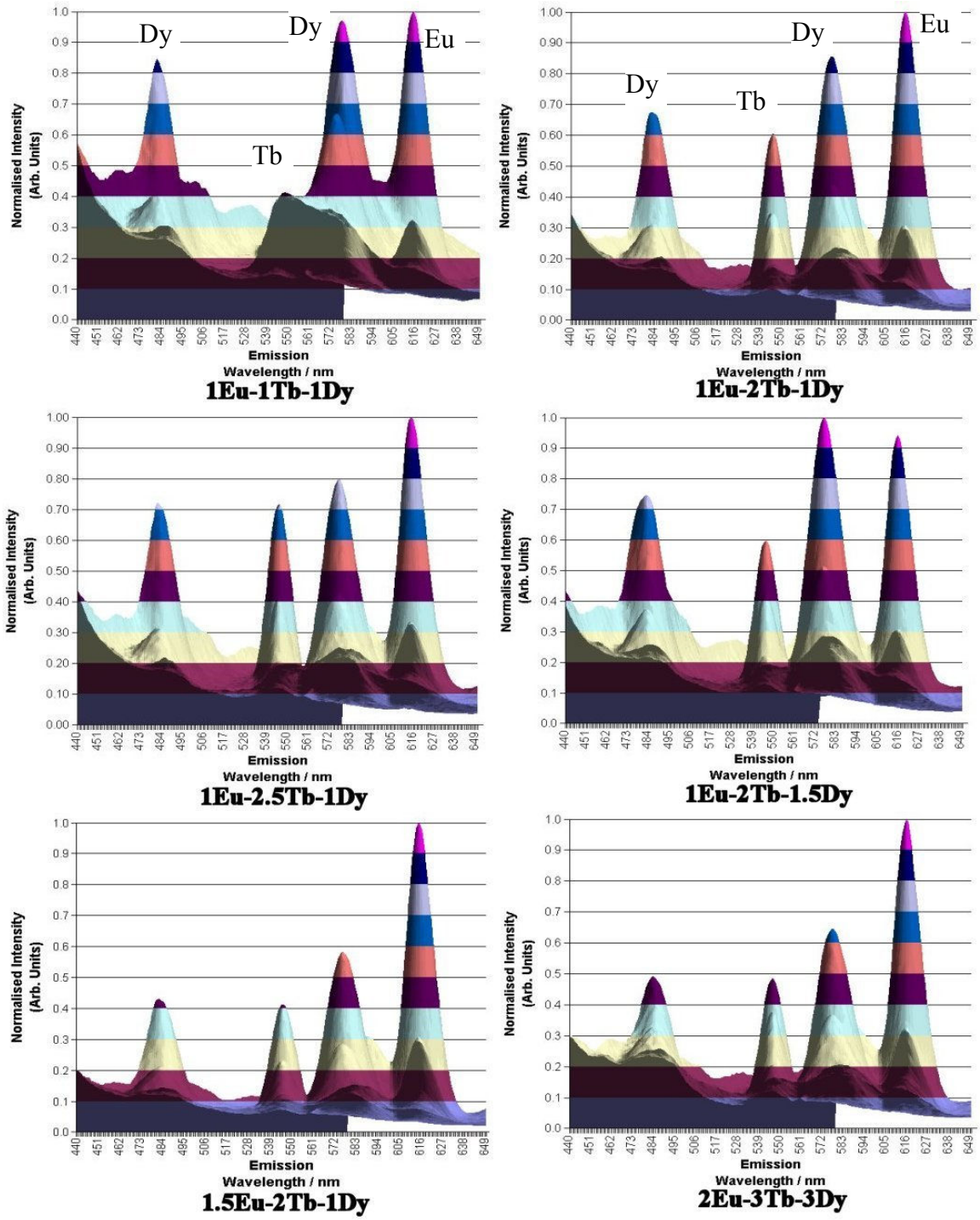

Figure 6-19. Normalised visible emission spectra of 6 different triple RE doped borosilicate glasses

6.6.3 Concentration Effects on Fluorescence

From the double doped results, it became clear that each dopant interacted with the other causing an enhancing or reducing effect on their fluorescence. This effect was further complicated with three different dopants in the same glass making this interaction harder to predict. A comparison of ratios between the strongest peak in each glass (395 nm excitation, 615 nm emission from Eu apart from 1Eu-2Tb-1.5Dy sample which was 387 nm excitation and 577.5 nm emission) and the peaks of interest in each glass is shown in Figure 6-20.

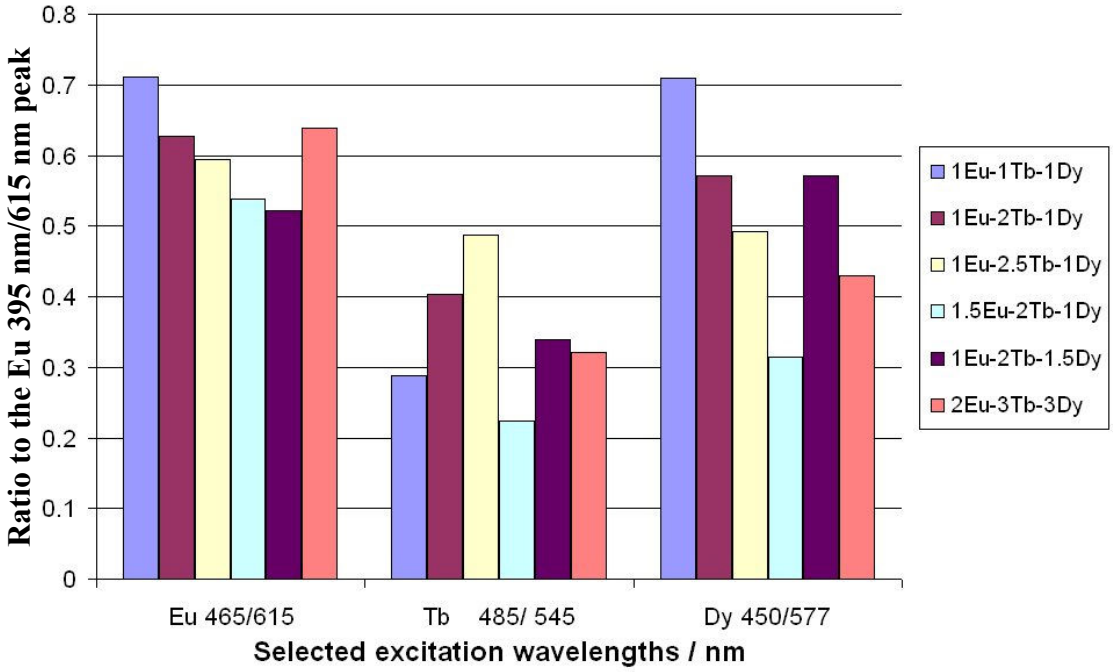

Figure 6-20. Comparison of the ratios between the peaks of interest in all of the triple RE doped glasses normalised to the Eu 395 nm/615 nm peak

This graph indicates the degree of change possible by varying the concentrations. This gives a good visualisation of how the security code could be changed by altering the dopant concentrations and that the results did not always follow the trend of increasing concentration causing a proportional increase in intensity due to the interactions between the dopants. Comparisons for each dopant can only be made when the other two dopant concentrations remained constant; therefore an investigation into the effects of changing each dopant concentration was carried out.

6.6.3.a Changes with terbium concentrations

To determine how the signal changed for each RE by altering the concentration of each dopant, tables of fluorescence intensity ratios were made. Each table allows for one RE concentration to change whilst keeping the other two constant. A factor that had to be accounted for was the energy transfer effects noted in the double doped samples. This meant that for the europium signal, the peak at 465/615 nm (normal fluorescence wavelength) and the peak intensity at 485/615 nm (due to energy transfer from terbium to europium) had to be added together. This also applies for terbium at 485/545 nm (normal fluorescence wavelength) and 450/545 nm (due to energy transfer from dysprosium to terbium) peak intensities being added together. Since no extra peaks were found to enhance the dysprosium signal, only the peak intensity at 450/577 nm was used. The first dopant concentration altered was terbium and the results shown in Table 6-9 using the data in Figure 6-21, Figure 6-22 and Figure 6-23. Columns (a) (b) and (c) involve the wavelengths selected for the detector system whilst columns (d) and (e) examine additional peaks that were noted in the double doped glass section due to energy transfer.

Concentration / mol%			**(a)**	**(b)**	**(c)**	**(d)**	**(e)**
Tb	Eu	Dy	Tb/Eu	Tb/Dy	Eu/Dy	(450/545 nm) / (450/577 nm)	(484/615 nm) / (484/545 nm)
1	1	1	0.67	0.67	1.00	0.40	NA
2	1	1	0.81	1.10	1.36	0.41	0.33
2.5	1	1	0.90	1.40	1.54	0.51	0.35

Table 6-9. Terbium concentration effects on triple doped samples

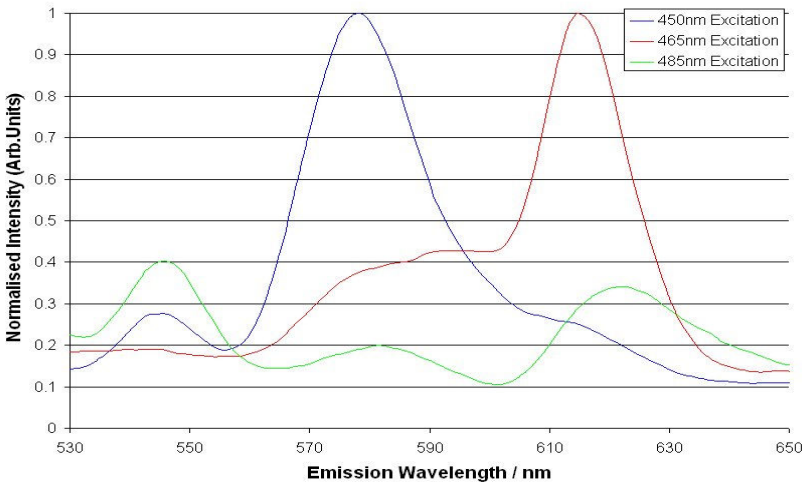

Figure 6-21. Fluorescence emission spectra for the three excitation wavelengths of interest in the 1Tb-1Eu-1Dy sample

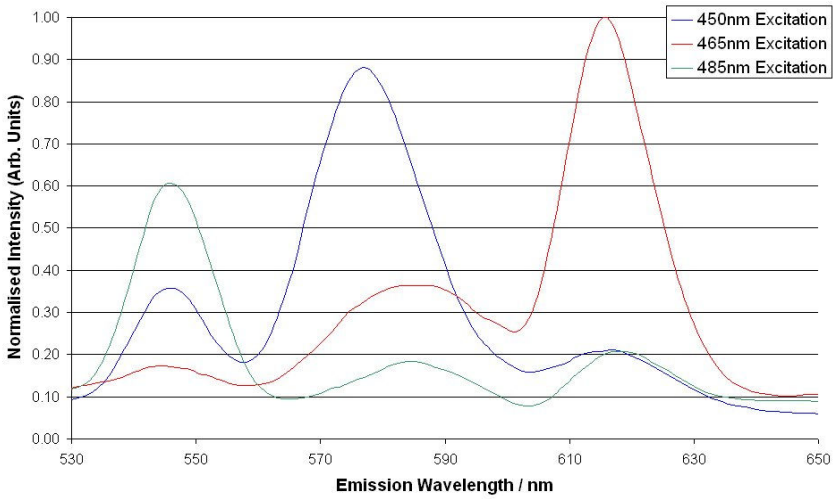

Figure 6-22. Fluorescence emission spectra for the three excitation wavelengths of interest in the 2Tb-1Eu-1Dy sample

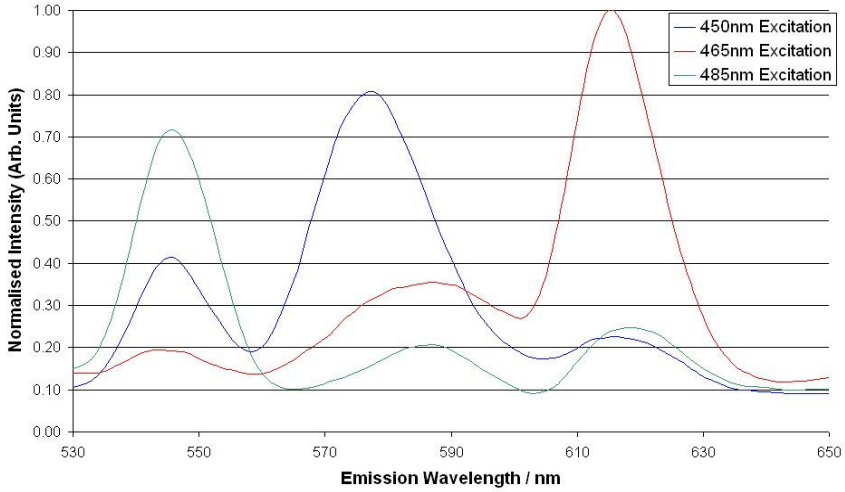

Figure 6-23. Fluorescence emission spectra for the three excitation wavelengths of interest in the 2.5Tb-1Eu-1Dy sample

As the terbium concentration increased so did the terbium signal. This caused column (a) and (b) to increase to 0.9 and 1.4 respectively. This implied that the terbium signal became stronger than dysprosium at 2 mol% and nearly equal to europium at 2.5 mol%. The ratio in column (c) also increased and was due to the dysprosium signal reducing (due to the energy transfer to terbium) and from terbium enhancing the europium signal. Column (d) shows the enhancing effect from dysprosium to terbium increasing as the terbium concentration increased. This can be due to the shorter distance between Dy-Tb bonds causing the probability of energy transfer to increase. This is similar to column (e) except the increase was not as pronounced perhaps by the higher probability of the Dy-Tb energy transfer in comparison to the Tb-Eu energy transfer. The result in column (e) for 1Tb-1Eu-1Dy was not applicable because the peak intensity was not strong enough to be detected.

6.6.3.b Changes with dysprosium concentrations

A table with the intensity ratios with changes in dysprosium concentration are shown in Table 6-10. Only two samples could be compared with constant europium and terbium concentrations and they are shown in Figure 6-24 and Figure 6-25.

Concentration / mol%			(a)	(b)	(c)	(d)	(e)
Dy	Eu	Tb	Dy/Eu	Dy/Tb	Tb/Eu	(450/545 nm) / (450/577 nm)	(484/615 nm) / (484/545 nm)
1	1	2	0.73	0.91	0.81	0.41	0.33
1.5	1	2	0.89	0.99	0.89	0.42	0.34

Table 6-10. Dysprosium concentration effects on triple doped samples

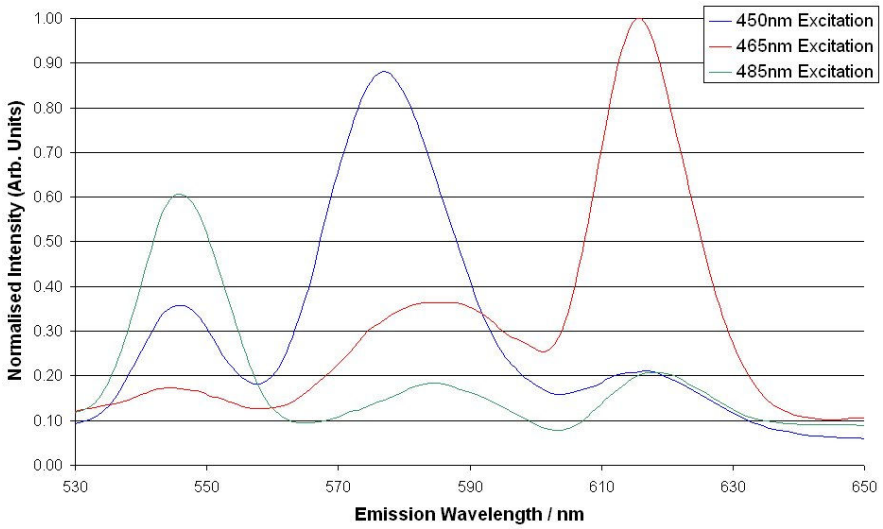

Figure 6-24. Fluorescence emission spectra for the three excitation wavelengths of interest in the 1Dy-1Eu-2Tb sample

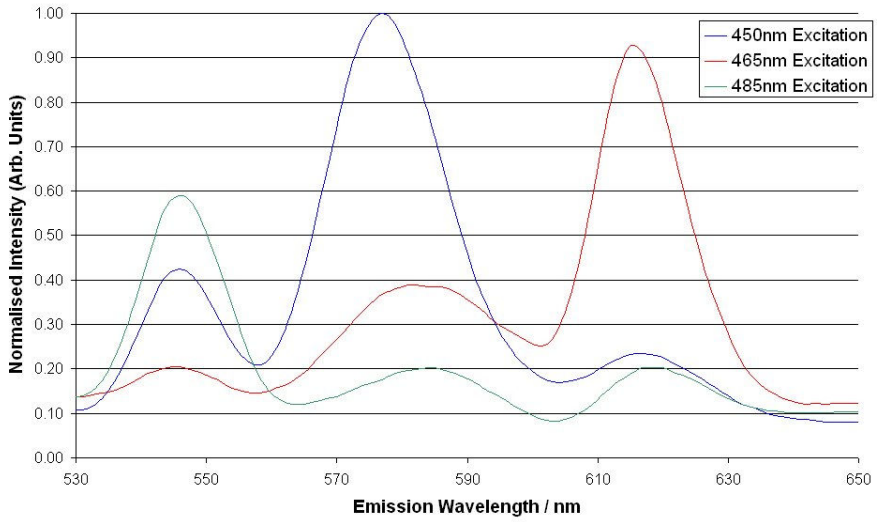

Figure 6-25. Fluorescence emission spectra for the three excitation wavelengths of interest in the 1.5Dy-1Eu-2Tb sample

As dysprosium increased so did its intensity to 0.89 and 0.99 in columns (a) and (b) respectively. This meant dysprosium had approximately an equal intensity with terbium and slightly lower than europium at a concentration of 1.5 mol%. Column (c) showed that the Tb/Eu ratio increased as the dysprosium concentration increased due to the enhancement of terbium by dysprosium. However, columns (d) and (e) did not increase significantly due to the small increase in the dysprosium concentration. A larger change might have been evident with higher dysprosium concentrations.

6.6.3.c Changes with europium concentrations

The intensity ratio changes with europium concentration are shown in Table 6-11. Similarly with dysprosium, only two samples could be compared with constant terbium and dysprosium concentrations and are shown in Figure 6-26 and Figure 6-27.

Concentration / mol%			(a)	(b)	(c)	(d)	(e)
Eu	Tb	Dy	Eu/Dy	Eu/Tb	Dy/Tb	(450/545 nm) / (450/577 nm)	(484/615 nm) / (484/545 nm)
1	2	1	1.36	1.24	0.91	0.41	0.33
1.5	2	1	2.02	1.80	0.89	0.41	0.45

Table 6-11. Europium concentration effects on triple doped samples

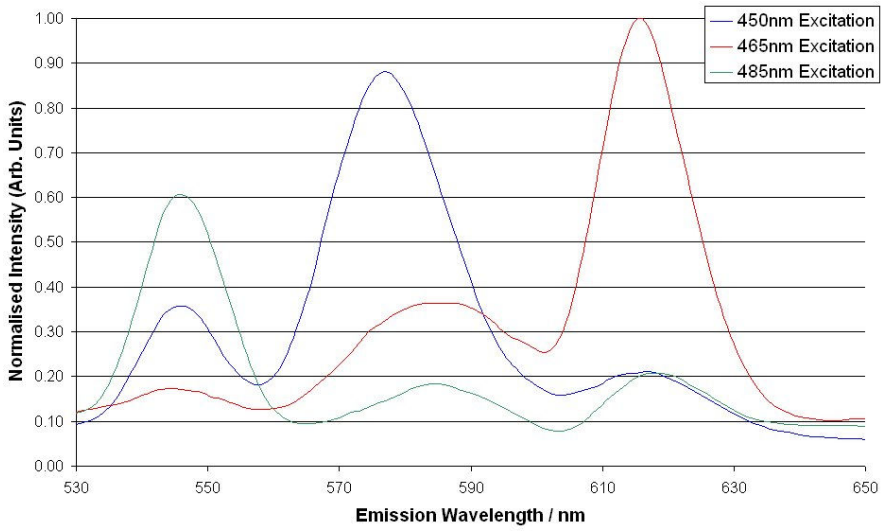

Figure 6-26. Fluorescence emission spectra for the three excitation wavelengths of interest in the 1Eu-2Tb-1Dy sample

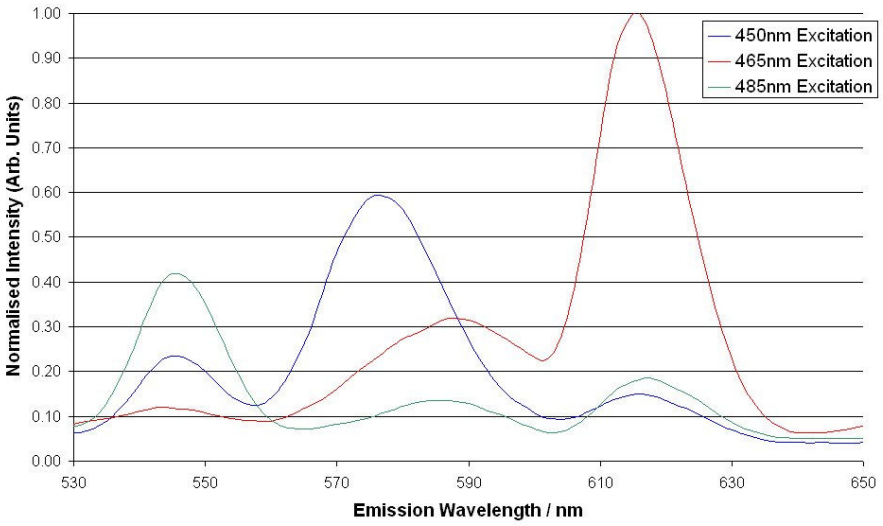

Figure 6-27. Fluorescence emission spectra for the three excitation wavelengths of interest in the 1.5Eu-2Tb-1Dy sample

With an increase in the europium concentration, its intensity ratio to dysprosium and terbium increased to 2.02 and 1.80 respectively. This was due to the europium intensity increasing. Column (c) showed the Dy/Tb ratio remained constant with the increase in europium as was the dysprosium enhancing effect on terbium (column (d)). Column (e) showed a slight increase in the terbium enhancing europium possibly due to the probability of terbium and europium ions becoming closer thereby increasing the efficiency of their energy transfer.

6.6.3.d Dopant concentration effects conclusion

From these results the concentration effects were evident in altering the intensity signals for all three dopants. This increases the complexity of the label if an attempt was made at reproducing the results. The largest alterations were found when the terbium concentration was changed due to its interaction with both dysprosium and europium.

6.7 HOMOGENEITY OF BATCHES

There was a need to investigate the homogeneity of each batch of glass to confirm the dopant ions were distributed throughout the glass instead of only on the glass surface. This involved random samples to be examined using the spectrofluorometer three times over a period of three months, with two examples shown in Figure 6-28 and Figure 6-29. All the peaks were expressed as the ratio to the Eu peak at 395 nm excitation 615 nm emission to normalise the data. If the samples were homogeneous throughout the batch, then the results should be consistent.

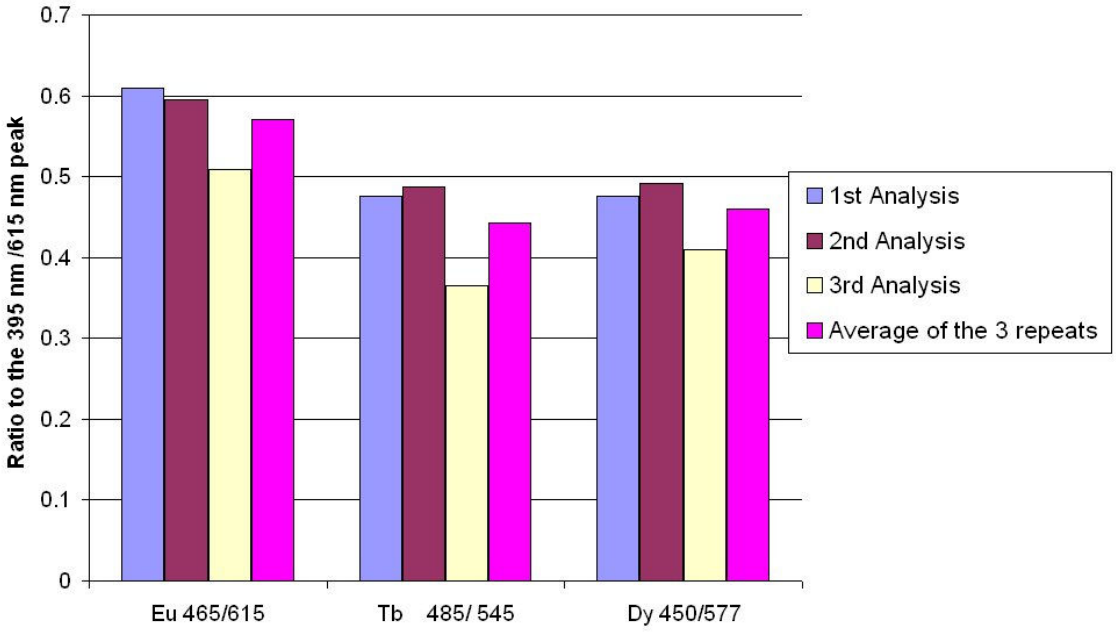

Figure 6-28. 1Eu-2.5Tb-1Dy ratio to the 395nm/615nm peak

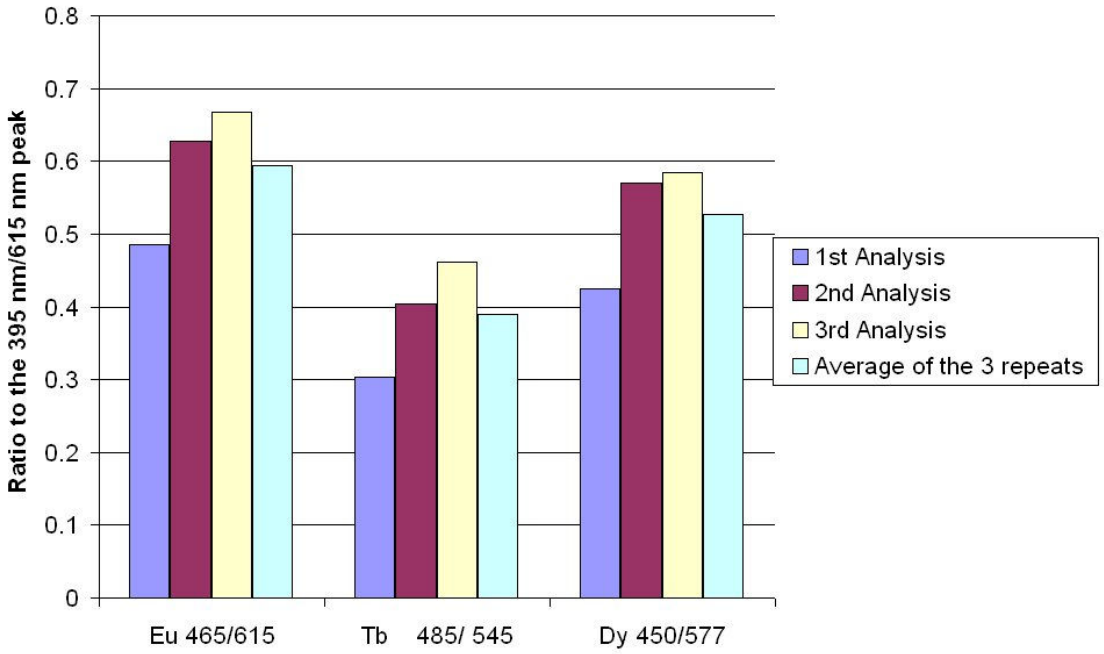

Figure 6-29. 1Eu-2Tb-1Dy ratio to the 395nm/615nm peak

Due to a slight variation between repeats, a one way analysis of variance statistical analysis was used to determine if the three runs came from a population of the same mean.

6.7.1 Analysis of Variance

There are two sources of variation when measurements are repeated under the same conditions with the first always present, due to random error, causing different results [113]. The second source is called controlled or fixed-effect factor; such as the method of analysis or due to the person carrying out the experiment. Analysis of variance (also called ANOVA) is a powerful statistical technique used to estimate and separate the different causes of variation.

For every significance test there is a null hypothesis. The term null implies that there was no difference between the observed and the known value other than due to random variation. If the null hypothesis is true, then statistical theory can be used to calculate the probability of the sample mean and true value results as random error. The null hypothesis is usually rejected if the probability of this observed difference is less then 1 in 20 (ie 0.05). To increase this certainty a higher level of significance can be used (0.01 or 0.001).

For checking the homogeneity of each batch there was more than one source of random error. Random samples from the same batch were chosen and replicate analysis was performed on these samples. Therefore there was a random error in the measurement of each sample and possibly variations in the homogeneity of the samples from the same batch. Since there was one random factor here (random samples taken from the same batch) in addition to random error, a one-way ANOVA was chosen for analysis using the Minitab version 13 software.

The F-test can be used to determine the random errors of two sets of data by comparing their standard deviations ($F=MS_{between}/MS_{within}$ where MS is the mean square) [114]. Where more than two sets of data are involved, ANOVA is used, although this also calculates an F value. ANOVA compares the amount of variability between groups to the amount of variability within groups. Between groups variability is due to the grouping factor whilst within groups variability is due to chance. If this ratio was equal to 1, then any differences between the groups would not be significant as the differences would be equal. If the difference between groups increased however, then the F value would increase and increases the probability that the difference was due to something other than chance.

6.7.1.a Results

The results from the ANOVA are shown in Table 6-12. For the results to be significantly different, the F_{calc} values for each sample in the top table would have to be greater than the F_{crit} value. Table 6-12 shows all the F_{calc} results were below the F_{crit} values which meant there were no significant errors and that they all came from a population of the same mean.

	1Eu-2Tb-1Dy	1Eu-2.5Tb-1Dy	1Eu-2Tb-1.5Dy	1.5Eu-2Tb-1Dy
Fcalc	2.09	1.77	0.11	0.27
Fcrit	3.707	3.707	3.707	3.707

	1Eu-2Tb-1Dy		1Eu-2.5Tb-1Dy		1Eu-2Tb-1.5Dy		1.5Eu-2Tb-1Dy	
	1	2	1	2	1	2	1	2
2	-0.4462		-0.3489		-0.2191		-0.6507	
	0.188		0.3855		0.21083		0.4364	
3	-0.4836	-0.3545	-0.3951	-0.4134	-0.12253	-0.1184	-0.5955	-0.4883
	0.1506	0.2797	0.3393	0.321	0.3074	0.31153	0.4916	0.5988

Fisher individual error rate of 0.01

Table 6-12. One way ANOVA results for determining the reproducibility of the spectrofluorometer results over a period of three months

The bottom table was used to compare between each of the three repeats with a confidence level of 1 % (Fisher individual error rate of 0.01 is the confidence interval for all pairwise differences between level means). In order for the results to be significantly different between repeats, the two values would not pass through zero. For example, between the first and second repeat for the 1Eu-2Tb-1Dy batch the values were -0.4462 and 0.188. Between these values passes through zero therefore there were no significant difference between the first two repeats. This was the case for all the samples in each batch, therefore no significant differences were found.

6.7.2 ANOVA Conclusion

The one way ANOVA results indicated, with a probability of less than 1 %, that the spectrofluorometer results did not differ significantly over a period of three months for the random samples taken from each batch. This, therefore, proved the dopant ions were distributed throughout the glass.

6.8 MULTI RARE EARTH DOPED GLASSES CONCLUSION

The results from the successfully produced double doped glasses have proved the capability of resolving the individual peaks from each of the dopants. This is in contrast with the fluorescence spectrum produced when mixing two different fluorescent dyes together. Additionally there was evidence of energy transfer in all three double doped glasses, which can be used to enhance the signal of certain dopants. With the enhancement of certain peaks, this can be utilised in order to increase the fluorescence signal of one or more dopants in order to increase the signal making it easier to detect.

From the triple doped glasses the first visualisation of how different security codes can be produced, by altering the concentrations of each dopant was shown. Altering the concentration of one dopant meant the fluorescence signal of the other two dopants can change therefore increasing the complexity of the signal. Furthermore, the results proved the spectrum of the three dopants do not overlap each other in comparison to a mixture of three fluorescent dyes. Although the fluorescence results changed with changes in concentration, the samples from the same batch were found to produce consistent results with the luminescence spectrometer over a three month period i.e. no photodecomposition was found.

6.9 ASSESSMENT OF PARTICLE SIZE

The ideal size for the security label was to be approximately 5 μm or smaller to be able to pass through the nozzles of an ink jet printer, therefore the original 100 μm soda lime beads have been ball milled and sieved to investigate particle size. A Malvern Particle Size Analyser was used for this analysis following Method C (section 3.3.3).

Two sets of experiments were carried out. The first was to show the effect of the ball milling time on the soda lime bead particle size, whilst the second investigated the effects of shorter ball milling intervals and sieving.

6.9.1 Effect of Ball Milling Time on Particle Size

One sample (2 g) of 100 μm soda lime beads were ball milled for 1 hour and analysed using particle size analysis with the distribution graph and table of important results in microns shown in Figure 6-30 and Table 6-13 respectively. The resulting powder was not passed through a sieve before analysis to allow the determination of the average size of the crushed glass and the particle size distribution.

Ball Mill Time/Mins	D[v,0.5]	D[4,3]	D[v,0.1]	D[v,0.9
60	7.77	17.71	1.54	42.15

Table 6-13. Particle size analysis of soda lime beads ball milled for 1 hour

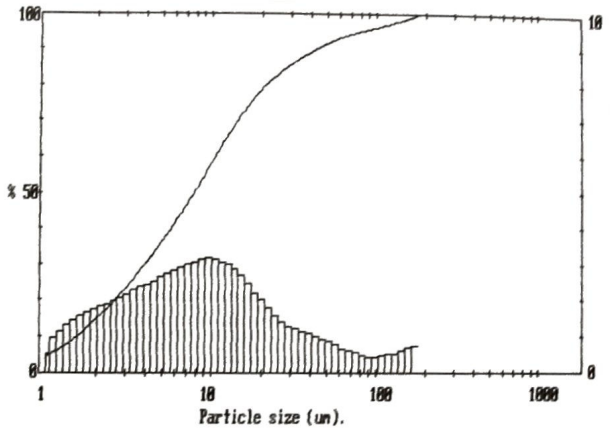

Figure 6-30. Particle size distribution of soda lime beads ball milled for 60 minutes

The computer program for the particle size analysis gave the data in various forms. From Table 6-13 the terms on the top row related to the following [84]:

- D [v,0.5] - Volume median diameter. This figure has 50 % of the distribution above and 50 % below this value. It divides the distribution exactly in half.

- D [4,3] - Volume mean diameter. This is the diameter of the sphere that has the same volume as an ideal sphere. $D\,[4,3] = \sum d^4 \Big/ \sum d^3$

- D [v,0.9], D [v,0.1] - These are 90 % and 10 % cut-offs respectively for the distribution. Where D [v,0.9] has 90 % of the distribution below this value and D [v,0.1] has 10 % of the distribution below this value.

6.9.2 Effect of Further Ball Milling of Sieved Glass

This experiment involved initial ball milling of the 100 μm soda lime beads for 5 minutes before passing them through a 45 μm sieve to remove any large aggregates formed during ball milling. The resulting powder was then analysed before being ball milled for a further 15 minutes. Each of the particle size distribution graphs are shown in Figure 6-31 (before ball milling), Figure 6-32 (after 5 minutes ball milling and sieving) and Figure 6-33 (after a further 10 minutes ball milling) and a comparison of the important results tabulated in (Table 6-14).

Total Ball Milled Time/Mins	D[v,0.5]	D[4,3]	D[v,0.1]	D[v,0.9]
0	97.21	98.47	77.86	122.15
5	12.65	15.7	1.76	32.41
15	8.88	22.01	1.36	52.93

Table 6-14. Particle size analysis of soda lime glass beads

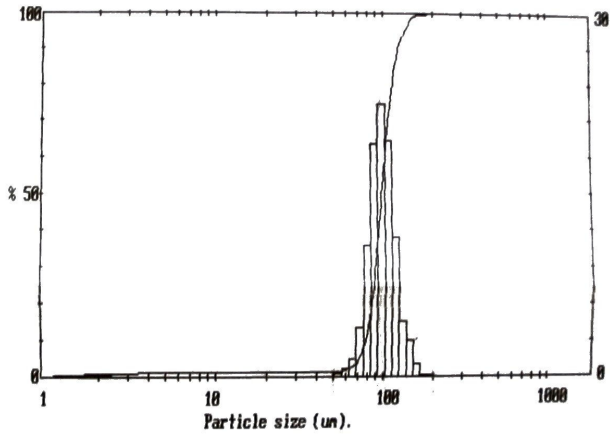

Figure 6-31. Particle size distribution for soda lime beads before ball milling

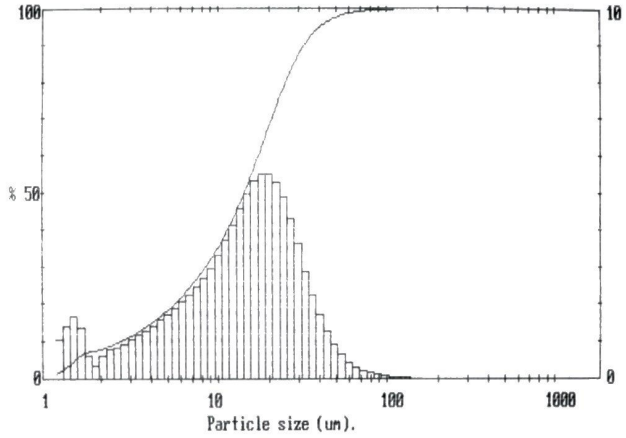

Figure 6-32. Particle size distribution graph for soda lime beads ball milled for 5 minutes

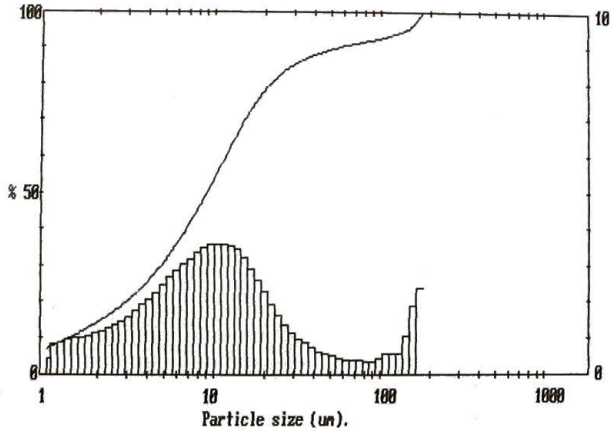

Figure 6-33. Particle size distribution of soda lime beads ball milled for a further 10 minutes

Some problems were found in the interpretation of the particle size results because the instrument could not distinguish between an air bubble, dust particles or larger aggregates (due to coagulation that resulted in a higher value) to the particle of interest. However, it did give a distribution of the size range for each sample. It was noted that after 15 minutes of ball milling the D[4,3] and D[v,0.9] values increased from the sample ball milled for 5

minutes. This was due to an increase in the number of aggregates formed by the ball milling process, as the sample was not sieved before analysis. This was further backed up as the D[v,0.5] and D[v,0.1] values decreased and a shift to lower sizes could be seen in the particle size distribution proving the ball milling had reduced the particle size.

6.9.3 Conclusion

These results demonstrated that it was possible to achieve single figure micron size samples by ball milling the 100 μm soda lime beads for 1 hour. Although micron sized particles were produced, there was a large distribution of sizes. Therefore sieves should be used to narrow the distribution. A very good distribution for the 100 μm beads without ball milling (time 0) was produced. This enabled good confidence in the other results as this acted as a calibration for the instrument. After 5 minutes ball milling, the particle size was reduced considerably (after sieving). In comparison with the results in Table 6-13 there was no significant reduction in particle size after 60 minutes in comparison with the results obtained after 5 minutes. Furthermore, after an additional 10 minutes, the particle size was not significantly reduced. Therefore, future analysis could be achieved with periods of 5 minute ball milling, before sieving and re-crushing to achieve the desired size. For future experiments with doped glass samples being analysed, a 5 μm sieve would be used to reduce the distribution range of the sample and set the maximum size at 5 μm.

6.10 PRODUCTION OF LESS THAN OR EQUAL TO 5 MICRON SAMPLES

Less than or equal to 5 μm particles were produced by crushing batches of small pieces, of the 2Eu-3Tb-3Dy sample, for 5-minutes. The resulting powder was then passed through a 45 μm sieve and the larger particles re-crushed until the entire sample had passed through the sieve. Although an attempt was made to sieve this through the 5 μm sieve by dry sieving, this was unsuccessful due to caking effects. Therefore the alternative method was to use wet sieving.

6.10.1 Wet Sieving

The wet sieving technique was adapted from Mullin [115] and a diagram of the experimental set up shown in Figure 6-34. The process involved placing the sieved sample (1 g) onto the sieve before lowering the sieve into a beaker of acetone so that the acetone was 1 cm above the immersed sieving surface. The beaker was then placed into an ultra sonic bath (Langford Ultrasonics Sonomatic SO575) and sonicated at 40 kHz for 2 minutes. The copper wire was used to hook onto the sides of the beaker to hold the sieve in place during sonication.

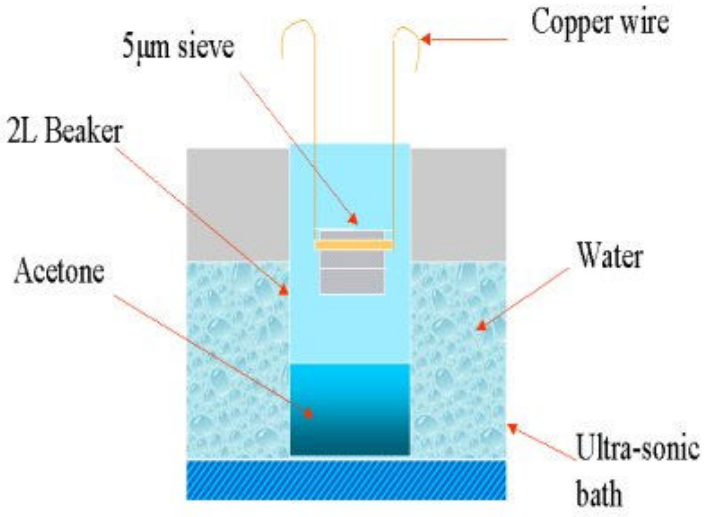

Figure 6-34. Wet sieving experimental setup

The sieved sample then became dispersed in the acetone below the sieve. The majority of acetone could be decanted off (after allowing time for the sample to settle) before allowing the rest to evaporate to dryness.

6.10.2 Particle Size Analysis

These samples were tested in the particle size analyser as before. Acetone was used as the dispersing agent and a drop of decon was added as surfactant to wet the sample. The surfactant was required to break up agglomerates and stop the sample from sitting on top of the acetone. The particle size distribution results are shown in Figure 6-35 with the important results tabulated in Table 6-15.

D[v,0.5]	D[4,3]	D[v,0.1]	D[v,0.9]
3.15	5.08	0.8	6.71

Table 6-15. Particle size analysis of the wet sieved sample

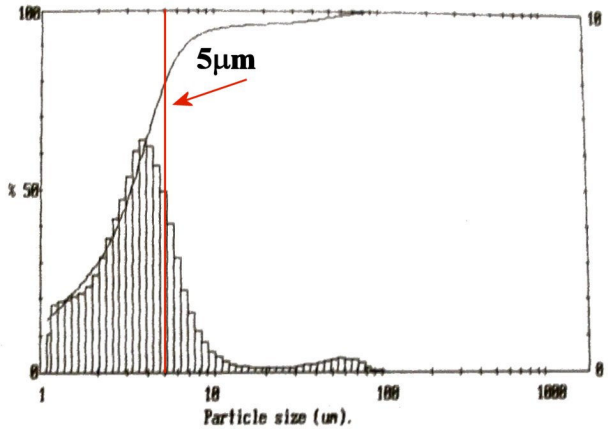

Figure 6-35. Particle size distribution of the wet sieved sample

The above results proved the majority of the sample analysed was less than 5 µm. Any signal found above the 5 µm line could have been produced by agglomerates. Although this process successfully produced samples less than 5 µm, the method was very laborious and time consuming with low sample production efficiency. Therefore, for larger quantities of samples a more automated procedure would be required such as the Endecotts Sonic Sifter.

6.10.3 SEM analysis

Now that the particle size was known, a scanning electron microscope (SEM) was used to take a micrograph of the sample to allow further analysis of the particle shape. All of the SEM work reported in this thesis was carried out on a LEO S430 digital SEM by Iain Tough (SEM Technician). These SEM images are shown in Figure 6-36.

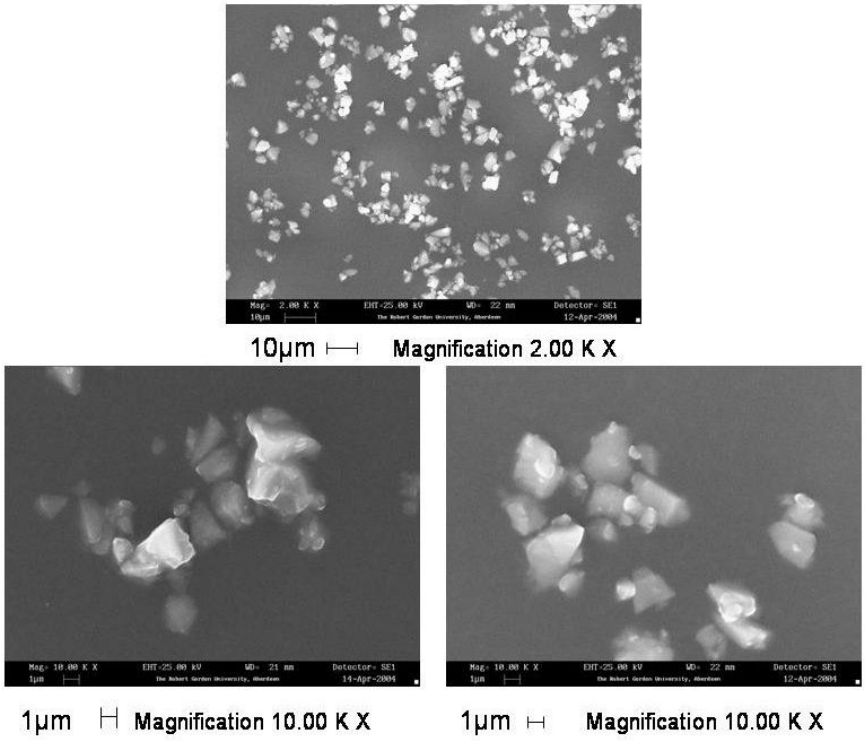

Figure 6-36. SEM images of 5 µm particles of 2Eu-3Tb-3Dy

These images show irregular shapes of particles between 1-4 µm in diameter. These were produced by the wet sieving technique and confirm the results from the particle size analyser. To determine whether each of the dopant ions were still present and that this was our glass sample, EDXA (energy dispersive x-ray analysis) was carried out with the spectrum shown in Figure 6-37.

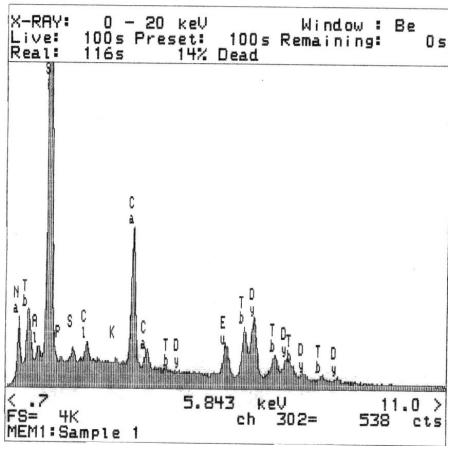

Figure 6-37. EDXA spectrum for the 2Eu-3Tb-3Dy 5 µm sample

Figure 6-37 showed peaks corresponding to europium, dysprosium and terbium proving that there were three dopant rare earth ions present in the 2Eu-3Tb-3Dy glass sample. The remaining peaks were due to the host matrix in the borosilicate glass although boron (from boric oxide) was not present due to the limitations of a beryllium window detector (detectable elements need a mass greater than 11 [116]). Furthermore, EDXA is only partially quantitative therefore concentrations of the dopants could not be confirmed.

6.10.4 Conclusion

These results have verified that the wet sieving technique can be used to successfully separate out 5 μm samples. Furthermore, the particle size analysis and SEM results confirmed that the particles were less than 5 μm in size and that they still contained all three dopant ions respectively. This process can be used in the future to produce more samples to use in ink jet printers and other printing applications.

CHAPTER 7 - ENVIRONMENTAL TESTING OF NOVEL DOPED GLASS TRACERS

7.1 ENVIRONMENTAL TESTING

A range of experiments was set up to simulate extreme environmental conditions that the security label may be exposed to and are tabulated below (Table 7-1).

Condition to simulate	**Experiments carried out**			
Water	Room temperature	60 ^{o}C	100 ^{o}C	
Chemical attack	Household bleach	Vinegar	Beer	Perklone (organic solvent)
Accelerated sunlight attack	Intense UV light			
Abrasion	Sand paper			

Table 7-1. Environmental tests carried out on the glass samples

Each test was carried out on different pieces of the doped glass, which were weighed before any testing and after each time interval to check for any weight loss. A visual inspection was also carried out to determine whether the glass became opaque or discoloured. The duration of time for each test depended on the nature of the test and any indication of change. It was decided not to prolong the testing for longer than it would take for a piece of paper to be destroyed by the test, as the paper document itself would lose its value by this stage.

The samples used in these tests were those in Table 7-2. These were the glasses available at the time of the testing and the peaks observed were the strongest peak (a) and the peak that would be used in the detection system (b). Graphs were then produced by taking the ratio of peak (b) to peak (a). This process normalised the data and removed any variance between the sample size and shape, as the ratios were intrinsic to each sample. All four samples could then be compared in the same graph for each of the nine tests.

Sample	Peaks observed
1.14 mol% Tb	(a)377 nm, (b)484 nm emission at 545 nm
1.14 mol% Eu	(a)395 nm, (b)465 nm emission at 615 nm
3 mol% Eu	(a)395 nm, (b)465 nm emission at 615 nm
3 mol% Eu and 3 mol% Tb	(a)377 nm, (b)484 nm emission at 545 nm and (a)395 nm, (b)465 nm emission at 615 nm

Table 7-2. Samples and peaks used in the environmental tests

7.1.1 Method

Since small pieces of glass were analysed for each test, their height position for placement in the spectrofluorometer for analysis had to be raised in order to detect the fluorescence. Therefore, broken pieces of pipette glass (that did not fluoresce) were placed at the bottom of a cuvette and the sample placed on top as shown in Figure 7-1. Furthermore, the positioning of the sample in the cuvette changed each time, therefore a positioning error had to be accounted for and is analysed later.

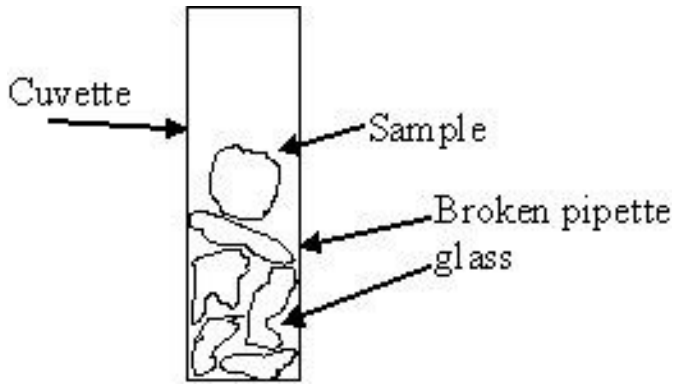

Figure 7-1. Picture of a sample raised by broken pipette glass in a cuvette

In order to produce enough suitably sized samples, the bulk glass samples were re-melted and formed into smaller sizes before analysis. This was not ideal as this can lead to greater internal stress in the glass.

7.1.2 Untreated Samples

The untreated samples were samples that had not been exposed to any environmental tests and would show how the glass surface should look initially.

7.1.2.a Blank

The SEM images for the blank untreated sample are shown in Figure 7-2. There are two images with different levels of magnification noted below each picture. From these images it can be seen that the surface was flat with no sign of cracks. The small fragments on the surface could be pieces of broken glass or powdered glass that had adhered to the sample surface.

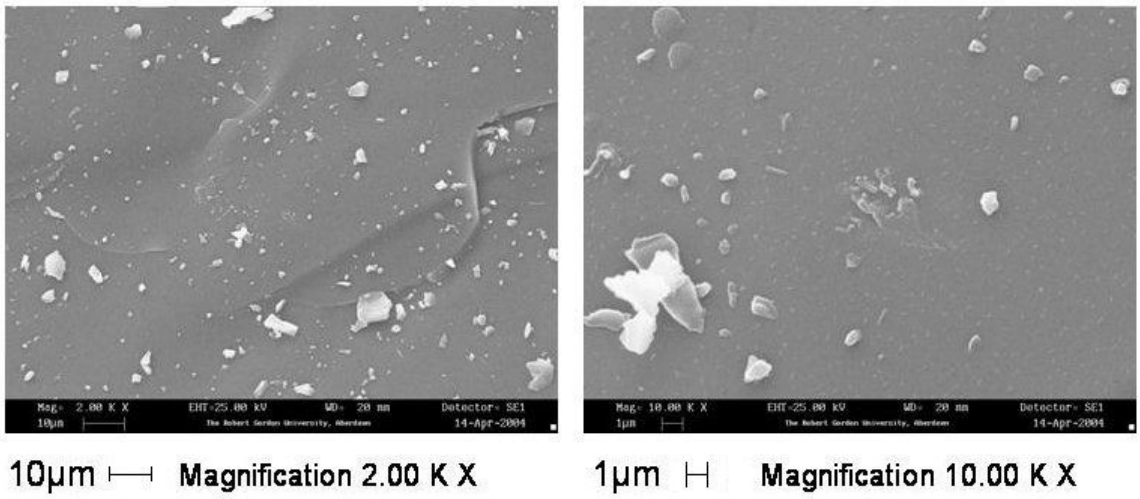

Figure 7-2. SEM images of a blank untreated sample

An example of the EDXA results for the blank untreated sample is shown in Figure 7-3. These results show the constituent atoms on the surface of the sample that have a greater atomic mass of 11. Therefore boron from boric oxide was not present, nor was oxygen. This result proved the fragments on the glass were of the same materials as the bulk as no contaminant atoms were detected in the EDXA results. This result was backed up with a similar EDXA results from the doped samples with the exception of the RE atoms being detected (not shown here).

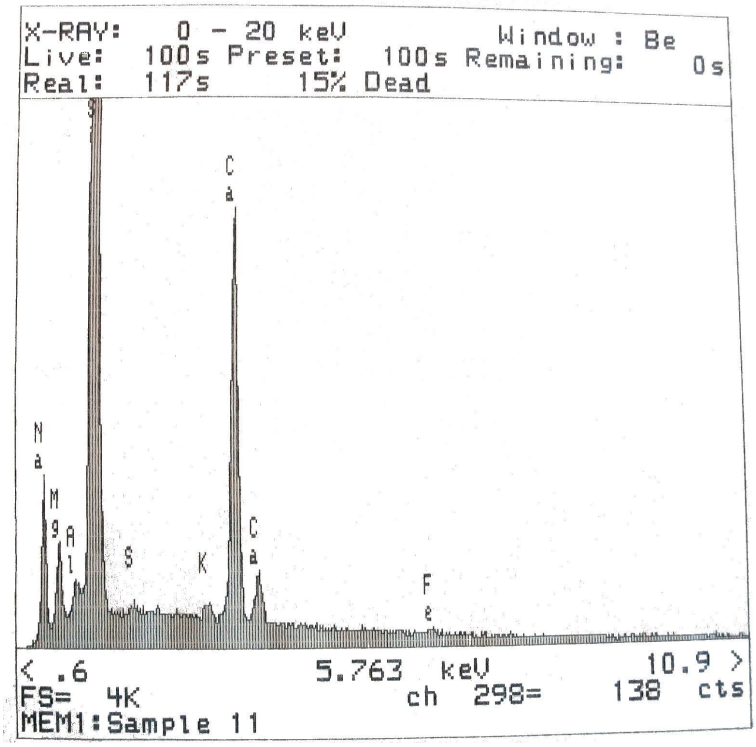

Figure 7-3. EDXA results for the blank untreated sample

7.1.2.b 3 mol% Eu

The SEM images for the 3 mol% europium doped glass are shown in Figure 7-4. These pictures were very similar to the blank sample in that there were no cracks present on the glass surface although again there were fragments of glass on the surface.

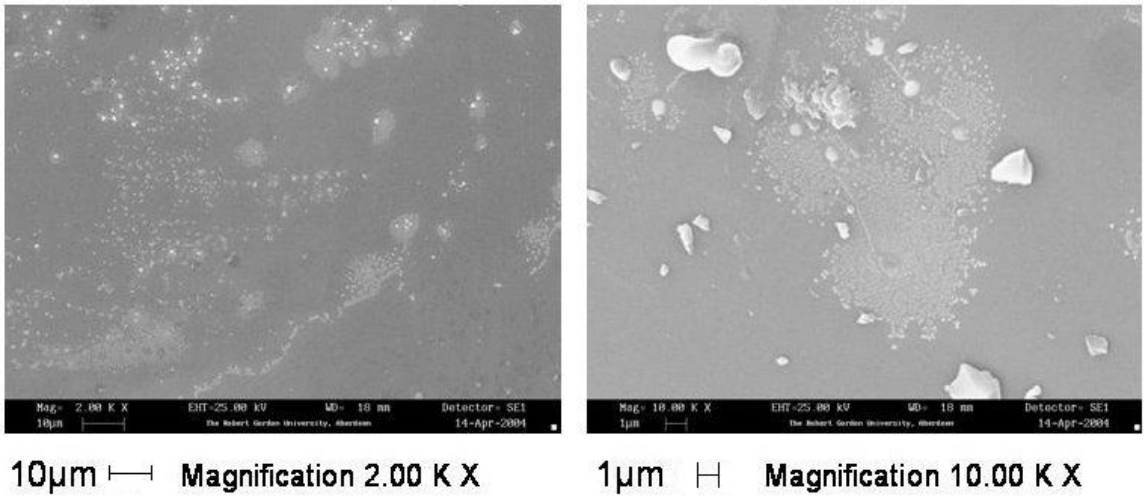

Figure 7-4. SEM images of a 3 mol% Eu doped glass sample

7.1.2.c 3 mol% Tb

The SEM images for the 3 mol% terbium untreated sample are shown in Figure 7-5. These images showed no cracks on the surface of the glass but again there were fragments of glass on the surface.

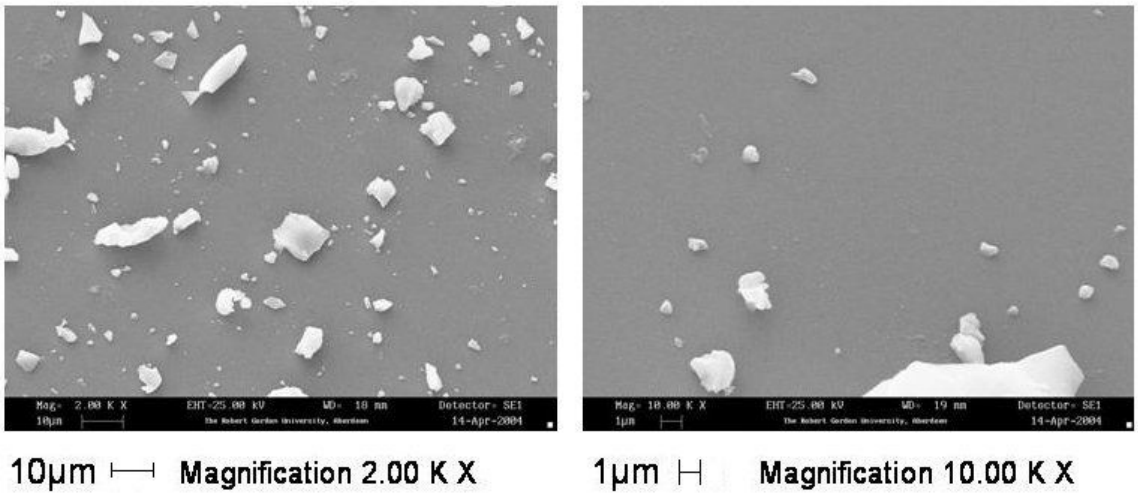

Figure 7-5. SEM images of a 3 mol% Tb doped glass sample

7.1.2.d Conclusion

All the samples analysed by SEM demonstrated that the glass surfaces were smooth and crack free. In each case, fragments of glass were found on the surface because none of the samples were polished before analysis. These images can be used for comparison against those from the environmental tests.

7.2 EXPOSURE TO WATER

The most probable water to come into contact with a security document is rain/tap water or the hot water in a washing machine. This led to testing the samples with room temperature, 60 ^{o}C (washing machine) and 100 ^{o}C (extreme/accelerated condition) distilled water.

7.2.1 Room Temperature Distilled Water

This test was carried out over a total period of two weeks soaking time and the fluorescence ratio results are shown in Figure 7-6.

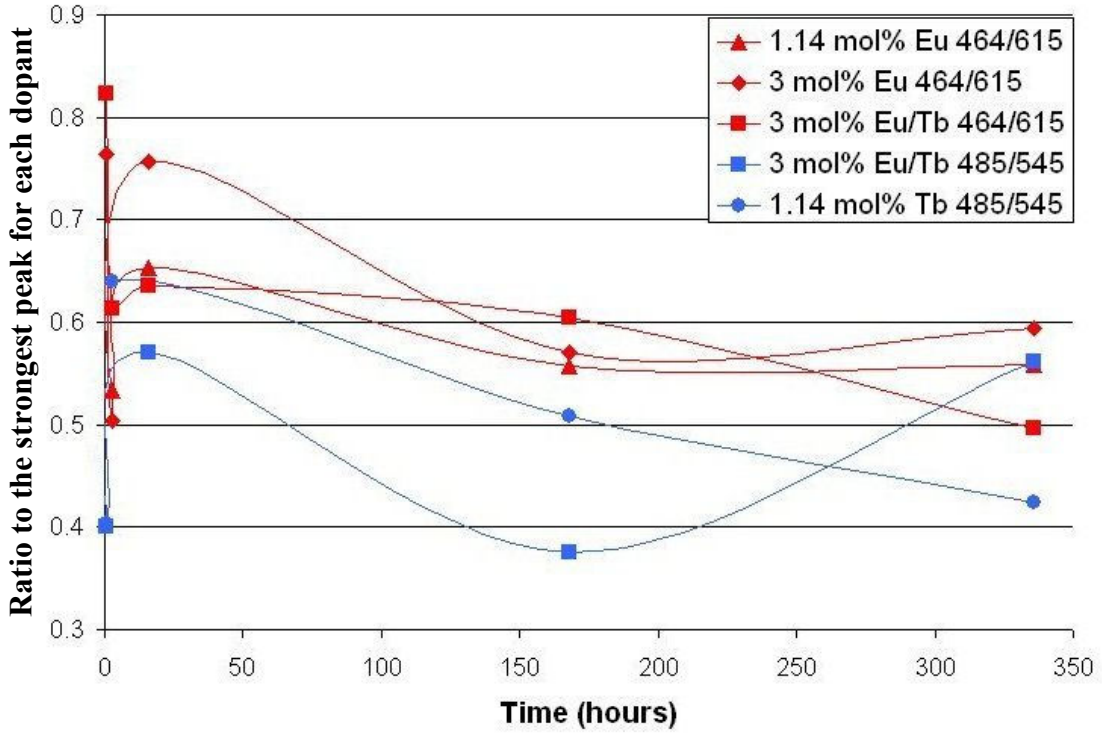

Figure 7-6. Effect of room temperature distilled water on doped samples

Although the graph does not show a perfect straight line, no definite trends can be drawn from these results. It was noted earlier that the position of the glass sample in the cuvette did alter the fluorescence signal greatly and therefore a positioning error standard deviation (SD) was found. This was determined by inserting and removing the sample 20 times from the cuvette and taking the reading at each of the wavelengths. The ratios between these peaks were then calculated and a standard deviation determined for each fluorescence ratio (see Table 7-3).

Peak	Standard Deviation
1.14 mol% Eu 464/615	0.0725
3 mol% Eu 464/615	0.0446
3 mol% Eu/Tb 464/615	0.0446
3 mol% Eu/Tb 485/545	0.0496
1.14 mol% Tb 485/545	0.0496

Table 7-3. Positioning standard deviations for each of the samples

To clearly show the size of the errors, the results for each series are shown in Figure 7-7 with the error bars added from the standard deviation results.

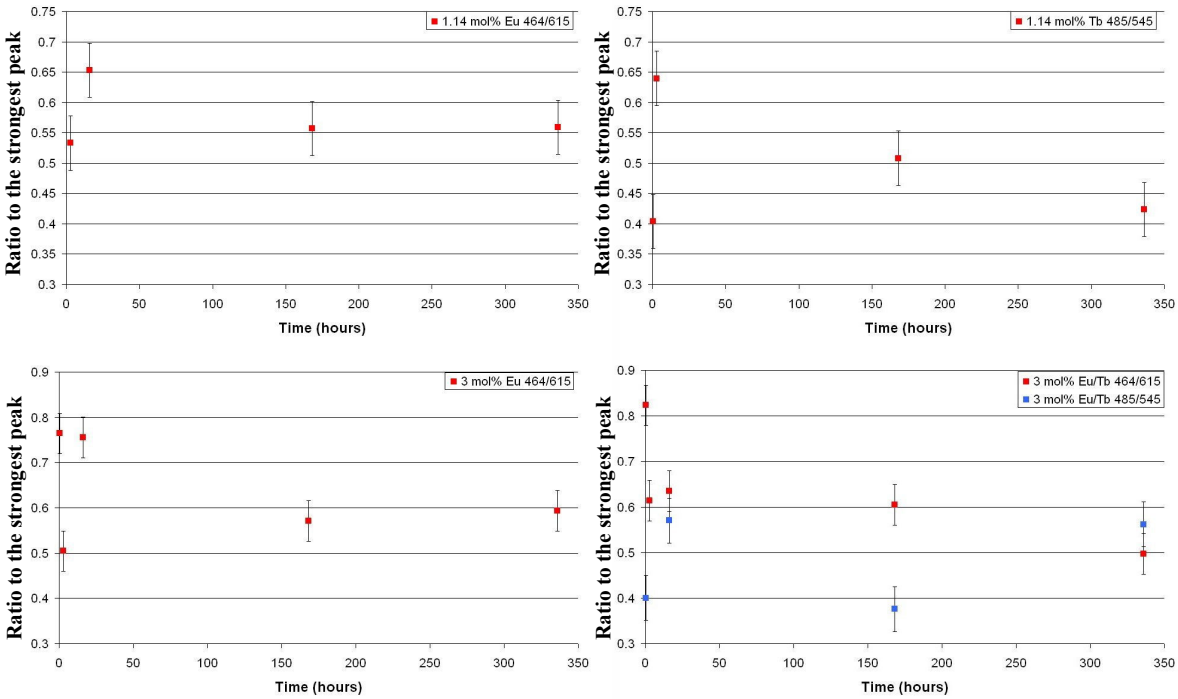

Figure 7-7. Positioning standard deviation for samples exposed to room temperature

Taking into account the standard deviation, it can be clearly seen that the variation of the results were either within their standard deviation or did not follow any definitive trend. As an additional check to help detect any change, the samples were weighed before and after each test interval. The calibration error of the balance was 0.0001g.

A table of the sample weights is shown below (Table 7-4) for the tests with room temperature distilled water. These results were shown to be within the standard deviation, which proved no effect was found.

	1.14 mol% Eu	3.0 mol% Eu	3.0 mol% Eu/Tb	1.14 mol% Tb
Initial	0.1668	0.0446	0.0867	0.0914
10mins	0.1664	0.0444	0.0862	0.0911
30mins	0.1668	0.0445	0.0865	0.0911
3hrs	0.1667	0.0446	0.0866	0.091
16hrs	0.1668	0.0446	0.0867	0.0912
1wk(168hrs)	0.1667	0.0445	0.0867	0.0912
2wks(336hrs)	0.1667	0.0444	0.0866	0.0913
Mean	0.1667	0.0445	0.0866	0.0912
SD	0.0001	0.0001	0.0002	0.0001

Table 7-4. Weights (g) of samples over two weeks of tests in room temperature distilled water

One observation made was the samples went opaque after the two-week test in cold water. Since there were no changes in weight to the samples, further investigation as to the cause of the visual alteration was carried out using SEM.

7.2.2 SEM Analysis

Considering the room temperature water samples appeared cloudy after the two weeks exposure, these samples were selected to try and understand what affect the water had on the glass surface.

7.2.2.a Blank

The SEM images are shown in Figure 7-8 and indicates large and small cracks throughout the glass surface.

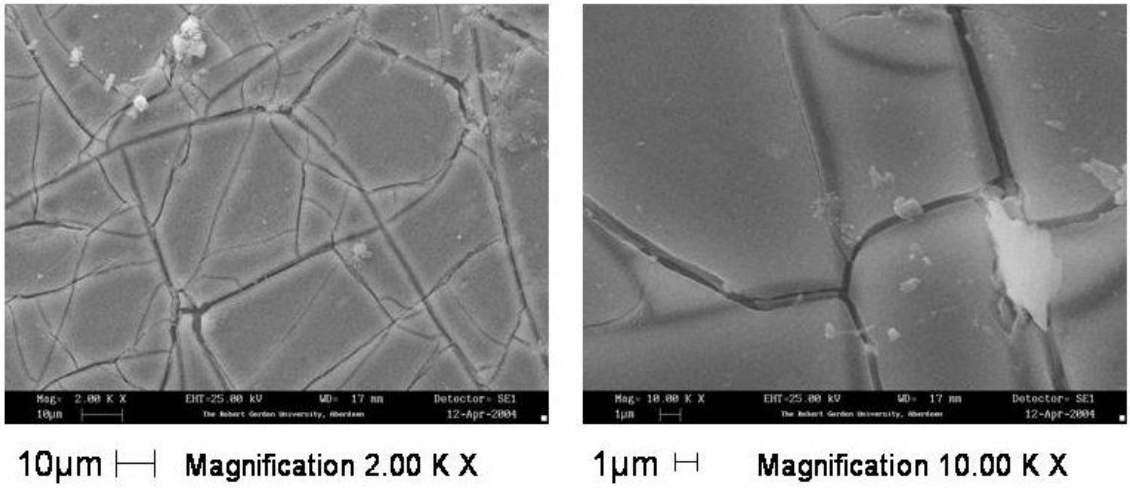

Figure 7-8. SEM images of the blank glass after two weeks exposure to room temperature water

In general, when glass comes into contact with water it may cause a series of complex chemical reactions resulting in an alkaline solution [117]. Water reacts slowly with the glass initially but increases with time as the alkali concentration of the solution increases. Faint whitening, which was observed in the room temperature testing, could therefore be due to an initial attack on the glass surface as it changed from a glassy silicate structure to a crystalline silicate structure on the surface. However, if this occurs then there would be a weight gain due to the added water molecules that had attached to the glass. Since this was not apparent, this would suggest that something happened to the glass prior to testing such as an increase in the stress during production. Additionally, an increased effect would be found for the 60 °C and 100 °C water tests analysed later if the cracks were due to the water. An EDXA analysis was carried out with the results shown in Figure 7-9. In comparison to the untreated blank glass, there did not appear to be any difference in the atoms found on the surface. This further enhances the view that the glass was affected by greater stresses during the production process rather than a water attack.

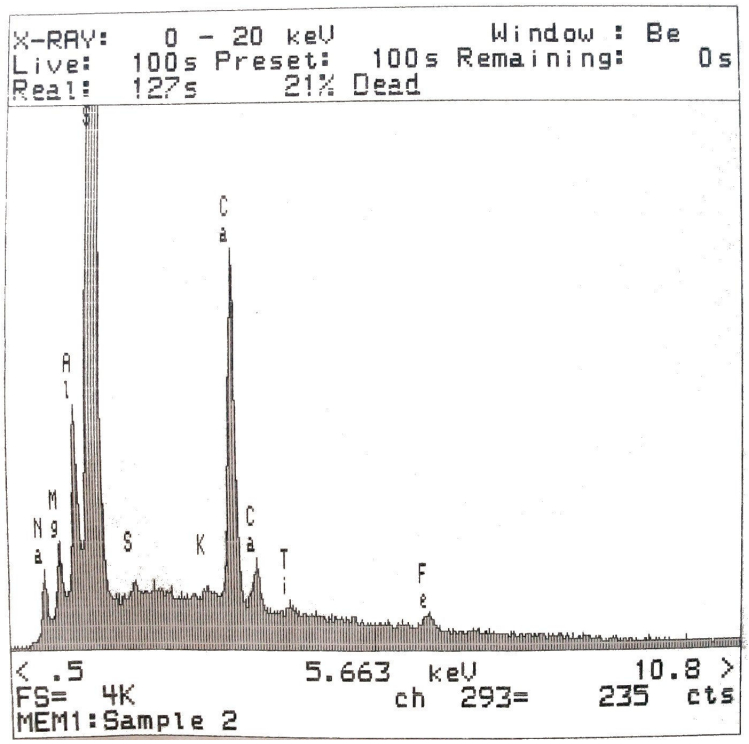

Figure 7-9. EDXA for the blank sample after two weeks exposure to room temperature distilled water

7.2.2.b 1.14 mol% Eu

The SEM images for the 1.14 mol% europium sample are shown in Figure 7-10. Cracks were again present on the surface and can be related to the cloudy appearance of the sample.

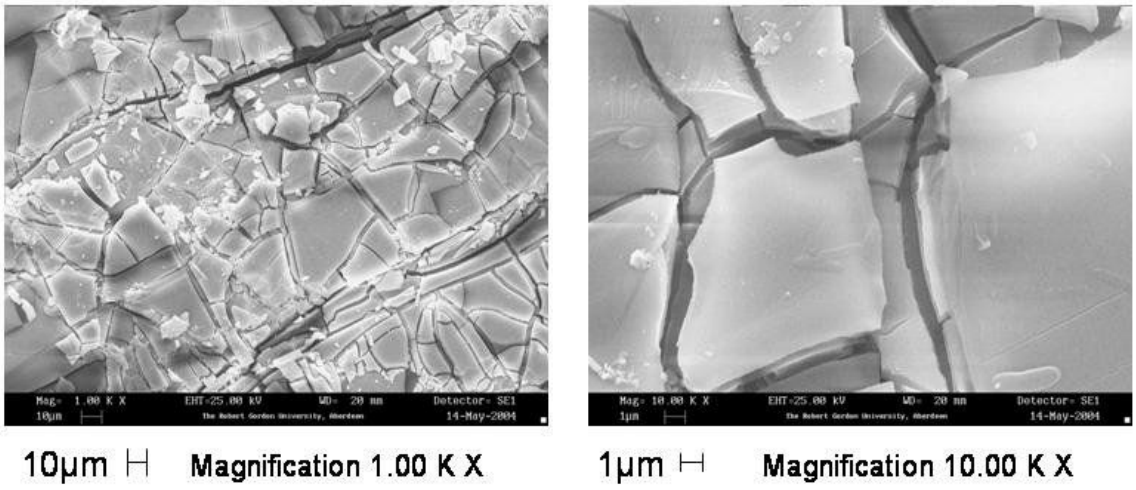

Figure 7-10. SEM images of the 1.14 mol% Eu doped glass after two weeks exposure to room temperature distilled water

7.2.2.c 1.14 mol% Tb

For the 1.14 mol% terbium doped sample, the SEM images are shown in Figure 7-11. The cracks present this time were not as severe as the europium doped sample but were still present.

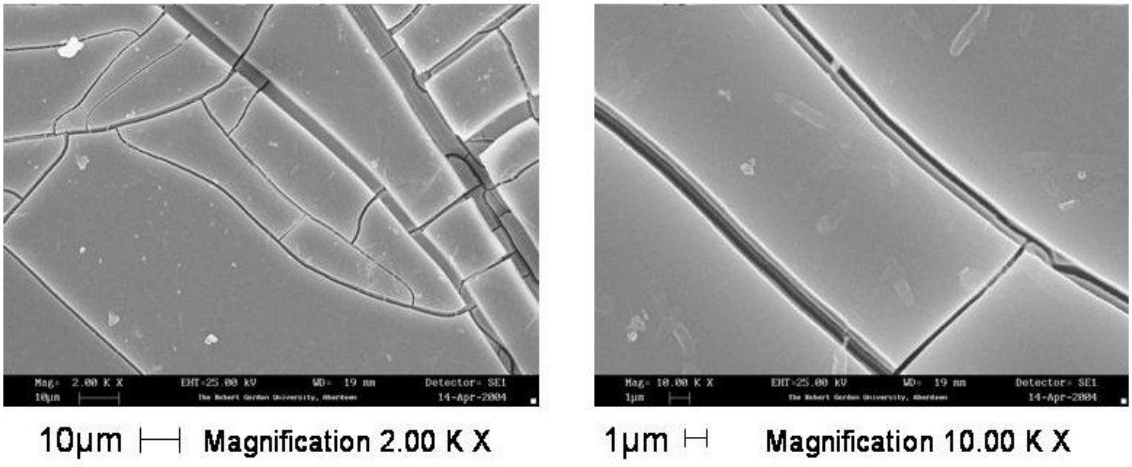

Figure 7-11. SEM images of the 1.14 mol% Tb doped glass after two weeks exposure to room temperature distilled water

7.2.2.d 3 mol% Eu

Figure 7-12 shows the SEM images for the 3 mol% europium doped glass. Once again the cracks were present showing some changes on the surface of the glass causing the sample to turn opaque.

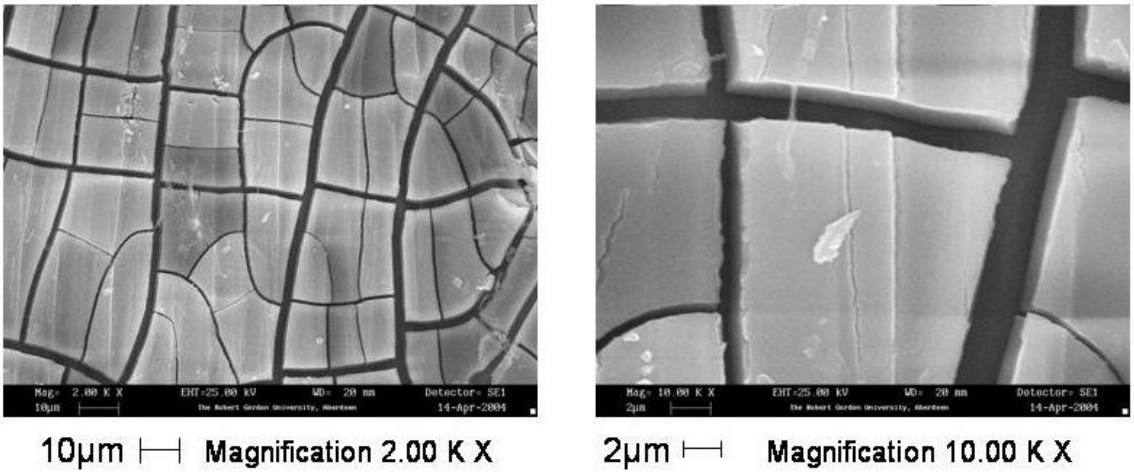

Figure 7-12. SEM images of the 3 mol% Eu doped glass after two weeks exposure to room temperature distilled water

7.2.2.e 3 mol% Eu and 3 mol% Tb

For the mixed europium and terbium doped glass, the SEM images are shown in Figure 7-13. These results showed the cracks were still present, therefore this sample contained defects on its surface.

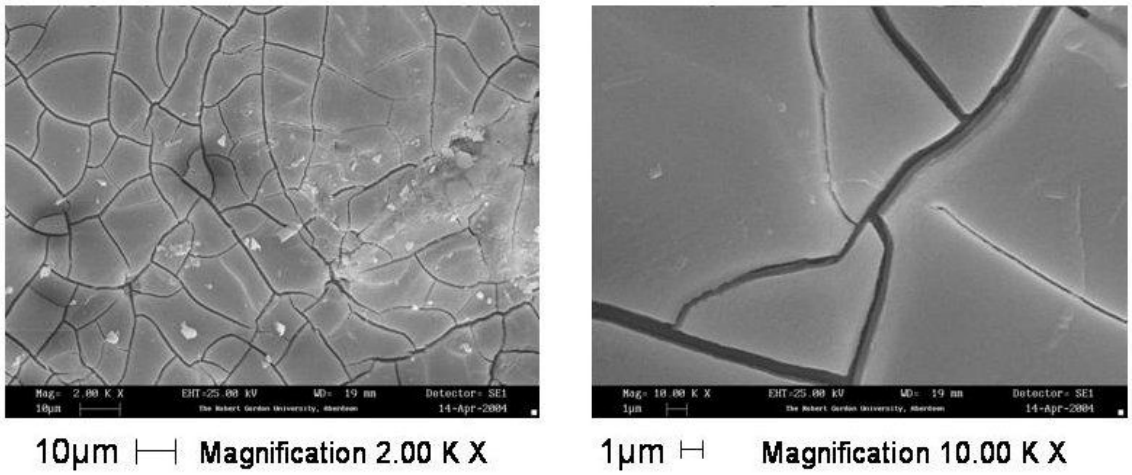

Figure 7-13. SEM images of the 3 mol% Eu and 3 mol % Tb doped glass after two weeks exposure to room temperature distilled water

7.2.3 Conclusion

For all the room temperature distilled water environmental tests, each sample was found to have a cloudy appearance after two weeks exposure. From the SEM images, this cloudy effect was due to the surface of the glass containing lots of very small cracks possibly due to the water attack described for the blank sample. However, it could be concluded from the environmental results that there were no significant changes in weight of the samples nor was there a significant change in the fluorescence ratio intensities; therefore, it appeared as though the cracks were only on the surface of the glass and did not affect the dopant signal. Furthermore, as there was no weight gain for any of the samples, it did not appear likely that the cracks were due to an interaction with water as the weight would increase with the addition of water molecules. The EDXA results of the blank glass also confirmed the absence of other atoms in comparison to the untreated glass meaning there was no effect caused to the glass chemically. Physically the glasses were affected with the appearance of cracks; however, the analysis would have to be repeated with fresh samples to determine whether the cracks were caused by the water or from internal stresses in the glass. These results can be confirmed in the 60 °C and 100 °C water tests as any water effects would be accelerated with an increase in temperature.

7.3 60 °C DISTILLED WATER

These tests were carried out for 120 minutes in 60 °C distilled water. Since the usual time for a washing machine to complete its cycle is approximately one hour, this would simulate an extreme case.

As can be seen in Figure 7-14, the point after 40 minutes for the 1.14 mol% Tb 484/545 peak appeared to be a suspect result that should be removed. To prove this, the Q-test was used to determine whether or not it was an outlier that statistically should be removed [113].

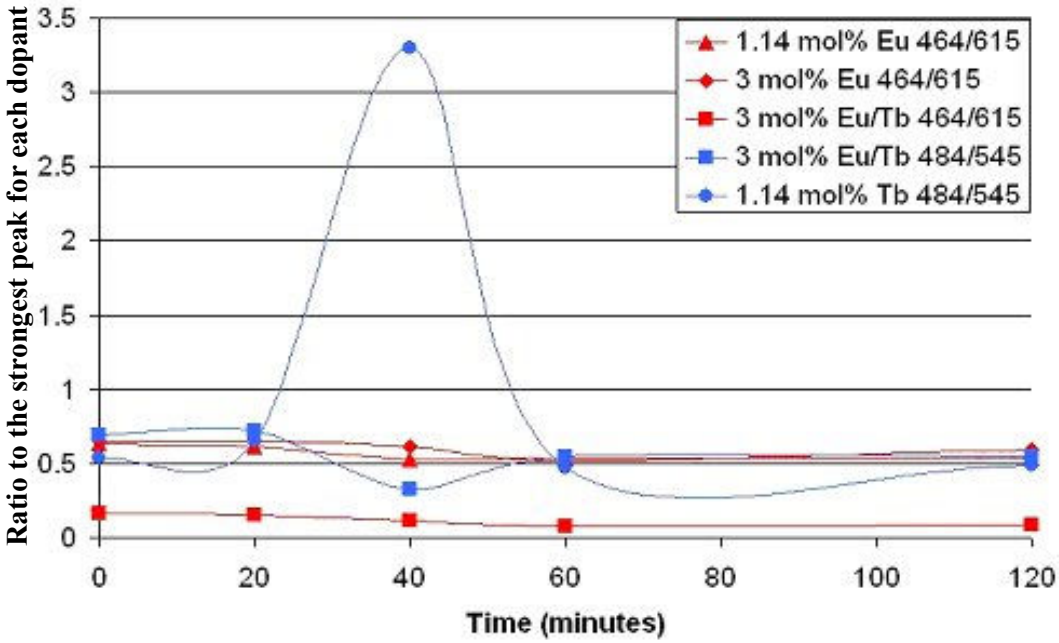

Figure 7-14. Effect of 60 °C distilled water on doped samples

Q = (suspect value – nearest value) / (largest value – smallest value)

Q = 0.936

Q_{crit} for 5 data sets = 0.717 therefore Q was greater than Q_{crit} and therefore should be removed. The corrected data set is now shown in Figure 7-15 using the standard deviations described previously.

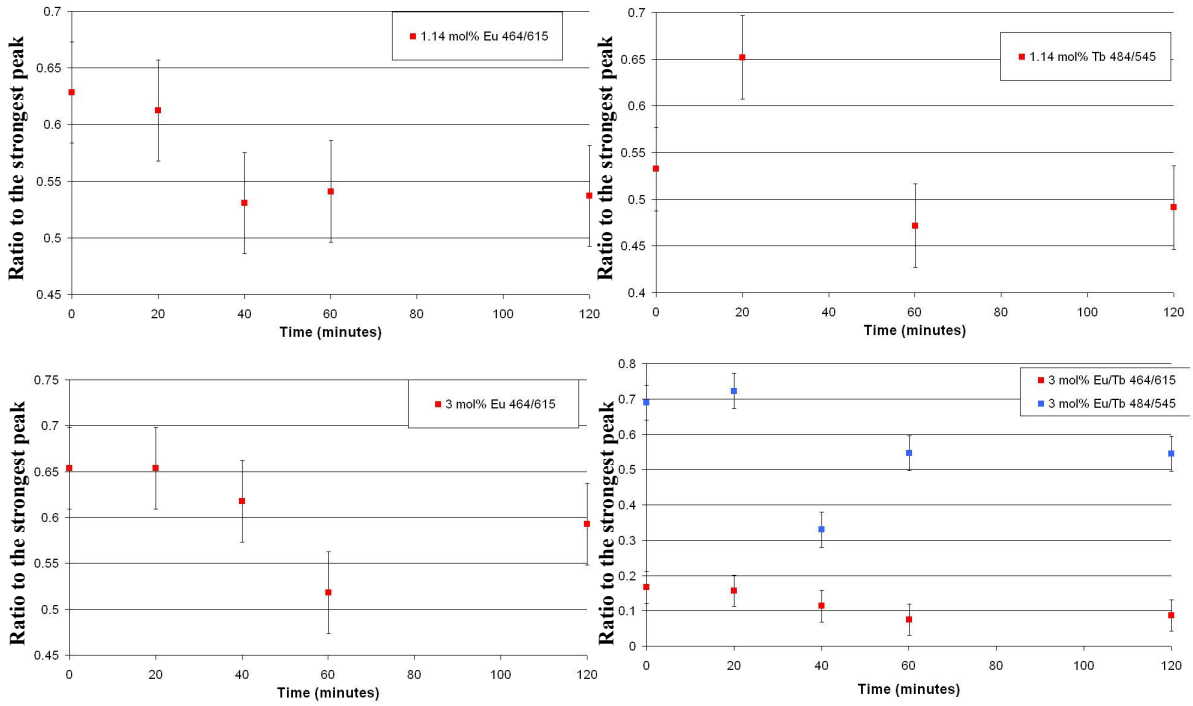

Figure 7-15. Positioning standard deviation for samples exposed to 60°C distilled water

These results did not show any real trends that were outside the error bars for each sample. Only the 3 mol% Eu/Tb 484/545 peak appeared to vary out with the error bars, however, the results fluctuated which made it difficult to determine whether or not there was actually any real change.

Table 7-5 shows that there were no significant changes in the weights of the samples and therefore backs up the claim that no significant effect was found. Furthermore, there was no visual change in appearance of the glass as reported for the cold water experiments. This would have been expected to become progressively worse as heating the water should accelerate any effects on the glass. Therefore, the cold water results were due to internal stresses during their production. This can be further investigated using a SEM.

	1.14 mol% Eu	3.0 mol% Eu	3.0 mol% Eu/Tb	1.14 mol% Tb
Initial	0.2055	0.1606	0.7645	0.5681
20mins	0.2054	0.1604	0.7643	0.5681
40mins	0.2055	0.1605	0.7645	0.5681
60mins	0.2056	0.1603	0.7644	0.5682
120mins	0.2054	0.1604	0.7644	0.5681
Mean	0.2055	0.1604	0.7644	0.5681
SD	0.0001	0.0001	0.0001	0.0001

Table 7-5. Weights (g) of samples over two hours of tests in 60 °C distilled water

7.3.1 SEM Analysis

After the samples were noticed to have turned cloudy when exposed to cold water, it was expected that the effects would be enhanced further by increasing the temperature. Although the 60 °C water environmental tests did not appear cloudy after their two hour exposure, SEM analysis was carried out to determine if there were still some cracks present from a water attack.

7.3.1.a Blank

The first sample analysed was the blank glass and the SEM images are shown in Figure 7-16. These images clearly showed no cracks on the surface and therefore no effect from the 60 °C water.

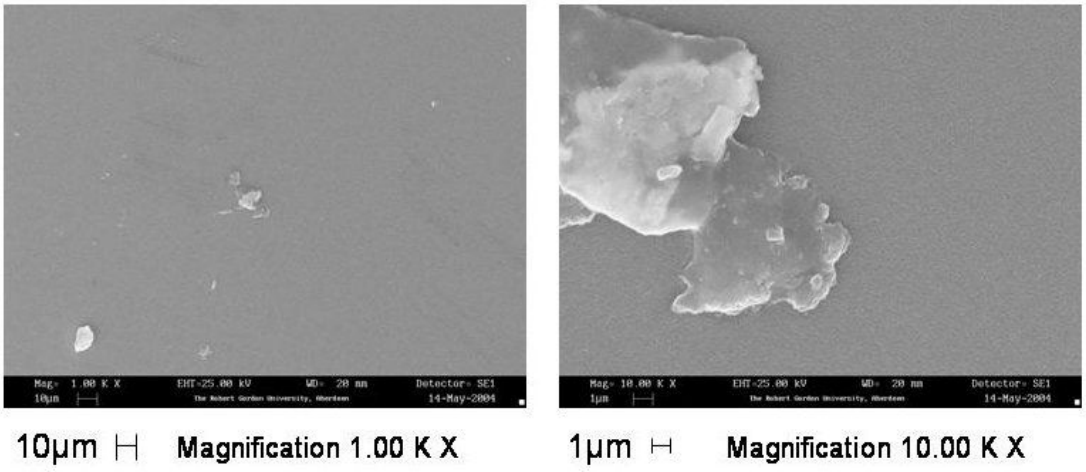

Figure 7-16. SEM images of the blank glass after two hours exposure to 60 °C distilled water

The EDXA result for the blank glass is shown in Figure 7-17. This showed no evidence of change from the untreated blank glass EDXA shown earlier and therefore no detrimental affects found on the glass.

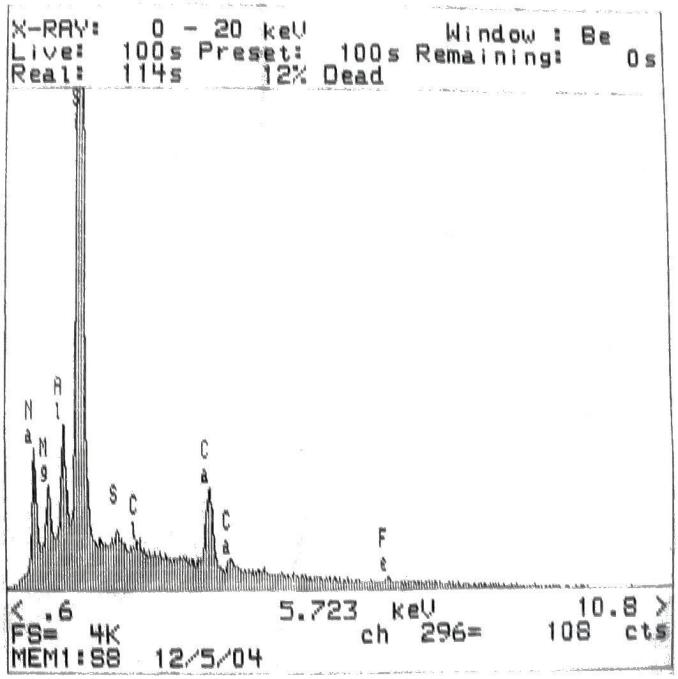

Figure 7-17. EDXA results for the blank glass exposed to 60 ^{o}C distilled water for two hours

7.3.1.b 1.14 mol% Eu

The 1.14 mol% europium doped glass SEM images are shown in Figure 7-18. Although the pictures did not look as smooth as the blank pictures, there were still no cracks on the surface.

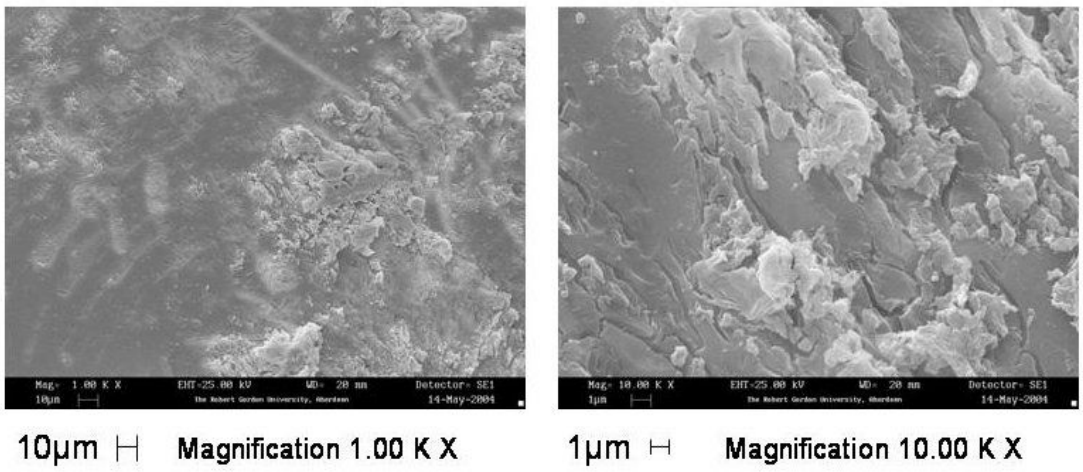

Figure 7-18. SEM images of the 1.14 mol% Eu doped glass after two hours exposure to 60 °C distilled water

7.3.1.c 1.14 mol% Tb

The SEM images of the 1.14 mol% terbium doped glass are shown in Figure 7-19. These showed no sign of any cracks on the glass surface and therefore no effect from the water.

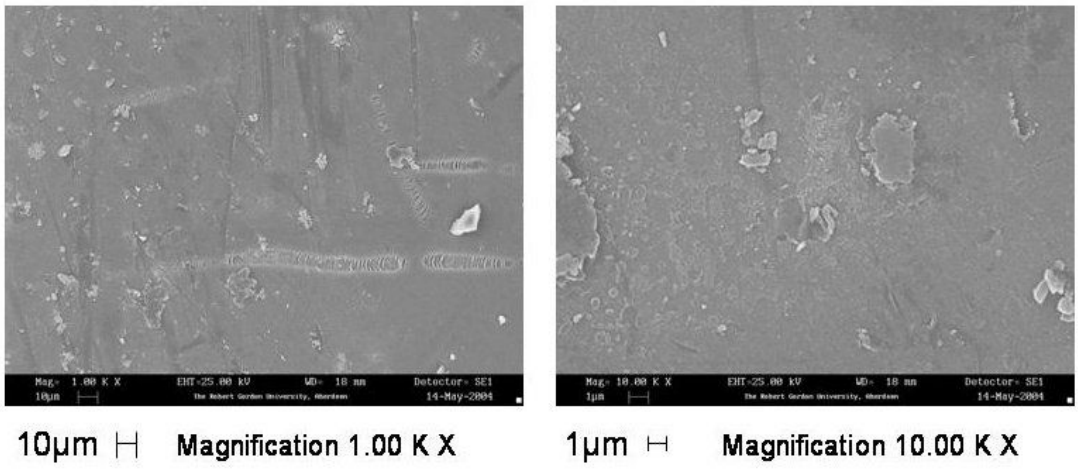

Figure 7-19. SEM images of the 1.14 mol% Tb doped glass after two hours exposure to 60 °C distilled water

7.3.1.d 3 mol% Eu

The 3 mol% europium doped glass images are shown in Figure 7-20. These images showed no sign of any cracks on the surface and therefore no effect from the water.

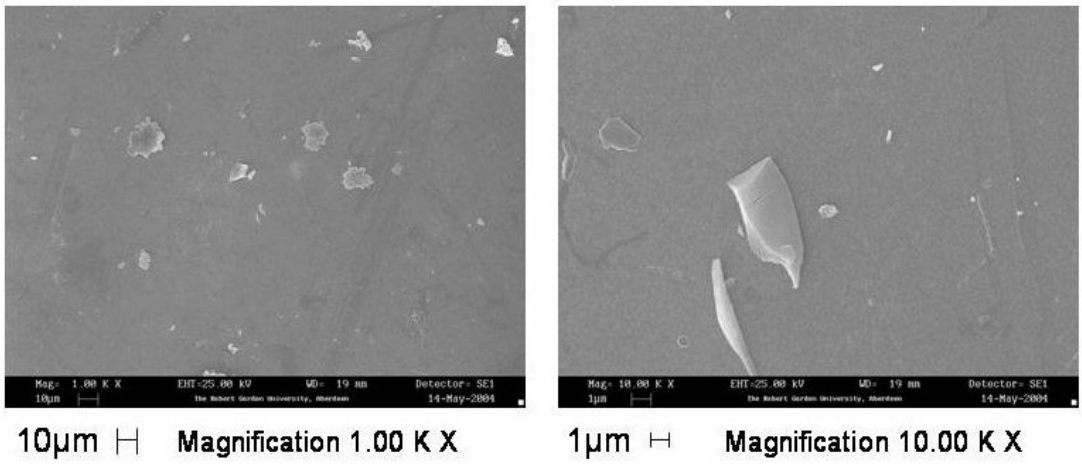

Figure 7-20. SEM images of the 3 mol% Eu doped glass after two hours exposure to 60 °C distilled water

7.3.1.e 3 mol% Eu and 3 mol% Tb

The final sample for the 60 °C water was the 3 mol% europium and 3 mol% terbium doped glass with their SEM images shown in Figure 7-21. These images also showed no signs of cracks appearing on the surface.

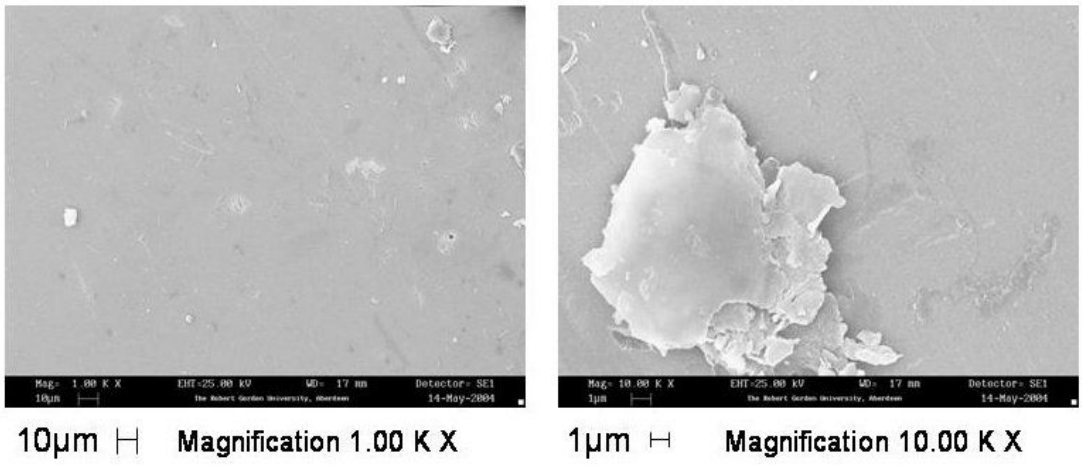

Figure 7-21. SEM images of the 3 mol% Eu and 3 mol% Tb doped glass after two hours exposure to 60 °C distilled water

7.3.2 Conclusion

For the 60 °C water environmental tests, no cloudy appearance was observed after two hours exposure. All the SEM images for all the samples confirmed there were no cracks on the glass surfaces and therefore the 60 °C water did not affect the samples. This appeared unusual as the temperature should have accelerated any effects the room temperature water had on the samples. Since this did not happen, it is possible that the time of exposure was not long enough to affect the samples in comparison to the room temperature samples. Additionally, it is possible that the samples used here were not produced by re-melting the bulk glass again but were produced by melting and quenching once. This would mean there were fewer internal stresses and therefore were less likely to crack. Furthermore, the results reported earlier showed no significant changes in weight of the samples nor was there a significant change in the fluorescence signal, therefore the 60 °C water did not cause a significant affect.

7.4 100 °C DISTILLED WATER

These tests were carried out for two hours in 100 °C distilled water to accelerate any affect from the water.

Figure 7-22 shows all of the points were within the error bars. The only series that appeared to follow a trend upwards was the 3 mol% Eu 465/615 which would indicate the 465 nm peak was becoming stronger. Although this was a change, it meant the peak for detection became stronger and therefore would not cause a problem for detection purposes.

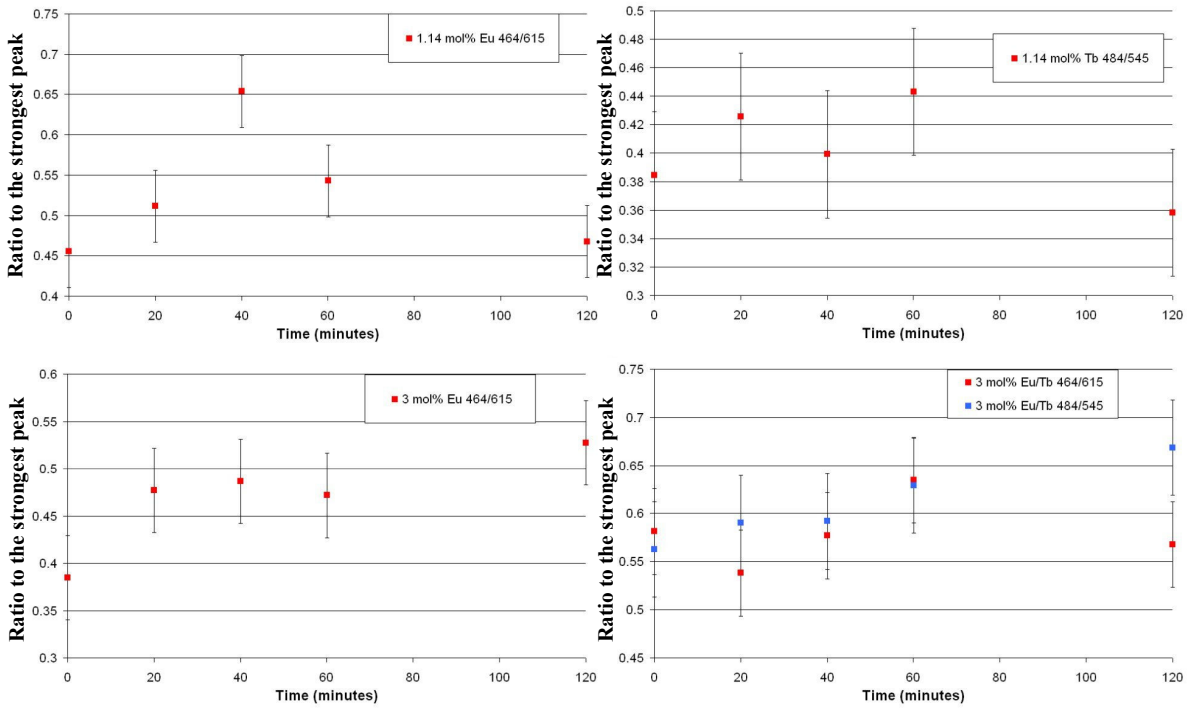

Figure 7-22. Positioning standard deviation for samples exposed to 100°C distilled water

Any change in results should be noticed in the sample weights, as with all of these environmental tests, however, Table 7-6 indicated no weight change for any of the samples. This along with no visual change in appearance suggested the slight increase for the two samples mentioned above would level out with further tests.

	1.14 mol% Eu	3.0 mol% Eu	3.0 mol% Eu/Tb	1.14 mol% Tb
Initial	0.1148	0.0787	0.5015	0.1792
10mins	0.1144	0.0786	0.5016	0.1793
20mins	0.1148	0.0786	0.5015	0.1791
40mins	0.1146	0.0787	0.5014	0.1792
60mins	0.1147	0.0786	0.5015	0.1792
Mean	0.1147	0.0786	0.5015	0.1792
SD	0.0002	0.0001	0.0001	0.0001

Table 7-6. Weights (g) of samples over one hour of tests in 100 °C distilled water

7.4.1 SEM Analysis

The 100 °C water environmentally tested samples, representing a further accelerated investigation of water attack, were analysed by SEM. The previously reported results suggested there was no significant difference in weight or the fluorescence intensities after two hours exposure for any of the samples and that no cloudy appearance was found.

7.4.1.a Blank

The first sample analysed was the blank and the SEM images are shown in Figure 7-23. Although these images did not show any cracks on the surface, it looked as though there were crystals forming. These could be the sign of an attack at the early stages with the formation of a crystalline silicate structure forming on the surface.

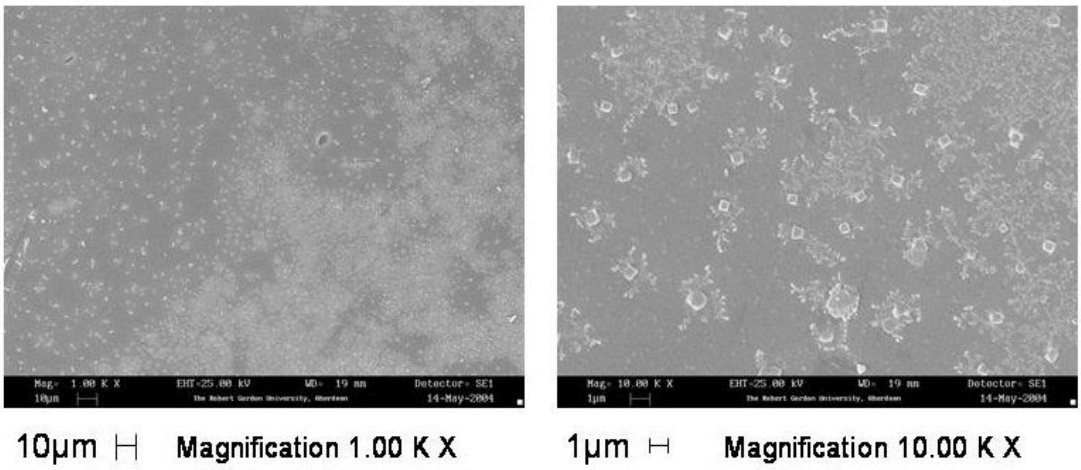

Figure 7-23. SEM images of the blank glass after two hours exposure to 100 °C distilled water

The EDXA result for the blank glass exposed to 100 °C water for two hours is shown in Figure 7-24. This did not contain any additional elements for the glass surface that were not present for the untreated sample.

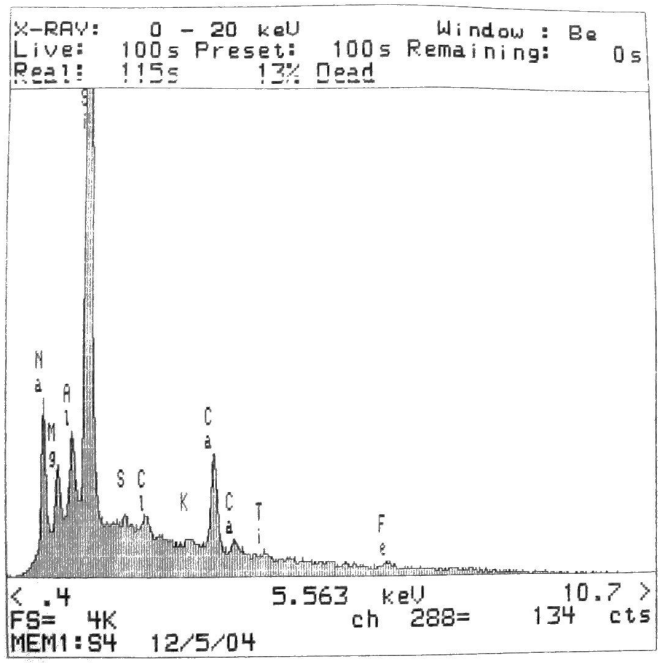

Figure 7-24. EDXA results for the blank glass after exposure to 100 ^{o}C distilled water for two hours

7.4.1.b 1.14 mol% Eu

The SEM images for the 1.14 mol% europium doped glass are shown in Figure 7-25. These images did not show any sign of cracks or crystals on the surface and therefore no effect from the water.

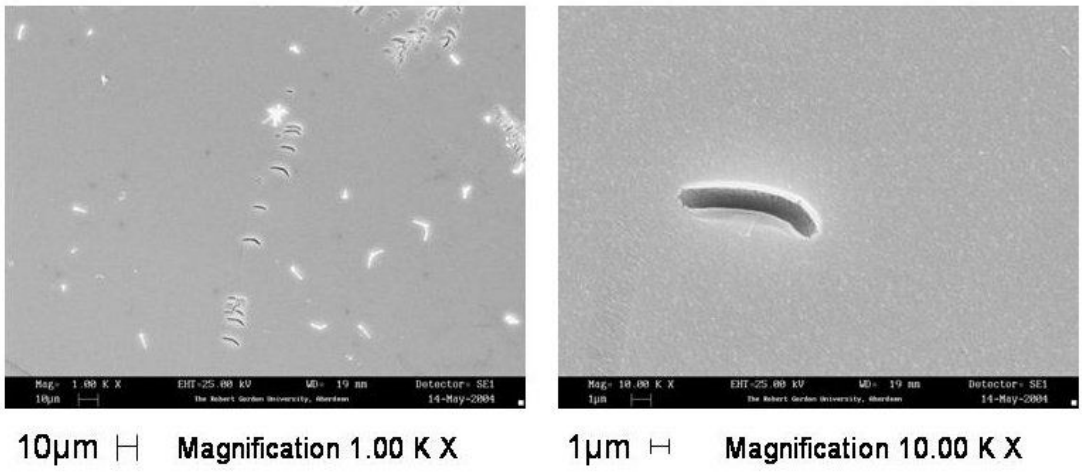

Figure 7-25. SEM images of the 1.14 mol% europium doped glass after two hours exposure to 100 °C distilled water

7.4.1.c 1.14 mol% Tb

For the 1.14 mol% terbium doped sample, the SEM images are shown in Figure 7-26. The large "crater" on the left hand side image, could be from an air bubble or pocket where an air bubble once was. Furthermore, these images showed no cracks on the surface and therefore no effect was found from the water.

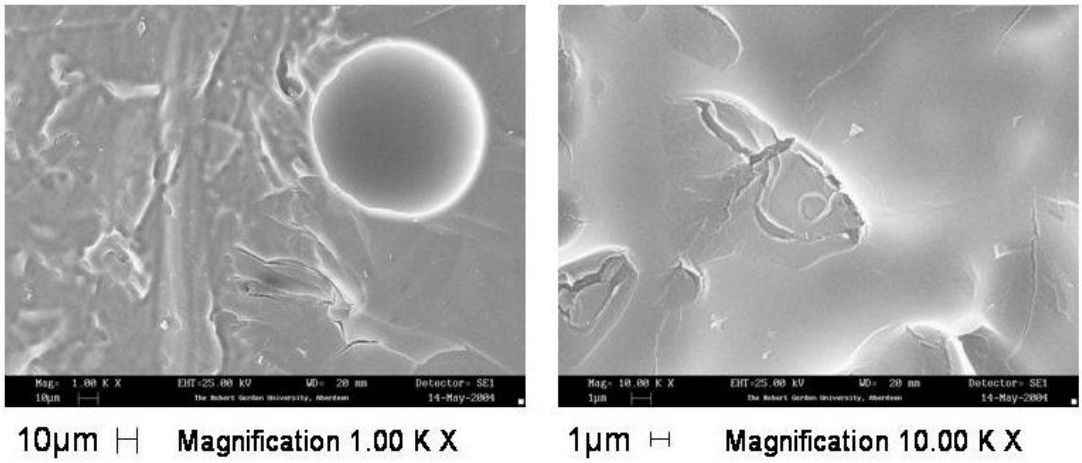

Figure 7-26. SEM images of the 1.14 mol% terbium doped glass after two hours exposure to 100 °C distilled water

7.4.1.d 3 mol% Eu

The 3 mol% europium doped glass SEM images are shown in Figure 7-27. The brighter lines on the left hand side image could be cracks on the glass. However, these could have been caused when the glass was broken off a larger piece of glass as the morphology is different from the cracks observed in the room temperature water samples.

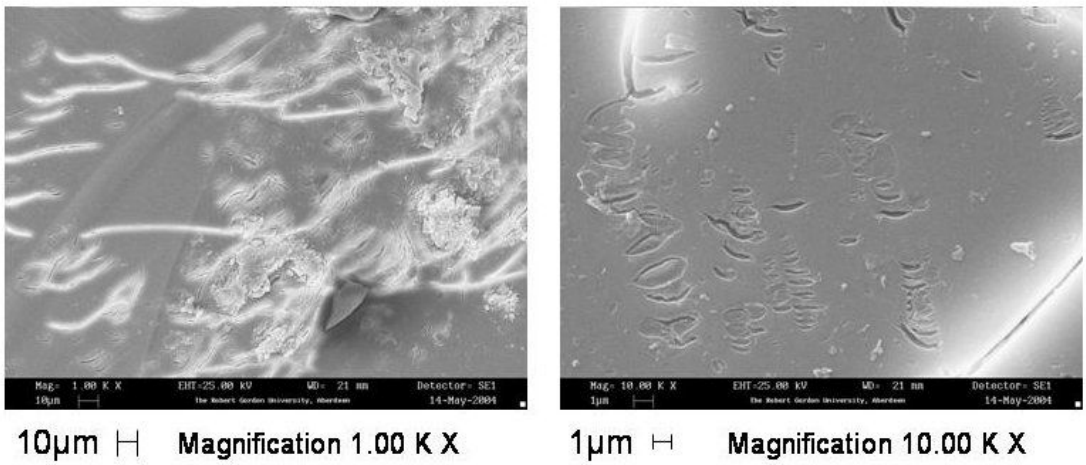

Figure 7-27. SEM images of the 3 mol% Eu doped glass after two hours exposure to 100 °C distilled water

7.4.1.e 3 mol% Eu and 3 mol% Tb

The double doped europium and terbium glass SEM images are shown in Figure 7-28. These appeared similar to the blank sample for the 100 °C water with small traces of crystals appearing on the surface. This could be a result of initial water attack on the surface of the glass although no cracks were present.

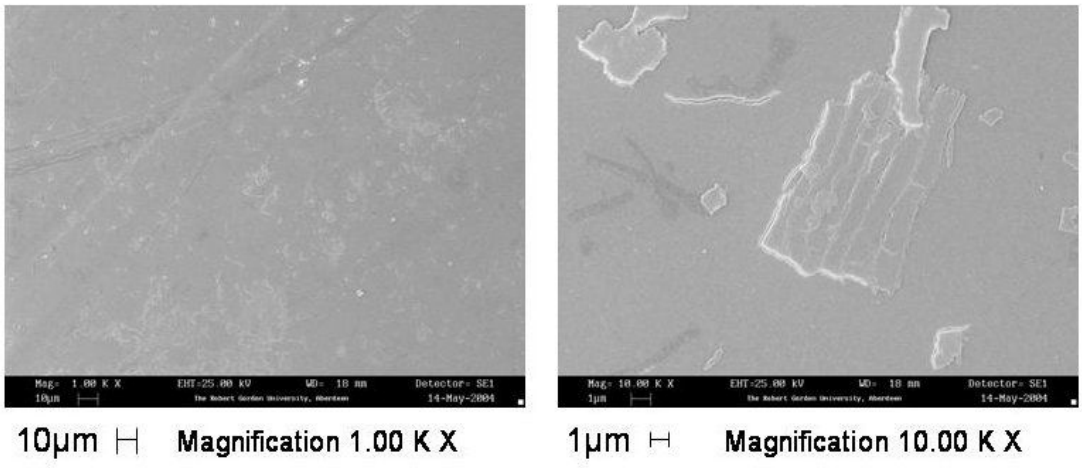

Figure 7-28. SEM images of the 3 mol% Eu and 3 mol% Tb doped glass after two hours exposure to 100 °C distilled water

7.4.2 Conclusion

For the 100 °C water environmental tests, the earlier reported results concluded by saying there were no significant changes in their fluorescence or weights and therefore that there was no affect from the water. The SEM results would tend to agree with this as there were no cracks observed on the surfaces although there were some crystals formed which may have indicated the beginning of a water attack. However, as the samples were not cloudy in appearance and the fluorescence signals did not change then there was no significant affect after two hours exposure to 100 °C distilled water.

These results have shown that the water does not cause the cracks on the sample surface as there were no indications of cracks in the 60 °C or 100 °C tests. Instead, internal stresses from the quenching of the samples may have been released by the two weeks exposure to the room temperature water. This affect was not observed for the heated water either because the samples heated at 60 °C and 100 °C had no quenching cracks or perhaps due to the shorter exposure time. However, as the fluorescence signals did not change in the

same time period, the affect was only to the glass and not the dopants. Therefore the water environment should not alter our ability to detect the label and would be surprising if the security item was subjected to a longer length of time immersed in water in the real world without affecting the security item itself.

7.5 CHEMICAL ATTACK

The strongest chemicals most likely to come into contact with any kind of security paper are bleach (alkali), vinegar (acid), beer (alcohol) and perklone (organic solvent used in dry cleaning). Therefore each of these conditions was tested.

7.6 EXPOSURE TO BLEACH

Household bleach was used in this test (Safeway basic bleach) to simulate a realistic environmental test. The experiment was run for 60 minutes, which would be a very long time for any paper to be in contact with bleach without destroying the document.

Figure 7-29 shows a spread of the fluorescence ratio results, however once the error bars were added, the results were within statistical error as shown in Figure 7-30. The point at 20 minutes for the 3 mol% Eu/Tb 484/545 was checked with the Q-test but was found to be lower than Q_{crit} and therefore had to remain. Only the 1.14 mol% Tb 484/545 peak after 60 minutes was outside its own error bars, although this could be an outlier result that would require more time exposed to bleach to determine whether this was starting a trend upwards or not.

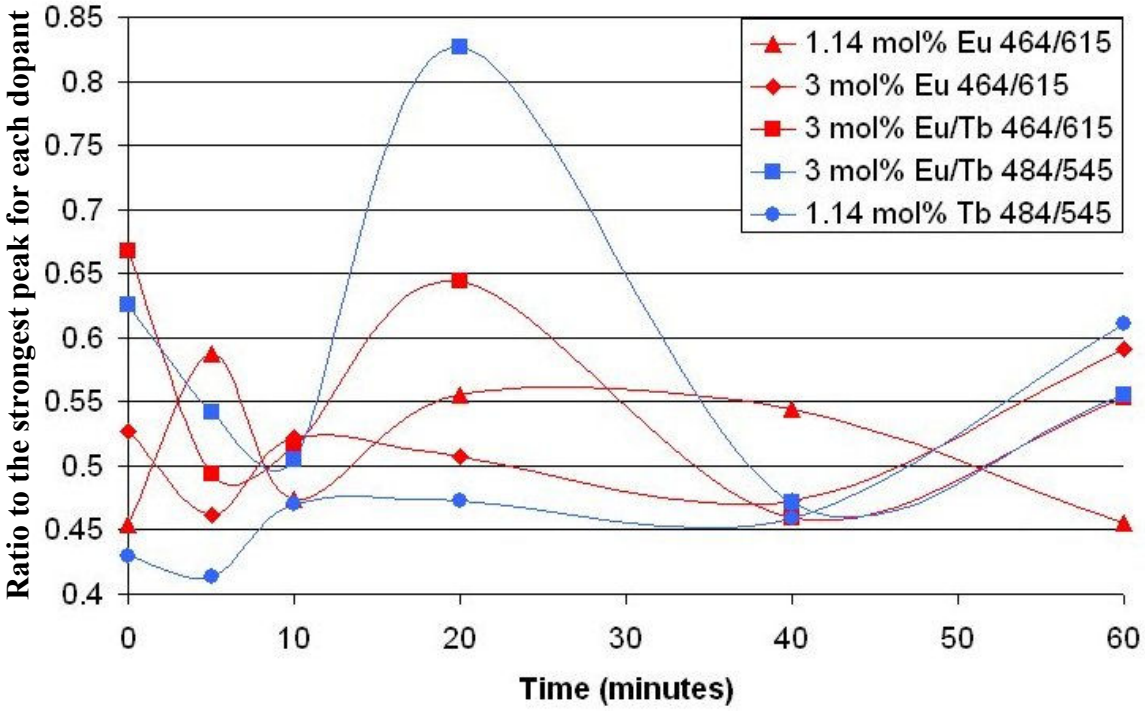

Figure 7-29. Effect of bleach on doped samples

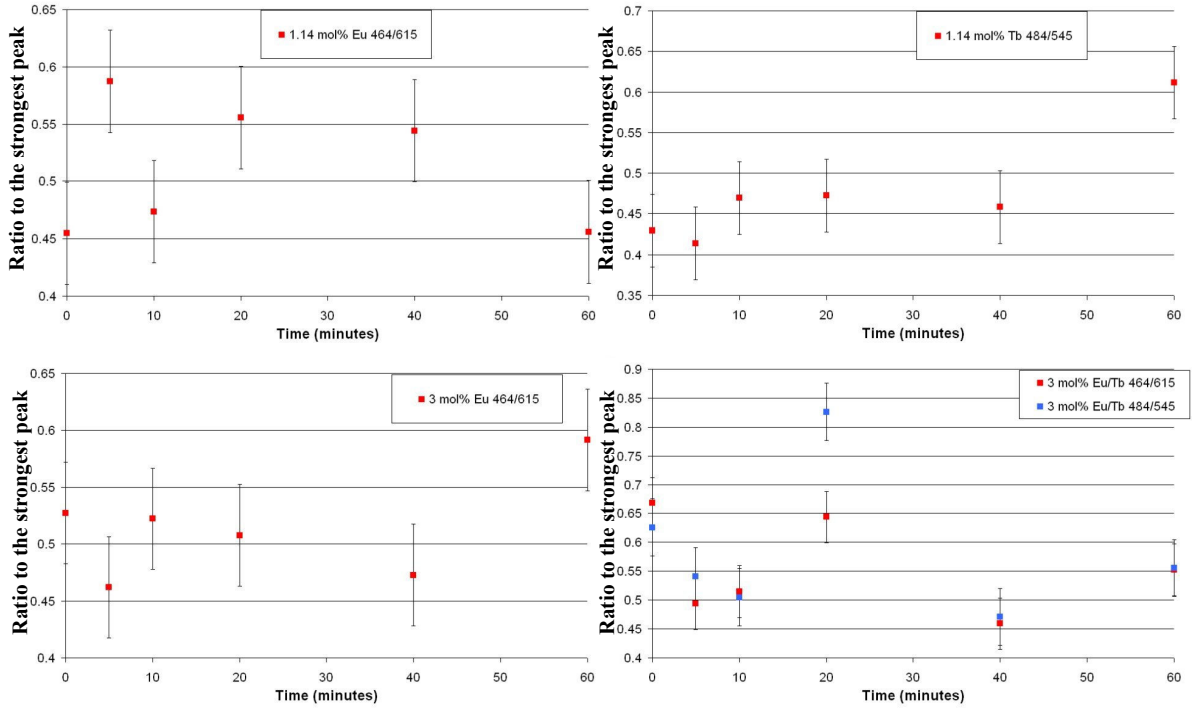

Figure 7-30. Positioning standard deviation for samples exposed to bleach

7.6.1 Conclusion

Table 7-7 shows no significant weight loss after the 60 minutes and no visual changes were observed for the glass samples. This would indicate that there was no change due to their exposure to bleach and therefore the samples were not analysed by SEM.

	1.14 mol% Eu	3.0 mol% Eu	3.0 mol% Eu/Tb	1.14 mol% Tb
Initial	0.2209	0.0825	0.1515	0.1316
5mins	0.2211	0.0823	0.1513	0.1314
10mins	0.221	0.0822	0.1515	0.1315
20mins	0.221	0.0824	0.1514	0.1316
40mins	0.2207	0.0821	0.1513	0.1316
60mins	0.2209	0.0822	0.1515	0.1315
Mean	0.2209	0.0823	0.1514	0.1315
SD	0.0001	0.0002	0.0001	0.0001

Table 7-7. Weights (g) of samples over 60 minutes in bleach

7.7 EXPOSURE TO VINEGAR

This experiment was run for 240 minutes with the samples exposed to clear vinegar, instead of brown vinegar to reduce the possibility of colour contamination, and the results shown in Figure 7-31.

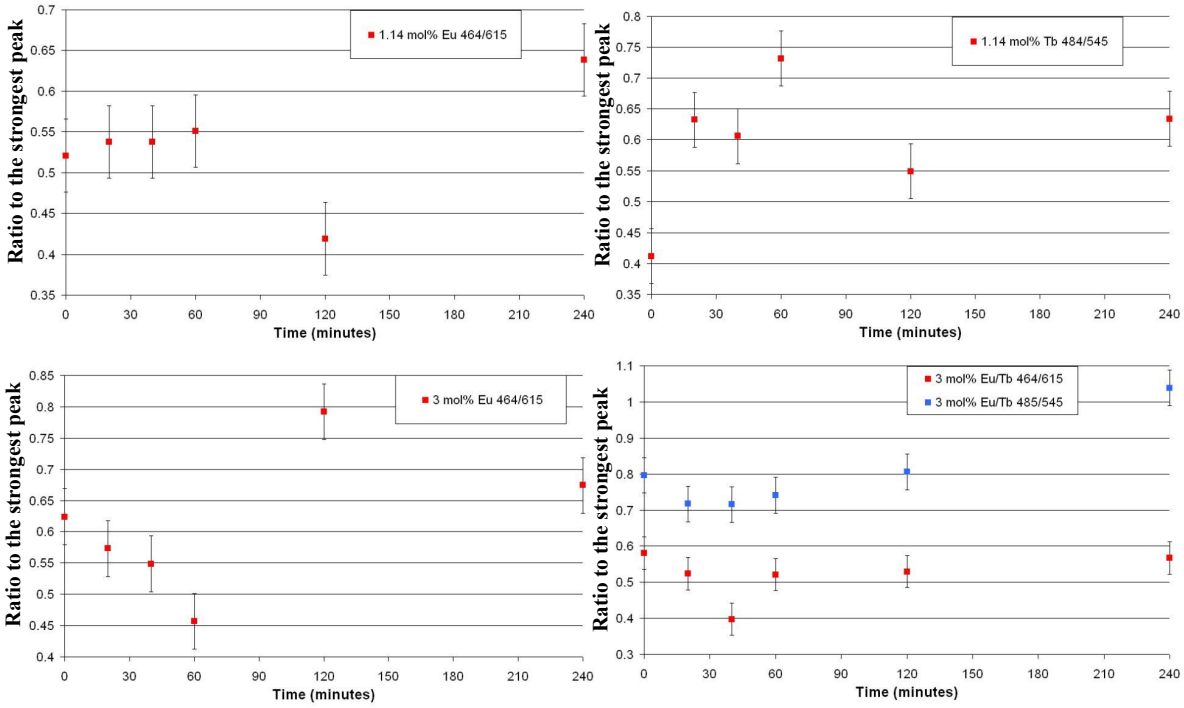

Figure 7-31. Positioning error for samples exposed to vinegar

Figure 7-31 shows a trend upwards for the 3 mol% Eu/Tb 484/545 series as the final point was much higher than the rest of the results even taking into account the standard deviation. Since the ratio results passed one, this meant the 485 nm excitation peak had become larger than the 378 nm excitation peak. Although this looked like a significant change, it meant the excitation peak used for the detector system became stronger after being exposed to the vinegar and therefore making it easier to detect the security label.

If there were a chemical attack on the glass, it would be expected that a weight change would occur. From the data in Table 7-8, there was no significant change in weight after four hours. However, there was a change in the appearance of the glass from clear to cloudy and would need to be investigated further.

	1.14 mol% Eu	**3.0 mol% Eu**	**3.0 mol% Eu/Tb**	**1.14 mol% Tb**
Initials	1.2179	0.8323	1.0275	1.1998
20mins	1.2179	0.8324	1.0276	1.1998
40mins	1.2179	0.8323	1.0274	1.1997
60mins	1.2178	0.8322	1.0275	1.1996
120mins	1.2178	0.8323	1.0275	1.1998
240mins	1.2179	0.8321	1.0273	1.1998
Mean	1.2179	0.8323	1.0275	1.1998
SD	0.0001	0.0001	0.0001	0.0001

Table 7-8. Weights (g) of samples over 240 minutes exposure to vinegar

7.7.1 SEM Analysis

The vinegar environmental tests observed the samples turning opaque after their four hours exposure in clear vinegar. These were therefore analysed by SEM to determine whether there were any surface defects caused by the acid.

7.7.1.a Blank

The first sample analysed was the blank glass and the SEM images are shown in Figure 7-32. These images did not show cracks on the surface although there were white marks appearing which could be the sign of a crystalline substance forming on the surface. The method of an acid attack is similar to a water attack where small amounts of mono- or divalent- cations such as Na^{+} or Mg^{2+} are leached out.

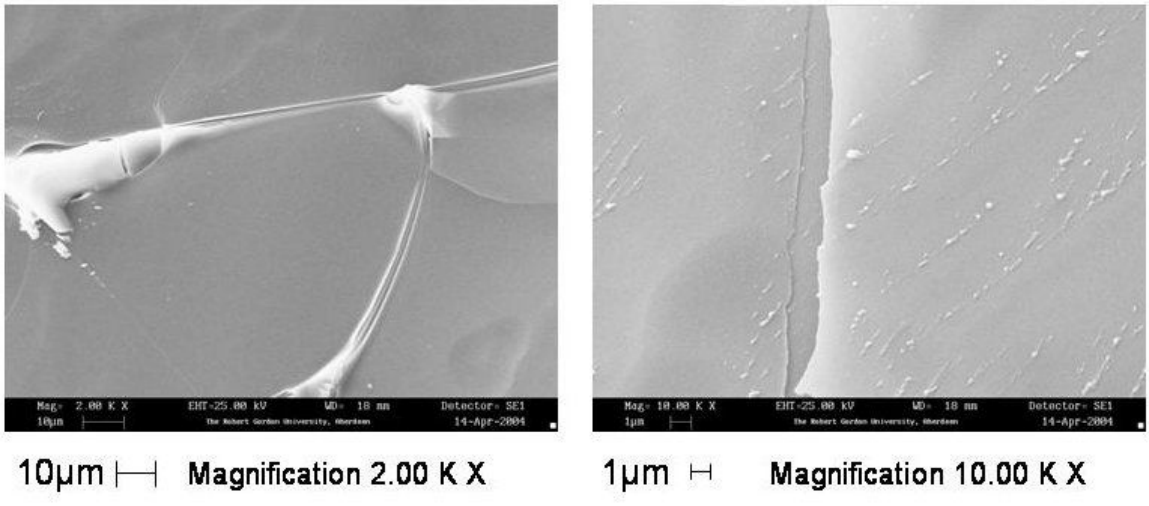

Figure 7-32. SEM images of the blank glass after four hours exposure to vinegar

7.7.1.b 1.14 mol% Eu

The 1.14 mol% europium doped glass SEM images are shown in Figure 7-33. The cracks shown in the images indicated the sample was affected by the vinegar. However, as there was no change in weight or fluorescence signal, this would indicate the vinegar would not affect the security label.

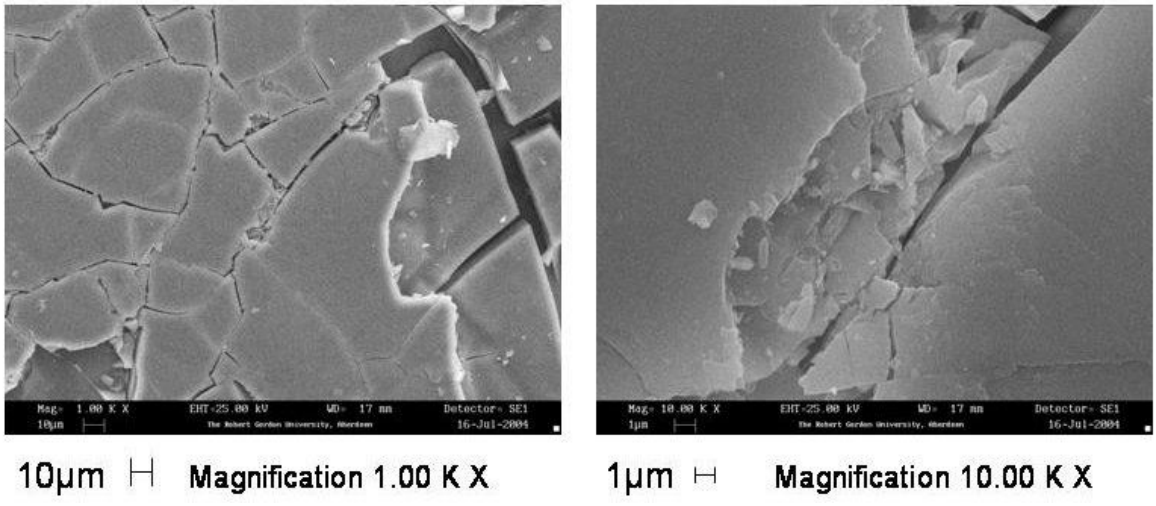

Figure 7-33. SEM images of the 1.14 mol% europium doped glass after four hours exposure to vinegar

7.7.1.c 1.14 mol% Tb

The 1.14 mol% terbium doped glass SEM images are shown in Figure 7-34. The cracks shown in these images indicated that the sample was affected by vinegar. However, the previously reported results concluded with no significant differences in weight or fluorescence signal and therefore would not hinder the detection of the label.

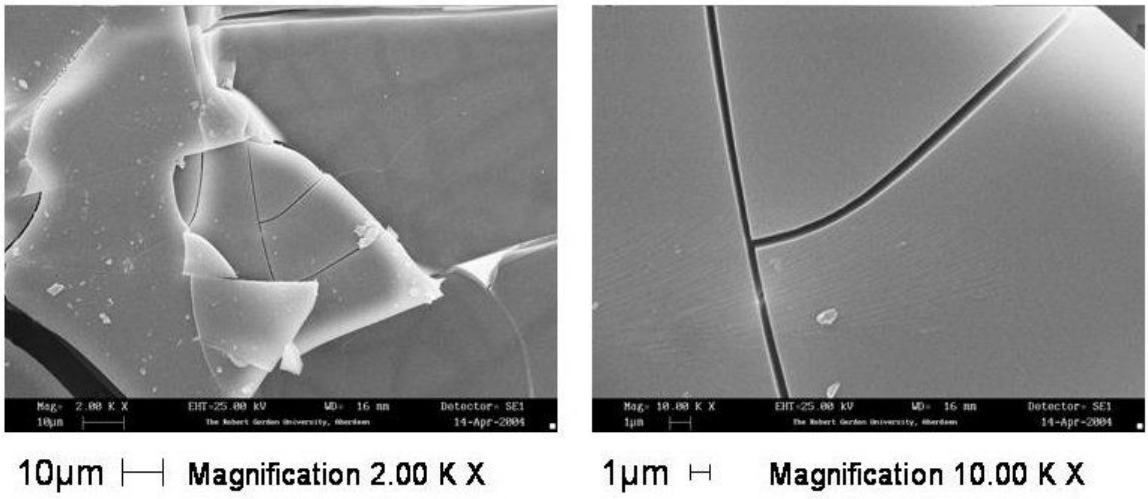

Figure 7-34. SEM images of the 1.14 mol% Tb doped glass after four hours exposure to vinegar

7.7.1.d 3 mol% Eu

The SEM images for the 3 mol% europium doped glass are shown in Figure 7-35. It was difficult to determine whether the images showed evidence of a film developed on the surface causing the lighter sections. Although no cracks were evident it could be the initial effects of the vinegar affecting the glass.

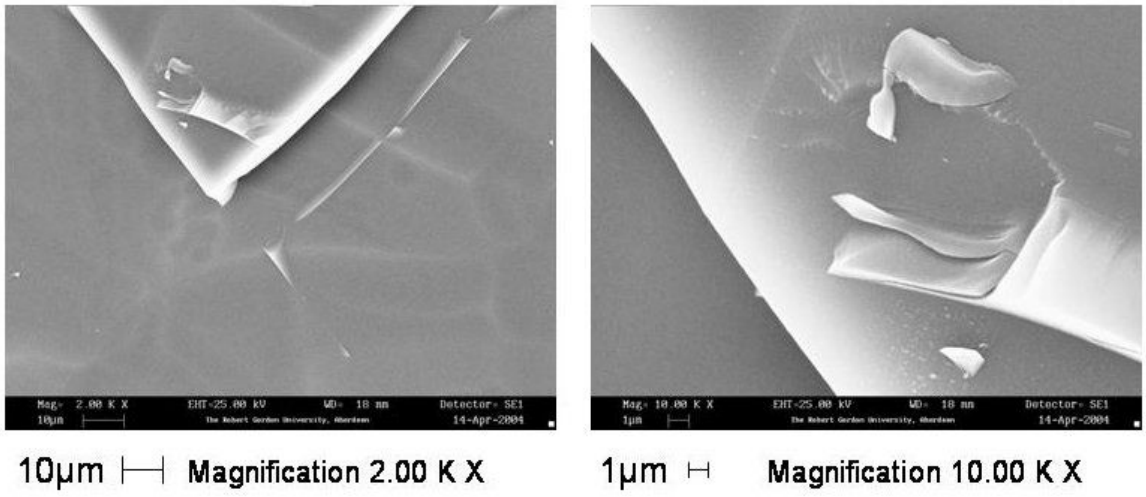

Figure 7-35. SEM images of the 3 mol% Eu doped glass after four hours exposure to vinegar

7.7.1.e 3 mol% Eu and 3 mol% Tb

For the 3 mol% europium and 3 mol% terbium doped glass, the SEM images are shown in Figure 7-36. These images did not show any cracks on the surface and therefore no significant detrimental affect. The small particles on the surface could be broken glass on the surface as shown previously for the untreated samples.

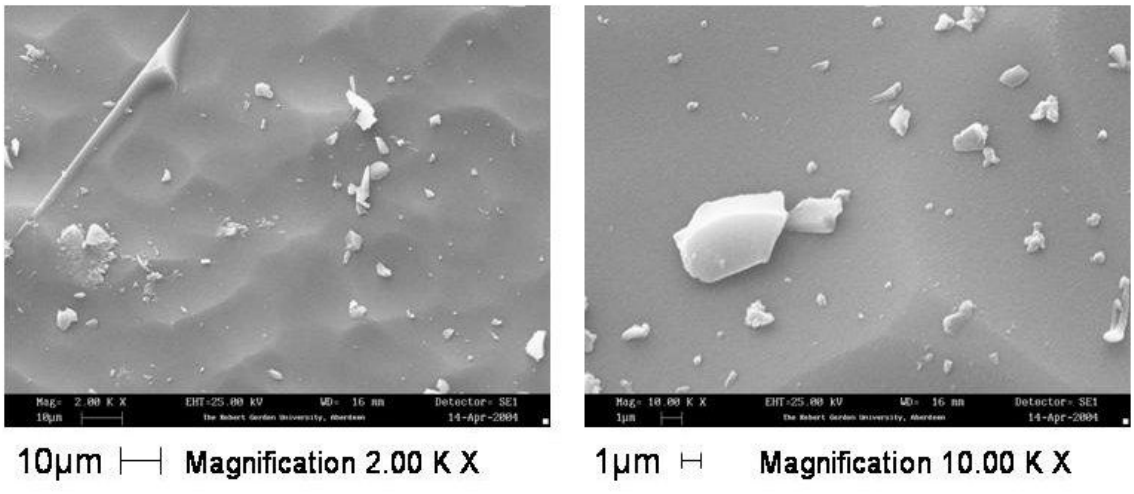

Figure 7-36. SEM images of the 3 mol% Eu and 3 mol% Tb doped glass after four hours exposure to vinegar

7.7.2 Conclusion

For the vinegar environmental tests, there were only cracks evident on the 1.14 mol% terbium and the 1.14 mol% europium doped glasses. Although all the samples appeared opaque after the four hours, it appeared as though some samples were affected more than others hence the cracks in two of the samples. These two samples might have had a greater internal stress throughout the sample in comparison with the other samples analysed. However, there were no significant changes in the weights of any samples or of the fluorescent signals therefore the detection of the label would not be hindered by the exposure to vinegar.

7.8 EXPOSURE TO BEER

The affects of beer were monitored for 60 minutes exposure time and the results shown in Figure 7-36 and the table of weights shown in Table 7-9. These results show possible trends upwards for some of the samples although there were fluctuations in the results. Figure 7-37 shows that for the 3 mol% Eu 464/615 peak, the variation was mostly inside the error bars whereas only the final point for 1.14 mol% Tb was outside the error bars but could have been an outlier result.

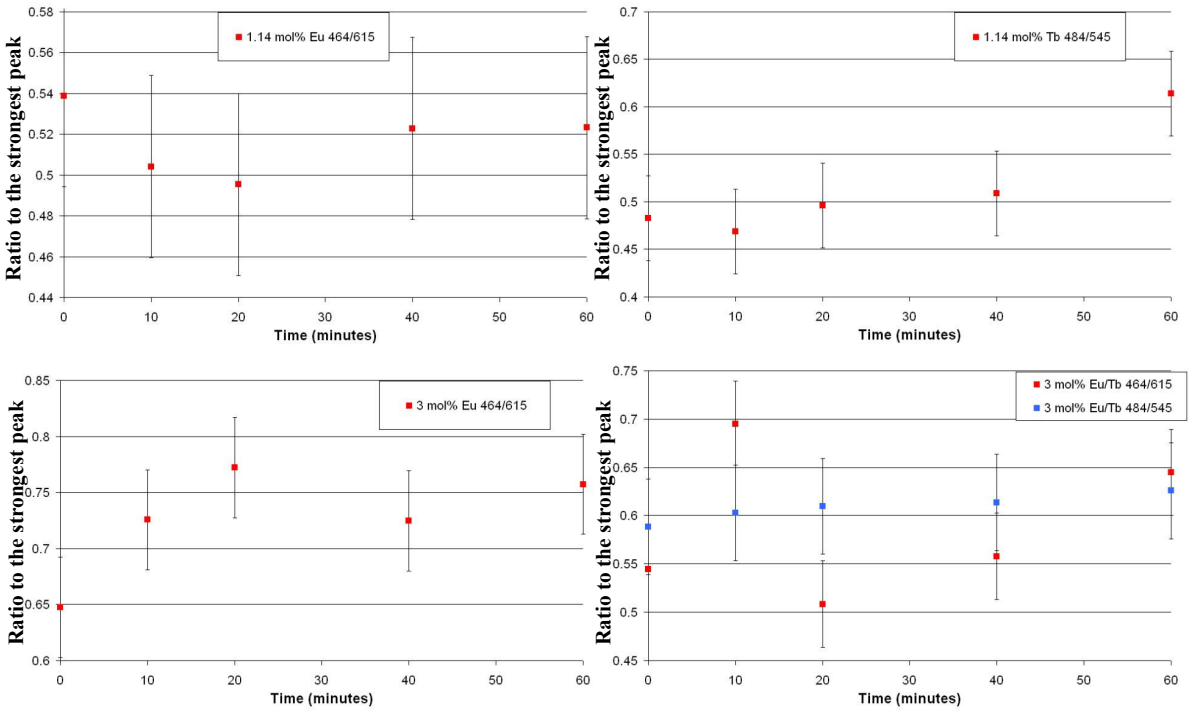

Figure 7-37. Positioning error for samples exposed to beer

	1.14 mol% Eu	3.0 mol% Eu	3.0 mol% Eu/Tb	1.14 mol% Tb
Initial	0.0635	0.2844	0.1519	0.0779
10mins	0.0636	0.2842	0.1516	0.0776
20mins	0.0634	0.2842	0.1516	0.0776
40mins	0.0635	0.2843	0.1518	0.0777
60mins	0.0635	0.2844	0.1517	0.0776
Mean	0.0635	0.2843	0.1517	0.0777
SD	0.0001	0.0001	0.0001	0.0001

Table 7-9. Weights (g) of samples after 60 minutes exposure to beer

7.8.1 Conclusion

The results in Table 7-9 showed that there was no significant change in weight after the 60 minutes. Furthermore, there was no visual change in appearance that would suggest any effects on the glass therefore the exposure to beer did not have any effect and the samples were not analysed by SEM.

7.9 EXPOSURE TO PERKLONE

It was decided to try and simulate the affects of a dry cleaning agent. As tetrachloroethylene (perklone) is a replacement for carbon tetrachloride which was the main solvent used in the dry cleaning industry, this was used for this experiment. The test was run for 60 minutes again and the results shown in Figure 7-38.

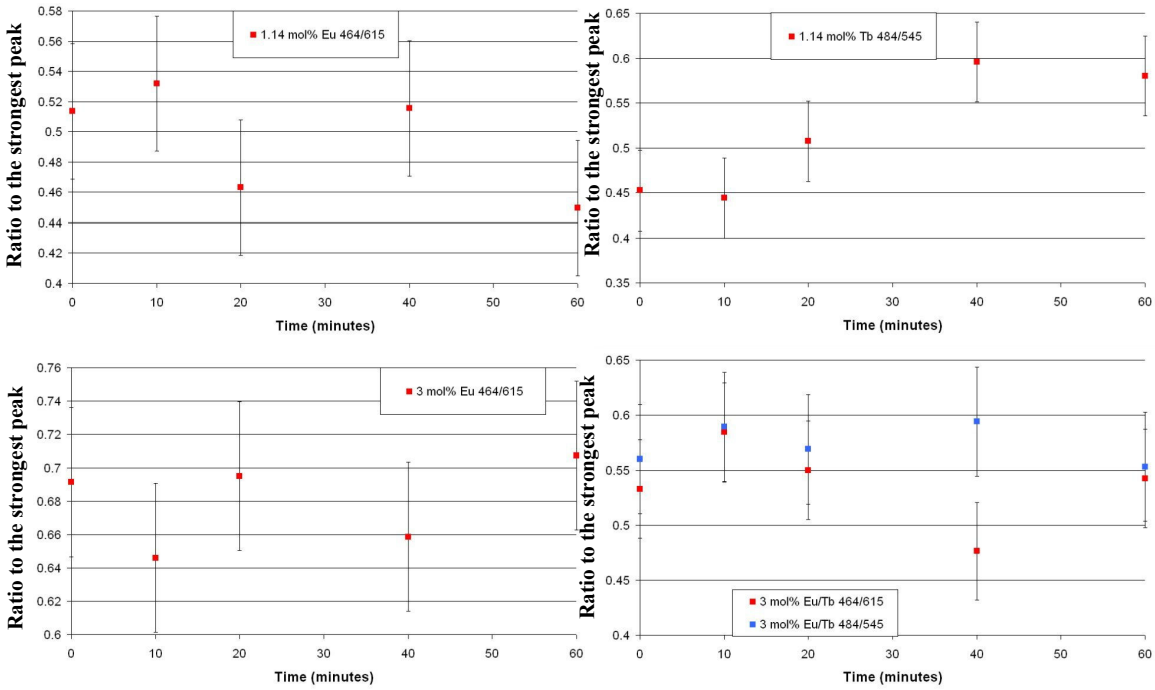

Figure 7-38. Positioning error for samples exposed to perklone

Figure 7-38 shows all the results are within statistical error. Only the 1.14 mol% Tb 484/545 series rises before levelling off but was still within the statistical error bars.

7.9.1 Conclusion

Table 7-10 shows that the weight remained constant over the 60 minutes exposure to the perklone and with no visual change in appearance, the perklone did not affect the fluorescent signal. These samples were therefore not analysed by SEM.

	1.14 mol% Eu	3.0 mol% Eu	3.0 mol% Eu/Tb	1.14 mol% Tb
Initial	0.1406	0.3863	0.1887	0.0999
10mins	0.1405	0.3863	0.1888	0.0995
20mins	0.1404	0.3862	0.1889	0.0998
40mins	0.1405	0.3863	0.1887	0.0998
60mins	0.1405	0.3861	0.1888	0.0997
Mean	0.1405	0.3862	0.1888	0.0997
SD	0.0001	0.0001	0.0001	0.0002

Table 7-10. Weights (g) for samples after 60 minutes exposure to perklone

7.10 ACCELERATED SUNLIGHT ATTACK

To accelerate the affect of sunlight on the samples, a 500W Dr Hönle AG UVASPOT 400T lamp was used to illuminate the sample for an exposure time of 60 minutes and the results shown in Figure 7-39. These results showed all the results were within the error bars for each sample.

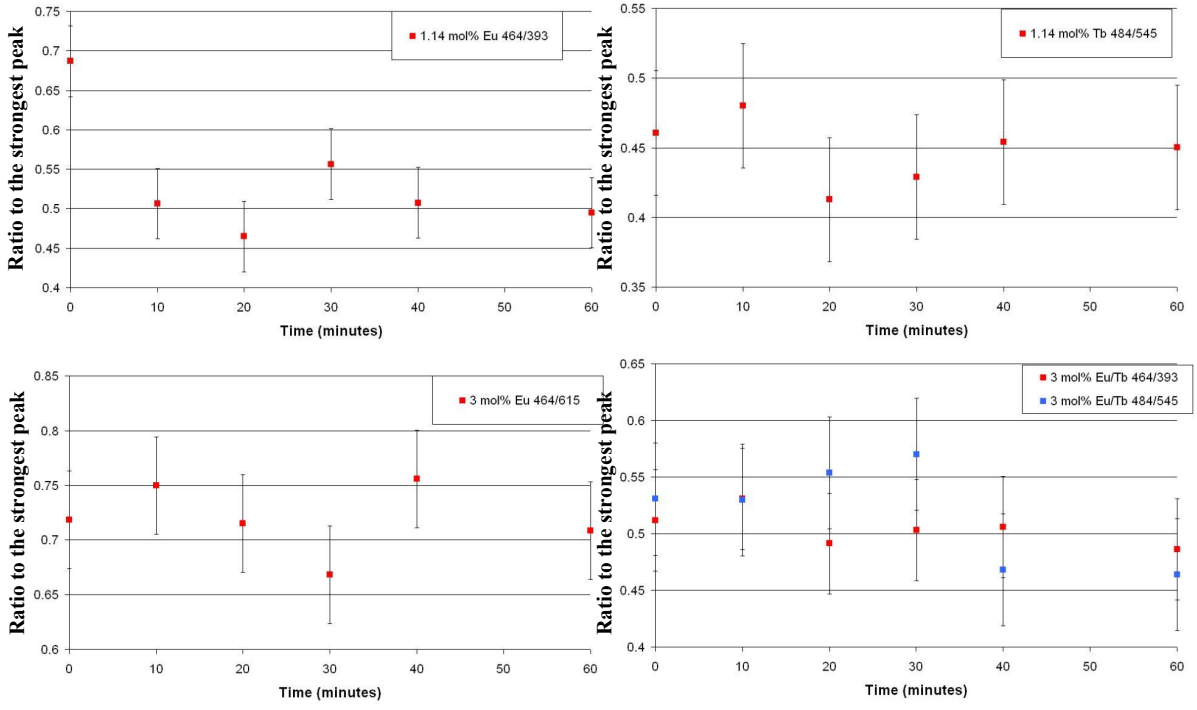

Figure 7-39. Positioning error for samples exposed to UV light

7.10.1 Conclusion

The results in Table 7-11 suggested that no physical effect was found from the UV lamp. Therefore no SEM analysis was carried out on these samples.

	1.14 mol% Eu	3.0 mol% Eu	3.0 mol% Eu/Tb	1.14 mol% Tb
Initial	0.1374	0.479	0.3783	0.1145
10mins	0.1375	0.4789	0.3784	0.1146
20mins	0.1375	0.4789	0.3782	0.1144
40mins	0.1376	0.4791	0.3782	0.1145
60mins	0.1375	0.479	0.3783	0.1145
Mean	0.1375	0.479	0.3783	0.1145
SD	0.0001	0.0001	0.0001	0.0001

Table 7-11. Weights (g) of samples after 60 minutes exposure to UV lamp

7.11 ABRASION

To simulate the affect of abrasion on the samples each sample was rubbed lightly with P400 sand paper for a time period of 20 minutes. At this point in time, a piece of paper would be too damaged to hold any value and therefore it would not matter if the sample was still present.

The results are shown in Figure 7-40 and depict each of the samples as having a constant fluorescence ratio. This was expected, as the abrasion would only affect the results if the dopant ions were only on the surface of the glass and not distributed throughout the whole sample. Additionally, this confirmed the dopant ions were distributed throughout the glass and not just on the surface.

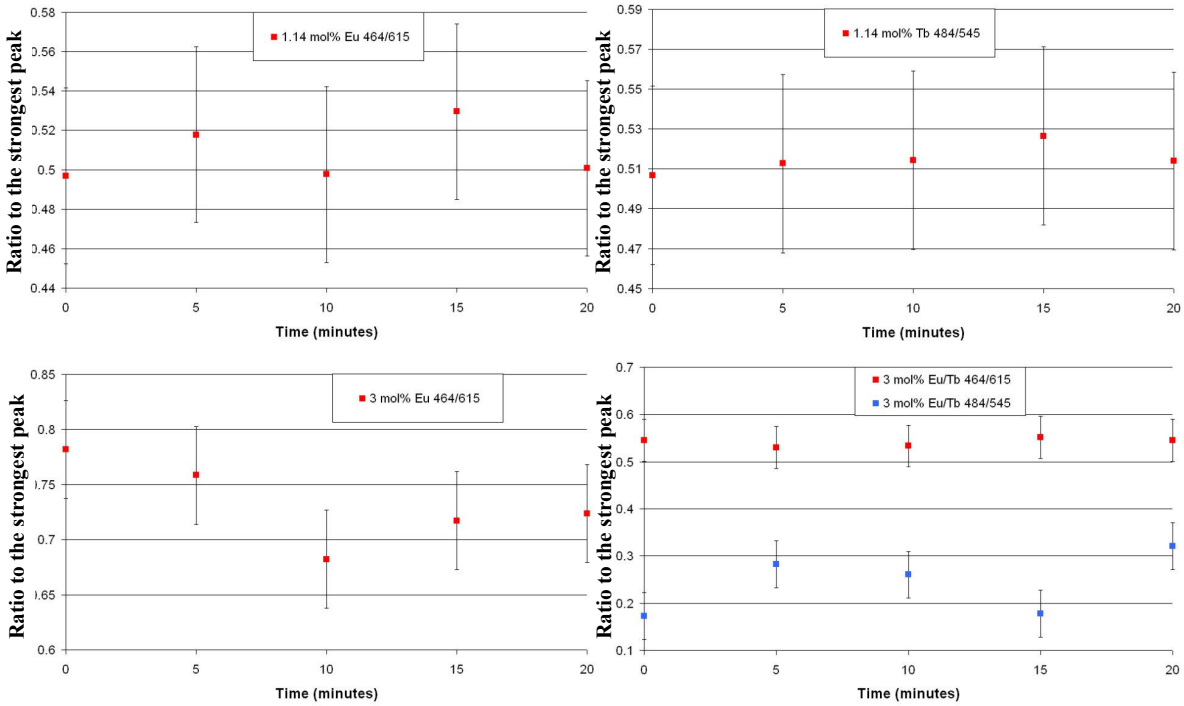

Figure 7-40. Positioning error for samples exposed to abrasion

Table 7-12 shows the weights of each of the samples over the time period and the calculated standard deviation was notably higher than any of the other weights previously mentioned. This again was expected as the abrasion affect would rub off some of the sample therefore making the samples lighter.

	1.14 mol% Eu	3.0 mol% Eu	3.0 mol% Eu/Tb	1.14 mol% Tb
Initial	0.0567	0.4231	0.2364	0.5279
5 mins	0.0565	0.423	0.2362	0.5277
10 mins	0.0563	0.4227	0.2361	0.5276
15 mins	0.056	0.4225	0.2359	0.5275
20 mins	0.0558	0.4222	0.2356	0.5273
Mean	0.0563	0.4227	0.236	0.5276
SD	0.0004	0.0004	0.0003	0.0002

Table 7-12. Weights (g) of samples after 20 minutes abrasion

7.11.1 Conclusion

This test demonstrated how steady the fluorescence intensity was as successive thicknesses of the doped bead were physically removed clearly showing a fairly homogeneous doping throughout the body of the novel taggant beads.

7.12 CONCLUSION OF ENVIRONMENTAL TEST RESULTS

From all the environmental experiments carried out, only the cold water and vinegar made any visual effect on the glass samples. However, the cold water effect was not enhanced during the 60 °C or 100 °C experiments and therefore it was concluded that the cold water only affected samples that contained higher internal stresses caused by re-melting.

The vinegar experiment also showed a trend upwards for the 3 mol% Eu/Tb 484/545 series of results. This change would actually enhance the signal for the detector system as the peak was found to increase in intensity with exposure to the vinegar. Although there was a visual change in colour on the glass surface, no negative effect was found for the fluorescence signal.

The abrasion experiment showed a variation in weight. However, this experiment showed no change in the fluorescence signal over the time period and confirmed that the dopant ions were distributed throughout the whole sample and not just on the surface.

All the other environmental experiments found no change in fluorescence signal or in the weight of the samples. For all practical purposes none of the environmental exposures have detrimentally affected the use of the doped glasses as a security label.

CHAPTER 8 - CONCLUSIONS AND FUTURE WORK

8.1 INTRODUCTION

The need for security features on a wide range of products has been well documented. According to the Organisation for European Co-operation & Development, an estimated 7-9 % of world trade each year is lost by the sale of fake goods [3]. In order to combat this problem, novel sophisticated security features have to be developed to hinder potential counterfeiters and to protect the customers.

The aim of this thesis was therefore to develop a novel covert security label based on a host matrix doped with RE ions. This label would be embedded into/onto a document or product and be excited and detected in the visible region of the spectrum, by an in-situ detector system.

The findings of this thesis can be separated into four parts addressing the objectives/milestones outlined in section 1.3:

- Those that address the development of the chosen host single RE doped glass samples and their spectral characterisation.

Objectives:
1. Analysis of different glass compositions to determine their suitability as a possible host matrix.
2. Development of methodologies for single rare earth ion doping of glass with selected rare earth ions.
3. Optimisation of rare earth doping methodologies.
4. Spectral analysis of the rare earth ion doped glasses
5. Rare earth doped glass lifetime studies by a modified laser induced scanning fluorescence microscope system

- Those that investigated the ability of multi-RE doped samples to form different codes due to the interactions between the dopants.

Objective: 6. Investigation of multi-ion doped glasses and their spectral characterisation.

- Those that investigated the effect of environmental conditions on the glass and dopant physical and spectral properties over time.

Objective: 7. Determination of any deterioration to the doped glass fluorescence and glass structure under various environmental conditions.

- Those that addressed the development of an in-situ detector system and the application and detection of the doped samples by the detector system.

Objectives: 8. Development of an initial in-situ detection system.

9. Testing of the doped glasses for their compatibility with the in-situ detection system.

10. Particle size analysis to determine the possibility of bead size production and verification of dopant ions presence in separate beads.

11. Incorporation of doped glass beads into or onto a paper document.

12. LISFM scans of paper samples with added doped glass beads to verify the detection capabilities and printing methods.

8.2 DEVELOPMENT OF SINGLE RE DOPED GLASS SAMPLES AND THEIR SPECTRAL CHARACTERISATION

From the RE solution analysis, suitable dopants appeared to be Eu, Tb, Dy and possibly Pr (Chapter 4). The investigation for a suitable host matrix found that a borosilicate matrix was suitable. This glass had a suitable working temperature that produced optically transparent samples with low hydrophilicity and low background fluorescence signal. The melting and quenching method was chosen for its ease of production and relatively high dopant concentration limit. Although other glass matrices could allow further transitions of the RE dopants due to different host phonon vibrational energies, borosilicate glass was still selected. This was because it had several other advantages, namely it altered the fluorescence response from the dopants, compared to in an aqueous solution, and this change would have to be replicated by anyone trying to reproduce the signal thus providing an additional security feature. Secondly the elemental analysis of the glass was complicated due to the large number of different constituents involved and this would therefore increase the number of permutations required in order to reproduce the exact matrix making it more difficult for a counterfeiter to copy.

Europium doped borosilicate glass confirmed the suitability of the host matrix by producing multiple strong, discrete rare earth fluorescence peaks. The spectroscopic analysis found the most suitable peak for europium detection purposes to be at 465 nm excitation and 615 nm emission. Praseodymium also produced very strong fluorescence when doped in the host. However, these peaks were not discrete and would cause problems in detection selectivity. Praseodymium was therefore not selected for further analysis but could have been investigated for its energy transfer capabilities as a sensitizer because of its strong absorption characteristics. Terbium doped glass produced another strong discrete fluorescence peak that was suitable for detection as it would not cause an overlap with the europium selected peak. This peak had an excitation of 483 nm and emission at 545 nm. Dysprosium doped glass produced a complex fluorescence signal which would further enhance the security due to the multiplicity of discrete peaks. The peak chosen for the detector system was at 452 nm excitation and 577 nm emission as this peak was spectrally discrete from both Eu and Tb.

The basis of applying and detecting the glass outside a cuvette was investigated in Chapter 5. Initial work demonstrated the need for selecting the correct filters when the security label would be on a white background. Furthermore, the need to investigate the fluorescence lifetimes of the RE ions, to enhance the selectivity of detection against background molecular fluorescence, was highlighted by the LISFM testing with molecular based beads and RE doped glass. Lifetime studies were therefore carried out utilising the wavelengths discussed for each dopant. The results demonstrated that the fluorescence lifetimes for Eu and Tb had a FWHM of nearly 2 ms whilst Dy was almost 7 ms. These times were sufficiently longer than molecular dyes that they can be used as a distinguishing feature for the detection system.

8.3 THE INVESTIGATION OF THE ABILITY OF USING MULTI-RE DOPED BEADS TO FORM DIFFERENT SECURITY CODES DUE TO THEIR INTERACTIONS WITH EACH OTHER

In order to increase the complexity of the security label, multi-RE ions were doped into the glass samples. Firstly a double doped RE mixture of Eu-Tb (3 mol% each) was successfully produced (Chapter 6). This sample produced a complex fluorescence spectrum with many peaks and demonstrated the first sign of energy transfer between the dopant ions with evidence of Tb enhancing the Eu signal. This effect further enhanced the security label as the net effect of any energy transfer would have to be known in order to replicate the same signal intensity. Two further double doped RE beads Eu-Dy and Dy-Tb were produced.

3 mol% of Eu had not caused any problems in the Eu-Tb glass so an investigation into the optimum concentration of Dy without causing phase separation showed even at 5 mol% Dy, the beads were produced without phase separation. 5 mol% was therefore selected as the optimum total dopant concentration to maximise the fluorescence intensity whilst avoiding phase separation. Further work would be required to investigate the maximum RE concentration of each RE dopant selected in the borosilicate glass matrix for single and double doped samples.

For the Dy-Tb mixture, the concentrations were altered to allow for the different signal intensities to be matched from previous results showing the Dy signal was much stronger than Tb (1 mol% Dy and 2.5 mol% Tb). This sample appeared to involve energy transfer from Dy to Tb again increasing the complexity of the label further although both peaks for the detector system were still detected and were spectrally discrete from each other.

Subsequently an investigation into the effects with triple-RE doped samples was carried out. This investigation successfully proved that the three dopants could be mixed together and their spectra resolved for each dopant without overlapping. This was in contrast to the inherent poor ability of molecular dyes to be spectrally resolved when mixed together due to their wide band widths. Examples of how altering the dopant concentrations could be used to advantage to produce various codes were also demonstrated as the intensities relative to each other were altered. The largest change appeared with the increase of Tb as this altered both Dy and Eu signals simultaneously reducing the Tb intensity.

8.4 THE EFFECT OF ENVIRONMENTAL CONDITIONS ON THE GLASS AND DOPANT PHYSICAL AND SPECTRAL PROPERTIES OVER TIME

Environmental tests were carried out to simulate the affects of extreme conditions that the security label may become exposed if applied to a paper document (Chapter 7). These tests were carried out for various times governed by how long an exposure would be required to destroy the paper document. Each sample was then measured for weight loss/gain, changes in appearance and fluorescence intensities.

Out of all the conditions tested, only the cold water and vinegar left any visual effect on the glass samples, in both cases turning the glass opaque. However, the cold water effect was not enhanced during the 60 °C or 100 °C distilled water experiments and therefore it was concluded that the cold water did not affect the glass through hydration. It was concluded that the cold water only affected samples that contained higher internal stresses caused by re-melting. Some original bulk samples were re-melted in order to form smaller sized samples due to the quantity of tests required per sample. This process appeared to have caused greater internal stresses in the glass due to the melting and quenching process and this was observed on SEM images. This highlighted the need for careful control of the

quenching process when preparing batches for security labelling. Further work could also investigate the effect of annealing on the properties of the glass to optimise the production process.

The vinegar experiment showed a trend upwards for the terbium peak in the Eu-Tb double doped sample. However, this change meant the relative intensity of the terbium peak of interest increased for the detector system when exposed to vinegar. Furthermore, the glass appearance became opaque although the other fluorescence intensities were not affected.

A weight loss was found after the abrasion experiment; however, this was expected as the glass surface was being removed by the sand paper. Nevertheless, the fluorescence signal over the time period remained the most consistent out of all the conditions tested. This confirmed the dopant ions were distributed throughout the whole sample and were not only on the surface of the glass bead.

All the other environmental conditions indicated no changes in the fluorescence signals or on the weight of the samples. Further work would be required in order to repeat the room temperature water experiment with freshly made samples that had not been re-melted. This would have confirmed whether the conclusions made about internal stresses being responsible for the cracks and not due to the glass being exposed to water, were correct. For all practical purposes, none of the environmental exposures detrimentally affected the use of the doped glass as a security label.

8.5 THE DEVELOPMENT OF AN IN-SITU DETECTOR SYSTEM AND THE APPLICATION AND DETECTION OF THE DOPED SAMPLES BY THE DETECTOR SYSTEM

The detection principle (Chapter 5) for the in-situ detection system was based on the spectral characterisation (Chapter 4) of each dopant and their respective long fluorescence lifetimes (Chapter 5). For each dopant selected, a single detector holder was made that incorporated a light source and detector with the required filters based on the discrete wavelengths selected in the spectral characterisation. The lifetimes were utilised to remove the background by using a slow pulsed excitation light. Since the RE fluorescence lifetimes were sufficiently long, their fluorescence did not have time to decay before the

next pulse producing a DC signal. Any molecular dye fluorescence in the background would have a much shorter fluorescence lifetime and would decay immediately after the excitation pulse. This would produce an AC signal that is filtered out using a low pass active filter, leaving the RE fluorescence signal.

The completed initial single channel detector was capable of detecting pieces of europium doped (3 mol%) borosilicate glass samples approximately 5 mm in diameter. This work demonstrated the possibility of the detector system for other dopants with the aim of producing a linear arrangement of detectors capable of detecting multi-RE doped samples.

Although this detector system could detect particles reduced to 5 mm in diameter, much smaller particles would be required for future applications. Particle sizes of under 75 μm are required for screen printing applications (to fit through the screen mesh) whilst particles under 5 μm would be required for ink jet printing (to fit through each print nozzle). The production of 5 μm particles (Chapter 6) was successfully demonstrated by ball milling and wet sieving of bulk samples. Particle size analysis confirmed the resulting size distribution was below 5 μm whilst SEM analysis displayed the random shapes and sizes to be between 1-4 μm. EDXA analysis provided evidence that the three RE dopants were present in these beads and indicated the possibility of producing single micron sized particles for printing applications.

Initial work was also reported on the incorporation of the doped beads into various inks and glues in order to produce barcodes to test the detector system (Chapter 5). This work successfully demonstrated the detection ability to selectively detect the beads on top of, inside and printed onto paper. However, the resolution would have to be improved to increase the spatial resolution of future barcodes. The LISFM system was utilised to increase the excitation power of the detector and was able to show the greater sensitivity that could be achieved.

8.6 OVERALL CONCLUSION

This research has successfully produced inert multi RE doped glass beads for use as covert security labels and taggants. The incorporation of these beads into various printing media and their application on top of and underneath paper surfaces, in the form of barcodes, was successfully demonstrated. Furthermore, these barcodes were successfully detected using the detector system designed in this thesis.

In order for this security label to be feasibly used in the mass market, the production cost for the whole system must be small. An initial study, based on quantities of reagents available to buy for small scale production, produced a total of 0.07 p per barcode. This cost was based on 0.1 g of borosilicate glass doped with 1 mol% Eu, 1 mol% Tb and 1 mol% Dy. However, this cost did not include the cost of manufacturing or the cost of the printing media (ink or paint for example) as these costs varied widely. This cost would be reduced significantly if large scale quantities were purchased and produced in bulk, therefore the actual price would be much smaller and would feasibly produce a competitive new security label.

A European patent and a US patent on the novel security taggants and detection system have been successfully published. A further patent has also been filed on the use of the technology in the multiple biomarker label field.

8.7 RECCOMMENDATIONS FOR FUTURE WORK

In order to progress this work to a commercial product, further work would have to be investigated in a number of areas. These can be separated into six parts:

1. Alternative dopants and dopant concentration.
2. Effects of altering the host matrix composition to alter the spectra.
3. Addition of sensitisers to maximise the fluorescence intensity.
4. Optimisation of single micron bead production.
5. Optimisation of the application of beads in various media.
6. Enhance sensitivity of the detector system.

8.7.1 Alternative Dopants and Dopant Concentration

To increase the number of security code permutations, new RE dopants are required. Based on the FT-IR results (Chapter 4) that investigated the host phonon energy of the glass and the energy difference between radiant energy levels of the REs, possible dopants included Pr, Sm, Gd and Yb although not all would produce visible fluorescence. These energy levels were separated by more than four phonons and therefore would not be quenched by multi-phonon relaxation. Additionally, dopants could be added in other oxidation states such as Eu^{2+} which is known in the literature [118, 119] to produce a blue fluorescence. Work would also be required to investigate the maximum concentration for each dopant in the host matrix. This would enable strong fluorescence signals to enhance the detector response. Furthermore, the investigation into the size of concentration increments required in order to be distinguished as a new code by the detector would have to be undertaken. There would have to be an area of certainty between concentrations therefore making it unlikely to be 0.1 mol% increments. This would have bearings on the permutations realistically possible and would emphasise the importance of knowing the concentration limits.

8.7.2 Effects of Altering the Host Matrix Composition to Alter the Spectra

Altering the network forming and network-modifying ions of the glass host, can change the fluorescence linewidths of the REs [74]. This feature could be utilised in order to reduce the possibility of peaks overlapping with multi-RE doped samples. The peak fluorescence wavelengths and their intensities are both host dependent and thus can be altered by changing the glass matrix, which can create greater site-to-site differences resulting in broader linewidths and shifts of the fluorescence wavelength peak. This work would further enhance the security of the label by increasing the number of permutations available to produce more security codes.

8.7.3 Addition of Sensitizers to Maximise the Fluorescence Intensity

The addition of sensitisers would further enhance the fluorescence intensity of the dopants without the need to increase their concentrations [73, 110-112, 120-123]. These would act in the same way as the energy transfer mechanisms described in Chapter 6 for the triple RE doped samples. Furthermore, this could change the wavelengths selected in the detection system as it could incorporate the excitation wavelength of the sensitiser and detect the emission of the dopant of interest. This would enhance the security as additional dopants could be added that were not necessarily being detected depending on the excitation and emission sources and filters in the detector system. This arrangement could then be changed to detect the sensitiser ion without the original RE dopant by swapping the detector heads. This would produce a new fluorescence signal for the same batch of glass with the same dopant concentrations.

8.7.4 Optimisation of Single Micron Bead Production

The methodology used for the production of single micron sized beads was very laborious with low production efficiency (Chapter 6). If the beads are to be tested further, a quicker automated process would be required. One option would be to use the Sonic Sifter from Endecotts Ltd. This machine would increase the production and purity of single micron beads as it does not require the use of liquids therefore decreasing the sieving time involved and removing any contaminates.

8.7.5 Optimisation of the Application of Beads in Various Media

Improvements in the application of the beads into ink and other media also need to be investigated. Optimisation of the printing methods onto various surfaces will increase the areas of possible applications for the security label. Sourcing of suitable inks and improved dispersion agents for each application would have to be found. With the improved production of single micron beads, the incorporation of the beads into ink used in suitable ink jet printers could be investigated. Additional work would be required to disperse the beads throughout the ink enabling the printing of the beads. If successful, this would further increase the application fields possible as this could be used in point-of-sale applications such as ticket printing.

8.7.6 Enhance Sensitivity of the Detector System

The initial detector system (Chapter 5) demonstrated the feasibility of detecting the RE doped glass. However, a lot of work would be required to optimise the sensitivity and selectivity in order to detect single micron sized particles. To achieve this, highly sensitive photodetectors and more powerful excitation sources such as lasers could replace the existing LED and photodiode. Although this would then increase the overall cost of the detector system (as the original aim was for a cheap design), the added benefits of detecting single micron beads should outweigh the cost for particular applications. The excitation pulse widths could be changed to optimise each channel to the fluorescence lifetime of the particular dopant (as Dy had a much longer lifetime than Eu and Tb). Different holder designs would be investigated to minimise stray light entering the detector thereby reducing the noise. Light guides can also be added to allow the excitation light and detector to be closer to the sample maximising the fluorescence collection efficiency. Furthermore, the detector system would become application driven with the ability to have a stand alone setup or a hand held device that could give authentication immediately.

CHAPTER 9 - REFERENCES

1. *Optical Document Security,* R.L. van Renesse, Second Edition, **1998,** London, Artech House
2. The Anti-Counterfeiting Group, *Essential Information - The extent of counterfeiting*, Accessed **13/09/04,** http://www.a-cg.com/docs/GuestEssentialextent.pdf.
3. VISA, *Targeting Fraud*, Accessed **13/09/04,** http://www.visa.co.uk/pressandmedia/pdf/targeting_fraud_brochure.pdf.
4. De La Rue, *Luxury brands under attack?*, Accessed **13/09/04,** http://www.delarue.com/DLR_Content/CDA/Pages/News/articles/199/0,1862,,00.html.
5. McCallien, D., *Marker of Distinction*, Chemistry in Britain, 38, **2002**, 31-33
6. Biocode, *The Biocode marking System*, Accessed **16/06/03,** http://www.biocode.com/.
7. Pabio, *Chemical labelling of objects,* Patent WO9617954, **1996**
8. Slater, J.H. and Minton, J.E., *A security device using an ultrasensitive microtrace for protecting materials, articles and items,* Patent WO9502702, **1995**
9. Silverschotz, S., Hipko, G.P. and Dennis, M., *Printed and encoded mass distributed response piece and method of making the same,* Patent US 5,087,805, Webcraft Technologies, Inc, **1992**
10. Davis, W.H., Goba, J.J., Riggs, D.D., Zeewy, A. and Flint, H.M., *Intercept system for intercepting stolen, lost and fraudulent cards,* Patent US 4,626,669, Fairview Partners, **1986**
11. Tobin, J.A., *Method for mastering and origination of covert machine readable barcode hologram in combination with overt hologram,* Patent AU3032595, **1996**
12. Payne, G., *Threads of Evidence*, Chemistry in Britain, 38, **2002**, 37-39
13. De La Rue, *High Security Paper*, Accessed **17/06/03,** http://www.delarue.com/dlr_content/cda/pages/portalsbathford/pbsecurity/0,2092,,00.html.
14. Jalon, M., *Security marking method, materials provided with security marks,* Patent US 4,736,425, Petrel Company, **1988**
15. Malmberg, T.A.H., Hogberg, K.G. and Sjoquist, S.R., *Checking an identity, authority or check document of the like,* Patent US 4,047,033, ID Kort AB, **1977**
16. Williams, C., *Conventionally used to protect banknotes, chequebooks and ID documents, security inks could be a cost-effective brand protection tool for*

packagers and brand owners seeking to stop counterfeiting attacks, Brand, **2002**, 4(May/June), 46-55

17. Winnik, F.M., Davidson, A.R. and Breton, M.P., *Porphyrin chromophore and dendrimer ink composition,* Patent US 5,256,193, Xerox Corporation, **1993**
18. Lent, B.A., Deng, G. and Ezpeleta, J.F., *Invisible fluorescent jet ink,* Patent US 5,837,042, Videojet Systems Int, **1998**
19. Otsubo, M., Tomura, T., Konno, E. and Kase, M., *Microbead containing fluorescent pigment and/or fluorescent dye,* Patent JP 8208976, Dainippon Ink & Chem Inc, **1996**
20. Okada, Y., Fukuoka, F. and Morita, Z., *Environmental effects of oxygen on the fading of monochlorotriazinyl reactive dyes on cotton fabrics,* Dyes and Pigments, **1998**, 37(1), 47-64
21. Smith, L.M., Sanders, J.Z., Kaiser, R.J., Hughes, P., Dodd, C., Connell, C.R., Heiner, C., Kent, S.B.H. and Hood, L.E., *Fluorescence detection in automated DNA sequence analysis,* Nature, **1986**, 321(12), 674-678
22. Cyr, M.J., Krutak, J.J., Clauberg, H. and Helton, T.W., *Security document and method using invisible coded markings,* Patent US 6,138,913, Isotag Technology Inc, **2000**
23. Berson, W., *Document authentication system utilizing a transparent label,* Patent US 5,514,860, Pitney Bowes, **1996**
24. Freeman, M.P., Halverson, D. and Halverson, F., *Process for recording and retrieving information employing photoluminescent inks which luminesce under ultraviolet illumination,* Patent US 3,473,027, American Cyanamid Co, **1969**
25. Butland, C.I., *Technique for labelling an object for its identification and/or verification,* Patent US 5,599,578, **1997**
26. Bratchley, R., Wallace, D.M. and Ranby, P.W., *An anti-stokes luminescent material,* Patent GB 2,258,659, De La Rue Thomas & Co Ltd, **1993**
27. Kaule, W., Schwenk, G. and Stenzel, G., *Security document with security features in the form of luminescing substances,* Patent US 4,442,170, Gao Ges Automation Org, **1984**
28. Kaule, W., Schwenk, G. and Stenzel, G., *Printed document having a value and comprising a luminescent authenticity feature based on a host lattice,* Patent US 6,344,261, Giesecke & Devrient GMBH, **2002**
29. Kaule, W. and Stenzel, G., *Security paper with authenticity features in the form of substances luminescing only in the invisible region of the optical spectrum and process for testing the same,* Patent US 4,598,205, Gao Ges Automation Org, **1986**

30. West, A.R., *Solid State Chemistry and its Applications,* **1984,** John Wiley & Sons
31. Pfaender, H.G., *Schott Guide to Glass,* **1996,** Chapman & Hall
32. Rawson, H., *Properties and applications of glass,* Glass science and technology, **1980,** New York, Elsevier science publishing company inc
33. Otsuka, M., *Tb- or Eu- containing fluorophosphate fluorescent glass,* Patent US 5,635,109, Sumita Optical Glass, **1997**
34. Silversmith, A.J., Boye, D.M., Anderman, R.E. and Brewer, K.S., *Fluorescence line narrowing and decay dynamics in sol-gel glasses containing* Eu^{3+}*,* Journal of Luminescence, **2001**, 94-95, 275-278
35. Popma, T.J.A. and Joormann, H.J.M., *Luminescent aluminoborate glass and luminescent screen provided with such a glass,* Patent US 4,751,148, Philips Corp, **1988**
36. Oversluizen, G. and Van Dongen, A.A., *Luminescent alumino-silicate and/or alumino-borate glass comprising lanthanum and/or gadolinium and luminescent screen provided with such a glass,* Patent US 4,798,768, Philips Corp, **1989**
37. Yamazaki, M., Otsuka, M., Nagahama, S. and Sawanobori, N., *Fluorophosphate fluorescent glass capable of exhibiting fluorescence in the visible region,* Patent US 5,755,998, Sumita Optical Glass, **1998**
38. Yamazaki, M., Otsuka, M., Takaku, H. and Sawanobori, N., *Oxide fluorescent glass capable of exhibiting visible fluorescence,* Patent US 5,961,883, Sumita Optical Glass, **1999**
39. Duffy, J.A. and Kyd, G.O., *Ultraviolet absorption and fluorescent spectra of cerium and the effect of glass composition,* Physics and Chemistry of Glasses, **1996**, 37(2), 45-48
40. Doweider, H., Moustafa, Y.M., Abd El-Maksoud, S. and H., S., *Properties of* Na_2O-Al_2O_3-B_2O_3 *glasses,* Materials Science and Engineering A, **2001**, 301(2), 207-212
41. Kamitsos, E.I., Patsis, A.P., Karakasside, M.A. and Chryssikos, G.D., *Infrared Reflectance spectra of lithium borate glasses,* Journal of Non-Crystalline Solids, **1990**, 126, 52-67
42. Duffy, J.A. and Ingram, M.D., *Establishment of an optical scale for lewis basicity in inorganic oxyacids, molten salts, and glasses,* Journal of the American Chemical Society, **1971**, 6448-6454
43. Duffy, J.A., Kamitsos, E.I., Chryssikos, G.D. and Patsis, A.P., *Trends in local optical basicity in sodium borate glasses and relation to ionic mobility,* Physics and Chemistry of Glasses, **1993**, 34(4), 153-157

44. Duffy, J.A., Ingram, M.D. and Fong, S., *Effect of basicity on chemical bonding of metal ions in glass and its relevance to their stability,* Physics Chemistry Chemistry Physics, **2000**, 2, 1829-1833
45. Duffy, J.A., Harris, B., Kamitsos, E.I., Chryssikos, G.D. and Yiannopoulos, Y.D., *Basicity variation in network oxides: distribution of metal ion sites in borate glass systems,* Journal of Physics and Chemistry B, **1997**, 101, 4188-4192
46. Barkatt, A. and Angell, C.A., *On the use of structural probe ions for relaxation studies in glasses. 1. Spectroscopic properties of cobalt (II) in chloride-doped potassium nitrate-calcium nitrate glasses,* Journal of Physical Chemistry, **1975**, 79, 2192-2197
47. Kumar, A., Rai, D.K. and Rai, S.B., *Luminescence of Gd^{3+} ions doped in oxyfluoroborate glass,* Solid State Communications, **2001**, 117, 387-392
48. Houde-Walter, S.N., Peters, P.M., Stebbins, J.F. and Zeng, Q., *Hydroxyl-contents and hydroxyl-related concentration quenching in erbium-doped aluminophosphate, aluminosilicate and fluorosilicate glasses,* Journal of Non-Crystalline Solids, **2001**, 286, 118-131
49. Zaccaria, S., Caesarin, M., Speghini, A., Ajo, D. and Bettinelli.M., *Optical spectroscopy of trivalent lanthanide ions in strontium metaphosphate glasses,* Spectrochemica Acta Part A, **1999**, 55, 171-177
50. Jiang, S., Luo, T., Hwang, B., Smekatala, F., Seneschal, K., Lucas, J. and Peyghambarian, N., *Er^{3+}-doped phosphate glasses for fiber amplifiers with high gain per unit length,* Journal of Non-Crystalline Solids, **2000**, 263 & 264, 364-368
51. Slooff, L.H., de Dood, M.J.A., van Blaaderen, A. and Polman, A., *Effects of heat treatment and concentration on the luminescence properties of erbium-doped silica sol-gel films,* Journal of Non-Crystalline Solids, **2001**, 296, 158-164
52. Haruvy, Y. and Webber, S.E., *Fast sol-gel preparation of glasses,* Patent US 5,272,240, The University of Texas System, **1993**
53. Stone, B.T. and Bray, K.L., *Fluorescence properties of Er^{3+}-doped sol-gel glasses,* Journal of Non-Crystalline Solids, **1996**, 197, 136-144
54. Fujiyama, T., Hori, M. and M., S., *Preparation of Nd-doped silica glasses by the sol-gel method,* Journal of Non-Crystalline Solids, **1990**, 121, 273-278
55. Nogami, M., Yamazaki, T. and Abe, Y., *Fluorescence properties of Eu^{3+} and Eu^{2+} in Al_2O_3-SiO_2 glass,* Journal of Luminescence, **1998**, 78, 63-68
56. Tonooka, K. and Nishimura, O., *Spectral changes of Tb^{3+} fluorescence in borosilicate glasses,* Journal of Luminescence, **2000**, 87-89, 679-681

57. Nogami, M., Nagakura, T. and Hayakawer, T., *Site-dependent fluorescence and hole-burning spectra of Eu^{3+}-doped Al_2O_3-SiO_2 glass,* Journal of Luminescence, **2000**, 86, 117-123

58. Nogami, M., *Fluorescent properties of Eu-doped GeO_2-SiO_2 glass heated under H_2 atmosphere,* Journal of Luminescence, **2001**, 92, 329-336

59. Guodong, Q. and Minquan, W., *Preparation and fluorescence properties of nanocomposites of amorphous silica glasses doped with lanthanide (III) benzoates,* Journal of Physics and Chemistry of Solids, **1997**, 58(3), 375-378

60. Almeida, R.M., Vasconcelos, H.C., Goncalves, M.C. and Santos, L.F., *XPS and NEXAFS studies of rare-earth doped amorphous sol-gel films,* Journal of Non-Crystalline Solids, **1998**, 232-234, 65-71

61. Nogami, M., Ishikawa, T. and Hayakawa, T., *Defect centres and room temperature persistent spectral hole burning in X-ray irradiated Eu^{3+}- doped glass,* Journal of Luminescence, **2002**, 96, 163-169

62. Pillonnet-Minardi, A., Marty, O., Bovier, O., Garapon, C. and Mugnier, J., *Optical and structural analysis of Eu^{3+} doped alumina planar waveguides elaborated by the sol-gel process,* Optical Materials, **2001**, 16, 9-13

63. Lochhead, M.J. and Bray, K.L., *Rare-earth clustering and aluminium codoping in sol-gel silica: Investigation using europium (III) fluorescence spectroscopy,* Chemistry of Materials, **1995**, 7, 572-577

64. Best, W.V. and Hughes, R.L., *Preparation of luminescent silica glass modified with a rare earth metal,* Patent US 3,459,673, Owens Illinois Inc, **1969**

65. Boffe, M. and Toussaint, F., *Diffusion methods and treating mediums for improving the properties of materials,* Patent US 3,807,980, **1974**

66. Kiefer, W. and Rodek, E., *Process for ion exchange on glass or glass ceramic,* Patent US 5,127,931, Schott Glaswerke, **1992**

67. Rinehart, D.W., *Ion exchange strengthening of soda-lime silica glass,* Patent US 4,192,689, PPG Industries Inc, **1980**

68. Dubiel, M., Schmitz, R., Kolb, U., Gutwerk, D. and Bertagnolli, H., *X-ray diffraction and absorption studies of ion exchanged glasses,* Physica B, **1995**, 208 & 209, 349-350

69. Dubiel, M., Brunsch, S., Kolb, U., Gutwerk, D. and Bertagnolli, H., *Experimental studies investigating the structure of soda-lime glasses after silver-sodium ion exchange,* Journal of Non-Crystalline Solids, **1997**, 220, 30-44

70. Skoog, D.A., West, D.M., Holler, F.J. and Crouch, S.R., *Analytical Chemistry, an Introduction,* 7th, **2000,** Saunders College Publishing
71. Fanderlik, I., *Silica Glass and its Applications,* **1991,** Amsterdam, Elsevier
72. Lee, J.D., *Concise Inorganic Chemistry,* 5th, **1996,** Blackwell Science
73. Jorgensen, C.K. and Reisfeld, R., *Chemistry and spectroscopy of rare earths,* Topics in Current Chemistry, **1982**, 100, 127-167
74. Weber, M.J., *Fluorescence and glass lasers,* Journal of Non-Crystalline Solids, **1982**, 47(1), 117-134
75. Weber, M.J., *Science and technology of laser glass,* Journal of Non-Crystalline Solids, **1990**, 123, 208-222
76. Shelby, J.E., *Rare earths as major components in oxide glasses,* Key Engineering Materials, **1994**, 94-95, 1-41
77. Aspinall, H.C., *Chemistry of the f-block elements,* Advanced chemistry texts, D. Phillips, P. O'Brian, and S. Roberts, **2001,** Amsterdam, Gordon and Breach Science Publishers
78. Kaplyanskii, A.A. and Macfarlane, R.M., *Spectroscopy of solids containing rare earth ions,* **1987,** Amsterdam, Elsevier Science Publishers
79. Knowles, A. and Burgess, C., *Practical absorption spectrometry,* Techniques in visible and ultraviolet spectrometry, **1984,** Cambridge, Chapman and Hall
80. Skoog, D.A., *Principles of instrumental analysis,* Third Edition, **1985,** London, Saunders College Publishing
81. Housecroft, C.E. and Sharpe, A.G., *Inorganic chemistry,* First Edition, **2001,** Essex, Pearson Education Limited
82. Macfarlane, R.M. and Shelby, R.M., *Coherent Transient and Holeburning Spectroscopy of Rare Earth Ions in Solids*, in *Spectroscopy of solids containing rare earth ions*,Amsterdam. 51-184, Editors A.A. Kaplyanskii and R.M. Macfarlane. **1987**, Elsevier Science Publishers B.V:
83. Cotton, F.A. and Wilkinson, G., *Advanced Inorganic Chemistry - a comprehensive text,* Third Edition, **1972,** London, Interscience Publishers
84. Rawle, A., *Basic principles of particle size analysis*, Accessed **26/05/03,** http://www.malvern.co.uk/malvern/kbase.nsf/0/5E3F5A148D336B0480256BF2006E2195/$file/Basic_principles_of_particle_size_analysis_MRK034-low_res.pdf.
85. *Malvern Mastersizer/E User Manual,*
86. Shelby, J.E., *Introduction to Glass Science and Technology,* **1997,** Cambridge, RSC Paperback

87. Li, Z., Wu, P., Jiang, X., Zhang, Z. and Xu, S., *The synthesis of rare earth borate glasses and their luminescence properties,* Journal of Luminescence, **1988**, 40 & 41, 135-136

88. Edelman, I.S., Malakhovskii, A.V., Potseluyko, A.M. and Zarubina, T.V., *Temperature dependencies of intensities of f-f transitions in Pr^{3+} and Dy^{3+} in glasses.,* Journal of Non-Crystalline Solids, **2002**, 306, 120-128

89. Rodriguez, V.D., Lavin, V., Rodriquez-Mendoza, U.R. and Martin, I.R., *Spectroscopy of rare earth ions in fluoride glasses for laser applications,* Optical Materials, **1999**, 13, 1-7

90. Erostyak, J., Buzady, A., Kaszas, A., Kozma, L. and Hornyak, I., *Time-resolved study of intramolecular energy transfer in Eu^{3+}, Tb^{3+} / β–diketone / o–phenanthroline complexes in aqueous micellar solutions,* Journal of Luminescence, **1997**, 72-74, 570-571

91. Levin, E.M., Robbins, C.R. and McMurdie, H.F., *Phase diagrams for ceramists,* **1964,** The American Ceramic Society Inc

92. Sarkies, J.R. and Rutt, H.N., *Spectroscopic and optical properties of the rare earth-doped liquid $PBr_3/AlBr_3/SbBr_3$,* Optical Materials, **1999**, 13, 231-238

93. Carnall, W.T., Fields, P.R. and Rajnak, K., *Electronic energy levels of the trivalent lanthanide aquo ions. IV. Eu^{3+},* The Journal of Chemical Physics, **1968**, 49(10), 4450-4455

94. Aruna, V. and Buddhuda, S., *Spectral properties of Tb^{3+}:B_2O_3-P_2O_5-R_2SO_4 glasses,* Materials Letters, **1998**, 36, 24-28

95. Kam, C.H. and Buddhudu, S., *Luminescence and decay behaviour of Tb^{3+}:ZrF_4-BaF_2-LaF_3-YF_3-AlF_3-NaF optical glasses,* Physica B: Condensed Matter, **2003**, 337(1-4), 237-244

96. Jayasankar, C.K. and Rukmini, E., *Spectroscopic investigations of Dy^{3+} ions in borosulphate glasses,* Physica B, **1997**, 240, 273-288

97. Reisfeld, R., *Spectra and energy transfer of rare earths in inorganic glasses,* Structure and Bonding, **1973**, 13, 53-98

98. Dixit, L. and Ram, S., *Quantitative analysis by derivative electronic spectroscopy,* Applied Spectroscopy Reviews, **1985**, 21(4), 311-418

99. Dejneka, M., Snitzer, E. and Riman, R.E., *Blue, green and red fluorescence and energy transfer of Eu^{3+} in fluoride glasses,* Journal of Luminescence, **1995**, 65, 227-245

100. Culea, E. and Bratu, I., *Structural and magnetic behaviour of some borate glasses containing dysprosium ions,* Journal of non-crystalline solids, **2000**, 262, 287-290

101. Henderson, D.O., George, M.A., Tung, Y.S., Mu, R., Burger, A., Morgan, S.H., Collins, W.E., White, C.W., Zuhr, R.A. and Magruder III, R.H., *X-ray photoelectron and infrared spectroscopies of Cu-implanted silica and borosilicate glasses,* Journal of Vacuum Science and Technology A, **1995**, 13(3), 1254-1259

102. Dejneka, M.J., Streltsov, A., Pal, S., Frutos, A.G., Powell, C.L., Yost, K., Yuen, P.K., Muller, U. and Lahiri, J., *Rare earth-doped glass microbarcodes,* The Proceedings of the National Academy of Sciences, **2003**, 100(2), 389-393

103. Dieke, G.H. and Crosswhite, H.M., *The spectra of the doubly and triply ionized rare earths,* Applied Optics, **1963**, 2(7), 675-686

104. Nachimuthu, P., Vithal, M. and Jagannathan, R., *Absorption and emission spectral properties of Pr^{3+}. Nd^{3+}, and Eu^{3+} ions in heavy-metal oxide glasses,* Journal of the American Ceramic Society, **2000**, 83(3), 597-604

105. Ishizaka, T. and Kurokawa, Y., *Optical properties of rare-earth ion (Gd^{3+}, Ho^{3+}, Pr^{3+}, Sm^{3+}, Dy^{3+} and Tm^{3+}) -doped alumina films prepared by the sol-gel method,* Journal of Luminescence, **2001**, 92(1-2), 57-63

106. Hormadaly, J. and Reisfeld, R., *Intensity parameters and laser analysis of Pr^{3+} and Dy^{3+} in oxide glasses,* Journal of Non-Crystalline Solids, **1979**, 30, 337-348

107. Bishop, O., *Practical Electronic Design Data,* **1996,** London, Bernard Babani publishing LTD

108. *3M™ Screen printing inks*, Accessed **23/06/04,** http://products3.3m.com/catalog/us/en001/graphicarts/scotchprint/node_ZVJJ34MXL9be/root_GST1T4S9TCgv/vroot_K9JT0N94GJge/gvel_Q9QB0Z97L6gl/theme_us_scotchprint_3_0/command_AbcPageHandler/output_html.

109. *Sample dispersion & refractive index guide,* Version 3.1, **1997**, Malvern Instruments ltd,

110. Joshi, B.C., *Enhanced Eu^{3+} emission by non-radiative energy transfer from Tb^{3+} in zinc phosphate glass,* Journal of non-crystalline solids, **1995**, 180, 217-220

111. Sobha, K.C. and Rao, K.J., *Luminescence of, and energy transfer between Dy^{3+} and Tb^{3+} in nasicon-type phosphate glasses,* Journal of physics and chemistry of solids, **1996**, 57(9), 1263-1267

112. Cabezas, A.Y. and DeShazer, L.G., *Radiative transfer of energy between rare-earth ions in glass,* Applied Physics Letters, **1964**, 4(2), 37-39

113. Miller, J.C. and Miller, J.N., *Statistics for analytical chemistry,* Analytical Chemistry, R.A. Chalmers and M. Masson, **1984,** Chichester, Ellis Horwood Limited

114. Salkind, N.J., *Statistics for people who (think they) hate statistics,* second edition, **2004,** London, Sage Publications, Inc

115. Mullin, J.W., *Particle size analysis with micro sieves using ultrasonic vibrations,* Chemistry and Industry, **1971**, 1435-1436

116. Lawes, G., *Scanning electron microscopy and x-ray microanalysis,* Analytical chemistry by open learning, A.M. James, **1987,** London, John Wiley & Sons

117. Pilkington, *Protecting flat glass surfaces*, Accessed **21/06/04,** http://www.pilkington.com/resources/ats104swprotectingglass20020306.pdf.

118. Kamata, N., Satoh, C., Tasaka, K. and Yamada, K., *Blue emission and energy transfer characteristics of Eu-doped sol-gel glasses without post-processing,* Journal of Non-Crystalline Solids, **2001**, 293-295, 595-599

119. Song, C.F., Yang, P., Lü, M.K., Xu, D., Yuan, D.R. and Liu, Z.Q., *Enhanced blue emission from Eu, Dy co-doped sol-gel Al_2O_3-SiO_2 glasses,* Journal of Physics and Chemistry of Solids, **2003**, 64, 491-494

120. Chang-xin, G., Wei-ping, Z. and Chao-Shu, S., *Enhancement mechanism of luminescence of RE^{3+} (Eu^{3+}, Sm^{3+}, Dy^{3+}) in Y_2O_2S phosphor by a trace of Tb^{3+},* Journal of Luminescence, **1981**, 24/25, 297-300

121. Choi, J.S., Baek, S.H., Kim, S.G., Lee, S.H., Park, H.L., Mho, S.-I., Kim, T.W. and Hwang, Y.H., *Energy transfer between Ce^{3+} and Eu^{2+} in $SrAl_{12}O_{19}$:Ce_x^{3+}, $Eu_{0.01}^{2+}$ ($x = 0.01$-0.09),* Materials Research Bulletin, **1999**, 34(4), 551-556

122. Dexter, D.L., *A theory of sensitized luminescence in solids,* The journal of chemical physics, **1953**, 21(5), 836-850

123. Reisfeld, R., Saraidarov, T., Ziganski, E., Gaft, M., Lis, S. and Pietraszkiewicz, M., *Intensification of rare earths luminescence in glasses,* Journal of Luminescence, **2003**, 102-103, 243-247

APPENDIX A - AQUEOUS SOLUTION SPECTRA

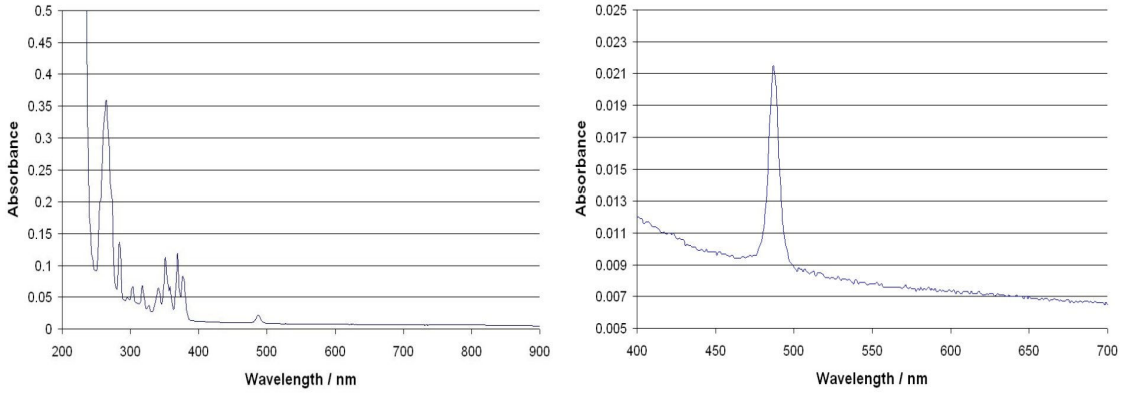

Figure A-1. UV-Visible absorption spectrum of 0.3 mol l^{-1} $TbCl_3$ solution

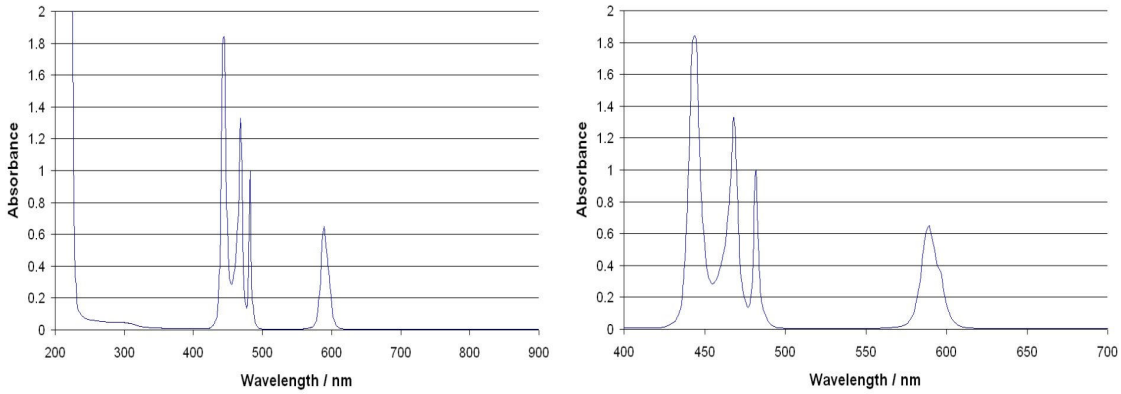

Figure A-2. UV-Visible absorption spectrum of 0.3 mol l^{-1} $PrCl_3$ solution

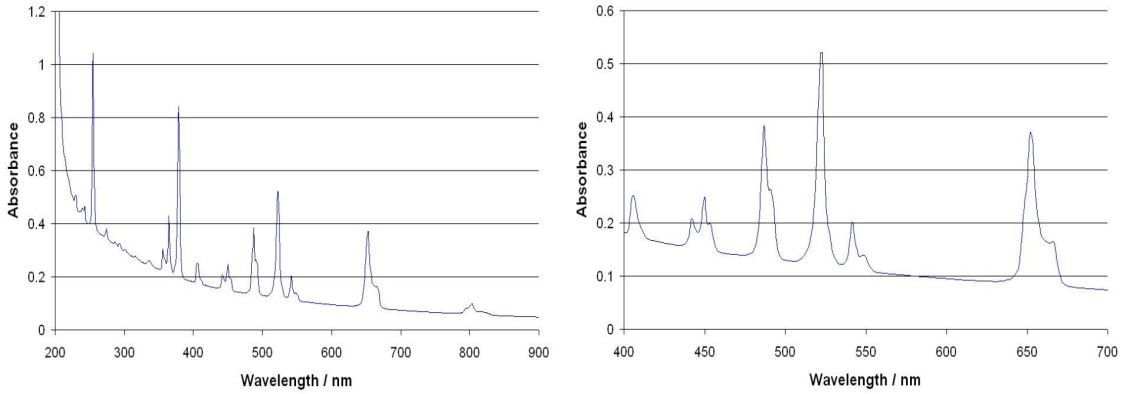

Figure A-3. UV-visible absorption of 0.3 mol l^{-1} $ErCl_3$ solution

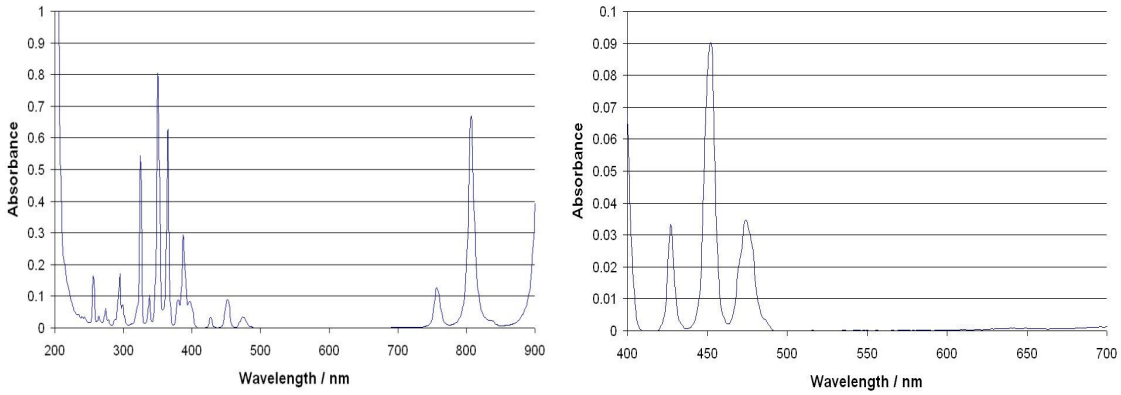

Figure A-4. UV-Visible spectrum of 0.3 mol l^{-1} $DyCl_3$ solution

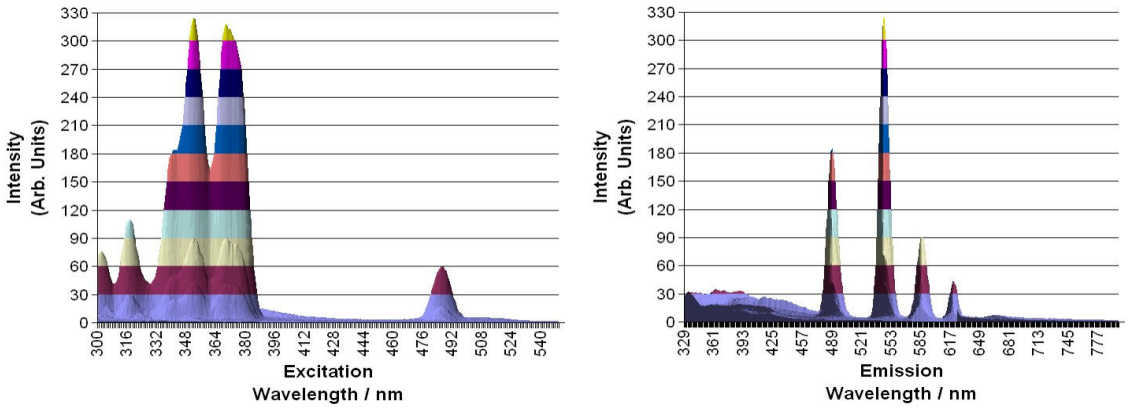

Figure A-5. Fluorescence spectrum of the 0.3 mol l^{-1} $TbCl_3$ solution

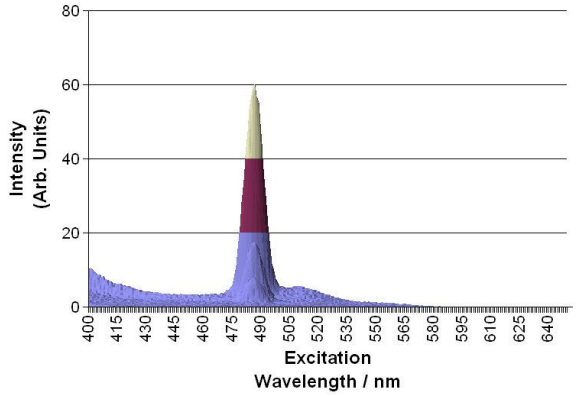

Figure A-6. Visible range excitation of 0.3 mol l^{-1} $TbCl_3$ solution

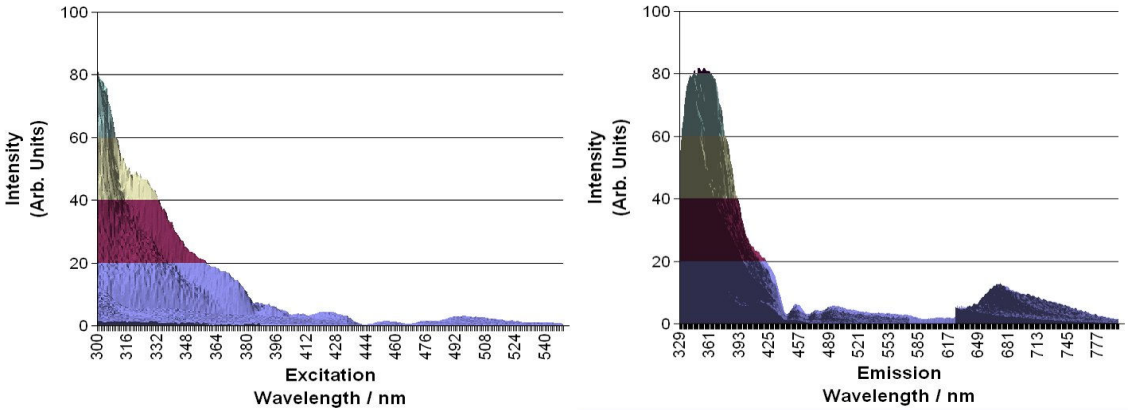

Figure A-7. Fluorescence spectrum of the 0.3 mol l^{-1} $PrCl_3$ solution

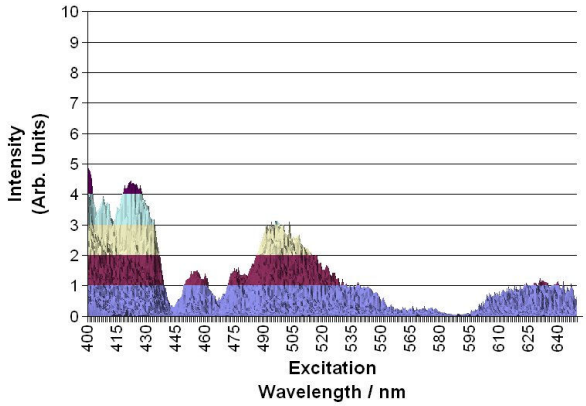

Figure A-8. Visible range excitation of 0.3 mol l^{-1} $PrCl_3$ solution

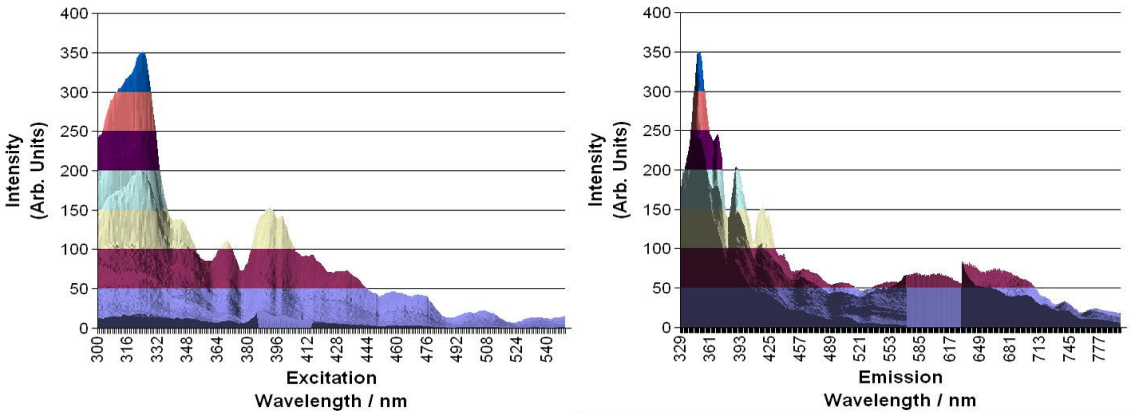

Figure A-9. Fluorescence spectrum of 0.3 mol l^{-1} $ErCl_3$ solution

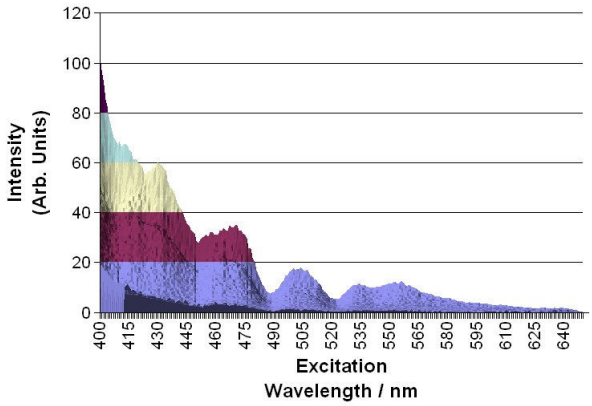

Figure A-10. Visible range excitation of 0.3 mol l^{-1} $ErCl_3$ solution

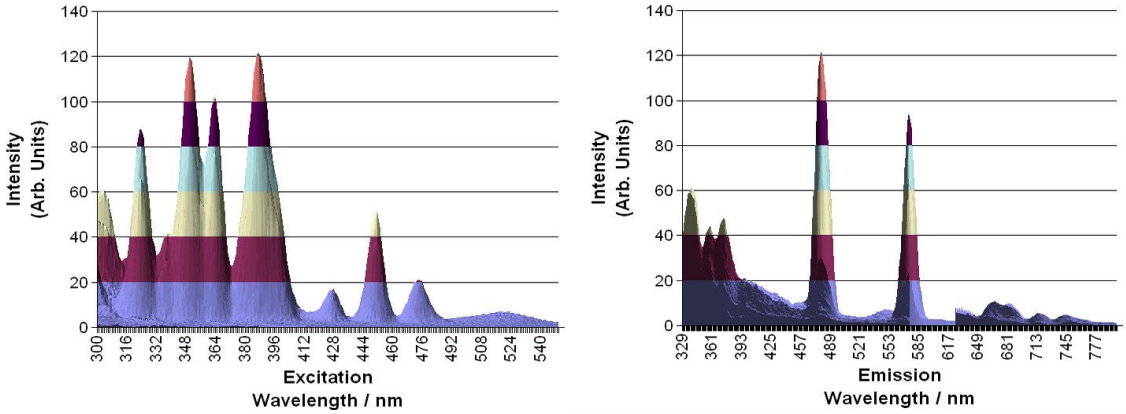

Figure A-11. Fluorescence spectrum of 0.3 mol l^{-1} $DyCl_3$ solution

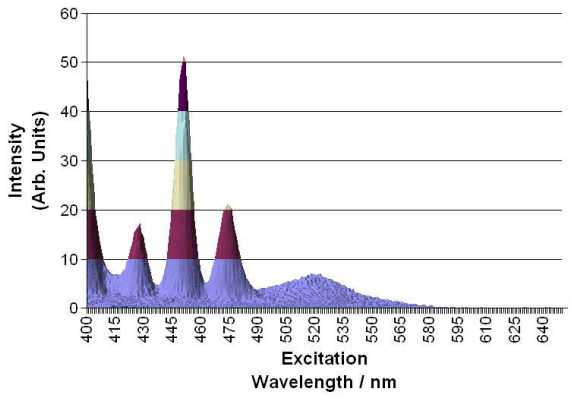

Figure A-12. Visible range excitation of 0.3 mol l^{-1} $DyCl_3$ solution

APPENDIX B - SINGLE RE DOPED GLASS SPECTRA

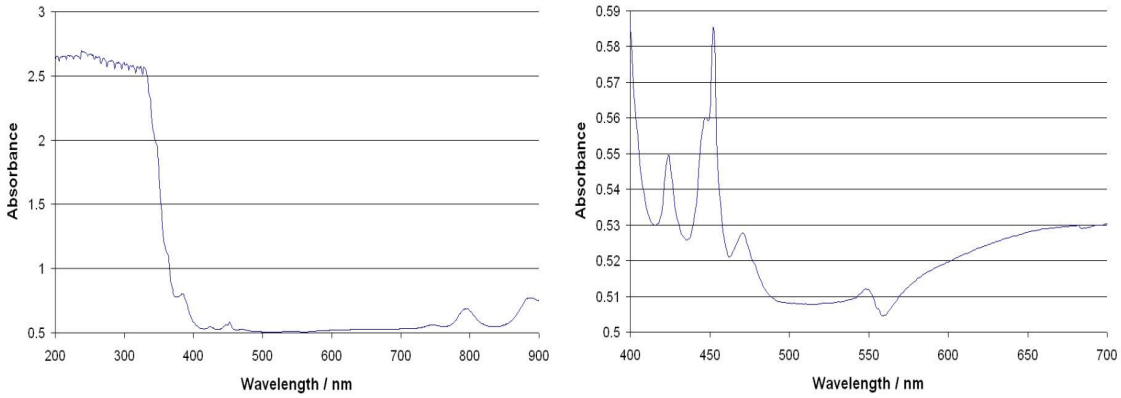

Figure B-1. Absorption spectra of 1 mol% Dy doped borosilicate

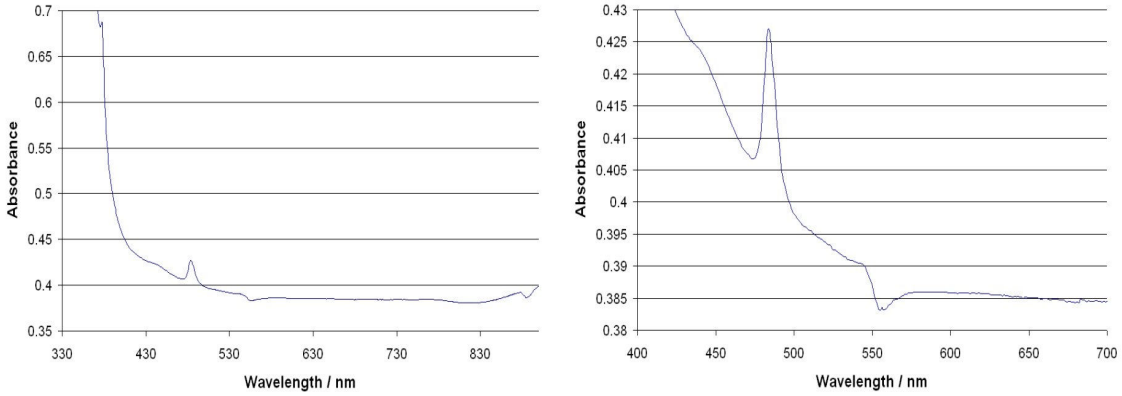

Figure B-2. UV-Visible absorption spectrum of 3 mol% terbium doped borosilicate glass

Terms from $^7F_6$	Excitation Wavelength / nm
$^5D_4$	484
$^5G_6$	378

Table B-1. Energy level assignments for Tb^{3+} doped in borosilicate glass

Terms from $^7F_{9/2}$	Excitation Wavelength / nm
	375
	381
$^4I_{13/2}$	385
$^4G_{11/2}$	424
	449
$^4I_{15/2}$	452
$^4F_{9/2}$	472
$^6F_{3/2}$	745
$^6F_{5/2}$	794
$^6F_{7/2}$	884

Table B-2. Absorption transitions of 3 mol% Dy^{3+} doped borosilicate glass

Excitation Wavelength / nm	Emission Wavelength / nm	Intensity	Transition
362	591.5	40.45	$^5D_0$-$^7F_1$
362	616	125.97	$^5D_0$-$^7F_2$
362	654.5	11.96	$^5D_0$-$^7F_3$
381	592	133.64	$^5D_0$-$^7F_1$
381	615.5	465.88	$^5D_0$-$^7F_2$
381	653.5	30.60	$^5D_0$-$^7F_3$
382	702.5	56.58	$^5D_0$-$^7F_4$
387	535	40.74	$^5D_1$-$^7F_1$
393	591.5	218.76	$^5D_0$-$^7F_1$
393	615.5	768.13	$^5D_0$-$^7F_2$
393	702	89.36	$^5D_0$-$^7F_4$
395	653	43.93	$^5D_0$-$^7F_3$
412	591	59.93	$^5D_0$-$^7F_1$
412	615.5	166.91	$^5D_0$-$^7F_2$
412	653.5	15.23	$^5D_0$-$^7F_3$
412	702.5	20.98	$^5D_0$-$^7F_4$
444	535.5	18.40	$^5D_1$-$^7F_1$
463	592	121.44	$^5D_0$-$^7F_1$
463	652	33.30	$^5D_0$-$^7F_3$
463	702.5	42.79	$^5D_0$-$^7F_4$
465	535	27.62	$^5D_1$-$^7F_1$
465	615.5	479.06	$^5D_0$-$^7F_2$
526	652.5	15.45	$^5D_0$-$^7F_3$
531	590	62.80	$^5D_0$-$^7F_1$
531	615.5	220.97	$^5D_0$-$^7F_2$
531	702.5	24.20	$^5D_0$-$^7F_4$
579	616	61.52	$^5D_0$-$^7F_2$
579	704.5	10.47	$^5D_0$-$^7F_4$
580	651.5	8.48	$^5D_0$-$^7F_3$

Table B-3. Table of fluorescence peaks their intensity and relative transitions for 3 mol% Eu doped borosilicate glass

Excitation Wavelength / nm	Emission Wavelength / nm	Intensity	Transition
352	588.5	23.69	$^5D_4$-$^7F_4$
354	488.5	65.29	$^5D_4$-$^7F_6$
354	546.5	164.13	$^5D_4$-$^7F_4$
354	622	14.31	$^5D_4$-$^7F_3$
359	385	17.35	$^5D_3$-$^7F_6$
375	546	382.28	$^5D_4$-$^7F_5$
375	588.5	55.88	$^5D_4$-$^7F_4$
376	415	64.87	$^5D_3$-$^7F_5$
376	438	65.12	$^5D_3$-$^7F_4$
376	488.5	139.36	$^5D_4$-$^7F_6$
377	622	32.75	$^5D_4$-$^7F_3$
379	458	27.26	$^5D_3$-$^7F_3$
483	545	200.31	$^5D_4$-$^7F_5$
483	588	35.09	$^5D_4$-$^7F_4$
483	622.5	30.03	$^5D_4$-$^7F_3$

Table B-4. Table of terbium fluorescence peaks, their intensities and relative transitions

Excitation Wavelength / nm	Emission Wavelength / nm	Intensity	Transition
324	577	15.25	$^4F_{9/2}$-$^6H_{13/2}$
325	483	9.31	$^4F_{9/2}$-$^6H_{15/2}$
352	483	51.09	$^4F_{9/2}$-$^6H_{15/2}$
352	577	101.13	$^4F_{9/2}$-$^6H_{13/2}$
352	662.5	3.84	$^4F_{9/2}$-$^6H_{11/2}$
364	483	56.20	$^4F_{9/2}$-$^6H_{15/2}$
364	577	100.68	$^4F_{9/2}$-$^6H_{13/2}$
365	665.5	3.82	$^4F_{9/2}$-$^6H_{11/2}$
389	483	96.76	$^4F_{9/2}$-$^6H_{15/2}$
389	577	197.69	$^4F_{9/2}$-$^6H_{13/2}$
391	665.5	8.65	$^4F_{9/2}$-$^6H_{11/2}$
391	752	3.59	$^4F_{9/2}$-$^6H_{9/2}$
425	758	1.80	$^4F_{9/2}$-$^6H_{9/2}$
426	483	30.20	$^4F_{9/2}$-$^6H_{15/2}$
426	577	50.74	$^4F_{9/2}$-$^6H_{13/2}$
426	664	3.37	$^4F_{9/2}$-$^6H_{11/2}$
451	758	3.19	$^4F_{9/2}$-$^6H_{9/2}$
452	483	55.22	$^4F_{9/2}$-$^6H_{15/2}$
452	577	111.25	$^4F_{9/2}$-$^6H_{13/2}$
452	669.5	5.00	$^4F_{9/2}$-$^6H_{11/2}$
470	577	38.25	$^4F_{9/2}$-$^6H_{13/2}$
471	658	4.24	$^4F_{9/2}$-$^6H_{11/2}$
471	756.5	2.29	$^4F_{9/2}$-$^6H_{9/2}$

Table B-5. Table of dysprosium fluorescence peaks, their intensities and relative transitions

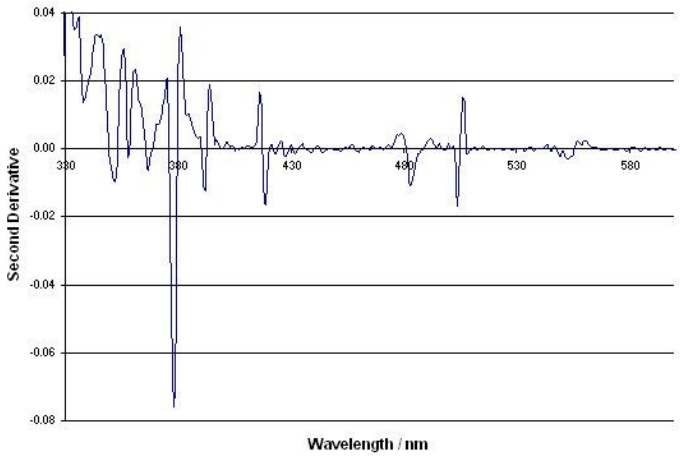

Figure B-3. Second derivative absorption spectrum of 3 mol% terbium doped borosilicate glass

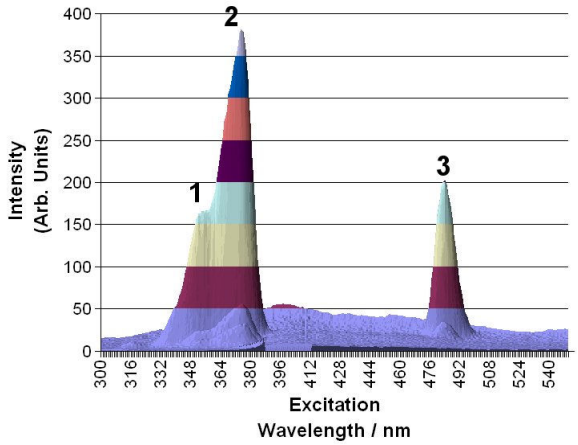

Figure B-4. Fluorescence spectrum of 3 mol% Tb^{3+} doped borosilicate glass with main peaks numbered

Label	Normal UV / nm	Second Derivative / nm	Excitation maximum on fluorescence spectrum / nm
1		338	
		352	354
		358	
2		367	
	378	378	375
		392	
3		419	
	484	483	483
		504	

Table B-6. Comparing UV results with second derivative and fluorescence results for terbium doped glass

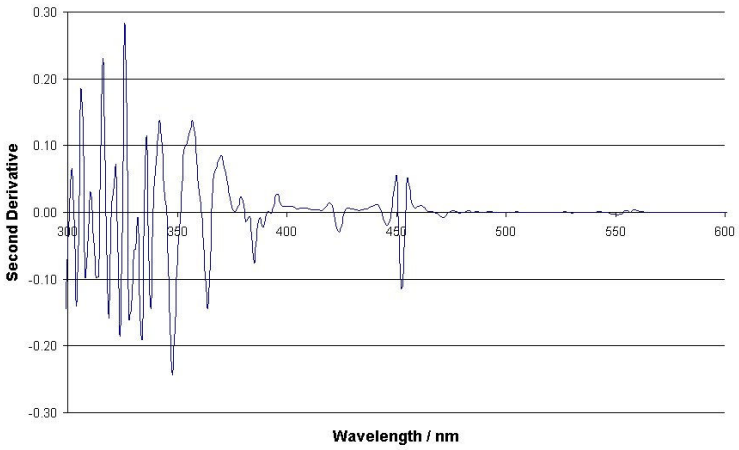

Figure B-5. Second derivative absorption spectrum of 3 mol% Dy^{3+} doped borosilicate glass

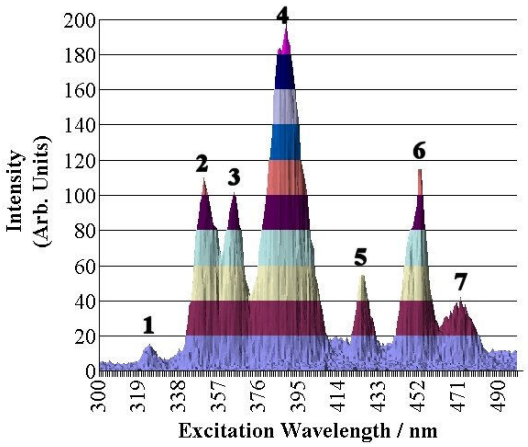

Figure B-6. Fluorescence spectrum of 3 mol% Dy^{3+} doped borosilicate glass with main peaks numbered

Label	Normal UV / nm	Second Derivative / nm	Excitation maximum on fluorescence spectrum / nm
1		319	
		324	324
		328	
2		334	
		338	
		348	352
3		364	364
4		377	
		382	
	385	385	
		389	389
		393	
5	425	424	425
6		446	
	452	452	452
7	472	472	471

Table B-7. Comparing UV results with second derivative and fluorescence results for dysprosium doped glass

Excitation Wavelength / nm	Emission Wavelength / nm	Intensity	Transition
444	489.5	43.76	$^3P_2$-$^3H_4$
444	529	13.14	$^3P_2$-$^3H_5$
443	604	336.29	$^3P_2$-$^3H_6$
443	698	10.81	$^3P_2$-$^3F_2$
469	530.5	14.60	$^3P_1$-$^3H_5$
468	606	238.90	$^3P_1$-$^3H_6$
468	699.5	9.31	$^3P_1$-$^3F_2$
479	527	14.11	$^3P_0$-$^3H_5$
481	606	223.77	$^3P_0$-$^3H_6$
481	698	9.53	$^3P_0$-$^3F_2$
582	604	88.34	$^1D_2$-$^3H_6$
586	698	5.16	$^1D_2$-$^3F_2$

Table B-8. Table of fluorescence peaks their intensity and relative fluorescence for Pr^{3+} doped borosilicate glass

APPENDIX C - FLUORESCENCE MICROSCOPE FILTER RESPONSES

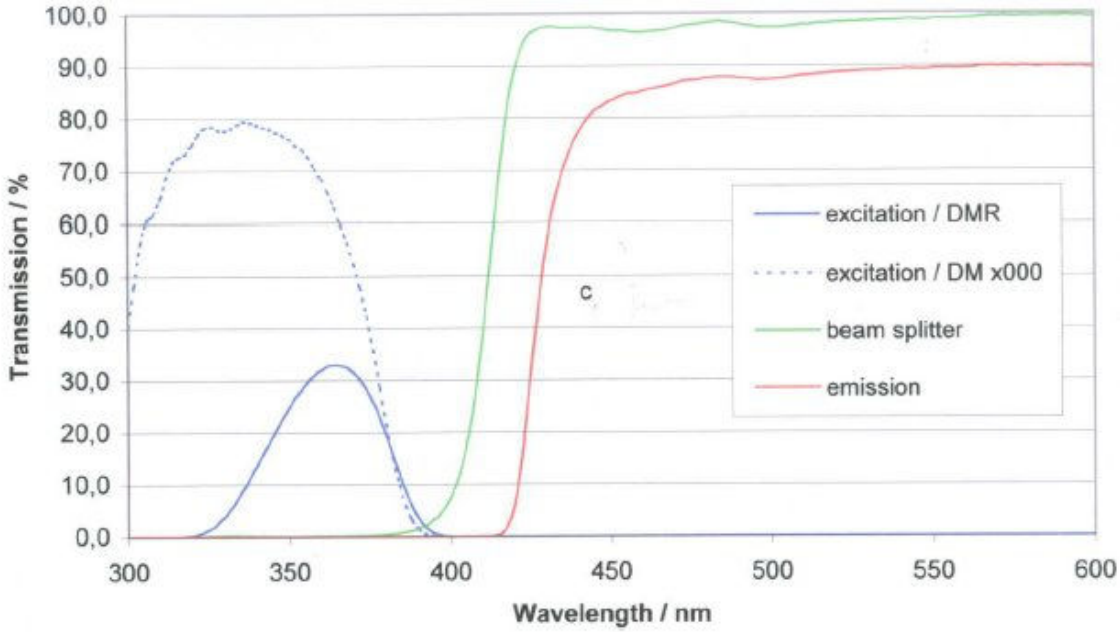

Figure C-1. Filter response of the UV filter used with the fluorescence microscope

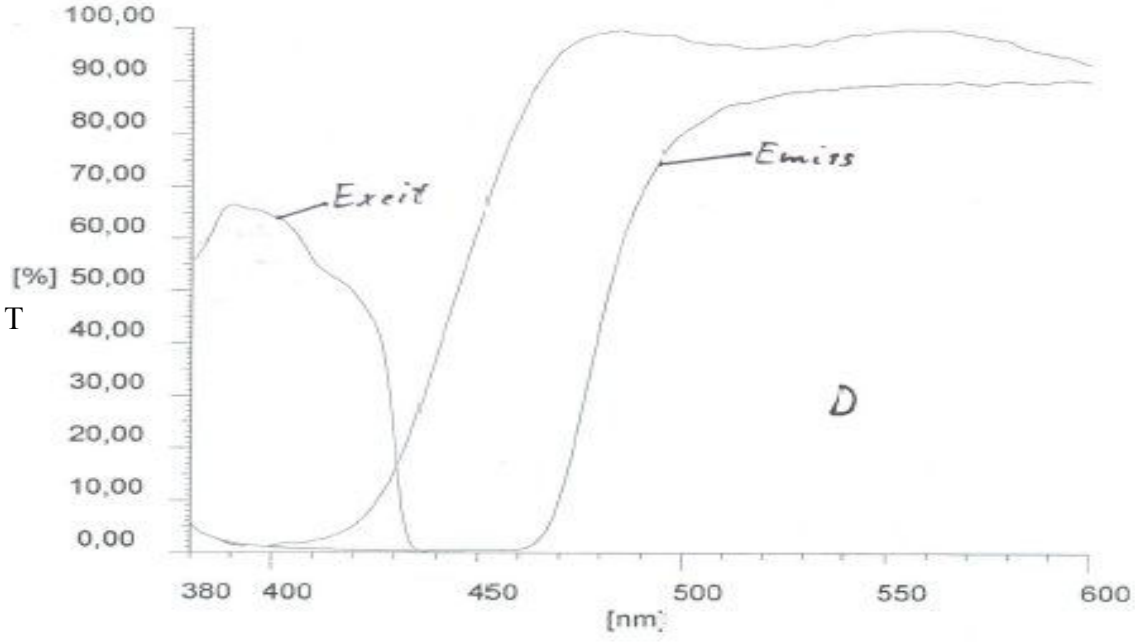

Figure C-2. Filter response of the Violet filter used with the fluorescence microscope

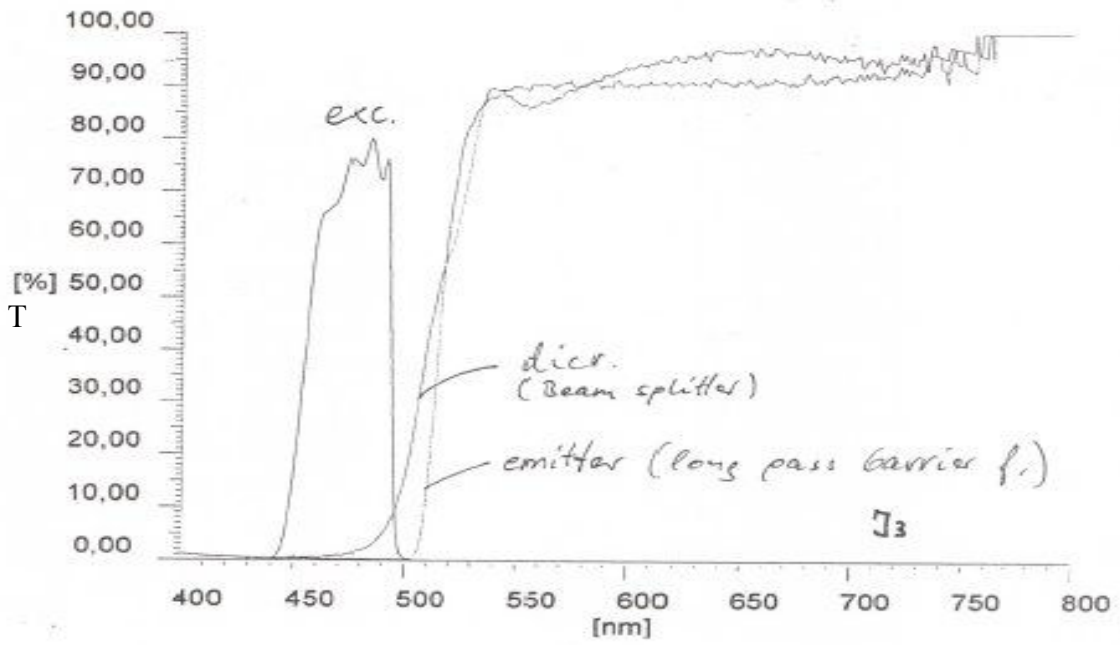

Figure C-3. Filter response of the Blue filter used with the fluorescence microscope

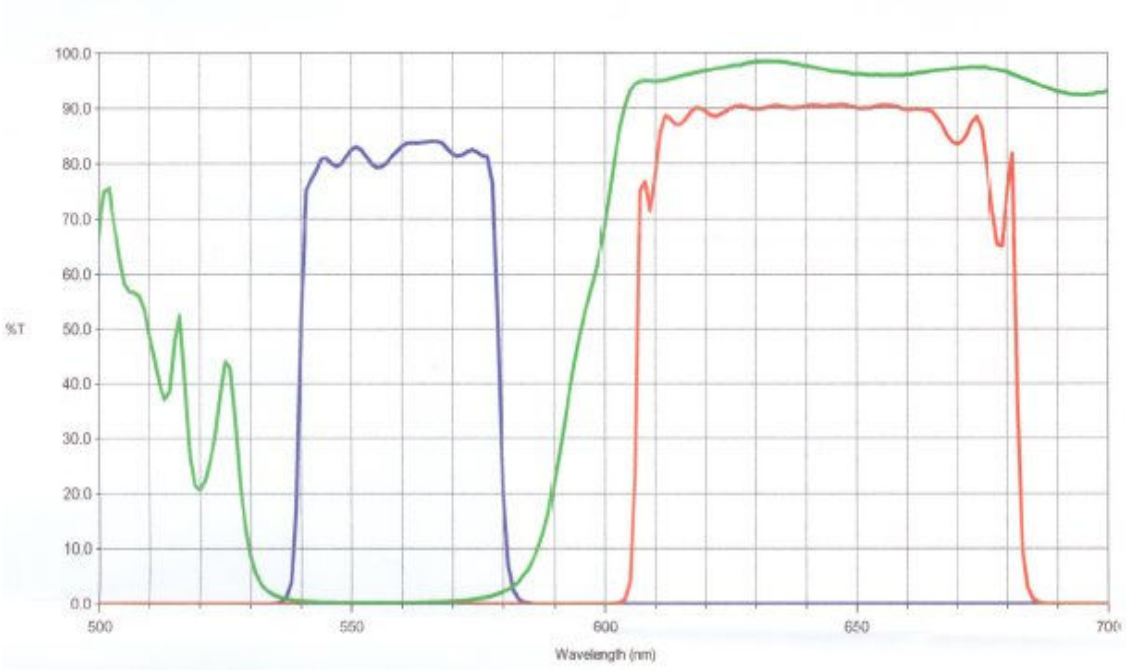

Figure C-4. Filter response of the Green filter used with the fluorescence microscope

APPENDIX D - PUBLICATIONS

Patents

Ross, G.A., Hunter, C., Officer, S., Prabhu, G.R. and Pollard, P., *Security Labelling,* Patent EP 1491350, **2004**

Officer, S., Ross, G.A., Hunter, C., Pollard, P. and Prabhu, G.R., *Security Labelling,* Patent US 2004262547, **2004**

Prabhu, G.R., Officer, S., Pollard, P. and Hunter, C., *Taggant Coated Glass Beads*, Patent Filed 24/12/04

Poster Presentations

Officer, S., Prabhu, G.R., Pollard, P., Hunter, C. and Ross, G.A. "Novel online security system based on rare-earth-doped glass microbeads". in *Optical Security and Counterfeit Deterrence Techniques V*, edited by R.L.van Renesse, Proceedings of SPIE-IS&T Electronic Imaging, SPIE Vol. 5310, 387-395, **2004**

Officer, S., Prabhu, G.R., Pollard, P., Hunter, C. and Ross, G.A. "Novel online security system based on rare-earth-doped glass microbeads". Presented at the *Set for Britain* annual presentation in the House of Commons, **2005**

Papers in the NCR Self-Service Strategic Solutions annual research reports

Officer, S. and Ross, G., *Security labelling: a review,* Advances II, **2002**, 50-55

Officer, S., Prabhu, R. and Ross, G., *Northern Light,* Advances III, **2003**, 61-68